
Science
1 June 2007 | $10
AAAS

A forecast you *can* predict: excellent results every time.

New Stratagene AffinityScript™ – Works at multiple temperatures.
Delivers high yields. Affordably Priced.

Our AffinityScript™ Multiple Temperature Reverse Transcriptase (RT)* is optimized for reverse transcription using your preferred reaction temperature from 37–55°C, making it the ideal choice for QRT-PCR experiments. With a 10-fold higher affinity to primer-template complexes compared to MMLV RT, our AffinityScript RT delivers high sensitivity and specificity without compromising cDNA yield or length.

- **Robust cDNA synthesis from 37–55°C**
- **Ten-fold higher affinity for primer-template complexes for high specificity and sensitivity**
- **Full length cDNA from 500 bp up to 20 kb**

Need More Information? Give Us A Call:

Stratagene US and Canada
Order: 800-424-5444 x3
Technical Service: 800-894-1304 x2

Stratagene Europe
Order: 00800-7000-7000
Technical Service: 00800-7400-7400

Stratagene Japan K.K.
Order: 3-5821-8077
Technical Service: 3-5821-8076

Ask us about these great products:

AffinityScript™ Multiple Temperature Reverse Transcriptase	10 rxn	600125
	50 rxn	600127
	200 rxn	600128
AffinityScript™ Multiple Temperature cDNA Synthesis Kit	50 rxn	200435
AffinityScript™ QPCR cDNA Synthesis Kit	50 rxn	600659

*Patent pending.

AffinityScript™ is a trademark of Stratagene in the United States.

STRATAGENE®

www.stratagene.com/affinityscript

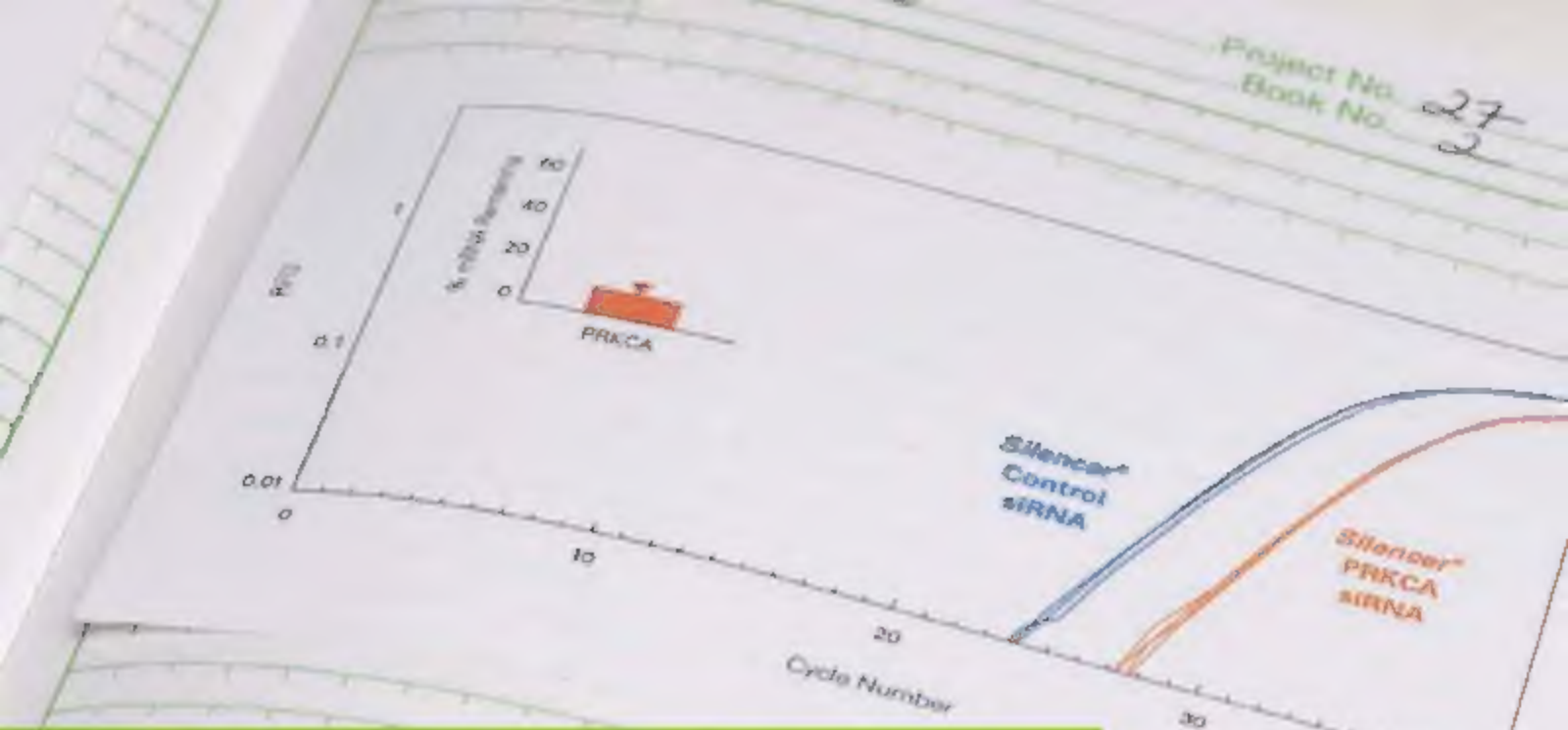

Ambion *Silencer*® Validated siRNA Gene Silencing is Confirmed Using Applied Biosystems TaqMan® Gene Expression Assays. The indicated *Silencer* Validated siRNAs were transfected into HeLa Cells at 30 nM. RNA was isolated 48 hours later and analyzed by one-step qRT-PCR using the appropriate TaqMan Gene Expression Assay. Results were normalized for input RNA amount using real time data for 18S rRNA. The inset graphs show the reduction in target gene expression compared to cells transfected with an equal concentration of *Silencer* Negative Control #1 siRNA.

Ambion Silencing. TaqMan® Assay Validation. All in Real Time.

RNAi Made Simple. With RNA interference, you can elucidate gene function in a matter of days—if you have the right reagents and protocols. Applied Biosystems and Ambion, now an Applied Biosystems Business, provide the most complete suite of premium quality reagents available that have been validated to optimally work together! Our potent, Ambion *Silencer*® siRNAs, gold-standard TaqMan gene expression assays, optimized Real-Time Reagents, trusted Real-Time Systems, and the protocols provided with them, streamline each step of an RNAi experiment. The result? Lower barrier to get started, reduced technical variability in your experiments, technical support throughout your experiment—all of which give you freedom to focus on making critical biological discoveries.

For a simple step-by-step RNAi experimental design guide that enables you to start exploring gene function quickly, visit: **www.ambion.com/ABsynergy**

Proven Performance. Proven Together.

Applied Biosystems

GE Healthcare

illustra™

Get attached to illustra for faster nucleic acid sample prep.

New illustra™ nucleic acid sample prep kits from GE Healthcare give you optimal yield and purity. What's more, they do this in as little as half the time it takes the best competing products. Whether you're purifying nucleic acids in plasmid, blood, tissue, cells or bacteria, you'll find that superior results and outstanding reproducibility come easily with illustra mini and midi kits.

With more than 20 years' experience in nucleic acid research, we're bringing science to life and helping transform healthcare. We call it Life Science Re-imagined.

www.gelifesciences.com/illustra

Speed is crucial to the sundew plant's success. It reacts rapidly, bending its tentacles to bind its prey. Some species can do this in just tenths of a second.

imagination at work

GE05-07 First printed 05/2007

Volume 316, Issue 5829

COVER

An orangutan (*Pongo abelii*) from Sumatra, Indonesia, in an upright posture. Orangutans, a more distant relative of humans than chimps or gorillas, move in a bipedal fashion on small flexible branches. Human bipedalism may thus reflect selection of a behavior that was present in the common great ape ancestor. See page 1328.

Photo: Art Wolfe/Getty Images

DEPARTMENTS

EDITORIAL

NEWS OF THE WEEK

NEWS FOCUS

Preparing Teachers


1270

LETTERS

BOOKS *ET AL.*


1286

POLICY FORUM

PERSPECTIVES

CONTENTS continued >>

RNAi solutions by QIAGEN

Knock down reliably

- Predesigned and validated siRNA
- Flexible, user-defined siRNA plates and sets
- Custom siRNA design and synthesis
- Matching siRNA and RT-PCR assays
- miRNA purification kits and assays

Contact QIAGEN today or visit www.qiagen.com/goto/RNAi .

QIAGEN®

Sample & Assay Technologies

Science

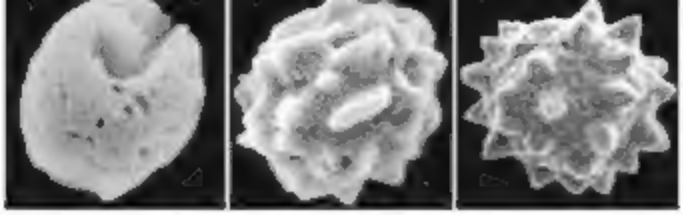

SCIENCE EXPRESS

www.sciencexpress.org

ASTROPHYSICS

Imaging the Surface of Altair
J. D. Monnier et al.
Optical interferometry of the surface of the star Altair suggests that its elongate shape and brightness may reflect unusual differential rotation near its equator.
10.1126/science.1143205

CLIMATE CHANGE

How Much More Rain Will Global Warming Bring?
F. J. Wentz, L. Ricciardulli, K. Hilburn, C. Mears
Humidity and precipitation unexpectedly increased at the same rate in response to global warming during the past 20 years, yielding more rainfall than predicted by models.
10.1126/science.1140746

EVOLUTION

Sponge Paleogenomics Reveals an Ancient Role for Carbonic Anhydrase in Skeletogenesis
D. J. Jackson, L. Macis, J. Reitner, B. M. Degnan, G. Wörheide
Analysis of an extant but evolutionarily ancient reef-building sponge shows how, through duplication, one early gene gave rise to later genes for calcification.
10.1126/science.1141560

MOLECULAR BIOLOGY

Genome-Wide Mapping of in Vivo Protein-DNA Interactions
D. S. Johnson, A. Mortazavi, R. M. Myers, B. Wold
Chromatin immunoprecipitation and high-throughput sequencing identify the nearly 2000 specific DNA binding sites for a neuronal transcription factor.
10.1126/science.1141319

TECHNICAL COMMENT ABSTRACTS

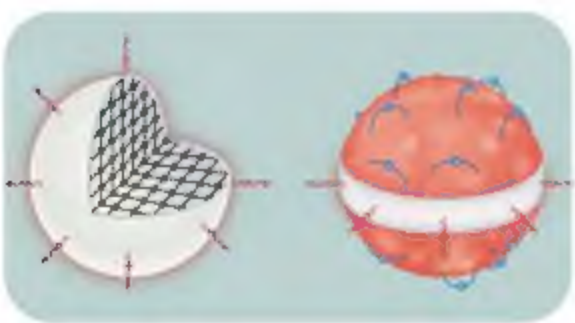

1290 & 1320

REVIEW

BREVIA

RESEARCH ARTICLES

CONTENTS continued >>

Delivery!

INNOVATION @ WORK

With MISSION® TRC shRNA – It's About Delivery!

As a member of The RNAi Consortium (TRC), Sigma offers a delivery solution for RNAi in non-transfectable, and non-dividing cells. The MISSION TRC shRNA libraries are a comprehensive collection of pre-cloned lentiviral shRNA designed to offer a variety of options for your RNAi experiments.

Better shRNA Delivery, Better RNAi Performance

MISSION TRC shRNA provides:

- **Delivery Solution**
  - Lentiviral system for transduction of most mammalian cells, including primary and non-dividing cells
- **Comprehensive Coverage**
  - 15,000 human and 15,000 mouse genes
  - 3-5 clones per gene
- **Efficient Knockdown**
  - Ideal for long-term gene silencing
  - Quality shRNA designed by the Broad Institute
- **Format Options**
  - Entire libraries, gene family sets, or individual genes offered in glycerol stock, DNA, or lentiviral formats
- **Custom Solutions**
  - Large scale lentiviral production and concentration
  - Custom packaging

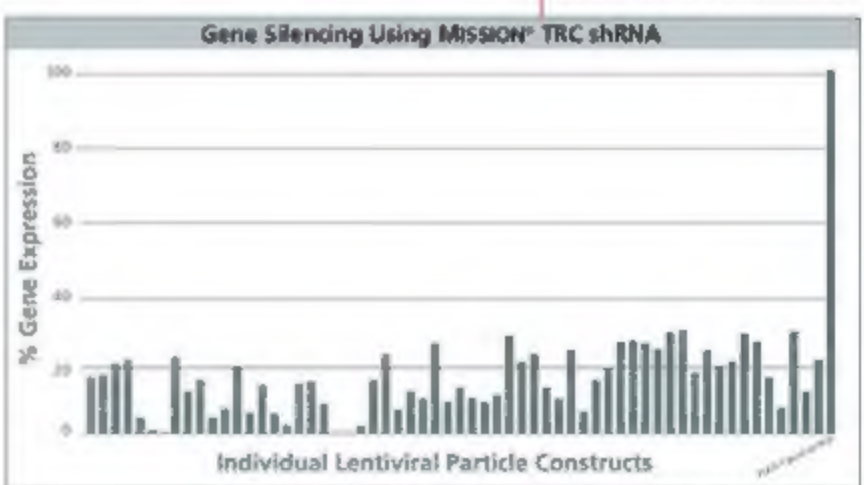

Gene Silencing Using MISSION shRNA. High-throughput validation of MISSION TRC shRNA lentiviral transduction particles. Gene silencing effect of 60 different genes was measured at the mRNA transcript level and compared to pLKO.1-puro empty control particles. For each target gene, approximately 70% or greater knockdown was achieved.

For more information on MISSION TRC shRNA, please visit us on the Web at sigma.com/shrna

SIGMA®

Accelerating Customers' Success through Leadership in Life Science, High Technology and Service
SIGMA-ALDRICH CORPORATION • BOX 14508 • ST. LOUIS • MISSOURI 63178 • USA

REPORTS

AAAS
ADVANCING SCIENCE, SERVING SOCIETY

SCIENCE (ISSN 0036-8075) is published weekly on Friday, except the last week in December, by the American Association for the Advancement of Science, 1200 New York Avenue, NW, Washington, DC 20005. Periodicals Mail postage (publication No. 484460) paid at Washington, DC, and additional mailing offices. Domestic individual membership and subscription (51 issues): $147 (GST #125416822). Domestic institutional subscription (51 issues): $750. Foreign postage extra: Mexico, Caribbean (surface mail) $55, other countries (air assist delivery) $85. First class, airmail, student, and retired rates on request. Canadian rates with GST available upon request. GST #125416822. Publications Mail Agreement Number 1069624. **Printed in the U.S.A.**

Change of address: Allow 4 weeks, giving old and new addresses and 8-digit account number. **Postmaster:** Send change of address to AAAS, P.O. Box 96178, Washington, DC 20090–6178. **Single-copy sales:** $10.00 current issue, $15.00 back issue prepaid includes surface postage; bulk rates on request. **Authorization to photocopy** material for internal or personal use under circumstances not falling within the fair use provisions of the Copyright Act is granted by AAAS to libraries and other users registered with the Copyright Clearance Center (CCC) Transactional Reporting Service, provided that $30.00 per article is paid directly to CCC, 222 Rosewood Drive, Danvers, MA 01923. The identification code for Science is 0036-8075. Science is indexed in the Reader's Guide to Periodical Literature and in several specialized indexes.

CONTENTS continued >>

New Electroporation Buffer!
Check out our new Gene Pulser® electroporation buffer for improved transfection efficiency and cell viability.

Bio-Rad and RNAi. Come have a look.

From design to detection, Bio-Rad supports your RNAi research.

With a broad range of proven delivery technologies, award-winning detection systems, and a suite of high-quality support products, it's clear that Bio-Rad has a vision for RNAi.

- High-performing, potent Dicer-substrate siRNAs that produce ≥85% knockdown with as low as 5 nM siRNA
- Broad selection of delivery technologies
- RNA and protein purification products
- Automated microfluidic system for nucleic acid analysis
- Sensitive, optimized cDNA synthesis kits
- Systems for both protein and mRNA detection and analysis

For a close look at Bio-Rad's tools for RNAi, visit us on the Web at **www.bio-rad.com/rnai/**

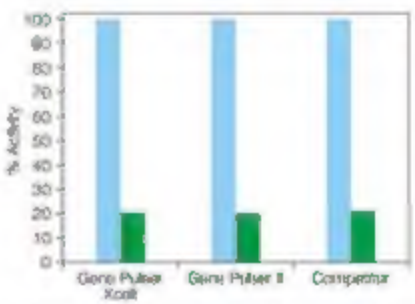

Electroporation with Gene Pulser electroporation buffer in different instruments. The Gene Pulser Xcell™, Gene Pulser II, and a competitor instrument were used to demonstrate the Gene Pulser electroporation buffer's flexibility across various instrument platforms. CHO cells were transfected in 0.4 cm cuvettes with a scramble siRNA (a) or a luciferase-siRNA (a). Similar transfection efficiencies were observed across all platforms.

To find your local sales office, visit **www.bio-rad.com/contact/**
In the U.S., call toll free at 1-800-4BIORAD (1-800-424-6723)

Visit us on the Web at discover.bio-rad.com

BIO-RAD

SCIENCE NOW

www.sciencenow.org

See Those Fingers? Do the Math
Boys with longer ring fingers are better at math

Putting the Hex on Fragile X
In mice, mental stimulation improves neural connections

Dinosaurs Charge Upstream
Discovery of ancient footprints suggests predators could swim hard.

Detecting protein complexes.

SCIENCE'S STKE

www.stke.org

PERSPECTIVE: The Biology of Regenerative Medicine
K. Muneoka
Can regenerative biology and regenerative medicine grow together into a single discipline?

PROTOCOL: High-Sensitivity Detection and Quantitative Analysis of Native Protein-Protein Interactions and Multiprotein Complexes by Flow Cytometry
A. G. Schrum, D. Gil, E. P. Dopfer, D. L. Wiest, L. A. Turka, W. W. A. Schamel, E. Palmer
Protein interactions can be quantitatively assessed using capture beads and flow cytometry in either a high-throughput or low-throughput format

Getting heard in the debate

SCIENCE CAREERS

www.sciencecareers.org

US: Who Speaks for Early-Career Scientists?
B. Bradley
In the debate about numbers of foreign scientific workers, voices of the Americans most directly affected are going unheard

EUROPE: Fruitful Collaborations With Industry
E. Pain
Academic scientists who interact with industry gain extra funding plus get their career horizons broadened.

MISCINET: Guiding Star
A. Spaeth
Jarita Holbrook moved from astrophysics training to studying the anthropology of astronomy by indigenous Africans.

GRANTSNET: June 2007 Funding News
GrantsNet Staff
Learn about the latest opportunities in research funding, scholarships, fellowships, and internships.

SCIENCE PODCAST

Listen to the 1 June *Science* Podcast to hear about the origins of human bipedalism, innovative programs for training science teachers, the effect of global warming on rainfall, and more
www.sciencemag.org/about/podcast.dtl

Separate individual or institutional subscriptions to these products may be required for full-text access.

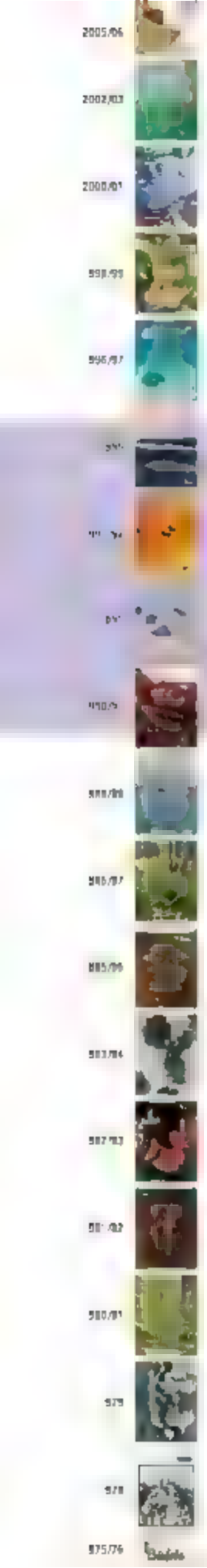

in a word, essential.

www.neb.com

NEW ENGLAND BioLabs® inc.

the leader in enzyme technology

New England Biolabs inc.
[illegible] • **China** [illegible] • **Japan** Tel [illegible]
UK Tel [illegible]
For a complete list of international offices, please visit www.neb.com

EDITED BY STELLA HURTLEY AND PHIL SZUROM

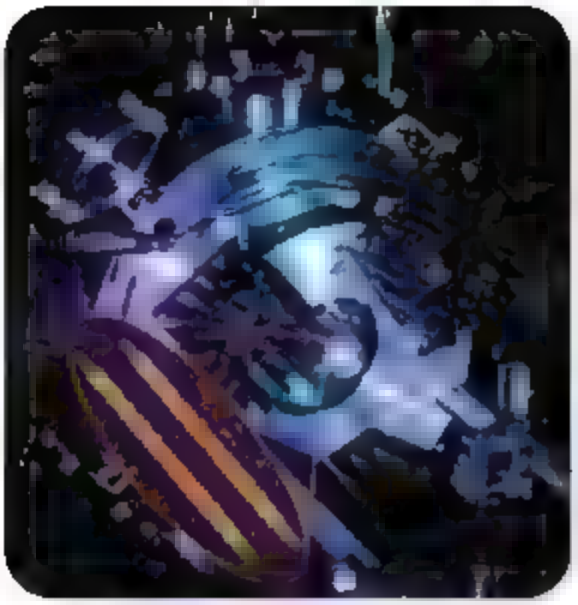

<< Quantum Storage and Repetition

Quantum registers allow the basic units of information, the qubits, to be transferred along channels and processed locally. **Dutt *et al.*** (p. 1312) demonstrate the coherent control and coupling of an electronic qubit and nuclear qubit stored in a single nitrogen vacancy (NV) center in diamond. Because the spin degree of freedom of the NV center is largely decoupled from the vibrational (and other kinetic) degrees of freedom, these two qubits can form a room-temperature quantum register where the electronic qubit could enable optical communication with other registers through state-dependent fluorescence, whereas the nuclear qubit could be used to store information. These registers can be used as a basis for scalable, optically coupled quantum information systems. The use of quantum processing in applications such as encryption requires the distribution of entangled quantum states over networks. These states have finite lifetimes, and networks will likely need to use quantum repeaters which would reliably pass on the information without actually destroying it. **Chou *et al.*** (p. 1316, published online 5 April) distribute an entangled state over a distance of 3 meters using two pairs of cold atomic gas clouds, thereby demonstrating the potential for long distance quantum communication.

West African Monsoon Paleohydrology

Monsoons account for much of the rainfall at low latitudes and are an important control of the moisture and heat budgets of the atmosphere. The West African monsoon affects a broad region of that continent, but it is unclear how it is connected to other large-scale climate processes, such as the El Niño–Southern Oscillation or nearby changes in sea surface temperatures (SSTs). **Weldeab *et al.*** (p. 1303; see the Perspective by **Barker**) analyzed the Mg/Ca and Ba/Ca ratios, as well as oxygen isotopic compositions of planktonic foraminifera from a marine sediment core recovered from the Gulf of Guinea, in order to document changes in SSTs and river runoff there during the past 155,000 years. The variability of freshwater input more closely resembled that of high northern latitude temperature than local SSTs for much of the record, which implies that high northern latitude climate exerted the dominant control on precipitation. Local SSTs were more closely related to low-latitude insolation.

Disobeying Transport Rules

The empirical Wiedemann-Franz law, which states that the ratio of thermal and electronic conductivities of metals is directly proportional to temperature, is one of the oldest relations in condensed matter physics. It has also been thought to be a robust property of metals because it is theoretically underpinned by quantum mechanics and the standard model of metals, Fermi-liquid theory. **Tanatar *et al.*** (p. 1320; see the Perspective by **Coleman**) present measurements of thermal and charge transport in $CeCoIn_5$ and report that this law is obeyed in one direction in the crystal lattice but violated in another. They discuss the consequences of this anisotropic violation in terms of how Fermi-liquid theory should or could be modified to describe the behavior of such strongly correlated systems.

Soft Iron Center

The core of Mars is widely thought to be similar to that of Earth—mostly iron with a smattering of light elements. In high-pressure experiments that mimic the conditions of the martian core, **Stewart *et al.*** (p. 1323) show that Mars' core is presently completely liquid and that its future crystallization behavior will differ from that of the Earth. Mars will not form an outwardly crystallizing iron-rich inner core as does the Earth. Instead, planetary cooling will lead to core crystallization following either a "snowing core" model, in which iron-rich solids nucleate in the outer portions of the core and sink toward the center, or a "sulfide inner core" model in which an iron sulfide phase crystallizes to form a solid inner core.

Preservation and Decay

Competition between degradation and preservation of organic matter in the sea and on the sea floor plays a central role in controlling how much oxygen is in the atmosphere, as well as how carbon, nitrogen, phosphorus, and other elements are cycled through the biogeosphere. Because the quantity of carbon in marine sediments is huge, small differences in the balance between these processes can have large impacts, which has made this problem challenging to model. **Rothman and Forney** (p. 1325; see the Perspective by **Middelburg and Meysman**) now present a consistent model in which the intrinsic reactivity of organic material is constant and that the rate of decay depends on bacterial abundance. This explanation is fundamentally different from chemical models in which organic matter degradation rates depend on intrinsic reactivity.

Not Like Peas in a Pod

Legumes, such as peas and beans, have residing within nodules on their roots symbiotic bacteria that fix atmospheric nitrogen. The rhizobial symbiont produces signaling molecules, the so-called Nod factors, that are recognized by the plant. **Giraud *et al.*** (p. 1307; see the Perspective by **Downie**) report the complete genomic sequences of two photosynthetic *Bradyrhizobium* strains that produce nodules in their host plant roots but lack the *nodABC* genes and Nod factors. Instead, during this atypical symbiosis, a purine derivative may act as a signal molecule to trigger root nodule organogenesis.

Continued on page 1251

www.roche-applied-science.com

PhosSTOP Phosphatase Inhibitor Cocktail Tablets

Protect your proteins before phosphatases attack

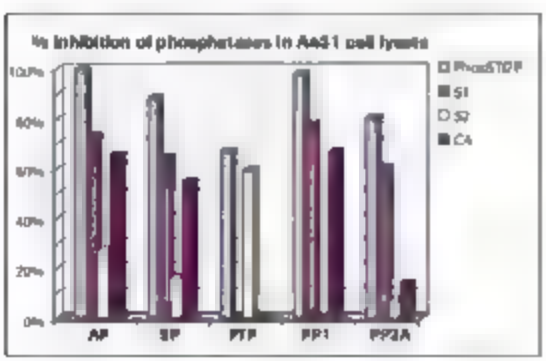

Figure 1. PhosSTOP Tablets deliver more effective phosphatase inhibition than other suppliers' liquid phosphatase inhibitor cocktails in lysate from A431 human cancer cell line.

S1, S2, and C4 = Phosphatase Inhibitor Cocktails 1, 2 and 4 from other suppliers
AP and SP = Alkaline (AP) and Acid (SP) Phosphatases
PTP = Tyrosine Protein Phosphatases
PP1 and PP2A = Serine/Threonine Phosphatases

Stop spending valuable time searching for the right phosphatase inhibitor mix or individual inhibitors or combining inhibitor cocktails. Conveniently, reliably prevent the dephosphorylation of proteins with new **PhosSTOP Phosphatase Inhibitor Cocktail Tablets**.

Simply drop one quick-dissolving tablet into 10 ml of buffer to

- **More effectively preserve proteins' phosphorylation state**
  Inhibit a broad spectrum of phosphatase types (Figure 1)
- **Instantly inhibit phosphatases in a variety of samples**
  Drop a tablet into extracts from mammalian tissue or plant cells or treat formalin-fixed, paraffin-embedded (FFPE) tissue sections
- **Protect proteins from both phosphatases and proteases**
  Fully protect your proteins by combining a PhosSTOP tablet with a cOmplete Protease Inhibitor Cocktail Tablet

Request a free sample or learn more at www.roche-applied-science.com

Roche

Roche Diagnostics GmbH
Roche Applied Science
68298 Mannheim
Germany

Continued from page 1249

Walking Tall with Hand Holds

The predominant bipedal locomotion of humans, which helps distinguish us from great apes, has generally been thought to have arisen since or with the last common ancestor between humans and chimps. **Thorpe *et al.*** (p. 1328, see the cover and see the Perspective by **O'Higgins and Elton**) show that orangutans, a more distant relative, move across thin branches in trees in a bipedal fashion, much like walking humans. These observations suggest that this more ancient ability was retained in the great apes and increasingly used by ancestral humans as they moved out of the trees, whereas chimps and gorillas essentially lost this ability.

Spaced Out

Methodological approaches for geospatial models of infectious disease encompass analyses of the effects of patches, distance transmission, multigroups, and networks. Within this framework, **Riley** (p. 1298) has reviewed key results on infections such as measles, foot-and-mouth, influenza, and smallpox, illustrating the significance of the epidemiological insights generated by these models.

A Growing List of Diabetes Genes

Type 2 diabetes, the most common form of diabetes, affects more than 170 million people worldwide, and its prevalence is increasing rapidly. An individual's propensity to develop the disorder is determined by a combination of life style and hereditary factors. Three independent international consortia—**Scott *et al.*** (p. 1341, published online 26 April), **Zeggini *et al.*** (p. 1336, published online 26 April), and the **Diabetes Genetics Initiative** (p. 1331, published online 26 April)—have conducted comprehensive surveys of the human genome to identify genetic variants that affect type 2 diabetes risk and then shared their data to increase the statistical power of their analyses. In addition to validating several variants previously implicated in the disorder, the authors identified several previously unknown susceptibility variants. At least 10 genetic loci have been now reliably linked to type 2 diabetes, each exerting a modest effect on risk.

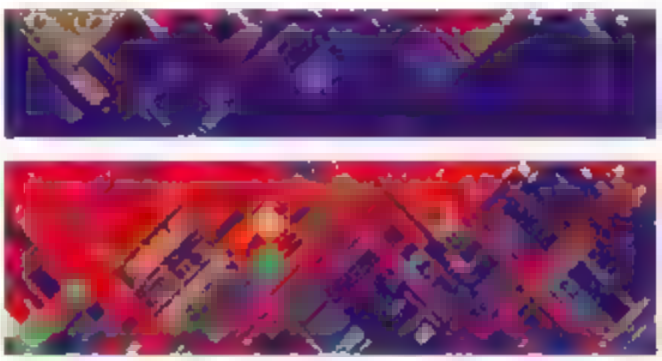

Let the RNA Do Its Business

Viruses need to ensure that infected cells survive long enough to allow the production of progeny. **Reeves *et al.*** (p. 1345) now show that human cytomegalovirus uses an unusual strategy to this end—an abundant noncoding RNA specifically interferes with an apoptotic trigger in the mitochondrion. In cells in which apoptosis has been triggered, the RNA binds to an enzyme in the mitochondrion and helps to maintain intact mitochondria, which prolongs the life of the infected cells. This mechanism obviates the need for the virus to translate a protein product to perform this function and may thus exploit the infected cell's resources more effectively.

Designer Proteasome

In the immune system, T cells respond to fragments of antigenic proteins presented at the cell surface by molecules encoded by genes of the major histocompatibility complex. This process is vital not only for recognition of antigens carried by pathogens and tumors, but also in the selection of T cells as they develop in the thymus. These peptides are generated by a large multisubunit complex called the proteasome, which exists in a variety of forms containing different catalytic subunits. **Murata *et al.*** (p. 1349, see the Perspective by **Bevan**) now identify a proteasome subunit, β5t, that was found exclusively in the thymic epithelial cells and directs positive selection of T cells. Indeed, mice lacking β5t showed significant disruption of T cell development.

CREDIT: SCOTT ET AL.

BIBLIOGRAPHY CENTRAL

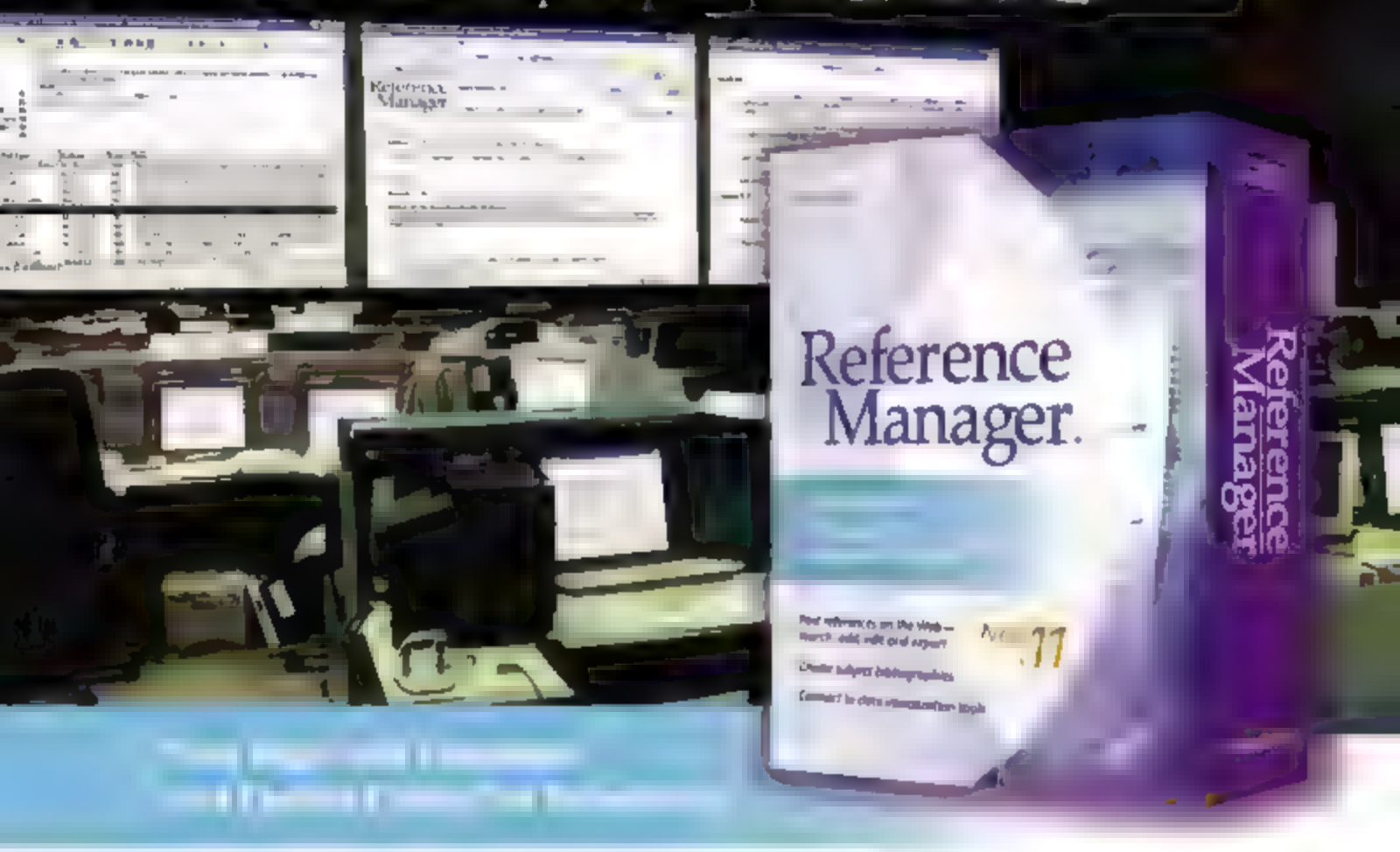

Introducing Reference Manager 11 a powerful upgrade to the bibliography software that streamlines research writing and publishing.

Reference Manager has served corporate, government and academic researchers worldwide for over 21 years. And now version 11 delivers new ways to share and view your reference collections. Post your databases to the Web. Collaborate with colleagues over a network or online by text and files.

These are just some of the powerful features that await you. Reference Manager is your command and control center for all things reference related.

What's new in v11

- Post Reference Manager databases to the Web or intranet
- Create & post bibliographies instantly
- Access new and updated content at www.refman.com
- Share files & libraries with colleagues
- Connect to data visualization tools

Put information into action. Order or upgrade today.

Available for Windows 2000 & XP desktop and network editions.

Phone Box 72[illegible] 2.7 • 760-438-5526 • info@isiresearchsoft.com

Download a Free Demo Today
www.refman.com

THOMSON
ISI RESEARCHSOFT

William A. Wulf is president of the National Academy of Engineering in Washington, DC

Changes in Innovation Ecology

GLOBALIZATION HAS INTRODUCED BOTH UNCERTAINTIES AND OPPORTUNITIES WORLDWIDE

In the United States, a flurry of recent books and reports has told the country how to be competitive in the 21st century, from Thomas L. Friedman's *The World Is Flat* to the National Academies' *Rising Above the Gathering Storm* and at least a dozen more. All note the historic strength of the United States in innovation and suggest that reinvigorating this capability is key to future prosperity. The resulting recommendations relate to an "ecology" of interrelated institutions, laws, regulations, and policies providing an innovation infrastructure: health care, education, research, tax policy, and intellectual property protection, among others. Clearly, this ecology is more fundamentally broken than is generally recognized.

It's broken for two reasons. First, its components were created in the context of old technologies and new of little use. Second, our processes for updating them are reactive, and we don't stand back and ask whether our changes are achieving the intended outcomes.

It isn't obvious, for example, that a patent system created for macroscopic physical machines is ideal for computer software, snippets of DNA, or business processes. A year ago, 30 Silicon Valley chief technology officers told me that the U.S. patent system was irrelevant to the original Constitutional intent to encourage innovation. Although their fast product cycles make them skeptical about decadal protection, their reaction shows that a system invented for an old technology won't necessarily fit a new one.

Also seemingly antiquated is a Web page with the copyright symbol © on it. That page was copied, in its digitized form, at least a half dozen times on the trip from its server to the screen; indeed, it would have zero value if it hadn't been copied. Of course the author didn't mean to prohibit those copies, but they are inextinguishable from the others that the author did mean to prohibit. Ironically, we must break the law to achieve one of its primary objectives. The notion of prohibiting copying, so protective and clearly creativity made sense when those values were expressed in physical media, but it makes no sense in a digital world.

A senior medical entrepreneur pointed out to me that the nation's gold standard of randomized double-blind clinical trials to ensure drug safety and efficacy simply doesn't work for therapies that are tailored to a small population of patients, an emerging trend in drug development. In those cases, a traditional clinical trial will lack the statistical power to reach a conclusion. It's worse: Ironically, a mechanism intended to protect us has the effect of preventing access to more effective drugs.

The antitrust laws are important for innovation. They create spaces in which small innovative companies can compete. A short-sighted loss in the United States was written in an era when scarcity usually determined economic value. In some fields today, ubiquity is what's valuable. For example, if I have the only telephone in the world, it has little value. Conversely, I use Microsoft software primarily because its ubiquity maximizes the probability that I can exchange documents with someone else. I shouldn't be surprised that laws based on assumptions that worked in a traditional industrial economic setting don't work perfectly for new technologies.

Although many commentators are ready to accept or even praise the loss of U.S. manufacturing to low-wage countries, production and marketing experts indicate that the future of manufacturing is not mass production, but mass customization. The key will not be the capacity to make a zillion size 10 D shoes cheaply, but rather manufacturing shoes to suit Bill Wulf's size, color, and style preferences. This is a knowledge-intensive business—one in which we are well equipped to compete. But we need the right institutional and policy ecology to do so.

Regarding these examples, the policy goal is still valid: protecting the public from unsafe or ineffective drugs, for example. It's the implementation that needs to be updated, and that can be done incrementally. To prosper, we need an international process that can, time after time, fundamentally rethink the elements of our innovation ecology.

William A. Wulf

10.1126/science.1145598

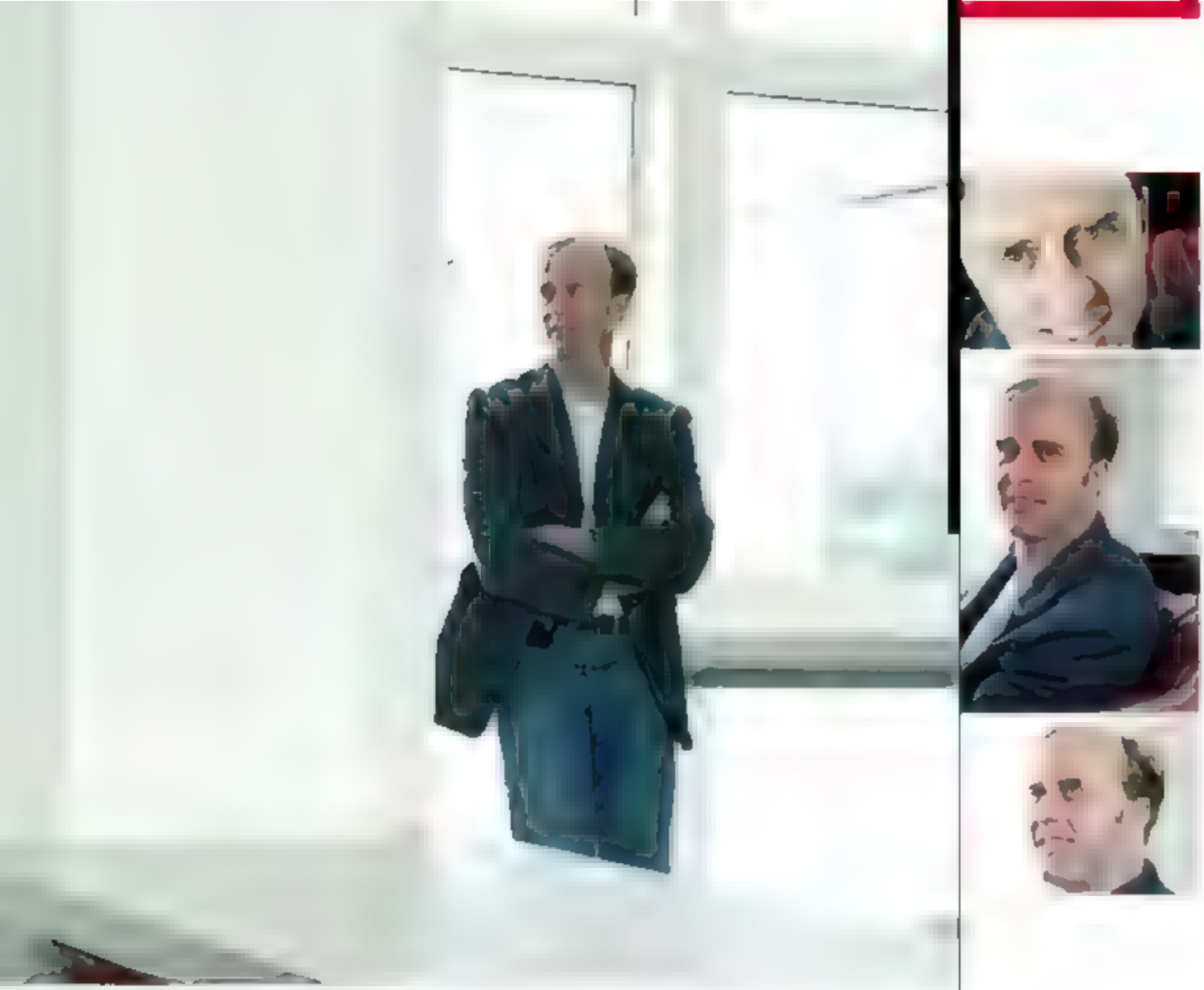

“The unknown has always fascinated me, and research is the best way to satisfy my curiosity.”

How do cells react to changed conditions? Which molecular processes control the regulation mechanisms? What genetic changes take place? Conversely, what is the effect on organisms when their genomes are transformed? Answering questions like these creates the foundation for breakthroughs in medicine, industry and agriculture. Finding these answers requires sharp cell images and accurate micromanipulation, now unified in a single system. With the **Leica AM6000** it is possible to view and manipulate cells simultaneously – with absolute reproducibility and minimum effort.

Prof. Stéphane Viville, Institute of Genetics and Molecular and Cellular Biology, Illkirch, France and Reproductive Biology Service SIHCUS-CMCO, Functional Unit Preimplantation Diagnostics, Schiltigheim, France

www.leica-microsystems.com

Leica

MICROSYSTEMS

Malaysian forest.

ECOLOGY EVOLUTION

Tropical Forest Slows Down

Tropical forests play a major part in the global carbon cycle. An understanding of the responses of tropical forests to climate change is an essential element in predicting the trajectory of global environmental change in the coming decades. Some studies have found increasing growth rates of trees, consistent with model predictions of CO_2 fertilization. However, others have suggested that growth rates might decrease, consistent with models of the effects of increasing temperature on tree respiration. Feeley *et al.* analyzed two detailed long-term data sets from forest plots in Panama and Malaysia, to reveal growth rates of individual species and whole communities over the past 25 years. In both places, growth rates decreased in the majority of species, and this pattern was also reflected at the community level. These decreases correlated with increasing temperature over the same period, suggesting the potential for positive feedbacks between decreasing tree growth and increasing atmospheric CO_2 concentration. — AMS

Ecol. Lett. **10**, 461 (2007).

MATERIALS SCIENCE

Aperiodic Polymer Tiles

Quasicrystals have sufficient long range order to produce a diffraction pattern, but do not show the three dimensional translational periodicity found in normal crystals. They have been observed in metallic and small molecular systems, often through small compositional changes in the materials, although in many cases the quasicrystals are of poor quality and stability. Hayashida *et al.* show this sort of patterning over a much larger length scale in three arm block copolymers made of polyisoprene (I), polystyrene (S), and poly(2 vinylpyridine) (P) mixed with a polystyrene homopolymer. Previously this system has been shown to form the (3.3.4.3.4) Archimedean tiling structure, with every vertex surrounded by a pattern of triangle (3) and square (4) cells. Upon changing the I:S:P ratio the ratio of triangles to squares shifted from the Archimedean value of 2 to 2.305, and a dodecagonal quasicrystal pattern emerged. The tiling, however, was not perfect. Transition regions led to sections showing sixfold symmetry and a triangle-to-square ratio of 8:3. When the composition of the blend was changed further, the overall quasiperiodicity of the triangles and squares was lost. Thus, it may be possible to tune the tiling patterns through small changes in the polymer composition. — MSL

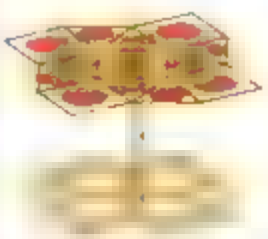

Polymer phase separation leading to quasicrystalline arrangement.

CREDITS: (TOP TO BOTTOM) PETER LAVERTY; SCOTT TAN; HAYASHIDA *ET AL.*, *PHYS. REV. LETT.* **98**, 195502 (2007)

Phys. Rev. Lett. **98**, 195502 (2007).

APPLIED PHYSICS

Patterned Graphene Transport

Graphene has received much recent attention both experimental and theoretical, because of its mechanical stability and promising electronic properties. These single sheets of graphite, or unzipped carbon nanotubes, are expected to display many interesting transport properties that are dependent on geometry and crystallographic orientation, in much the same way in which the electronic properties of carbon nanotubes are dependent on their chirality, or how they are rolled up. Working with single sheets of graphene extracted from bulk graphite and patterned into strips of various widths (ranging from 10 to 100 nm) and a selection of crystallographic orientations, Han *et al.* have probed the ensuing transport properties. They found that the energy band gap widens with decreasing width, as expected from theory, but that there is no systematic variation with orientation. The results suggest a route to engineer the band gap of graphene nanostructures with potential applications for devices. — ISO

Phys. Rev. Lett. **98**, 206805 (2007).

GENETICS

A Powerhouse Conversion

Animal cells contain not only their nuclear genome, which is inherited equally from both parents, but they also within their mitochondria carry a further, much smaller genome, which is generally maternally inherited. Mitochondrial DNA is thought not to undergo recombination and to represent a relatively stable record of the evolutionary history of a species. By examining duplicated genes within the mitochondria of killifish, Tatarenkov and Avise found evidence of gene conversion within the mitochondria, suggesting that recombination does occur. Sequences from both copies of the control regions of the mitochondrial DNA identified 28 examples where both copies contained the same nucleotide substitution, resulting in an overestimate of genetic distance between individuals on the basis of paralogs, which arise from gene duplications, in comparison to that estimated from orthologs, which represent genes sharing the same evolutionary history. Thus, recombination and gene conversion are ongoing in the mitochondria of killifish and, by extension, probably in other animals as well. — LMZ

Killifish.

Proc. R. Soc. London Ser. B 10.1098/rspb.2007.0169 (2007).

Continued on page 1257

Continued from page 1255

GEOLOGY

Death Valley in Slow Motion

The San Andreas Fault is thought to mark the right lateral slip between the North American and Pacific plates, but a large amount of the slip (~20 to 25%) occurs on a set of faults farther inland extending from Death Valley in eastern California up through western Nevada. These faults have produced some of the largest earthquakes within North America, comparable in size to temblors on the San Andreas itself, and this slip is responsible for the great depth of Death Valley. Today, the fault network near Death Valley is moving at about 12 mm/year, but whether this represents the long-term rate has been hard to determine. Frankel *et al.* measured cosmogenically produced radionuclides in boulders to date offsets in an alluvial fan in Death Valley. The long-term rate for the fault system for the past 70,000 years is indeed close to the current rate, whereas farther south, where several recent earthquakes have occurred, the current strain rate seems to be exceeding the long-term average. — BH

J. Geophys. Res. 10.1029/2006JB004350 (2007)

PSYCHOLOGY

You Did It, It Did It

One of the many kinds of psychological processing we perform effortlessly is the recognition of actions as being motivated by animate versus inanimate agents. Two groups of brain areas have been proposed to subserve this function: the mirror neuron system and the social network. Mirror neurons become active both when a person performs an action and when a person observes that action being performed by another. Neurons within the social network become active in social contexts, such as during the assessment of emotion in others, or while imagining another's state of mind. Wheatley *et al.* examined the differential activation of these networks under conditions in which the central figure and its movements remained constant, but the backgrounds were changed to bias the interpretations of the scene as representing animate or inanimate agency. The mirror neuron system does indeed engage in the neural processing of motion, during both observation and imagination of the figure. On the other hand, the brain areas within the social network are specifically more active when people perceive the motion as biological or animate. — GJC

Psychol. Sci. **18**, 469 (2007)

CHEMISTRY

How H-Bonding Helps

Although hydrogen bonding has long been known to be prevalent in enzymatic substrate-binding motifs, its use in nonmetallic small molecule catalysis has been adopted comparatively recently. Jensen and Sigman have quantified the impact of catalyst acidity on the rate and enantioselectivity of the hetero-Diels Alder reaction in one such system. The catalyst is a chiral quinoline derivative that binds aldehydes through the N-H group of a pendant amide; the authors systematically varied the acidity of this group by adding differing numbers of Cl or F atoms to the amide α-carbon. They observed linear free energy relationships correlating both rate and enantioselectivity with increased acidity, which they tentatively attribute to a tighter transition state. — JSY

Angew. Chem. Int. Ed. **46**, 10.1002/anie.200700298 (2007)

www.sciencemag.org

Science

1200 New York Avenue, NW
Washington, DC 20005
Editorial: 202 326-6550, FAX 202-289-7562
News: 202-326-6501, FAX 202 371-9227

Bateman House, 82-88 Hills Road
Cambridge, UK CB2 1LQ
+44 (0) 1223 326500, FAX +44 (0) 1223 326501

Subscription Services For change of address, missing issues, new orders and renewals, and payment questions: 866-434-AAAS (2227) or 202 326-6417 FAX 202-842 1065 Mailing addresses: AAAS, PO Box 96178, Washington, DC 20090-6178 or AAAS Member Services, 1200 New York Avenue NW Washington, DC 20005

Instructions for Licensed please call 202 326-6755 for any questions or information

Reprints Author inquiries 800-635-7181
Commercial inquiries 803 359-4578

Permissions 202 326 6582 FAX 202 682 0816

Back Issues Current & Recent Issues: AAAS Publications/Nobles (or back issues www.aaas.org/pubs), Car purchase discount: Subaru VIP Program 207 326-6417 Credit Card: MBNA 800-847 7378, Car Rentals: Hertz 800-654-2200 CDP#343457 Dollar 800 800-4000 #AA-115 AAAS Travels: Getchart Expeditions 800 252 4910 , Life Insurance: Seabury & Smith 800-424 9883 Other Benefits AAAS Member Services 202 326 6640 or www.aaasmember.org

science_editors@aaas.org	(for general editorial queries)
science_letters@aaas.org	(for queries about letters)
science_reviews@aaas.org	(for returning manuscript reviews)
science_bookrev@aaas.org	(for book review queries)

Published by the American Association for the Advancement of Science (AAAS). [illegible] Periodicals Mail Postage Paid at Washington, DC, and at additional mailing offices. The editorial content of this publication, including any material on which a commercial interest may exist, is solely the responsibility of the AAAS editorial staff. Science—including all articles published in Science—including editorials, news and comment, and book reviews—are signed and reflect the individual views of the authors and not official points of view adopted by the AAAS or the institutions with which the authors are affiliated.

AAAS was founded in 1848 and incorporated in 1874. Its mission is to advance science for the benefit of all people. The goals of the association are to foster communication among scientists, engineers and the public, enhance international cooperation [illegible] and increase the effective use of science in government and society, support the science and technology workforce and infrastructure, increase public understanding and appreciation of science and technology, and strengthen support for the science and technology enterprise.

Information for Authors

See pages [illegible] of the 5 January 2007 issue or access www.sciencemag.org/feature/contribinfo/home.html

25 years of delivering next-generation systems

Accelerate your time to publish

To find out more, visit nfo.appliedbiosystems.com/bdx

Applied Biosystems

Science Alerts in Your Inbox

Get daily and weekly E-alerts on the latest breaking news and research!

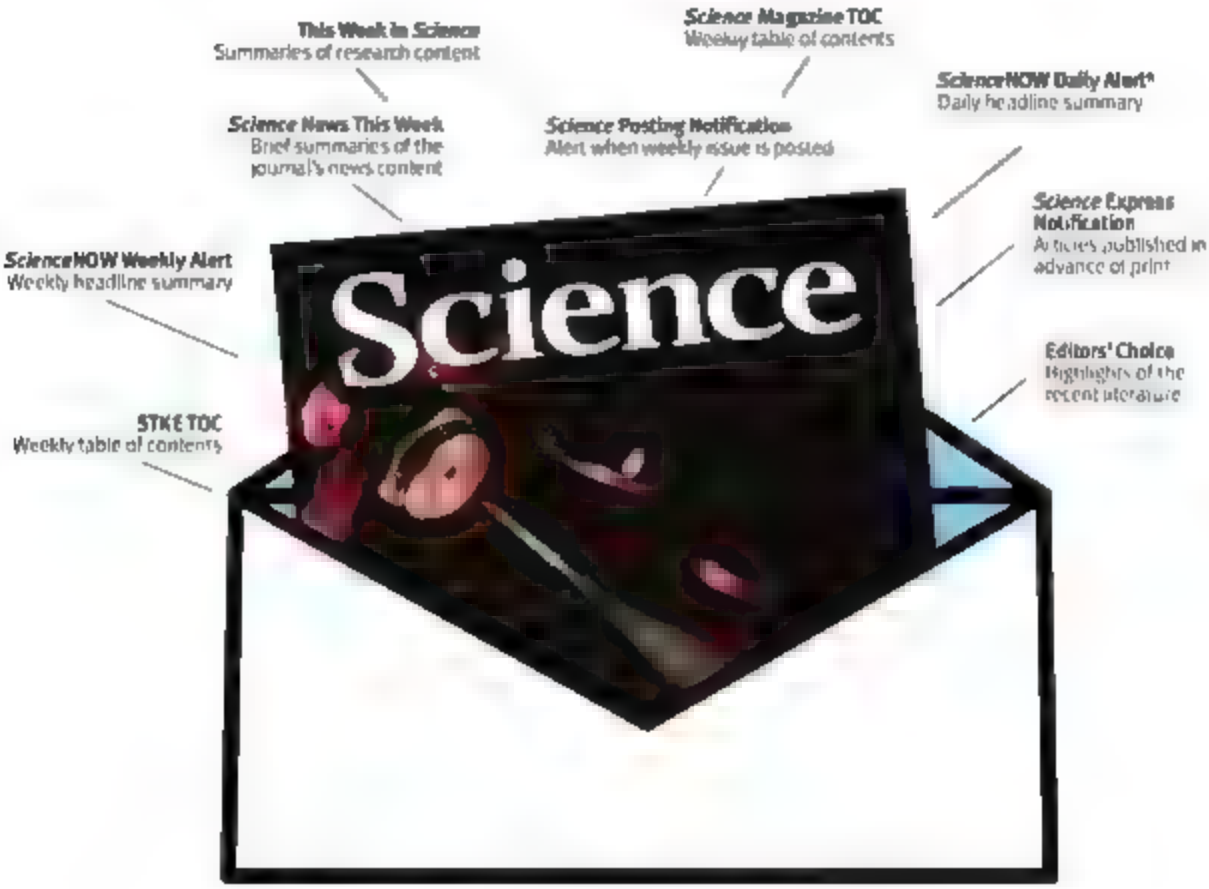

Get the latest news and research from *Science* as soon as it is published. Sign up for our e-alert services and you can know when the latest issue of *Science* or *Science* Express has been posted, peruse the latest table of contents for *Science* or *Science*'s Signal Transduction Knowledge Environment, and read summaries of the journal's research, news content, or Editors' Choice column, all from your e-mail inbox. To start receiving e-mail updates, go to:

http://www.sciencemag.org/ema

Science

AAAS

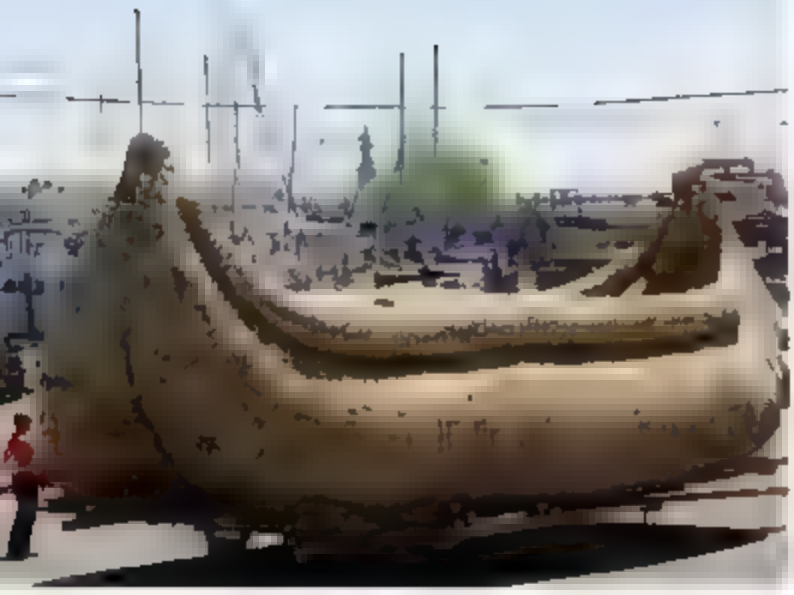

Abora III at New Jersey port.

In the Wake of *Kon-Tiki*

A German biology teacher and amateur archaeologist plans to launch a reed boat this month in New York harbor, in preparation for an ocean voyage to Spain.

Dominique Goeritz, currently a Ph.D. student in invasion biology at the University of Bonn, wants to prove that prehistoric humans could have crossed the stormy North Atlantic, bringing with them Old World plants such as bottle gourd and cotton, thousands of years before Columbus.

The 12 ton, 12-meter-long boat, built of reeds from Lake Titicaca in Bolivia and sporting linen sails, is based on rock drawings made in upper Egypt and Spain during the 4th and 5th millennia B.C.E. "This will be a high-tech laboratory" loaded with instruments to monitor the ship's progress, adds Goeritz, whose funding for the half million-dollar project so far has come from a private loan. Jürgen Böhmer, a vegetation ecologist at the University of Bonn, notes that the unusual effort could help clarify how plant species spread between continents. Goeritz, 40, has experimented with earlier versions of the boat in the Mediterranean. The *Abora III* will set sail in July with a crew of 12 for the 2-month voyage.

Iceman's Final Hours

A team of botanists and anatomists has produced a close-up view of the last wanderings of Ötzi the Iceman, the frozen 5200-year-old mummy found in the Alps in 1991, from the pollen in his digestive tract.

By various delicate procedures, researchers led by botanist Klaus Oeggl of the University of Innsbruck in Austria extracted five gut samples—representing at least three different meals—from the end of the small intestine to the rectum. Comparing the pollen with modern reference samples from known locations, the scientists tracked Ötzi's path in roughly his last 33 hours. "Background" pollen in the intestine closer to the rectum reflected alpine vegetation, whereas the transverse colon had pollen from tree species common in the valley. Contents of the ileum indicated that he ate his last meal back in the subalpine pine and spruce forests.

The scientists, whose analysis appears in the latest issue of *Quaternary Science Reviews*, say the results lend new weight to the "disaster" theory of Ötzi's death. It holds that he walked down from subalpine regions perhaps to his native village, got in a fight, and fled to the mountain glacier, where he apparently died from an arrow wound in the upper back. The reconstruction of the Iceman's final journey is "an extremely exquisite piece of work," says geoscientist Wolfgang Müller of the Royal Holloway University of London in Surrey. "Before, it was largely speculation. Now it's pinned down with scientific evidence."

The Breast Cancer List

NET WATCH

French fries, car exhaust, and shampoo have one thing in common. They can contain breast cancer–causing compounds. To find out more about suspect chemicals and lifestyle factors, including obesity, implicated in breast cancer, check out this new two-part database from the Silent Spring Institute, a women's health nonprofit based in Newton, Massachusetts.

Researchers pored over literature data to compile a roster of 216 compounds that trigger mammary tumors in animal tests. For chemicals such as acrylamide, a byproduct of cooking starch-laden foods, the site offers information on uses, routes of exposure, and health risks. The database also summarizes and critiques the methodology of 450 studies on links between human breast cancer and nongenetic factors. www.silentspring.org

Rachel Carson, author of *Silent Spring*, died of breast cancer in 1964.

INTERSPECIES MISCOMMUNICATION

A silverback gorilla went on a King Kong–style rampage in a Rotterdam zoo on 18 May, and ethologists are speculating that a misunderstanding with a female fan may have pushed him over the edge.

Eleven-year-old Bokito jumped a 3-meter-wide moat at Blijdorp Zoo, attacked a 57-year-old woman, and dragged her along a path before smashing a glass door and entering a restaurant, where zoo staff shot him with tranquilizer darts. The victim—hospitalized with a crushed hand, broken arm, and more than 100 bite wounds—had visited Bokito almost daily with her husband. "When she arrived at him, he stirred back," she told the Dutch newspaper *De Telegraaf*.

Bokito on the loose.

The frequent visits may have made the woman a group member in the gorilla's mind, says Zief Preeboom, head of research at the Antwerp Zoo in Belgium. But primates use eye contact to establish dominance relations, and they can misinterpret human signals, he says. "He is the silverback, the dominant male in his group, and he may have felt that she did not respect his dominance." The gorilla's "smile" may actually have been a threat, other ethologists say.

The victim wants the zoo to pay damages but said Bokito "will remain my darling."

CREDITS: (TOP TO BOTTOM) DOMINIQUE GOERITZ; TAKE A BITE PICTURES/GETTY IMAGES; ASSOCIATED PRESS

Get published in *Science*, win a trip to Stockholm, $25,000 – and earn the respect of Nobel laureates

Grand Prize winner Irene Chen presents her research to an applauded audience

Chen and fellow Premiumer Bor Mir find common ground with Nobel laureate Craig Mello

* For the purpose of this prize, molecular biology is defined as "that part of biology … [that] attempts to interpret biological events in terms of the physical properties of molecules." (Watson-Hall Dictionary of Scientific and Technical Terms, 6th Edition)

**Nobel Prize winners in Medicine for their discovery of RNA interference gene silencing by double-stranded RNA

MOVERS

SEEING THROUGH HYPE. Educational psychologist Robert Slavin has been chosen to lead a new center for education research at the University of York in the United Kingdom. The Institute for Effective Education (IEE) is being funded with $22 million from the Bewland Charitable Trust. Slavin will continue to direct the Center for Research and Reform in Education (CRRE) at Johns Hopkins University in Baltimore, Maryland.

Slavin's message to educators is to pay attention to what works, "not necessarily to what is popular or well marketed." For too long, education has been ruled by "fads and fashions," says Slavin, who also runs the nonprofit Success for All Foundation that offers curricula that has first been evaluated in research institutions. He hopes that IEE can also increase evidence-based learning in schools by using proven methods to boost literacy, language science, and numeracy.

Two CRRE professors, Nancy Madden and Bette Chambers, will join Slavin at IEE, dividing their time between the new institute and their current base.

FOLLOW-UP

A MUST NOT READ. An Indian court has struck down a state-imposed ban on a book by a U.S. religious studies scholar that offended Hindu nationalists and triggered riots 3 years ago. But the publisher of *Shivaji: Hindu King in Islamic India* has no plans to sell the book in India.

The book, by James Laine, a professor at Macalester College in St. Paul, Minnesota, tells the story of Shivaji, a 17th century Hindu king who built an empire in western India amid Muslim domination of much of the subcontinent. Right-wing Hindu groups slammed the book for questioning Shivaji's lineage, and the Maharashtra government banned it in 2004 and threatened to arrest Laine if he ever returned to the state (*Science*, 30 January 2004, p. 623). The ban was moot, however, as the book's publisher, Oxford University Press, had already withdrawn it from stores.

In April, India's Supreme Court ruled that the charges brought against Laine were baseless, and the Bombay High Court instructed the state government to lift the ban. But Hindu extremists have warned bookstore owners not to carry the title.

ON CAMPUS

BLOWN AWAY. Tulane University mechanical engineering chair Monte Mehrabadi spent last week house hunting in southern California in preparation for becoming chair of the mechanical engineering department at San Diego State University. It's an involuntary move. Mehrabadi's 113-year-old department is dissolving this month as part of the New Orleans university's plan for restructuring after Hurricane Katrina. It's "heart-wrenching," he says. Although he's landed on his feet, two of the department's 12 faculty members are still looking for work.

A new 67-page report from the American Association of University Professors (AAUP) takes five New Orleans universities to task for their response to the August 2005 disaster. It says Tulane, which cut more than 200 positions overall, failed to give financial or academic reasons for abolishing the mechanical engineering department. AAUP also says the universities paid little heed to tenure and dismissed staff without offering clear explanations. Although Tulane offered many 12 months severance pay, Louisiana State University Health Sciences Center laid off 61 full-time medical faculty members, about 9% of the total, without pay and with "virtually no notice," the report says.

Tulane has called the report "seriously flawed" and tainted by "advocacy." Louisiana's higher education commissioner responded that the usual standards "barely apply" to such a catastrophe.

Got a tip for this page? E-mail people@aaas.org

Three Q's >>

Maize (corn) biologist **Michael Fernandez** has worked himself out of a job. This spring, the Pew Charitable Trusts declared victory and shut down its 6-year-old Initiative on Food and Biotechnology that he directed. The program provided objective information on genetically modified plants and animals and focused attention on the U.S. regulatory system.

Q: Who won the debate over agbiotech?

I'm not sure I want to talk about winners and losers. Public opinion hasn't changed very much over these 6 years. A relatively small proportion of U.S. consumers are opposed, and the vast majority are somewhere in the middle. We've had big increases in the acreage planted [and] farmers clearly see a benefit to insect- and herbicide-resistant crops.

Q: How good is our regulatory system?

It's a mixed bag. For products with incremental changes, the system works pretty well. When you start to get into products that don't fit neatly into a category like plant-made pharmaceuticals, there are questions about whether the system is adequate.

Q: What's coming down the pike?

Bioengineered] animals are something that we will have to deal with, including moral and ethical issues. The U.S. will have to figure out how to deal with imports of products that we've never seen before. It's in our best interest to have a regulatory system that is flexible enough and has the tools to assess the risks so that we can all get the benefits.

CREDITS (TOP TO BOTTOM): STAFF; TULANE UNIVERSITY; JOHNCE MICHAEL FERNANDEZ

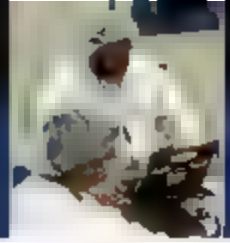

1268

1269

PALEONTOLOGY

Mammoth-Killer Impact Gets Mixed Reception From Earth Scientists

ACAPULCO, MEXICO—A headline-grabbing proposal that an exploding comet wreaked havoc on man and beast 13 000 years ago got its first full scientific airing at a meeting here last week.* Many geoscientists who attended nearly a day of talks and posters on the putative impact called the idea "cool." But they are not dashing off to rewrite the textbooks yet.

A loose consortium of more than 25 scientists is arguing that a massive comet exploding in the atmosphere over North America wiped out the mammoths, terminated the fluted, Paleo-Indian culture and triggered a millennium-long reversion to an ice age climate. "We're quite sure there was no impact," says analytical chemist Richard Firestone of Lawrence Berkeley National Laboratory in California, one of the consortium's two leaders.

Not so fast, say veterans of decades-long wrangling over how cosmic collisions have affected Earth and the life on it. "There is some interesting evidence that deserves study," says crater-ing researcher Peter Schultz of Brown University, a member of the consortium who did not attend the meeting. But the evidence for an impact is too new and unconventional to be convincing.

The "impact wars" have been raging since scientists first began working out geologic markers for ancient impacts in the 1960s. By the 1980s, researchers found 65 million year-old sediments that contained too much of the element iridium—rare on Earth but enriched in meteorites. That discovery pointed the way to nanometal grains scarred by the shock of the impact that killed off the dinosaurs. Geologists eventually found the crater from that impact.

In the 1990s, geochemist Luann Becker of the University of California, Santa Barbara, and colleagues said they had found impact markers at the mother of all mass extinctions, the Permian-Triassic 251 million years ago (*Science*, 23 February 2001, p. 1469). These markers included metallic grains and molecular cages composed of carbon—called buckyballs or fullerenes—filled with extraterrestrial helium. Three years later, however, Becker's group has failed to make its case for a Permian-Triassic impact. In fact, despite considerable effort, no one else has found fullerenes or extraterrestrial helium at the Permian-Triassic boundary.

Now Firestone and some of his consortium colleagues, including Becker, say they have found nearly a dozen kinds of recent impact markers at 26 sites from California to Belgium. Most of the supposed markers are new types, many have never before been reported in the geologic record.

The consortium got its start in 1999 when retired archaeologist William Topping of Denang, New Mexico, approached Firestone with unusual mineral grains from seconders at Gurney, Michigan. The grains came from the base of a black layer rich in organic matter left during the Younger Dryas, a cold snap that began 12 900 years ago and lasted 1000 years. The "black mat" lies just above the last arrowheads and spear points crafted by the Paleo-Indian Clovis people, as well as the last bones of the mammoths the Clovis hunted.

From the odd composition of the Gurney samples, Topping and Firestone inferred that the sediments had been tapped 12 900 years ago by radiation from a nearby supernova that devastated the Western Hemisphere. In late 2004, Allen West, a retired geophysical consultant in Prescott, Arizona, offered to help with the by-then-stalled project. Other specialists soon came on board. West collected most of the samples and funded much of the work with $70 000 of his own "fun money."

Given new evidence, the researchers have discarded the supernova scenario in favor of a major collision. They believe the impacting object contributed many of their proposed markers. Indeed, irregularly shaped metallic grains, some exotically [illegible] in the same metallic grains melted into microspherules, nanodiamonds, fullerenes carrying extraterrestrial helium, and excess potassium-40. These markers have "no way of being produced except by impact," Firestone said at a press conference at the meeting. The collision with Earth, they propose, produced other markers, soot and charcoal from global wildfires, vesicular carbon microspherules, and melted, glasslike carbon. The latter two carry the nanodiamonds.

Because they have found no crater or shocked minerals, West and Firestone say the alien object probably did not slam into the ground. They believe it was some several kilometers in diameter and dirtied with rock and carbon approached Earth and broke up into bits, as comet Shoemaker-Levy did before it hit Jupiter in 1994. Each fragment exploded in the atmosphere, ▶

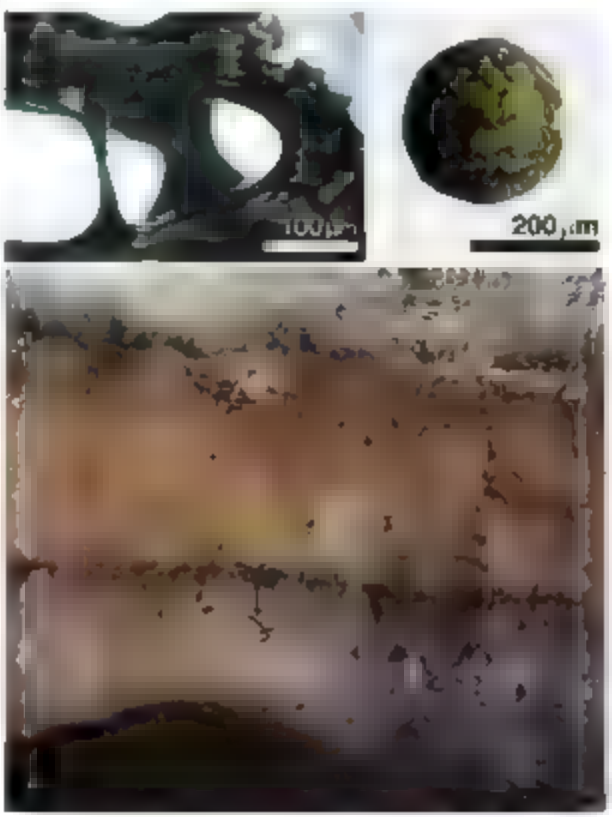

ET debris? Possible impact markers such as glasslike carbon (*left*) and carbon spherules (*right*) are found in the [illegible] layer (*bottom*).

CREDITS: ALLEN WEST

* Joint Assembly of the American Geophysical Union, 22–25 May.

over North America before reaching the ground. In their scenario. The resulting shock waves and heat would have devastated the plants, animals, and humans below. The heat could also have melted enough of the ice sheet then on North America to put a freshwater lid on the North Atlantic, shutting down the warm-water ocean "conveyor" and plunging much of the hemisphere into the Younger Dryas cold spell.

Most listeners at the meeting gave the Younger Dryas impact a polite, sometimes welcoming reception. But the one specialist in impact markers who heard out the presentations was so skeptical. "It's similar to the situation with the Permian-Triassic impact proposal," says David Kring of the Lunar and Planetary Institute in Houston, Texas. The proposed signatures for an impact event shouldn't be discussed, but they need to be tested. Until they are, one has to look at them a little skeptically. Iridium, for example, might have been concentrated by slowed sedimentation or even by algae. The charcoal could well be from forest fire pits. And Kring says the extreme uranium levels and the nanodiamonds embedded in melted carbon make no sense at all.

A paper in review at the *Proceedings of the National Academy of Sciences* may answer a few key questions about the comet clash—and perhaps lure combat-weary impact specialists back into the fray.

–RICHARD A. KERR

ANIMAL STUDIES

NIH to End Chimp Breeding for Research

The U.S. National Institutes of Health (NIH), the world's largest owner of chimpanzees used in biomedical research, announced last week that it was effectively phasing itself out of the business. Officially, it's a money-saving move, although animal advocates are taking credit for making it happen.

Barbara Alving, director of NIH's National Center for Research Resources (NCRR), revealed at her institute's advisory council meeting on 22 May that NCRR had decided to make permanent its longstanding moratorium on breeding chimpanzees for research, which was set to expire in December. NCRR currently owns or supports 650 research chimpanzees, and Alving said the institute could not afford to breed more animals, which can require up to $500,000 each over a lifetime. In fiscal year 2006, NCRR spent $10.9 million on its chimpanzees. Without breeding, this population may die out within 30 years (*Science*, 26 January, p. 450).

Although animal advocates hailed the move, researchers who do studies with these chimpanzees decried it as shortsighted. "It's a horrible decision," says Evan Eichler, who does genomic comparisons between chimps and humans at the University of Washington, Seattle. "There are so many levels where we could regret this day." Neuroscientist Todd Preuss, who does noninvasive brain studies with chimpanzees at Yerkes National Primate Research Center in Atlanta, Georgia, notes that chimpanzees are endangered and can no longer be imported. "This is not a resource that can be reconstituted," says Preuss of the research chimpanzees. "Fifty years from now, people will wonder why we did this."

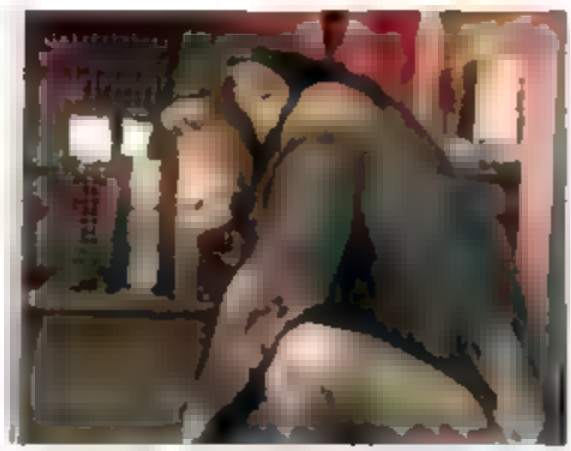

Guest of the state. Without NIH support for breeding of research chimpanzees, today's aging population will steadily be retired or die within the next 30 years.

Preuss, Eichler, and other critics of NCRR's move say maintaining this large genetically diverse population of chimpanzees could help answer pressing biomedical questions for humans about diseases such as Alzheimer's and hepatitis B and C. It also serves as an insurance policy should chimpanzees become extinct. "It's penny-wise and pound foolish," says Ajit Varki, a glycobiologist at the University of California, San Diego, who studies disease differences between humans and chimps. (Another 500 or so chimps available for biomedical research are funded by primate facilities, pharmaceutical companies, and other grants.)

Both the Humane Society of the United States and the New England Anti-Vivisection Society have called for ending the use of chimpanzees in "invasive" biomedical research. Indeed, the Humane Society claims that its campaign—including nearly 22,000 letters to NCRR—was in part responsible for the decision. John Harding, who heads primate resources for NCRR, says the society is mistaken and that it was purely a fiscal issue.

NCRR instituted the breeding moratorium in 1995 largely because AIDS vaccine researchers ended up abandoning the expensive chimp model when they realized that the animals typically suffer no harm from HIV. After seeking input from outside experts, NCRR extended the moratorium three times. No outside body—including NCRR's chimpanzee working group—has recommended ending breeding completely. "It's very inappropriate," says Varki. Although the working group has been consulted on the moratorium before, Harding says it made no recommendation on this topic at its last meeting in March.

Varki hopes several NIH branches might each chip in a few million dollars to restart the program. But if history is any indicator, the institutes enjoy their distance from this contentious issue.

–JON COHEN

CREDIT: ROBERT GALLAGHER/AURORA/GETTY IMAGES

You could be next

Yes, it *can* happen to you.

If you're a young scientist making inroads in neurobiology research, the next Eppendorf and *Science* Prize for Neurobiology could be yours!

This annual research prize recognizes accomplishments in neurobiology research based on methods of molecular and cell biology. The winner and finalists are selected by a committee of independent scientists, chaired by the Editor-in-Chief of *Science*. Past winners include post-doctoral scholars and assistant professors.

To be eligible, you must be 35 years of age or younger. If you're selected as this year's winner, you will receive $25,000, have your work published in the prestigious journal *Science* and be invited to visit Eppendorf in Hamburg, Germany.

Get recognized!

Deadline for entries

June 15, 2007

www.eppendorf.com/prize
www.eppendorfscienceprize.org

$25,000 Prize

eppendorf & Science PRIZE FOR NEUROBIOLOGY

PROGRAM EVALUATION

Researchers Fault U.S. Report Critiquing Education Programs

A new Education Department report that scolds U.S. science agencies for doing a poor job of evaluating their combined $3 billion education programs is itself getting a harsh evaluation from researchers. In particular, they object to its recommendation that randomized controlled trials (RCTs) should be the gold standard to judge how a program has affected students. RCTs, they argue, are ill-suited to handle the complexity of most classroom settings and fail to tell evaluators why a particular intervention has worked.

The 87-page report* was written by an interagency panel chaired by Education Secretary Margaret Spellings. "We've laid out the metrics for agencies to follow," says Kenneth Zeff, senior consultant for policy development within the Education Department. "And we think that RCTs, when appropriate and possible, are the best way to learn if something works."

The report includes an inventory of all federal science, technology, engineering, and mathematics (STEM) efforts—some 105 programs across 12 Cabinet departments and independent agencies, covering everything from museum exhibits to graduate research fellowships. The panel, called the Academic Competitiveness Council (ACC), also requested studies that had evaluated the effectiveness of those programs. "We asked them to give us your best stuff," says one federal official involved in the process who requested anonymity. The council received 115 studies but concluded that only 10 met its test for rigor—and of those, only four showed "a meaningful positive impact" on students.

There's a reason that total is so paltry, say researchers. RCTs, commonly used to test the efficacy of new drugs or medical treatments, aren't appropriate for most education programs because they can't handle the complexity of the classroom or other real-world settings. Students are not pills, and evaluations that are blind to why a particular intervention works aren't very useful. "It's hard to not be for rigor," says Iris Weiss, head of Horizon Research Inc., a contract research firm in Chapel Hill, North Carolina. "And they are right that an RCT is well-suited to demonstrating impact. But if you can't say when, for whom, and under what conditions it works, what good does it do you to know that something was effective?"

Math educator Jere Confrey of Washington University in St. Louis, Missouri, says that the report reflects "business as usual" by the Bush Administration. The Education Department has heavily promoted the use of RCTs through its research arm, the Institute of Education Sciences (*Science*, 25 March 2005, p. 1861). By putting RCTs at the pinnacle of a so-called hierarchy of study designs (see drawing), Confrey says, the report reinforces an "outdated model" of evaluation. Confrey, who chaired a 2004 study by the National Academies' National Research Council on evaluating precollege math programs that the ACC report cites approvingly, says the ACC "picked up from our report [the fact] that most evaluations did not meet our standards. But they missed the idea of multiple evaluations, using multiple methods, to come up with a theory of change."

The agency with the biggest stake in federal STEM education, the National Science Foundation (NSF), has funded precisely that type of work for decades. NSF officials have declined to comment publicly on the report, which was released 10 May by the Education Department, and researchers say that they aren't surprised. As one researcher who requested anonymity noted, "I think they are hunkering down and hoping that the emphasis on RCTs fades once this Administration leaves office."

–JEFFREY MERVIS

*www.ed.gov/about/inits/ed/competitiveness/acc-mathscience-report.pdf

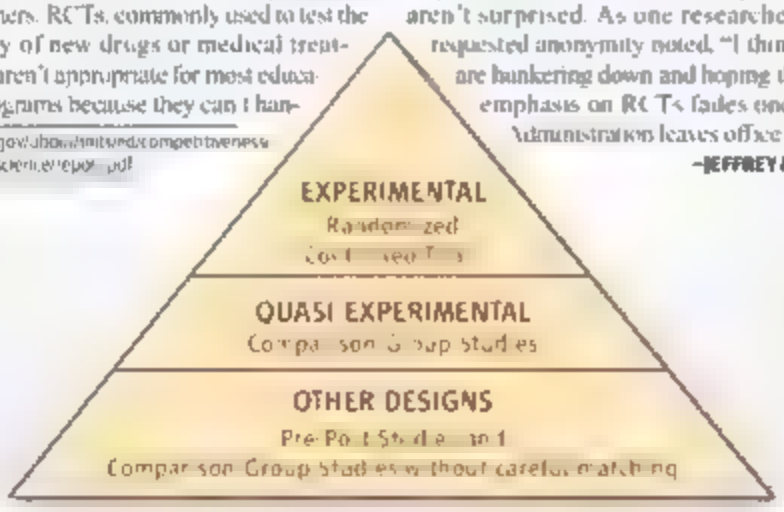

SOURCE: COALITION FOR EVIDENCE BASED POLICY, 2006

Hunting for Genes . . .

Canada has joined the growing lineup of countries setting up large databases in hopes of finding links among genes, the environment, and common diseases. Last week, the Canadian government and the province of Quebec agreed to spend $28.7 million over 3 years for CARTaGENE, a long-term health study that will begin by recruiting 20,000 Quebecans aged 40 to 69. Another $6 million will fund a consortium based at the University of Montreal helping CARTaGENE and other biobanks to harmonize their data. –JOCELYN KAISER

. . . and Martian Ions

BEIJING—With two successful crewed space flights under its belt and a moon mission on tap for later this year, China has announced plans for its first voyage to another planet—with Russia as its partner, in October 2009. Russia will launch a pair of probes to Mars and Phobos, one of two martian moons. The Russian half of the duet is a lander that will collect soil samples on Phobos and return them to Earth, while China is contributing a 110-kilogram satellite called Fluorescent Light One that will study the martian ionosphere. The work will accelerate the development of Chinese remote-control technology, says chief technical engineer Chen Changyu of the Shanghai Institute of Satellite Engineering. Chen says that China and Russia have no plans to share mission data with other countries, apart from what's released in published papers. The Chinese mission budget is also under wraps. –GONG YIDONG

Strong Start for Physics

House Democrats have trumped the White House in their support for physical sciences. Last week, a spending panel allocated $4.5 billion for the U.S. Department of Energy's (DOE's) Office of Science, a 16% boost over current levels and $116 million more than the White House request. "I'm thrilled," says Michael Lubell of the American Physical Society.

The appropriators were silent, however, on a new DOE entity modeled after the Pentagon's Defense Advanced Research Projects Agency that was proposed by the influential 2005 National Academies *Gathering Storm* report as a way to "sponsor creative, out of the-box" energy studies. The House Science and Technology Committee has authorized $4.9 billion over 5 years for such an agency, but competing bills in the House and Senate on innovation and energy cast some doubt on the future of the entity, called ARPA-E. –ELI KINTISCH

SCIENTIFIC WORKFORCE

U.S. Immigration Bill Would Extend Warmer Welcome to Highly Skilled

A clock began ticking for India's Anjali Mahajan as soon as she finished her Ph.D. in biophysics from Ohio State University in Columbus last December. Under U.S. immigration rules, Mahajan had 1 year to find an employer willing to sponsor her for a work visa known as an H1-B. The window seemed far too short to find the job she wanted, as a research scientist in the pharmaceutical industry. Returning to India wasn't an attractive option, either, because her husband had a good U.S. job.

And so, in April, she settled for plan B, which was to remain in academia. By accepting a position as a postdoc at the University of Illinois, Chicago (her husband got a transfer there), she's all but guaranteed a timely work visa because of a rule exempting academic jobs from the annual H1-B cap of 65,000.

Foreign students may have more choice than Mahajan did if Congress passes a massive immigration reform bill that the U.S. Senate began debating last week. Two provisions in the 628-page legislation would help somebody in Mahajan's position. One would increase to 2 years the time allowed for foreign students to obtain an H1-B. The second would increase the H1-B cap from 65,000 to 115,000, with the option of raising it to 180,000.

The overall bill would alter the landscape of high-tech immigration. One of its pillars is a framework for a new merit-based system of granting permanent residency to immigrants that would strongly favor young workers with advanced degrees in science and engineering fields, including Mahajan. Under this system, individual applicants would be awarded points toward their so-called green card based on specific criteria such as a graduate degree, employment in a STEM (science, technology, engineering, and mathematics) occupation, a recommendation from a U.S. employer, and fluency in English. (Mahajan's score would be 90 points out of 100, a fairly high rating.) The 140,000 applicants with the best scores would receive green cards annually. After 8 years, the number would rise to 380,000 a year.

The bill (S. 1348) has drawn mixed reactions. "Allowing students 2 years to find a job in their field is a good move that would help draw more global talent to U.S. universities," says Debra Stewart, head of the Washington, D.C.–based Council of Graduate Schools. But Stewart is ambivalent about the point system. "It appears to have been successful in some countries, but its specifics will determine whether it would increase our competitive position."

Those specifics are already causing heartache. Businesses feel they are being pushed aside. Unlike the current system, which hinges on employer sponsorship, a recommendation from an employer earns only a handful of points. "The points don't ensure that the worker will be fully employed and beneficial to the economy," says B. Lindsay Lowell, a demographer at Georgetown University in Washington, D.C. Lowell would like the employer's word to carry more weight.

Observers say that the system could also mean fewer foreign students at U.S. universities, as a graduate degree has the same value regardless of where it is earned. A better way of attracting and retaining foreign talent would be to "staple green cards to the degrees of foreign students graduating with master's and Ph.D.s from the U.S.," says Lynn Shotwell of the American Council on International Personnel in Washington, D.C. "These are people that we simply don't want to turn away."

Shotwell says the point system also leaves applicants guessing whether they will qualify for permanent residency. In contrast, Canada and Australia allow individuals who reach a set passing mark to become residents. "The message it sends to a skilled foreign worker is 'I don't care your opinion,'" she says. "If one country says you can get residency, buy a house, get settled, and move on with your life, and the other country says, 'We can't guarantee that you will get in,' where would you rather go?"

Although Shotwell thinks the bill doesn't go far enough in welcoming foreign talent, others say it recklessly flings open the doors. Jack Martin of the Federation for American Immigration Reform in Washington, D.C., which favors stricter laws, says that some of the bill's provisions will continue to depress the wages of U.S. workers. Instead of raising the H1-B cap, Martin says, Congress should "restructure the program so that it responds to real market need for foreign workers" through metrics such as "rising salaries for workers in a particular job classification."

Martin also opposes doubling the time allowed for foreign students to find a job. He says that the change simply creates "a new category of workers who can be taken advantage of by American employers before being hired permanently."

Legislative aides predict that the provisions increasing the H1-B cap and the time to find a job will remain in the bill, which will be voted on later this summer, but that the merit-based system will face close scrutiny. —YUDHIJIT BHATTACHARJEE

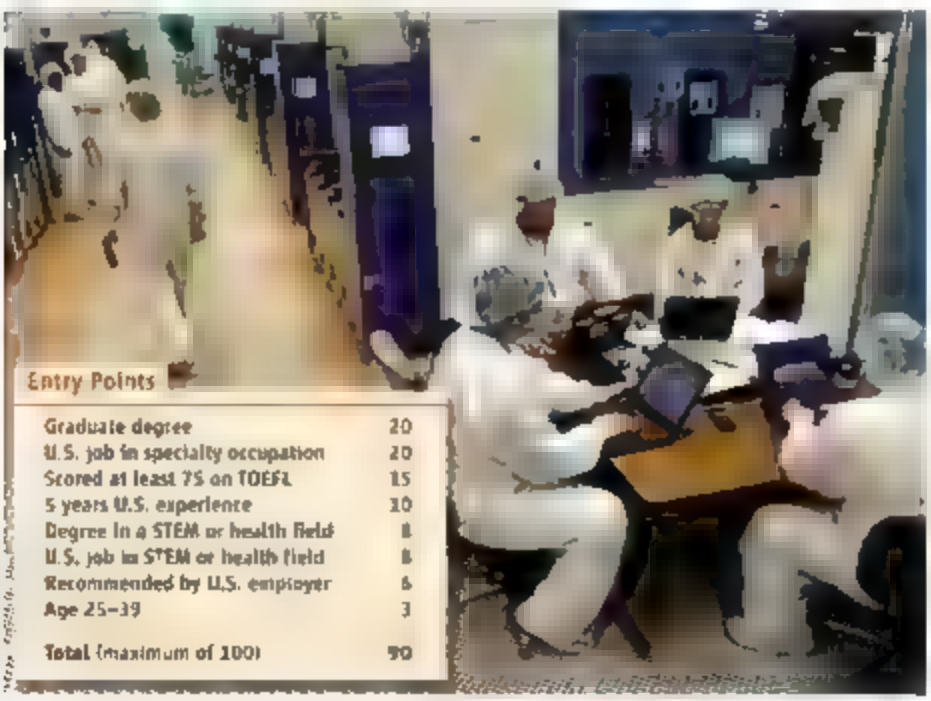

Top scorer. A foreign-born scientist with a graduate degree who has worked in the United States for 5 years would earn 90 points toward a green card under the Senate bill.

PHOTO CREDIT: CHIP EAST/REUTERS

SPACE SCIENCE

Stern Looks for Way Out of NASA's Budget Squeeze

His $5.4 billion budget is stretched thin, but NASA's new science chief doesn't plan to cancel space projects nearing launch or ask for more money. Instead, Alan Stern says he intends to beef up lunar science, champion smaller and less complex spacecraft, and insist on hard-nosed cost estimates before larger missions can win approval.

Stern, a planetary scientist who took over on 2 April, laid out his plan to revamp the agency's troubled science effort in his first wide-ranging discussion with reporters on 24 May. Facing the rising cost of several missions on a science budget that's unlikely to grow beyond the 1% increase for 2008 proposed by the Bush Administration, he's clearly a priority. "I don't have to kill any missions," he insists. But he said NASA will consider firing those principal investigators in charge of missions that spiral out of control.

He also wants upcoming decadal studies by the National Academies to put a ceiling on the cost of any particular mission, and says that NASA is willing to plow millions of dollars into independent estimates for use by the academies' panels. A 1 May academies' report agrees that better cost estimates are critical. Joseph Alexander, study direc-

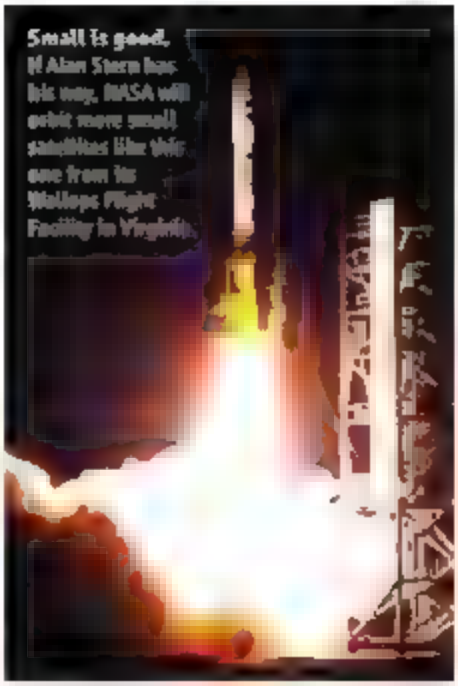

CREDIT: NASA

tor of that report, says that scientists on the panel are "sympathetic in principle" to including what Stern calls "a trapwire." But he cautioned that it's not clear how specific a survey can or should be in laying out costs.

Stern also wants to do for the moon what NASA did in the 1990s for Mars, when it committed to flying a mission to the Red Planet every 2 years. Starting with a $20 million fund in 2008, Stern wants to create a buzz for what he calls "spectacular" lunar science. That effort, along with targeted missions to the moon, could make use of spacecraft already planning to use Earth's gravity on their way to other destinations as well as space telescopes. "Good results lead to good results," he says. "You don't conscript people into scientific fields, they go where the excitement is."

He also defended NASA's approach to earth sciences, which has been criticized for a lack of attention to global climate change. "We'll be very aggressive" in backing the academies' recent decadal study of the field, he says, citing the recent restoration of the Global Precipitation Measurement mission. He also promised greater use of cheaper suborbital missions from NASA's Wallops Flight Facility in Virginia. "We're going to advance the ball on earth sciences," he says, "and we're going to turn heads in doing it."

–ANDREW LAWLER

HIGHER EDUCATION

Australian University Is Latest to Pull Up Stakes in Singapore

Singapore's hopes of becoming a regional center for higher education suffered a setback on 23 May when the University of New South Wales (UNSW) in Sydney, Australia, announced it is abandoning plans to establish a comprehensive university there. The new school was to be a key part of Singapore's "Global Schoolhouse" vision, which aims to foster a knowledge-intensive economy.

Both sides had high hopes 3 years ago when Singapore chose UNSW from among 15 aspirants to build a university to complement three existing local institutions (*Science*, 30 April 2004, p. 663). Plans called for the campus to eventually enroll 15,000 students and house biotechnology and related research that would fit with Singapore's push to become a biomedical powerhouse.

UNSW Asia opened its doors last March with 148 students, less than half of the 300 it had hoped for. Second-semester enrollment was also anticipated to fall short of the university's target. The venture is "unsustainable," UNSW vice-chancellor Fred Hilmer said in a statement. UNSW Asia is slated to shut down on 28 June. A key factor behind the decision's timing is that construction was to begin soon on $96 million worth of buildings, says UNSW spokesperson Lady Bronkman. The university will assist current students in transferring to its Sydney campus or to Singaporean institutions.

This is not the first time that Singapore has hit a snag in its efforts to lure foreign universities to the island nation. In 2005, talks with the University of Warwick, U.K., to establish a second comprehensive university collapsed, reportedly after concerns about costs and academic freedom. And last June, Singapore's government and Johns Hopkins University in Baltimore, Maryland, shot down a joint research and education program amid acrimonious claims over who was to blame for failures to meet goals on faculty recruitment, student enrollment, and technology transfer to local industry, among other issues.

Singapore says it is undeterred by the latest defection. "We are fully committed to developing Singapore into a premier education hub," the Economic Development Board (EDB), which is spearheading Global Schoolhouse, said in a statement. An EDB spokesperson says that the few failures must be viewed against a long list of successes, including a branch of INSEAD, a French business school offering MBA programs since 2000. And plans are afoot for Duke University Medical Center and the National University of Singapore to establish a medical school using Duke's curriculum.

One lesson from UNSW's about-face is that "it is not easy" to set up an offshore campus, especially one combining teaching and research, says Philip Altbach, director of the Center for International Higher Education at Boston College. Universities with international ambitions have been unable to persuade key faculty members to uproot and move to unfamiliar locations, he explains. "There is no successful example" to follow, Altbach says. UNSW could not succeed where others have failed.

–DENNIS NORMILE

A New Twist on Training Teachers

Major U.S. research universities are beginning to steer some of their best students into the classroom in order to address a serious shortage of quality science and math teachers

HEATHER MCKNIGHT DIDN'T THINK SHE was "throwing away her career" by wanting to become a science teacher. But that's what her professor warned when McKnight broached the idea of teaching in the public schools during a summer research stint in a nanofabrication laboratory at Cornell University. McKnight had gotten a similar reaction from faculty members—and fellow students, for that matter—at Carnegie Mellon University in Pittsburgh, Pennsylvania, another research powerhouse, where she spent her freshman and sophomore years as a physics major. "They just didn't seem to care about teaching, or about me," she recalls. "All they cared about was their research."

The next year McKnight did a summer research project at Brigham Young University (BYU) in Provo, Utah, and loved it. "The teachers cared, and the classes were more fun." So McKnight transferred to BYU—and last month she graduated with a physics degree and a certificate to teach secondary school science. She's finishing up an on-campus job—designing an online virtual science program for an academic publisher—while she sifts through several offers for a high school teaching spot back east.

Last year, BYU, a private institution run by the Mormon Church, graduated roughly 5% of all the new physics teachers produced by U.S. colleges and universities in 2006. Its class of 16 dwarfs the production of any other university and even most states. McKnight didn't know that fact when she arrived in Provo after completing a 2-year church mission in Spain. But she knew the introductory science teaching classes she had taken, from former Utah state physics teacher of the year Duane Merrell, "was incredible. And what I loved most," she says, "was the linkage between the laboratory and the classroom, the science and the pedagogy. That's what had been missing everywhere else."

McKnight's odyssey may suggest some answers to perhaps the most pressing

CREDIT: WENDY DOOLEY/BYU

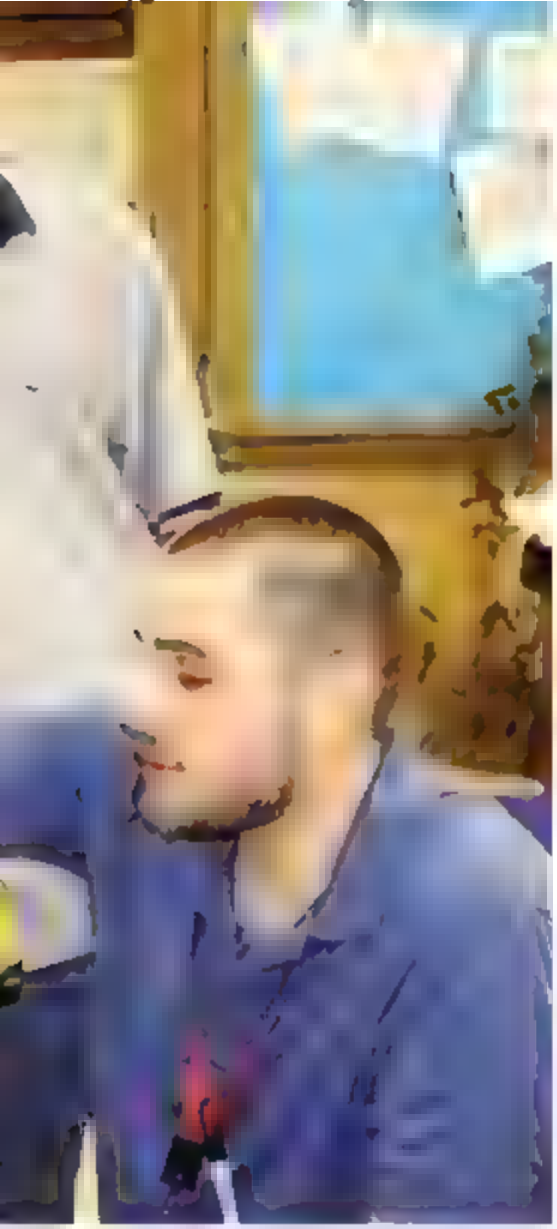

CREDITS (TOP TO BOTTOM): MARK A. PHILBRICK/BYU; VALERIE K. OTERO

Teaching trailblazers. Utah graduate Marshal Hester (*left*) has taught biology for the past 5 years at Travis High School in Austin, Texas. Science educator Duane Merrell (*top*) works with BYU undergraduates in a physics class. Above, an "Ask the student" (*in compound*) helps other University of Colorado, Boulder, students in his role as a learning assistant for an undergraduate physics class.

question of the day for U.S. science policy makers. How can the country produce more and better science and math teachers? This spring, *Science* visited BYU and two other campuses—the University of Texas (UT), Austin, and the University of Colorado, Boulder (CU-B)—that are tackling the question in different ways. Administrators on each campus have data to back up their claims that what they are doing is working.

At Texas, the effort is called UTeach, a multifaceted 10-year-old program that has become a national role model for turning STEM (science, technology, engineering, and mathematics) majors into classroom teachers. The UT approach, well-funded and comprehensive, begins with a frontal assault on the problem by encouraging all entering STEM majors to consider teaching. Those attracted into UTeach get classroom experience in local schools beginning in the freshman year and take courses in pedagogy in parallel with their STEM major. The goal is to graduate students in 4 years with a science major and a teaching certification (see p. 1275).

Colorado is pursuing an innovative strategy that uses learning assistants (LAs) for peer-assisted teaching in introductory science and math courses. The program gives STEM majors their first taste of teaching, as aides to the professors. Concurrently, all the LAs attend a weekly class on education and learning theory that is taught by master science and math teachers. A small percentage of LAs who decide to become teachers later get classroom experience in local schools and take additional pedagogy courses (see p. 1276).

The BYU program is built upon old-fashioned nurturing of every STEM undergraduate with an interest in teaching. It's rooted in the idea that science and math departments should take responsibility for training future teachers, working with master classroom teachers who know how to combine content and pedagogy. It also takes advantage of the fact that many students, including McKnight, have already completed a 2-year mission for the Mormon Church that has often given them their first taste of teaching along with their religious activities. Those students tend to be more certain of their career goals, say BYU administrators, and ready to take advantage of a program that combines research and

Continued on page 1273

BYU TAKES TEAM APPROACH LED BY A MASTER TEACHER

PROVO, UTAH—Duane Merrell looks like a high school science teacher. Which is a good thing, because that's exactly what Brigham Young University (BYU) wanted when it hired the award-winning Utah physics educator 3 years ago into a new position as a clinical faculty member. But driving around in his Isuzu pickup to visit student teachers and their mentors in schools across the Wasatch Valley, the rumpled, laconic 47-year-old Mormon also comes across as a modern-day sheriff of higher education, out to restore order on the nation's chaotic frontier of training science and math teachers.

So far, Merrell is making his presence felt. BYU's annual production of science teachers exceeds those for many states, let alone individual institutions, which suggests he's doing something right.

Although its affiliation with the Mormon Church adds a distinct service component to its educational mission, BYU traditionally did little better than the average U.S. research university in producing science teachers. "We had seen a decline to about one or two graduates, in a program that resided within the College of Education," explains Earl Woolley, dean of the College of Physical and Mathematical Sciences (MPS) at BYU. To help turn things around, Woolley says, "the college of education agreed to transfer the program and faculty slot [to MPS]. We realized that we had to increase the engagement of our science faculty in educating teachers. And we needed the right person to make that happen." He adds: "The biggest single thing that we've done in the past 10 years for training science teachers was our hiring Duane."

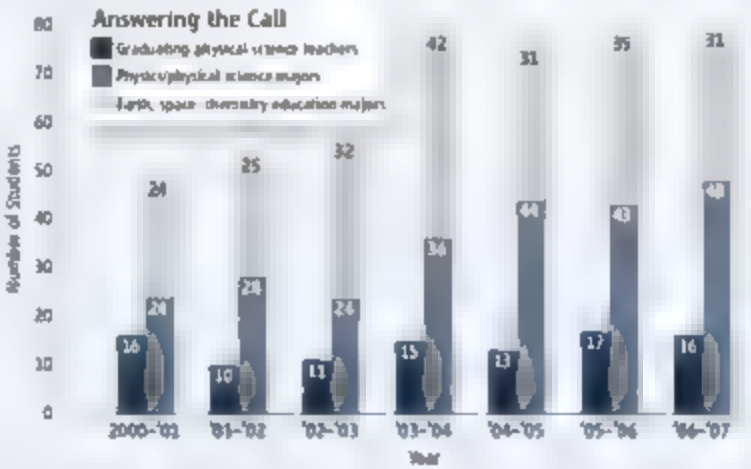

Full-service education. BYU's annual output of secondary school science teachers dwarfs that of most universities, and even some states.

Merrell, who has received a presidential teaching award and numerous state teaching honors, teaches three courses that form the core of the physics education curriculum (along with more traditional education courses and student teaching). Students must complete all but three courses of what's needed for a traditional physics degree, and many students find a way to cram those additional courses into their schedule. Merrell's goal is to connect the pedagogy with the science so that these future teachers "will have multiple ways to engage their students." Despite a heavy teaching load, he tries to get off campus and into the schools as much as possible, checking on the progress of the students, offering tips on how to present a lesson or lab, and helping them prepare for the profession they have chosen. Merrell hand-selected many of the students' mentors and created a teachers' advisory council to tap their expertise. "It's the first time we had asked their opinion about what we were doing," he notes.

"Duane is something special," says Tom Erekson, a mentor physics teacher at Lone Peak High School, who graduated from nearby BYU in 1994 as "the only physics teacher in my class." Erekson says Merrell is proof of how much one person can do to invigorate a program.

Merrell holds an open-ended faculty appointment, which gives him the institutional staying power absent from other programs in which educators spend 1 year on campus as a teacher-in-residence. "My first year went by in a blur," he recalls. "It was the end of the year before I realized all the changes that I'd need to make in the second year."

Despite his celebrity status among his peers, Merrell says his work is far from over. He's on the prowl for master teachers to cover STEM (science, technology, engineering, and mathematics) fields in which he is not expert. The so-called clinical faculty assistants will help out with large introductory courses and—if they so choose—take graduate courses to further enhance their skills. He's recruited one in biology and one in math, and in the earth sciences, he's just found a "hybrid" who will keep one foot in the classroom. And then there's a new "Physics for Inquiry" class. It's designed to give students enough confidence to stick with that hands-on approach to teaching science, even when the going gets tough, rather than fall back on the traditional lecture style of teaching. It's all in a day's work for a pedagogical sheriff. **—JEFFREY MERVIS**

SOURCE: BYU. CREDIT: MARK A. PHILBRICK/BYU

Prime Mover: Robert Clark

It was 1969, and physicists with newly minted Ph.D.s were allegedly driving taxis because they couldn't find academic positions. So BYU physicist Robert Bent Clark, then a junior faculty member at the University of Texas, decided to expand young physicists' career choices. He scoured the country and came up with 75 job openings for high school science teachers. Then he posted those openings—more than the total from academia—at the job fair during the next meeting of the American Physical Society in a performance that elicited gasps from older members but heartfelt thanks from the ranks of his unemployed colleagues. The effort also launched Clark, a particle theorist, on a parallel 30-plus year career in physics education that would include the presidency of the American Association of Physics Teachers.

The avuncular Clark has never worried about going against the grain. At Yale, where he earned his undergraduate and graduate degrees, he chuckles that "I was known as the married Mormon football player." And when a faculty opening in 2000 gave him and his wife a chance to return to Utah, Clark says that "those who were expecting to hire someone right out of grad school. But they went with a graybeard."

His colleagues say Clark is the tinder that has rekindled the university's commitment to preparing physics teachers. And when the education department handed over its slot to the College of Physical and Mathematical Sciences, Clark called up Merrell and twisted his arm to apply.

Continued from page 1271

education objectives (see p. 1272).

These are not the only U.S. universities and colleges experimenting with ways to improve the supply and training of teachers for the nation's schools. By far the largest test bed is in California, which has begun a two-pronged attempt to massively increase the output of STEM teachers by its state-supported universities (see p. 1279). Some programs, including a portion of the California initiative, are consciously modeled after UTeach. But the decentralized nature of U.S. higher education, as well as different state requirements for teacher certification, mean that even a highly regarded program must be adapted to local conditions.

Shopping for data. BYU student teacher Heather McKnight enlisted sandbags and shopping carts to help a middle school science class understand the concept of acceleration.

Despite these differences, educators seem to agree on the essential ingredients for a successful program. They include

- Sending talented undergraduates the message that teaching is valued.
- Giving students an opportunity for early classroom experiences so they can find out whether teaching is right for them.
- Enlisting experienced classroom teachers in shaping courses and mentoring students, and working with faculty members.
- Teaching the subject matter along with the pedagogy courses.
- Strengthening links between science departments and schools of education on campus.
- Persuading faculty members that good teaching is part of their job.

Incorporating these ingredients into their programs hasn't been easy for BYU, CU-B, and UT, however. And the transformation is far from over.

The challenge

The push to improve U.S. math and science education is being fueled by a depressing stream of state and national assessments documenting poor performance, as well as international tests showing that U.S. students do progressively worse than their peers as they move through the education system. The sense of urgency is captured in the title of a 2005 report by the National Academies (*Science*, 21 October 2005, p. 429), *Rising Above the Gathering Storm*. The report asserts that more and better science and math teachers are essential for continued U.S. leadership in science, the engine driving the U.S. economy.

The current shortage of math and science teachers in middle and high schools is the result of many factors, including the lure of higher-paying industry jobs, high attrition and burnout, an aging workforce, and a growing school-aged population. Unlike vacancies in the private sector, however, a teacher shortage doesn't translate into a teacherless classroom. Rather, too often the position is filled by an "out-of-field" teacher, that is, someone with little or no college training in the subject. In 2000, for example, two-thirds of high school physics students were taught by teachers who didn't major in physics. Even for a core subject like math, the figure is 31%.

A move is under way to change that. The current Congress is awash in legislation that embraces the *Gathering Storm* report's call for "10,000 teachers, 10 million minds" by expanding federal support for undergraduates majoring in STEM fields (*Science*, 4 May, p. 672). Bills passed recently by the Senate (S. 761) and the House (H.R. 362 and H.R. 2272) would authorize hundreds of millions of dollars a year for the Robert Noyce Scholarship program at the National Science Foundation (NSF), which gives money to STEM majors who agree to teach in high-need school districts. Another set of bills just introduced (H.R. 2204 and S. 1339) would create a similar program at the Department of Education. Spending bills to

Junior High Means a Senior Commitment

Doug Panee has seen a lot in his 18 years as a junior high school science teacher. But it's what he hasn't seen that makes Panee such an asset to BYU's science teaching training program. "You can never think of all the things that the kids will ask," he says, with a nod toward his eighth-grade class at nearby Oak Canyon Junior High in Orem, Utah. "Their creativity hasn't been stifled." He retains a similar respect for the 14 student teachers that he has mentored over the years, the latest being Heather McKnight (see main text). "After all these years, I'm still learning how to teach. I certainly don't have all the answers."

Panee is being modest, says BYU's Duane Merrell. Master teachers like Panee who are willing to share their classroom expertise and their knowledge of the profession with students have a great deal to offer the program, says Merrell. They allow students to make their own mistakes—"I've had teachers try to hand my kids a set of lesson plans, but that's not what the practicum is supposed to be like," Merrell explains—while at the same time providing useful guidance on classroom management and pedagogy.

The relationship nurtures students through their internships and into the profession, giving them the type of support Panee wished he'd had when he began his career after graduating from BYU. "I was ready to quit after 3 days," he recalls. "My wife and mother told me to stick it out." Nearly 2 decades later, McKnight is glad he did.

Hot science. Doug Panee lights up his physical science class.

CREDITS (TOP TO BOTTOM): COURTESY OF JAN NATHAN

fund such programs starting next year are just beginning to move through Congress. In the meantime, the private sector is stepping. This month, the ExxonMobil Foundation will hold a meeting in Texas about its $125 million National Math and Science Initiative (NMSI) that hopes to replicate the UTeach program at dozens of college campuses (nationalmathandscience.org).

Although money is always needed, many science departments actually have a bigger problem with the very idea that they should help prepare the next generation of science and math teachers. That job has traditionally been left to schools of education. "It's a sea change for major research universities who traditionally have never prepared teachers," says Bruce Alberts, a biochemist at the University of California, San Francisco, and past president of the National Academy of Sciences, who made improving science education one of his priorities during his 12-year tenure.

Equally radical is the concept—eagerly embraced at BYU, UT and CU-B—of tapping into the knowledge of experienced classroom teachers to improve campus-based instruction. By hiring people with many years of experience teaching science in the local schools, the three universities have challenged the sanctity of disciplinary boundaries and overturned the conventional wisdom that faculty members in each department are the font of all wisdom in their subject.

"When I started out, I thought that anyone who had a degree could teach college," says Mary Ann Rankin, dean of the UT College of Natural Sciences who created the UTeach program. "And students at a major research university like UT probably can survive any type of teaching. But it's so easy to turn off kids from science. By working with the college of education, we can help faculty acquire the tools to do better." Adds Michael Marder, a UT physicist and director of UTeach, "The real keys to our program are the former K–12 teachers serving as master teachers, who will be the role models for our students. These are the people who wake up every day saying, 'How can I improve my teaching?'"

Most STEM teacher-training programs assume that the best teachers will have both a solid grasp and love of their subject matter. But the way most universities treat their undergraduates undercuts that assumption. Historically, students who have done well in high school science and math classes are channeled into undergraduate programs that emphasize research, not teaching. Then the best collegiate performers are encouraged to go on to graduate school. In contrast, STEM majors who choose a career in the elementary or secondary school classroom are regarded as washouts, not winners. That was certainly the message conveyed to McKnight, who grew up in a college town outside New York City with a biology professor as a father and who assumed that her interest in science would lead to a career as an academic researcher.

The BYU, CU-B and UT programs broadcast the opposite message, and officials at each school say that is an important ingredient in their success. Every incoming UT freshman, for example, gets an invitation from Rankin to check out the UTeach program, part of an ongoing and aggressive recruitment effort by the university. Each class in the first pedagogy course for Colorado's LAs begins with pizza and soda. Both Texas and Colorado also offer Noyce scholarships, which provide up to $10,000 a year for 2 years. "We're telling those who want to go into teaching that they are our elite. That's the opposite of what we have traditionally told them," says Richard McCray, a professor emeritus of astrophysics at CU-B and a co-founder of the LA program. "We're showing them that we plan to treat them well—with scholarships and pizza."

For love and money

None of these programs is hugely expensive. The biggest of the three, with about 450 students enrolled, UTeach has an annual operating budget of nearly $2 million drawn from a variety of sources, including a $9 million endowment for

Continued on page 1277

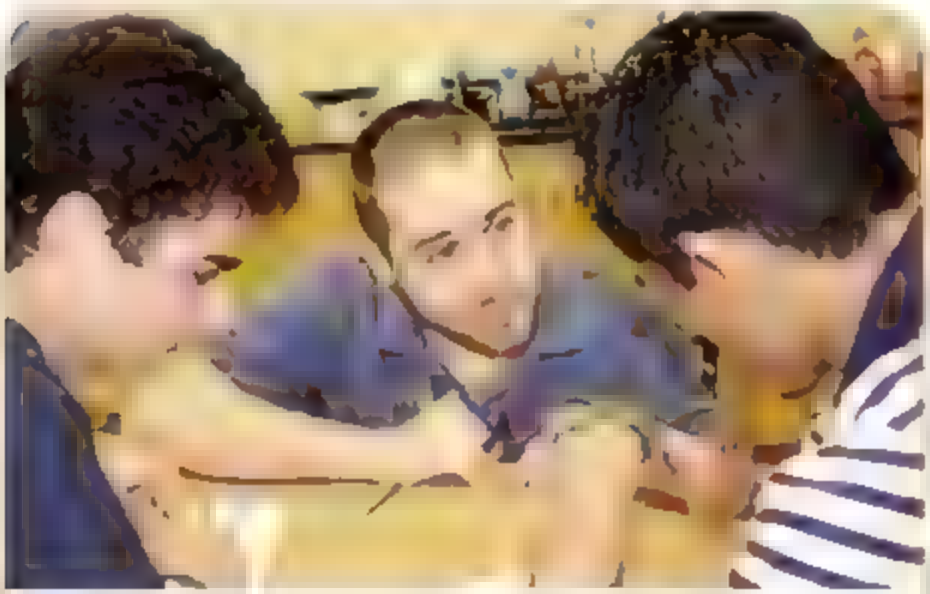

CREDIT: WENDY DOUGLEHUS

UTeach Makes Marshall Hester a Lifer

An overcast, humid spring day in this capital city finds Marshall Hester sweating through another biology class at Travis High School in Austin, Texas. It's an ESL—English as a second language—class in a high needs school, and Hester wrestles with his less than fluent grasp of Spanish, the dominant language for his students. Winding down a 3-week unit on plants, he uses his laptop computer to display a warm-up exercise showing a cross section of a leaf.

"What process is going on here?" he good-naturedly pumps the students, pointing to the top layer of the drawing and straining to hear someone toss out the word photosynthesis. Then he moves down the image. "And why is this layer on the bottom?" he asks, hoping for a mention of respiration. "I know, it's not easy," he says encouragingly. But there's also a note of frustration in his easy bantering. "We just did this, and I'm a little disappointed that you don't remember."

A graduate of the University of Texas with a degree in biology and certification to teach secondary school science, Hester was part of the second class of the university's UTeach program. Teaching was in the back of his mind after a high school biology teacher turned him on to the wonders of plants, although the initial education classes he took at UT were a drag. "But the Step I and II classes were great—it wasn't easy, but it was fun," he recalls. Now Hester is hooked. He's in his fifth year of what he expects to be a career at Travis. Asked why, he responds: "Is it corny to say that I'm doing it for the kids?"

UTEXAS TELLS SCIENCE MAJORS: WE WANT U (TO) TEACH

AUSTIN, TEXAS—The University of Texas's UTeach is the most visible of the new wave of teacher-preparation programs. It earned an accolade in an influential 2005 National Academies' report on U.S. competitiveness, and this spring, the ExxonMobil Foundation created a National Math and Science Initiative to replicate it. Its 10-year track record is impressive: From a pool of highly qualified students, the university has more than tripled its annual production of STEM (science, technology, engineering, and mathematics) teachers and kept most of them in the classroom.

But its success was far from preordained. In 1987, Texas changed its school certification laws to require future secondary school teachers to earn a degree in a disciplinary field. Designed to make sure that teachers acquired more content knowledge in science and math, the law was actually driving students away from those fields because of its stiffer requirements. At the same time, the state's flagship university was a bit player in STEM teacher training: Out of some 12,000 students in the UT graduating class of 1996, only five were certified to teach secondary science and only 16 in math.

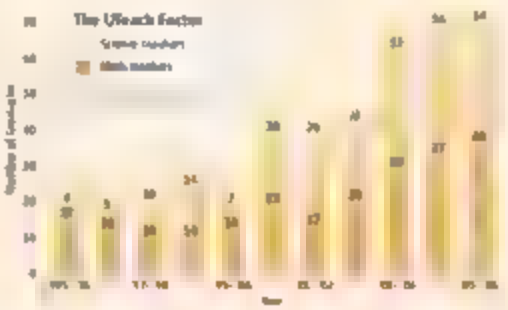

Positive trend. Texas's output of science teachers has soared since UTeach began in 1997.

Mary Ann Rankin, dean of UT's College of Natural Sciences, decided that something had to be done to get more STEM majors into teaching. So in the summer of 1997, she asked a group of master teachers from the area's public schools to design a curriculum that could be ready to go by fall. "The dean told us to assume that nothing would remain the same and not to worry about the cost," recalls Mary Long, the program's first master teacher, who remains a guiding light. "And a month later we enrolled the first students."

What Long and her colleagues drew up remains the basis for the current UTeach program. Its essential elements include aggressive recruitment of potential teaching candidates, an early exposure to the classroom as part of two tuition-free courses, a strong network of teachers in local schools who mentor UT trainees in field placements, a new sequence of pedagogy classes taught by master teachers in STEM fields, and disciplinary classes with faculty members modeling best teaching practices. Jere Confrey, a prominent math educator who helped create the curriculum before moving 4 years ago to Washington University in St. Louis, Missouri, says that one key change was linking each of the three new pedagogy courses—knowledge and learning, classroom interactions, and project-based instruction—to the subject matter, namely, math and science. "Non-content-based methods courses are silly," she explains.

The program acquired "instant credibility" among the faculty when UT physicist Michael Marder agreed to sign on as director, says Rankin. "He's also absorbed an incredible amount about the world of education that has been extremely valuable." Forging a partnership between the College of Natural Sciences and the School of Education, says Rankin, was another critical element. "Previously, a STEM major who wanted to be a teacher would get their major in our college and then take their gened [general education] requirements, which, to be honest, were not the most exciting courses." The new courses, she says, "are relevant to what they need to know to teach science, and they get to use their knowledge in the classroom."

In addition to an enrollment of nearly 500, UTeach officials are especially proud of what happens once students graduate from the program. More than 80% actually go into teaching, and since 2000, some 92% of that pool have remained in the classroom. That's an impressive retention rate for a profession in which 40% of teachers leave within their first 5 years.

From the beginning, Rankin and Marder have sought to make the program self-sustaining without cutting back on elements—such as the tuition reimbursement for the initial field experience courses, called Step 1 and 2 internships, so that students can pursue education-related summer jobs rather than work at the mall; and stipends to mentor teachers—that could not be funded by the state. The solution, they decided, was an endowment. That's how Jeff Kodosky became the program's financial godfather.

"I was on the dean's advisory council when she first talked about it, and I was intrigued by the idea," says Kodosky, a New York native who moved to Austin for graduate school and in 1976 co-founded National Instruments, which provides measurement and automation software. "It was clear we weren't producing many science and math teachers. And having an education major decide to teach science always seemed backward to me. Why not start with someone who loves science?" After providing seed money for the initial curriculum, Kodosky and his wife, April, agreed in 1999 to donate $5 million. The endowment has grown to $9 million, with a goal of $35 million. **–JEFFREY MERVIS**

Prime Mover: Mary Ann Rankin

Team player. Rankin with UT mascot.

Mary Ann Rankin launched the UTeach program because she believed that the College of Natural Sciences, of which she is dean, needed to become more involved in preparing secondary school science and math teachers. But it wasn't just an academic exercise. Rankin's daughter, then in fourth grade and attending a suburban school district with an excellent reputation, suddenly went from loving school to refusing to do her homework. An uninspired teacher, she recalls, had made math "boring and repetitive, and the science program was nonexistent." With a little bit of guilt, Rankin says she transferred her to a private school, where she resumed her stellar academic career.

This fall, her daughter will start college (at UT, as it happens). But elementary school science and math are still on Rankin's mind. She's thinking about jettisoning the two current science courses for elementary education majors and replacing them with a three-course sequence that would begin with a research methods course "tailored to their level," followed by a science component in the early classroom experience all UTeach students get. "They would learn so much more, and we would be reinforcing the importance of science in the elementary grades," she explains. "So many elementary school teachers shy away from science because they don't like it or don't understand it, and it turns off the kids at a young age."

SOURCE: UTEACH; CREDIT: COURTESY OF THE UNIVERSITY OF TEXAS, AUSTIN

COLORADO ALSO SEEKS IMPACT ON CAMPUS

BOULDER, COLORADO—The goals of the Physics Education Research (PER) group at the University of Colorado, Boulder (CU-B), are as big and bold as the Rocky Mountains that loom over the campus. To improve undergraduate student learning and to produce more STEM (science, technology, engineering, and mathematics) teachers. But rather than getting their feet wet by teaching in the public schools, as with most such programs, Colorado students first interact with their peers—an approach that also aims to improve undergraduate education.

"Back in the 1990s, I won lots of teaching awards," explains Jim Curry, chair of the applied mathematics department and an early convert to the program. "But then I found out that the kids in my introductory calculus class were struggling later on in thermodynamics, and the professor would come by and ask me why I hadn't taught them. Well, we do teach this stuff, but 2 years later they've forgotten it. The problem is that they never really learned it."

The program, which Colorado officials have dubbed course transformation, begins with faculty members inviting top-performing undergraduate students in their introductory classes to become learning assistants (LAs) in their course the next semester. It's the first step on the ladder toward becoming a teacher. Along the way, they earn $1500 by assisting the professor during lectures as well as running weekly tutorials. In addition to helping students with homework sets, the peer tutors explain the basic concepts being covered in class. Concurrently, the LAs begin a series of pedagogy classes taught by experienced science educators intended to meld their content knowledge with the skills they will need to become effective teachers.

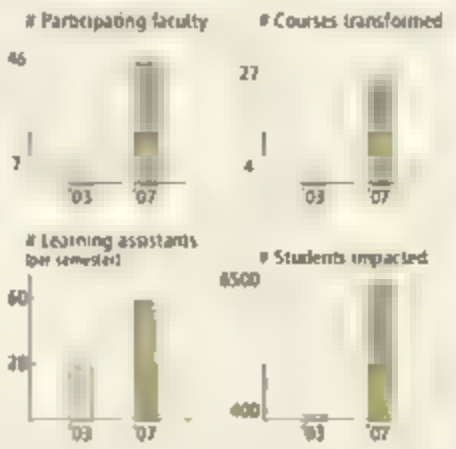

Campus revolution. The Colorado program is affecting many aspects of university life.

The LA program is directed by faculty from the school of education and the physics department, building upon the pioneering work on physics education research done by Lillian McDermott and others at the University of Washington, Seattle. "She convinced the field that physics education was really physics," says group member Steve Pollack, a physicist who migrated from nuclear theory to education after using a sabbatical to pore over the scientific literature on how students learn. "We've managed to do that here, too."

Valerie Otero, the effervescent physics educator who runs the LA program, calls Pollack one of the "seekers." Together with Noah Finkelstein, the duo is studying student outcomes in LA-assisted courses at the same time they expand the number of courses, departments, and faculty using LAs. Although the group has won converts across the university, Pollack admits that most faculty members "stay where I was 6 years ago. They say, 'This is good material, leave it with me and I'll use it.' But they won't do the research themselves that could take them to the next level."

Part of the reason is that course transformation is hard work. Gabe Thatcher, who took a quantum mechanics class from Finkelstein last fall and then served as an LA for the same course this past semester, marveled at how much Finkelstein tailored his "clicker questions"—an interactive method of instruction developed by physicist Erik Mazur at Harvard that provides immediate feedback on how well students understand a particular concept—to the needs of the students in each class. "He probably only used about 60% of the questions he had asked when I took the course," says Thatcher. "I was really impressed."

Preliminary results show that both LAs and their peers learn more science than do those not in classes with LAs, and about 15% of the LAs decide to pursue teaching as a career. (Because of high demand for a limited number of these paid slots, only students who agree to become teachers can be an LA for more than two semesters.) This fall, the program's first 11 graduates, armed with teaching certificates, will enter the classroom. That's half of the state's entire output in 2005, a year that saw CU-B graduate exactly one STEM major certified to teach.

The on-campus component of the program also dovetails with a systematic effort to improve the teaching of undergraduate science begun by physicist Carl Wieman with money from his 2002 Nobel Prize. Last year, Wieman moved to the University of British Columbia in Vancouver, Canada, which offered him more resources. But he retains an appointment at Colorado, and the staff of his science education initiative work alongside the LA program staff.

—JEFFREY MERVIS

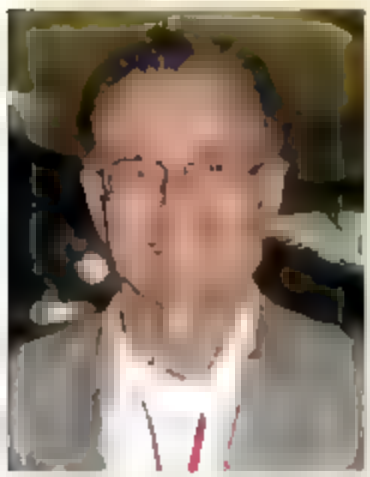

Prime Mover: Richard McCray

CU-B's Richard McCray has done pioneering work in theoretical x-ray astronomy that earned him election to the National Academy of Sciences. But he says that his late-career quest to understand how students learn—to improve undergraduate instruction and prepare the next generation of science teachers—"is more of a challenge and more interesting" to him. He also thinks it's more important. "Bright students don't want to sit passively and listen to a lecture; they want to interact. These huge intro courses are acting as a filter. And we all need to do something about that."

McCray stumbled onto the idea of using learning assistants (LAs) after getting a grant from the Pew Charitable Trust. The goal was to increase technology in the classroom in ways that could be sustained without more money. "But I couldn't make it compute," he confessed. The traditional model, using graduate students as teaching assistants, wasn't economically feasible, he says. "The only way I could do it was by using LAs, you could get seven undergraduates for the price of one grad student. And when I found that the LA experience was extremely powerful for these students, and that it got them interested in teaching, I thought, 'Let's exploit that.'"

This spring, he also found a way to put the LA program on the road to self-sustainability, offering $120,000 if the university agreed to a three-to-one match. (The donation was made anonymously because he felt a public announcement would be too boastful.) Now retired, he's only working about 70% of the time. "I helped get this started, so I'd like to keep lending a hand."

SOURCE: CU-B; CREDIT: COURTESY OF RICHARD MCCRAY

Continued from page 1274

activities not covered with state funding. And Marder has an expansionist bent. Last year, for example, UT began a program to provide more first-year students with early research experiences, using a grant from NSF and the Howard Hughes Medical Institute. By involving science faculty members and enlisting second-year students as peer instructors, the initiative mirrors some aspects of Colorado's LA program. Marder's goal is to reach one-quarter of each freshman class, with the hope that some of them will decide to be teachers.

First steps. Amanda Geist (*left*) and Michelle Stachurski explore how children learn science in a class for learning assistants at the University of Colorado, Boulder.

Valerie Otero, who directs Colorado's LA program, has also been adept at attracting outside funding. The LA program began officially in 2003 with a $900,000 NSF grant, and the next year it got a $300,000 boost from a physics teacher education consortium (physteconorg) funded by NSF and the American Physical Society. Last year, NSF gave the Colorado team $1.5 million over 3 years to study its success in improving student learning and filling the teacher pipeline. It's in line for $1 million more from NSF in 2009. Otero says, thanks to the university's recent decision to commit $360,000 over the next 3 years.

At BYU, university administrators say they don't need to rely on outside funding because the cost of their program is so modest. There are no stipends for LAs, no tuition waivers for initial classroom experiences, no payments to mentor teachers. Not even free food. Carl Wuellner, dean of the College of Physical and Mathematical Sciences, says the budget for the science education program is "nothing" compared to the $100,000 or so that it costs to support a single graduate student. By his calculation, "once we got [Merrell's] position, we spent $25,000 the first year on equipment for field experiments and anything else that he asked for. But he scrounged most of it."

Universities new to the game can get help in adopting some or all of the program from the UTeach Institute, which was formed last year to disseminate the programs' findings after Marder and Rankin started getting calls from universities wanting to know more about what they had accomplished. Next month, the institute is hosting a conference for applicants to ExxonMobil's initiative, which this fall hopes to give out 10 or so $2.4 million grants to universities interested in replicating the UTeach program. If the initiative raises enough money, says CEO Tom Luce, a retired Dallas lawyer who came back to Texas last fall after a stint as assistant secretary for policy in the U.S. Department of Education, the number could eventually swell to 50 sites.

CU-B has applied for a grant, seeing it as a way to grow its program. "We have about 50 math and science majors in the pipeline, and our goal for year 4 would be to quadruple that number," says Colorado's Otero. "We feel that's doable, if their program is as good at recruiting students as they say it is."

In contrast, BYU declined to submit an application. University administrators didn't see the need to seek outside funding for something that they were already doing and would eventually have to finance themselves, anyway. Indeed, the final $4 million of the NMSI grant, which would create an endowment, is contingent on a university match that demonstrates a commitment to sustaining the changes made possible with NMSI funding.

For one of UTeach's newest master teachers, 32-year-old Jason Erman, becoming a teacher was never about the money. A computer science major at Carnegie Mellon, he walked away from a well-paying job at an Austin software company during the height of the dot-com boom that he says "was paying me more money in my first year out of school than I'll probably ever earn as a teacher." After completing UTeach's master's program, he taught math for 5 years at Kealing Middle School in Austin before signing up last fall to help train the next generation of teachers. Likewise, McKnight says that she turned down a full-time job at the publishing company that would pay her a lot more than what she'll earn as a teacher.

Their career paths affirm the importance of what's happening at UT, CU-B and BYU. "It just feels like the right thing to do," says Erman. "And it's something that the country needs."

–JEFFREY MERVIS

Teaching for a Living or for Life

Gabe Thatcher isn't a classroom teacher. And the senior electrical engineering major at the University of Colorado, Boulder (CU-B), may never become one. "I like teaching. It's really stimulating. But I also like money," says the 27-year-old California native, speaking candidly about the anticipated gap between a $60,000-a-year starting salary as an engineer and the $35,000 he can expect to earn in the classroom. His calculations include a wife who's planning to return to school and the couple's desire for a family.

But Thatcher is closer to teaching than most students in his field, having served as a learning assistant (LA) this past semester for an introductory physics course that he took last fall. As an LA, he also attended weekly classes on how students learn, taught by CU-B's Valerie Otero and Steve Iona, a retired local high school science teacher. Both experiences deepened his appreciation for what it takes to convey information to someone else. "Even if I'm not a classroom teacher, I need to understand how my kids learn and how my co-workers learn," he explains. "As a working engineer, I think being a good teacher is a key tool."

CREDITS (TOP TO BOTTOM): VALERIE K. OTERO; JENNIFER L. VAN HOECKE

One FailSafe™ PreMix is guaranteed to work

Keep a dozen on hand for your PCR challenges

Using a unique blend of thermostable enzymes and a set of 12 standardized premixes, optimization of any PCR reaction is quick, easy and reproducible

The FailSafe™ PCR System Amplifies—

- Up to 85% GC-rich templates
- Any templates up to 20 kb
- Multiplex PCR, consistently
- Low copy number templates

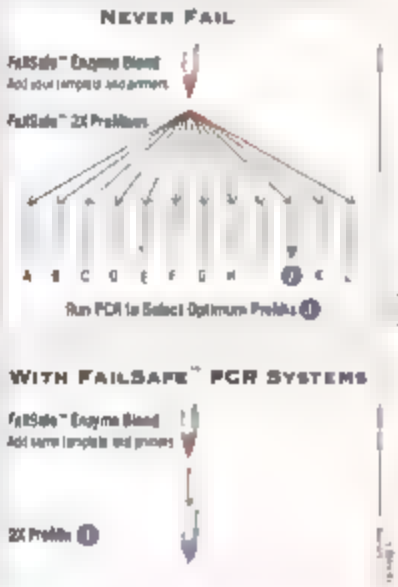

Amplification of an 80-85% GC-rich region of the human fragile X gene. PCR was performed using the FailSafe™ PCR System. Lanes A–L [illegible] molecular weight marker. Optimal amplification was obtained with FailSafe PCR PreMix J.

Start using FailSafe and get your PCR to work the first time and every time

EPICENTRE offers a money-back guarantee for successful PCR with one or more PreMix. If you're not happy, you don't pay.

To order yours, go to **www.EpiBio.com** and enter QuickCode **FSA3X**

Epicentre Biotechnologies

California Heads Down Many Roads In Search of Best Training Model

The state's research powerhouses are feeling their way while the CSU system goes full speed ahead in producing more high-quality teachers

In the nation-state of California, producing more math and science teachers has become a high-stakes numbers game—with a bewildering number of players and more than one set of rules.

Staring at a projected need for 33,000 new math and science teachers over the next decade, which dwarfs the state's current output, Governor Arnold Schwarzenegger won pledges in 2005 from the state's two public university systems to tackle the problem in return for increased state aid. The 23-campus California State University (CSU) system, which now produces about 60% of the state's teachers in all fields, agreed to double its output of 750 math and science teachers by 2010. The University of California (UC) system set a more ambitious goal, from a lower base, to quadruple the 200 students now graduating from its 10 research-oriented campuses with science and math teaching credentials.

So far, so good. But those similar goals hide important differences in how the two systems are tackling the problem. For CSU, its Mathematics and Science Teacher Initiative means building on a long proud history of training teachers. Accordingly, its changes are evolutionary, involving new paths to credentialing, improved tracking of its graduates, more partnerships with federal agencies, and novel ways to deliver high-quality coursework.

CSU schools have already increased output by 37% since 2005, raising from 6.3% to 8.8% the percentage of science and math teachers among the total annual production of 12,000 teachers. "It's a top priority for all our campuses, and we're doing it through a range of different strategies," says Joan Bissell, head of teacher education programs within the CSU chancellor's office.

In contrast, training lots of teachers will require wrenching changes for most UC campuses, their science departments, and individual faculty members. Many of them bristled at the idea of taking a top-down approach, so last year the Science and Mathematics Initiative (SMI), which implements the system's promise to the governor, was transformed from a program run out of the office of UC Chancellor Robert Dynes to a decentralized effort in which each school is allowed to set its own priorities and decide how best to achieve them.

The effort to improve STEM [science, technology, engineering, and mathematics] teaching has been on the back burner nationally for 20 years," observes Fred Eiserling, a UC Los Angeles microbiologist who heads the school's SMI program and who also serves as coordinator for all UC campuses. "At UCLA, we've built up our program with the help of outside grants. But it's never received the attention it deserves. SMI will allow each campus to ratchet up its efforts."

Teachable moment. Chancellors Charles Reed (*left*) and Robert Dynes (*right*) have promised California Governor Arnold Schwarzenegger that their Cal State and University of California campuses will graduate more science and math teachers.

One striking example of the different challenges facing the UC and CSU systems is their reaction to the new National Math and Science Initiative (NMSI) funded by ExxonMobil to replicate a 10-year-old Texas program called UTeach (see p. 1275). Half of UC's 10 campuses have submitted applications in hopes of expanding their fledgling activities. In contrast, none of the 23 CSU schools is bidding for the money.

Bissell says CSU plans to stay the course with students earning a bachelor's degree followed by full certification as part of a master's program before they began teaching, rather than veer toward the UTeach model, in which students combine classroom experience, pedagogy, and core science studies in a 4-year program. Part of the reason is that Texas has different certification requirements, she says. But she also points to a recently completed 6-year analysis of 1500 California math and science teachers. It found that those who had gone through the "full preparation model" were better prepared and performed better in the classroom than so-called interns, a category that Bissell says would apply to most UTeach graduates.

In comparison, UC schools were drawn to the NMSI program. SMI's second name, in fact, is CalTeach, in honor of the Texas program. But a similar name doesn't necessarily mean the same type of sweeping changes. UCLA's proposal, for $2.4 million over 4 years, for example, would permit education courses to be counted as part of the degree requirement for STEM majors.

Eiserling makes no apologies for the incremental approach. "We have 26 tenured science persons across nine departments," he says. "So making this change will take time, cost a lot of money, and require buy-in from a lot of people. If we can get departments to agree to allow students to substitute one of the CalTeach courses for, say, an astronomy course, it will send a message that teaching is important. And that will help change the culture."

If history is any guide, however, even incremental changes won't come easily. In 1993, Heather Calahan graduated from UCLA and became a high school math teacher. Two years ago, she returned to help administer, as well as teach in, the school's Joint Mathematics Education Program. JMEP is a 20-year-old effort with essentially the same goals as SMI but that has limped along without any of the hoopla or resources of the new initiative. The program runs on a shoestring, however, and so far SMI hasn't meant any additional resources. In fact, a JMEP request last year for some administrative help was turned down.

This spring, Dynes told a congressional science committee that as SMI ramps up, "I predict we are going to see real magic happen." Calahan can only hope that some of the magic will rub off on those working in the trenches to prepare more science and math teachers.

–JEFFREY MERVIS

CREDIT: LAUREL MAGGINFORD

LETTERS

edited by Etta Kavanagh

Biodiversity Loss in the Ocean: How Bad Is It?

THE RESEARCH ARTICLE "IMPACTS OF BIODIVERSITY LOSS ON OCEAN ECOSYSTEM SERVICES" BY B. Worm *et al.* (3 Nov. 2006, p. 787) projects that 100% of seafood-producing species stocks will collapse by 2048. The projection is inaccurate and overly pessimistic.

Worm *et al.* define the "collapse" as occurring when the current year's catch is <10% of the highest observed in a stock's time series. However, fish catch is rarely an adequate proxy for fish abundance, particularly for rebuilding stocks under management. A variety of biological, economic, and social factors and management decisions determine catches. Low catches may occur even when stocks are high (e.g., due to low fish prices or the effects of restrictive management practices), and vice versa. The inadequacy of Worm *et al.*'s abundance proxy is illustrated by the time series of data for Georges Bank haddock (*Melanogrammus aeglefinus*). The highest catch for haddock occurred in 1965 at 150,362 tons (*1*). This catch occurred during a period of intense domestic and international fishing (*1*). In 2003, haddock catch was 12,576 tons, or 8% of the time series maximum. Under the Worm *et al.* definition, the stock would be categorized as collapsed in 2003. However, stock assessment data (*1*) estimate the total magnitude of the spawning biomass in 2003 to be 94% of that in 1965. Comparing the estimate of spawning stock biomass in 2003 to the level producing maximum sustainable yield (MSY), the stock was not even being overfished in 2003 (*2*).

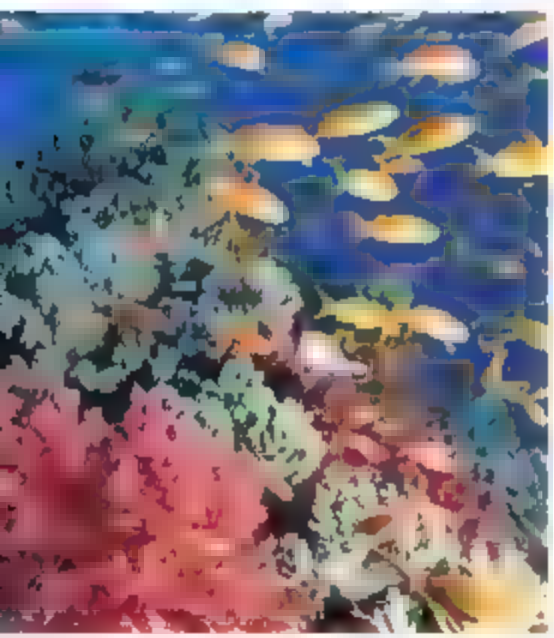

Because adequate stock abundance measures exist for only a portion of world fish stocks, this purported worldwide meta-analysis required using data that represent the lowest common denominator of data—the total magnitude of the catch. However, if the catch ratio metric is so prone to misrepresentation of the true status of populations as illustrated above, a synthesis of world fisheries based on these data is equally flawed. At the least, the authors should have conducted a calibration of their stock collapse metric with more complete stock abundance data available from the many worldwide sources where such data exist.

The extrapolation of their stock collapse metric to 100% by 2048 does not agree with the recent history of stock status, particularly in the United States. National Marine Fisheries Service data indicate that for 2005, about 76% of stocks were classified as "overfished" (*2*). For most stocks, overfished status occurs when the population size drops below 50% of the population required to support MSY. Even under this more conservative definition of stock rebuilding, the proportion of stocks classified as overfished is actually declining slightly—in 2004, 28% of stocks were so classified. Extrapolating a 2% decrease in the number of overfished stocks per year leads to a prediction that no stocks in U.S. jurisdiction would be overfished by the year 2018. However, such a meaningless projection does not incorporate a large number of complex factors, such as the differing life histories of species, impacts of variable ocean conditions on recruitment, and the increasing effectiveness of management measures, all significant shortcomings of the prediction method and data of Worm *et al.*

To address persistent overfishing issues, in December 2006 the U.S. Congress passed and the National Marine Fisheries Service is now implementing provisions of the Magnuson-Stevens Fishery Conservation and Management Act Reauthorization Act (MSRA). The law mandates that overfishing be eliminated for all federally managed species by 2010 and that science-based annual catch limits will be calculated for all of the 532 stocks currently under regulation.

STEVEN MURAWSKI,[1] RICHARD METHOT,[2] GALEN TROMBLE[1]

[1]Director of Scientific Programs and Chief Science Advisor, National Marine Fisheries Service, National Oceanic and Atmospheric Administration, Silver Spring, MD 20910, USA. [2]Office of Science and Technology, National Marine Fisheries Service, National Oceanic and Atmospheric Administration, Seattle, WA 98112, USA. [3]Chief, Domestic Fisheries Division, Office of Sustainable Fisheries, National Marine Fisheries Service, National Oceanic and Atmospheric Administration, Silver Spring, MD 20910, USA.

1. J. Brodziak, M. Traver, L. Col, S. Sutherland, Stock Assessment of Georges Bank Haddock, 1931-2004 (National Marine Fisheries Service, Northeast Fisheries Science Center Reference Document 06-01, 176, 2006).
2. NOAA, Status of the U.S. fisheries for 2005, available at www.nmfs.noaa.gov/sfa/domes_fish/StatusOfFisheries/2005/finalSOS/Report_text_FINAL.pdf)

THE PROJECTION FROM B. WORM *ET AL.* ("Impacts of biodiversity loss on ocean ecosystem services," 3 Nov. 2006, p. 787) that all of the world's wild fish will be collapsed by 2048 attracted international media attention. Such a projection is fallacious and inappropriate to appear in a scientific journal. The use of catch data to indicate stock status is misleading for several reasons. Catch may be low due to management restrictions,

and healthy, well-managed stocks may be classified as collapsed. Many stocks naturally fluctuate dramatically in abundance, and as the length of the time series of data becomes longer, the chance that any particular low in abundance will cause catches to fall below 10% of the historical high catch becomes greater. Finally, many examples of dramatic declines in catch can result from political or market forces, such as declaration of the 200-mile zone. Worm *et al.* should have demonstrated that their index of collapse corresponded to stock abundance–based indices. This test clearly fails for U.S. fisheries, where the proportion of stocks classified as overfished is declining, not increasing.

Furthermore, the Worm *et al.* analyses fails to recognize that jurisdictions such as the United States, New Zealand, Iceland, and Australia have good fisheries management systems where the proportion of stocks that are overfished is decreasing. All of the fish will not be gone by 2048. Most importantly, Worm *et al.* advocate Marine Protected Areas as a way to rehabilitate collapsed fisheries. None of the well-managed jurisdictions use Marine Protected Areas as essential parts of their management strategy. Methods that have been shown to work in well-managed countries involve eliminating the competitive nature of fisheries by incentives and application of conservative harvest levels (*1*, *2*).

RAY W. HILBORN

School of Aquatic and Fisheries Sciences, University of Washington, Box 355020, Seattle, WA 98195, USA.

References

1. R. Hilborn, M. Orensanz, A. M. Parma, *Philos. Trans. R. Soc. London Ser. B Biol. Sci.* **360**, 47 (2005).
2. R. Q. Grafton *et al.*, *Can. J. Fish. Aquat. Sci.* **63**, 699 (2006).

IN THEIR IMPORTANT RESEARCH ARTICLE ON THE precarious condition of ocean ecosystems ("Impacts of biodiversity loss on ocean ecosystem services," 3 Nov. 2006, p. 787), B. Worm *et al.* introduced some confusing terminology that needs to be clarified. Although the term "biodiversity" is sometimes used to mean the general abundance of life in publications on conservation biology, it is almost always used to indicate the relative number of species present in a given area or ecosystem. The conservation problem that the authors intended to emphasize is that the populations of many commercially valuable species have been reduced to the point that they no longer play important roles in the communities to which they belong. Although the phrase "population loss" may provoke less public reaction than "biodiversity loss," it would have been more accurate.

Additional confusion was introduced when it was stated that records over the past millennium revealed a rapid decline of native species diversity since the onset of industrialization. Surely this statement, and the specific reference to extinctions (100% decline) of some species, must refer to some very limited localities. A thorough study of historic extinctions in the sea published in 1999 (*1*) showed that no fish species and only four or five invertebrate species had become extinct. Although many valuable species have suffered severe declines, they are still with us and may yet be saved. The authors also observed that the number of species invasions over time coincided with the loss of native biodiversity. But my own research on this subject has shown that almost all invasions have not resulted in the loss of native species and have produced gains in biodiversity (*2*). Increases in species diversity generally produce an increase in ecosystem services.

JOHN C. BRIGGS

Department of Fisheries and Wildlife, Oregon State University, Corvallis, OR 97333, USA.

References

1. J. J. Carlton, J. B. Geller, M. L. Reaka-Kudla, E. A. Norse, *Annu. Rev. Ecol. Syst.* **30**, 515 (1999).
2. J. C. Briggs, *J. Biogeogr.* DOI: 10.1111/j.1365-2699.2006.01584.x (2006).

Response

MURAWSKI AND COLLEAGUES STATE THAT OUR assessment of the impacts of global marine biodiversity loss is overly pessimistic. They imply that management interventions are likely to reverse current trends of overfishing, and that the U.S. National Marine Fisheries Service (NMFS) has already met that goal. They cite Georges Bank haddock as an example and contest that catch metrics (as used in our global analysis) are sufficient to track the status of this particular fish stock and possibly others. We agree that precise biomass data are preferable but these are rarely available. Here, we illustrate that catches are a good proxy of the status of haddock, although there can be a short delay in detecting recovery under intense management. While NMFS's own data show that full recovery is still uncommon (<5% of overfished stocks) (*1*), we strongly agree that destructive trends can be turned around and that rebuilding efforts need to be intensified to meet that goal. But we must not miss the forest for the trees: Continuing focus on single, well-assessed, economically viable species will leave most of the ocean's declining biodiversity under the radar.

The Georges Bank example illustrates well how intensive management can reverse the loss of marine biodiversity and ecosystem services (see figure) and was in fact included in our own recovery analysis. Haddock stocks collapsed from foreign overfishing in the 1960s and from domestic fleets in the 1980s. The first collapse was reversed by establishing a 200-mile Exclusive Economic Zone in 1977, the second by an emergency closure of half of the fishing grounds in 1994. Haddock biomass increased promptly in both cases, and catches followed with a 1- to 6-year delay (panel A of figure), indicating that fishing became again economically viable. The importance of large-scale protected areas for such unprecedented recovery is well documented (*2*).

The definition of "collapse" we used refers to a loss in catches of 90% below the historic maximum (*3*). According to this metric, the Georges Bank haddock stock, or more precisely the ecosystem service it supplied, collapsed from 1970 to 1977 and 1983 to 2003 (panel A of figure). Using stock assessment data from NMFS (*4*), we find that stock biomass similarly collapsed from 1970 to 1977 and from 1982 to 1997. The stock biomass was considered overfished under NMFS rules from 1967 to 2002 and in 2004 (panel A of figure).

Thus, available data suggest that catch records tracked biomass changes, overfishing status, and stock collapses reasonably well.

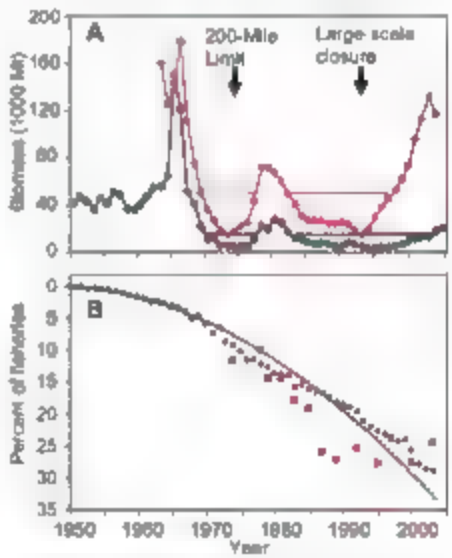

Comparison of fisheries catch and biomass trends. (**A**) Georges Bank haddock (*Melanogrammus aeglefinus*) catches (white diamonds) and spawning stock biomass (red diamonds). Black line indicates collapsed status based on 90% reduction in catches, red solid line indicates collapse based on 90% reduction in biomass, and red dotted line indicates overfished status as defined by NOAA/NMFS. (**B**) Global fisheries trends. Shown is the proportion of fisheries where catches in a given year declined 90% or more below the historic maximum (black diamonds and trend line from our paper), and those that have been assessed by FAO as overfished, depleted, or recovering from depletion (red squares, from (*5*)). The latter are only a subset of all stocks, i.e., those that have biomass estimates available.

linear regression: catch against biomass 1963 to 2004, $r = 0.90$, $P < 0.0001$). By 2004, catches had increased to >10% of the maximum, or "recovered" by our definition. This example implies that use of stock biomass data (as opposed to catch data) would not change our overall conclusions.

The Georges Bank example is built on some of the best fisheries data in the world and on effective but still uncommon management practices. In our global analysis, we could obviously not rely on precise stock assessments available only for a fraction of the world's fisheries. Even in the United States half of the 903 species recognized by fisheries management are not assessed because of data gaps, and out of the 74 species that are assessed as overfished, 34 still experience further overfishing, while only 3 have recovered (*1*).

Myrawski *et al.* imply that if we had used a different metric of collapse or had access to global stock abundance data, we would not have seen the steady decline in fisheries stocks that our analysis revealed. They provide no reanalysis of global fisheries data and rely on a single positive example to suggest that the future of seafood is currently safe. Our paper concentrates on the ability of high-diversity ecosystems to support services such as fisheries catch and suggests that efforts to support natural levels of marine diversity will be a powerful force in preventing the seafood collapse of which we warned. We share the fervent hope of Myrawski *et al.* that changes in fisheries management can help reverse this troubling trend, and suggest that an honest recognition of the global problems we face, combined with a comprehensive assessment of successes and solutions, will be the best way forward.

Hilborn also raises concerns about the use of catch data in our analysis and calls for demonstration that catch trends approximate fish stock abundance trends. Although measures of stock abundance are critically important to fishery management, our study focused on the flows of goods and services from marine ecosystems to humankind: food supply was one of these critical services, and fisheries catches are the appropriate metric in this context. Recent assessments of the status of world fisheries used different approaches and data sources, yet they all reach pessimistic conclusions about the direction of global fisheries trends (*5*–*7*).

For example, Hilborn and co-authors [(*7*), p. 359] state that "we anticipate further declines in abundance, further loss of jobs and fishing communities, and potential structural change to marine ecosystems." They used catches in the same way as we do to distinguish well-managed, abundant fisheries from failed, depleted ones. Their "landings indicator" (current yield over maximum historic yield) [(*7*), tables 2 and 3] ranges from 0.28 to 1 for well-managed fisheries, from 0 to 0.11 for depleted stocks, and 0.14 for a recovering stock (*7*). Thus, our cutoff for "collapsed stocks" at 0.1 seems well supported, as suggested by others (*3*).

Hilborn does not provide any documentation to substantiate the argument that stock abundance data (as opposed to catches) may show a pattern different to ours. When we compare the United Nations Food and Agriculture Organization's (FAO) assessments of world fisheries (available since 1974) with our catch trends, the general magnitude of change appears similar (panel B of figure). There is more variability in the FAO estimates, as they are based on a smaller subset of fisheries, i.e., those that have proper

abundance data available. The fact that within the last 7 years, both indices fall above the long-term trend may be optimistically interpreted as an early sign of positive change (panel B of figure).

Hilborn asserts that we have disregarded recent management successes in some jurisdictions. We focused on the relationship between biodiversity and services, not on fisheries management, in our paper. The maintenance and restoration of biodiversity consistently emerge as our critical management recommendation; this is consistent with previous work on the importance of stock complexity (*8*). In the context of our study, Marine Protected Areas (MPAs) provided a replicated experimental framework for studying recovery of biodiversity and services. We are not advocating the establishment of MPAs as the sole policy solution to resolving the problems of fisheries management. Rather, we suggest that sustainable fisheries practices, pollution control, maintenance of essential habitats, and creation of marine reserves all need to be part of a broader strategy to manage ocean ecosystems for their biodiversity and associated services. We fully support Hilborn's call to create incentives for conservative harvest levels as part of that broader strategy.

Briggs asks for clarification of some terminology. Although the term "biodiversity" is used in many ways, it has been clearly defined by the Convention on Biological Diversity as "the variability among living organisms from all sources including, *inter alia*, terrestrial, marine and other aquatic ecosystems and the ecological complexes of which they are part; this includes diversity within species, between species and of ecosystems" (*9*). Our study focused on the variability within and between species. Briggs suggests that the term "population loss" would more accurately describe our study than "biodiversity loss" and felt that we mostly dealt with commercially valuable species. This is not the case. Our study concerns the accelerating loss of populations and species, both are essential elements of biodiversity (*9*).

Briggs is further concerned about the role of species extinctions in coastal ecosystems. We do not refer to "global" but "regional" extinctions within the 12 estuarine and coastal ecosystems studied, but these include several species that are now globally extinct. Local and regional extinctions are much more common than extinctions on a global scale (*10*, *11*) and are relevant for considering the effects of diversity on ecosystem services, because these are often provided at a local or regional level. In other words, the ecosystem consequences of species loss occur long before global extinction (*11*).

Finally, Briggs is confused about our statement that an increased number of species invasions over time coincided with the loss of native biodiversity, which he interpreted as invasions causing extinctions. However, the reference we cited (*12*) shows mechanistically that declining biodiversity can facilitate invasion and that diversity loss could be a contributing cause rather than a consequence of invasions in these systems. Briggs also suggests that invasions produce gains in biodiversity, which in terms of sample number of species is correct. However, we stated in our paper that invasions did not compensate for the loss of native biodiversity because they are comprised of other species groups (*13*). Briggs implies that biodiversity gains from invasions may enhance ecosystem services. This is an interesting idea. Although some invasive species may contribute to specific ecosystem services (such as invasive clams filtering the water of San Francisco Bay), there was no evidence in our study that invasions halted or reversed the marked loss of ecosystem services in coastal oceans.

BORIS WORM,[1] EDWARD B. BARBIER,[2] NICOLA BEAUMONT,[3] J. EMMETT DUFFY,[4] CARL FOLKE,[5,6] BENJAMIN S. HALPERN,[7] JEREMY B. C. JACKSON,[8,9] HEIKE K. LOTZE,[1] FIORENZA MICHELI,[10] STEPHEN R. PALUMBI,[10] ENRIC SALA,[8] KIMBERLEY A. SELKOE,[7] JOHN J. STACHOWICZ,[11] REG WATSON[12]

[1]Biology Department, Dalhousie University, Halifax, NS, Canada B3H 4J1. [2]Department of Economics and Finance, University of Wyoming, Laramie, WY 82071, USA. [3]Plymouth Marine Laboratory, Plymouth PL1 3DH, UK. [4]Virginia Institute of Marine Sciences, Gloucester Point, VA 23062–1346, USA. [5]Department of Systems Ecology, Stockholm University, Stockholm, SE 106 91 Sweden. [6]Beijer International Institute of Ecological Economics, Royal Swedish Academy of Sciences, SE-104 05 Stockholm, Sweden. [7]National Center for Ecological Analysis and Synthesis, Santa Barbara, CA 93101, USA. [8]Center for Marine Biodiversity and Conservation, Scripps Institution of Oceanography, La Jolla, CA 92093–0202, USA. [9]Smithsonian Tropical Research Institute, Box 2072 Balboa, Republic of Panama. [10]Hopkins Marine Station, Stanford University, Pacific Grove, CA 93950, USA. [11]Section of Evolution and Ecology, University of California, Davis, CA 95616, USA. [12]Fisheries Centre, University of British Columbia, Vancouver, BC, Canada V6T 1Z4.

References

1. A. R. Ricebery, J. H. Swasey, M. Bowman, *Front. Ecol. Environ.* **4**, 303 (2006).
2. S. A. Murawski, R. Brown, H.-L. Lai, P. J. Rago, L. Hendrickson, *Bull. Mar. Sci.* **66**, 775 (2000).
3. R. Froese, K. Kesner-Reyes, *Impact of fishing on the abundance of marine species*. ICES Council Meeting Report CM 2002/A: 12, 2002).
4. J. Brodziak, M. Traver, L. Col, S. Sutherland, *Stock assessment of Georges Bank haddock, 1931–2004* (Northeast Fisheries Science Center Reference Document 06-11, NOAA/NMFS Northeast Fisheries Science Center, Woods Hole, MA, 2006).
5. FAO, *The State of World Fisheries and Aquaculture 2004* (United Nations Food and Agriculture Organization, Rome, 2005).
6. R. Watson, D. Pauly, *Nature* **414**, 534 (2001).
7. R. Hilborn *et al.*, *Annu. Rev. Environ. Res.* **28**, 359 (2003).
8. R. Hilborn, T. P. Quinn, D. E. Schindler, D. E. Rogers, *Proc. Natl. Acad. Sci. U.S.A.* **100**, 6564 (2003).
9. UN, Convention on Biological Diversity (United Nations, New York, 1992) (www.biodiv.org/convention/convention.shtml).
10. M. K. Dulvy, Y. Sadovy, J. D. Reynolds, *Fish Fish.* **4**, 25 (2003).
11. E. Sala, N. Knowlton, *Annu. Rev. Environ. Res.* **31**, 93 (2006).
12. J. J. Stachowicz, R. B. Whitlatch, R. W. Osman, *Science* **286**, 1577 (1999).
13. H. K. Lotze *et al.*, *Science* **312**, 1806 (2006).

Problems of Searching in Web Databases

THE ISSUES DESCRIBED IN THE ARTICLE "European Union steps back from open-access leap" (M. Enserink, News of the Week, 23 Feb., p. 1065) mask a deeper problem. Simply putting scientific content into Web-accessible databases will not make it easily available because commonly used search engines do not crawl databases.

The vast majority of Web-accessible scientific material resides in databases that can only be searched sequentially using manual input of search terms. This makes it prohibitively laborious for individuals to search more than a small fraction of the hundreds or thousands of existing databases. These databases are commonly called the "deep Web."

The U.S. R&D agencies have made a start at addressing this problem with www.science.gov, which allows simultaneous search across 35 massive federal document databases. A new project, Science.world, will extend this model to include content housed by other national governments. But in the long run, someone needs to coordinate searches to all the major Web-accessible document databases in the world, most of which are nongovernmental.

Simple Web accessibility is a necessary condition for the dissemination of scientific knowledge, but it is not sufficient. The issue of open access, although important, pales in comparison to the problem of deep Web access.

WALTER WARNICK

Office of Scientific and Technical Information, U.S. Department of Energy, 1 Science.gov Way, Oak Ridge, TN 37830, USA.

CORRECTIONS AND CLARIFICATIONS

Reports: "A single *IGF1* allele is a major determinant of small size in dogs" by N. B. Sutter *et al.* (6 Apr., p. 112). Affiliation 4 should have been the Department of Ecology and Evolutionary Biology. Also, in the Fig. 1B legend, the labels for two genotypes in the histogram were reversed. The black line with closed triangles represents *A/A*, and the gray line with closed circles represents *B/B*.

Policy Forum: "The obvious war" by M. R. Samardzija (12 Jan., p. 190). In paragraph 5, line 31, in the sentence "For

example. In 1991, U.S. companies spent over $1 billion enforcing or defending against patent lawsuits, while only spending roughly $300 million on R&D expenditures (12)." "$300 million" should read, "$3.7 billion." The last sentence of the penultimate paragraph is incorrect. It should read "Mandel indicates that neither the Federal Circuit's test nor the Supreme Court's test completely resolve the hindsight problem (21)."

TECHNICAL COMMENT ABSTRACTS

COMMENT ON "Impacts of Biodiversity Loss on Ocean Ecosystem Services"

John Jaenike

Worm *et al.* (Research Articles, 3 November 2006, p. 787) used a power relation to predict a global collapse of fisheries by the year 2048. However, a linear regression of the data for the past 40 years yields an excellent fit, with a predicted [illegible]114. Thus, long-term projections of fisheries collapse are highly dependent on the specific statistical models used.

Full text at www.sciencemag.org/cgi/content/full/316/5829/1285a

COMMENT ON "Impacts of Biodiversity Loss on Ocean Ecosystem Services"

Michael J. Wilberg and Thomas J. Miller

Worm *et al.* (Research Articles, 3 November 2006, p. 787) reported an increasing proportion of fisheries in a "collapsed" state. We show that this may be an artifact of their definition of collapse as a fixed percentage of the maximum and that an increase in the number of managed fisheries could produce similar patterns as an increase in fisheries with catches below 10% of the maximum.

Full text at www.sciencemag.org/cgi/content/full/316/5829/1285b

COMMENT ON "Impacts of Biodiversity Loss on Ocean Ecosystem Services"

Franz Hölker, Doug Beare, Hendrik Dörner, Antonio di Natale, Hans-Joachim Rätz, Axel Temming, John Casey

Worm *et al.* (Research Articles, 3 November 2006, p. 787) investigated the importance of biodiversity to marine ecosystem services across temporal and spatial scales. In projecting the extent of future fisheries collapse, we argue that the authors inappropriately extrapolated beyond their available observations and used data on marine reserves and fishery closures that are not representative of global fisheries.

Full text at www.sciencemag.org/cgi/content/full/316/5829/1285c

RESPONSE TO COMMENT ON "Impacts of Biodiversity Loss on Ocean Ecosystem Services"

Boris Worm, Edward B. Barbier, Nicola Beaumont, J. Emmett Duffy, Carl Folke, Benjamin S. Halpern, Jeremy B. C. Jackson, Heike K. Lotze, Fiorenza Micheli, Stephen R. Palumbi, Enric Sala, Kimberley A. Selkoe, John J. Stachowicz, Reg Watson

We show that globally declining fisheries catch trends cannot be explained by random processes and are consistent with declining stock abundance trends. Future projections are inherently uncertain but may provide a benchmark against which to assess the effectiveness of conservation measures. Marine reserves and fisheries closures are among those measures and can be equally effective in tropical and temperate areas—but must be combined with catch, effort, and gear restrictions to meet global conservation objectives.

Full text at www.sciencemag.org/cgi/content/full/316/5829/1285d

COMMUNICATING SCIENCE

Because Science Matters

Barbara Kline Pope

Recently I was sitting with my five-year-old son in a dingy yellow leather chair in the uncomfortable quiet of our dermatology specialist's waiting room. As I was absent-mindedly reading a Magic School Bus book to him, I heard the words, "Well, I can sort of believe in evolution..." Immediately looking up, I saw a woman in her mid-30s with an open book on her lap. She was relating her opinion to a returning elderly man seated beside her. I listened intently, hoping for a lively discussion about a topic that is occupying much of my time these days. She continued, "but I just can't see that the big bang really happened."

Most of us are familiar with the dismal state of science literacy. Basic science concepts and facts escape many people. A majority of Americans say that they do not accept the validity of some of the most established scientific theories—as witnessed on that visit to the doctor. And perhaps the most important feature of the woeful state of public understanding of science is the average American's lack of a firm grasp of the process of science itself (*1*).

The science community and policy-makers point to many ills that result from the public's failure to understand, appreciate, or engage with science and technology. The concept of "science literacy" implies that knowledge of basic scientific ideas is necessary for adequate citizen participation in decision-making, preparation for employment, and the practical aspects of daily life (*2*). The increasing number of science and technology–related public issues makes science literacy an essential component of public participation, informed public policy, support for science (*3*), and ultimately robust global competitiveness.

These motivations and others underlie programs to educate the American public about science abound. A quick browse of the Web sites of several scientific societies reveals that most have at least one program designed to address the problem. Public schools and universities are reacting to this need, as are most other sectors of society. Given the increasing importance of science and technology in all of our lives, individual scientists themselves have a responsibility to take the lead in communicating their research findings and offering insight into the scientific process to decision-makers and the public.

Scientists can participate in many ways—speaking with community groups and schools and directly with business leaders and politicians. Speaking to the public through the media offers a way that scientists can efficiently reach many people with their messages. But how can scientists ensure that reporters represent their science accurately? Will they be held in high esteem by their peers for promoting their work—or will colleagues think that they are wasting precious time that could be spent on "real" work? How can scientists attract reporters' attention in this media-fragmented society in such a way that others will benefit from their insights? All these questions and a host of others are answered in *A Scientist's Guide to Talking with the Media* by Richard Hayes (media director of the Union of Concerned Scientists) and Daniel Grossman (a science journalist). This superbly organized and well-written primer guides scientists through the process of talking to the public through the media.

At first glance, one might think that this is all just common sense. And much of it is. But the book is full of common sense not commonly practiced. We all know that we should choose a few major messages and stick with them throughout an interview with a reporter, but how many people actually use a "message compass" to keep themselves from wandering from the most important points? Hayes and Grossman offer lists of specific things to ask a reporter prior to an interview as part of doing our homework—items that we just might not think about on our own. Their sections on creating effective messages includes examples and helpful advice on specific wording. They remind us that "long-winded statements rarely end up in newspaper articles," so we should make sure that our messages have "a certain something extra"—something that is surprising, catchy, humorous, or sobering.

Missing from the book are an emphasis on the fragmentation of the media and how to communicate effectively in an environment where consumers of science information have thousands of choices including the ubiquitous Web. What's the best way to engage blogger journalists?

One of the book's most useful sections attempts to narrow the cultural divide between scientists and journalists. Many science journalists do an excellent job reporting on complicated issues under very tight deadlines. Many scientists jeopardize their process by not providing the most relevant messages and framing their work in ways that are meaningful to people's lives. This and many other actions detailed in the book suggest that there can be a happy, productive partnership between scientists and journalists. But fewer and fewer science-trained journalists are employed by the news media today. General reporters with little or no science expertise often cover science beats and are carrying a heavier load in general (*4*). The authors tell eye-popping stories about science news articles gone awry, detailing ways in which both the scientists and journalists could have prevented misunderstandings and miscommunications that caused sometimes life-threatening problems. They say, "We have focused on such outrageous cases not to scare you away from contact with the press, but because such stories starkly illustrate that the scientific community needs to communicate better. The situation desperately needs to be improved." I hope that more scientists will embrace communicating with the public and use this book as one of their tools for improving the situation.

The reviewer is at the National Academies, 500 Fifth Street, NW, Washington, DC 20001, USA. E-mail: bkline@nas.edu

References

1. National Science Board, *Science and Engineering Indicators 2006* (National Science Foundation, Washington, DC, 2006), 7-17–7-22; www.nsf.gov/statistics/seind06/pdfstart.htm.
2. B. S. P. Shen, in *Communication of Scientific Information*, S. P. Day, Ed. (Karger, Basel), pp. 44–52.
3. J. D. Miller, R. Pardo, F. Niwa, *Public Perceptions of Science and Technology: A Comparative Study of the European Union, the United States, Japan, and Canada* (Fundación BBV, Bilbao, Spain, 1997).
4. C. Russell, "Covering controversial science: Improving reporting on science and public policy," Working paper, Center on the Press, Politics, and Public Policy, Kennedy School of Government, Harvard Univ., Cambridge, MA, 2006, pp. 7–13, http://ksghibbs.harvard.edu/press/pdf/research_publications/papers/working_papers/2006_4.pdf.

10.1126/science.1141343

PUBLIC HEALTH

Bumpy Road to Vaccination Policies

Rino Rappuoli

Although vaccines may well be the most effective form of medical intervention ever introduced, factors having nothing to do with science or medicine have greatly influenced their acceptance and use. The history of vaccination shows the importance of the passions surrounding the social, legal, political, and industrial problems associated with convincing healthy people to be vaccinated against severe, debilitating, and often lethal diseases.

James Colgrove's *State of Immunity* captures the emotions that shaped the course of vaccination efforts in the United States from the beginning of the 20th century to contemporary times. Colgrove (a Columbia University historian of public health) describes the bumpy road that led to the remarkable status of health now enjoyed by children. His breathtaking narrative is effectively supported by the illustrations (historical photographs and advertisements) and a rich list of references. Colgrove discusses the episodes that followed public health efforts to deploy vaccines against smallpox, diphtheria, pertussis, poliomyelitis, measles, swine flu, rotavirus, and bioterrorism. Therefore, the book is not about the history of vaccine development per se; in fact, many good vaccines that were introduced without generating emotional opposition are barely mentioned.

Colgrove describes a history of repeated cycles of "expansion and backlash." The use of a new vaccine spreads as campaigns of mass persuasion fuel countrywide enthusiasm for the conquest of another disease. Complacency then sets in as the threat of the disease wanes. The ever-present perceptions of vaccine-associated risk now lead people to question the value of the vaccination. During the backlash phase, more attention is given to the question of whether individuals must freely choose vaccination or should be directly or indirectly compelled to be vaccinated.

Discussing the early 1890s smallpox epidemic in Brooklyn, New York, Colgrove shows that people were already debating whether vaccination campaigns should rely solely on persuasion or also involve compulsion, police enforcement, and quarantine. Even at that date, efforts that constrained the liberty of individuals to protect the health of the public generated strong opposition, legal suits, and the emergence of antivaccination activists. Eventually, public health authorities adopted the solution of keeping vaccination voluntary but using "indirect compulsory" methods such as requiring vaccination to attend school, a procedure that became universal in the United States in the 1970s under the slogan "No shots, no school." But debates over mandatory vaccination of public school children continue today.

The book also provides historical background for understanding how vaccination became accepted as a cost-saving procedure. During the 1910s and 1920s, the major insurance companies were heavily involved in public health activities through the gathering of mortality data and the preparation of educational materials. In 1927, medical statisticians working for Metropolitan Life calculated that the cost of diphtheria to American society was $200 million per year in medical and nursing costs alone, without considering the disruption to commerce and business caused by quarantine and other procedures. Convinced that an infant is an economic asset that has the potential to increase wealth, Met-Life actively supported the introduction of vaccines.

Among the other topics Colgrove explores are the conquest of poliomyelitis by the Salk and Sabin vaccines, the efforts to eradicate measles, the substantial obstacles to vaccinating the poor, the concept of product liability, and the controversies surrounding informed consent and mandatory vaccinations.

The backlash against vaccination that began in the 1970s was accelerated by a dramatic 1982 television program that described diphtheria-pertussis-tetanus vaccine as a roulette that risked causing permanent neurological damage. The program led directly to the formation of the activist group Dissatisfied Parents Together. There was an enormous increase in the number of legal actions against vaccine manufacturers, and several companies abandoned the vaccine market. This situation accelerated the introduction of a federal compensation program (through the 1986 National Childhood Vaccine Injury Act), which reimbursed medical and rehabilitative expenses for those who suffered a severe reaction from vaccination.

Due to successful research and development programs, the last 15 years have seen the introduction of several new vaccines (such as those for *Haemophilus influenzae*, hepatitis B, acellular pertussis, and *Pneumococcus*). These have increased the number of shots given to each child and the fear that too many immunizations may be responsible for a variety of child health problems, including asthma, sudden infant death, diabetes, and autism. The concern has been taken up by Representative Dan Burton (R-IN), who is fully convinced that either a measles-mumps-rubella vaccine or a thimerosal-containing vaccine caused his grandson's autism.

On the whole, *State of Immunity* is an excellent resource for physicians, researchers, and policy experts in the field as well as for lay readers. Colgrove helps one understand the history of vaccination policies. While the science and the safety of vaccines made a quantum jump during the 20th century, the basic social, legal, and political aspects of vaccination have remained much the same—e.g., the current controversy surrounding cervical cancer vaccine. Because we still face problems similar to those Colgrove discusses, the book should be very helpful for tackling them today and into the future.

CREDIT: BILL BRANSON/NATIONAL CANCER INSTITUTE/TIME AND LIFE PICTURES/GETTY IMAGES

The reviewer is at Novartis Vaccines, Via Fiorentina 1, 53100 Siena, Italy. E-mail: rino.rappuoli@novartis.com

10.1126/science.1141443

INTERNATIONAL SECURITY

Energy Security for North Korea

North Korea should be provided with energy assistance based on technical and economic realities rather than on nuclear politics

David Von Hippel and Peter Hayes

In the 13 February 2007 Six-Party Talks in Beijing, members, wrestling with the DPRK's (Democratic People's Republic of Korea's) nuclear weapons program, stated that the promise of energy aid was a key part of the bargain whereby the DPRK is to freeze its plutonium production (1, 2). Energy loomed large because the DPRK's energy insecurities must be overcome if it is to reverse course and disarm its nuclear weapons and dismantle its nuclear fuel cycle as demanded by the other five parties at the talks. The first Six-Party Talks energy working group meeting, held in Beijing on 17 March 2007, was dominated by foreign affairs officials. Their negotiators should avoid falling into the same traps that resulted in the failure of the energy cooperation dimension of the 1994 U.S.-DPRK Agreed Framework. Technical and economic factors were subordinated to the political imperative of "getting to yes," resulting in many elements that were in many ways not practicable on the time scales expected.

At the end of the Cold War, the DPRK economy went into a precipitous decline, and the energy sector went with it (3, 4). Total primary energy demand in 2005 was about 642 petajoules; total delivered energy to meet end-use demand was about 520 petajoules (5). For comparison, the DPRK's 22 million people consume about three times the fuel used by Washington, D.C.'s slightly more than half a million people (6).

The DPRK economy is powered today much more by biomass such as wood fuel, charcoal, and agricultural waste than by oil (see chart, above). In this regard, the DPRK sits today about where the South Korean energy economy was in 1965. The rest of the DPRK's energy supply is dominated by coal (7).

Hit hard by the floods of the mid-1990s, the DPRK coal industry operates well below its nominal capacity. Recent compiled statistics (8) indicate that the DPRK produced ~22 million metric tons of coal in 2002, about 35% lower than in 1990.

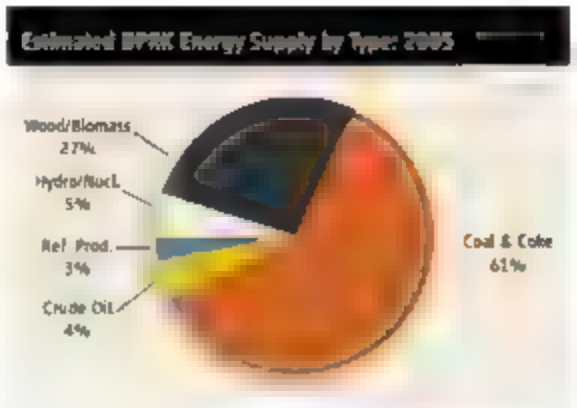

Energy supply. Hydro/Nucl., hydroelectric and nuclear plants. Ref. Prod., refined petroleum products. Further discussion of the estimates for this figure can be found in the supporting online material (5).

The DPRK's overall generating capacity is nominally about 10 gigawatts of electric power (GWe), where it has remained since about 1990, but only about 5.9 GWe, and quite possibly less, is actually operable today (9). Of this, about 3.9 GWe is hydroelectric, and about 2 GWe is thermal-powered (mostly coal). A figure the North Koreans confirmed in Beijing at the first Six-Party Talks energy working group meeting. Thus, the entire DPRK is running at most on the equivalent of two to four large-sized power plants, depending on the season and availability of operable supply.

The thermal (fossil fuel based) power generation system in the DPRK has eroded significantly (3, 4). In virtually all of the large power stations, only selected boilers and turbines are operating, and those that are still in use operate at low efficiency and capacity owing to maintenance problems and lack of fuel. (There have been reports of some refurbishing of selected plants in recent years.) Losses in the power system are high, perhaps 20%, and the grid has collapsed into subgrids on different frequencies and subject to huge voltage and frequency variations. The capacity factor of generators, especially hydroelectric plants, is low, and the DPRK has built many small- to medium-sized hydropower dams and generators of dubious efficacy. Recently, the DPRK installed card-type electricity meters in some households in Pyongyang as an initial step toward reforming how electricity is priced and sold.

Crude oil is imported from China for the DPRK's one operating major refinery. Since the end of heavy fuel oil shipments in 2002 by the Korean Peninsula Development Organization (set up under the 1994 Agreed Framework), most imported petroleum products are also from China (10), with small quantities coming from Russia and elsewhere.

DPRK Energy Demand

Buildings, especially residential buildings, took the biggest share of energy use in the DPRK as of 2005 (see the chart on page 1289). This fact reflects the survival needs of the impoverished population and the significant use of biomass fuels at low efficiency for cooking and heating, particularly in rural areas. The relatively small fraction of household and commercial energy use that is electrical varies greatly in terms of availability by region, city, season, and time of day. The bigger cities and some industrial areas hooked directly into new hydropower plants or the more reliable thermal power plants have more electricity more of the time, but some areas receive electricity only rarely.

Most cooking and heating, particularly in rural areas, is fueled by wood and biomass. Because of supply constraints, household coal use has declined since 1990. Many offices, most commercial buildings, and almost all factories are unheated. Based on remote sensing data, it is now possible to estimate that the DPRK has suffered a roughly 10% deforestation since 1995 (11).

In recent years, the DPRK economy has begun to grow again, albeit very slowly and unevenly, and mostly in sectors that are not energy-intensive. Some light industry and retail or service activity has been observed, but other than increased mining (especially of magnesite, iron ore, copper, lead, and zinc) (12), heavy and medium industry remains stagnant. Agriculture accounts for about 7% of total energy demand, though 70% of estimated agricultural-sector fuel use is wood and biomass for crop processing. The transport sector remains a relatively small user of fuels in the DPRK, because most people walk from place to place. The DPRK has imported a few thousand cars annually from China, and each year, tens of thousands of bicycles have been imported (10). Finally, the DPRK multi-

Nautilus Institute, Eugene, OR 97401, USA, and Melbourne, Australia; dvonhip@igc.org and peter.hayes@rmit.edu.au

tary sector accounts for about 7% of coal use (troops living in bases, plus military-run factories) and about one-third of refined oil usage or overall, about 9% of total energy demand (*13*).

International Cooperation

The pervasive nature of the DPRK's energy-sector problems means that an approach that focuses on one or several massive projects simply will not work. A multipronged approach is required, with a large suite of coordinated, smaller, incremental projects.

Several specific energy-sector initiatives that will assist in the process of rapprochement with the DPRK, help the DPRK to get its economy and energy sector working in a sustainable (and peaceful) manner, and help to pave the way for additional cooperative activities in the energy sector include:

1. *Assistance for internal policy, economic, and legal reforms to stimulate and sustain energy-sector rebuilding.* This could include reform of energy-pricing practices and providing physical infrastructure to implement them; capacity building for careful energy planning to allow aid to be based on need and rational objectives; training for energy-sector actors; strengthening regulatory agencies and educational and/or research institutions in the DPRK; and involving the private sector in investments and technology transfer.

2. *Rebuilding of the electrical transmission and distribution (T&D) system.* The most cost-effective approach for international and Republic of Korea assistance in this area will be to work with DPRK engineers to identify and prioritize a list of T&D sector improvements and investments, and to provide limited funding for pilot installations in a limited area.

3. *Rehabilitation of power plants and other coal-using infrastructure.* An initial focus should be on improvements in 19,000 small, medium, and district heating boilers for humanitarian end-uses such as residential heating. Targeting improvements in (nonmilitary) industries with good prospects for foreign-exchange earnings is also needed.

4. *Rehabilitation of coal supply and coal transport systems.* Strengthening of the coal supply and transport systems must go hand-in-hand with boiler rehabilitation if the amount of useful energy available in the DPRK is to increase.

5. *Development of alternative sources of small-scale energy and implementation of energy-efficiency measures.* The North Koreans we have worked with have expressed a keen interest in renewable energy and energy-efficiency technologies. Such projects should be fast, small, and cheap and should (especially initially) emphasize agricultural and humanitarian applications.

6. *Rehabilitation of rural infrastructure.* Rural energy rehabilitation goals are likely to provide the modern energy inputs necessary for North Korean agriculture to exceed sustainable production level and to meet basic needs of the rural population.

7. *Begin transition to a system of liquid petroleum gas (LPG) networks.* LPG is more expensive than natural gas, but the infrastructure to import LPG, relative to liquefied natural gas (LNG) is much easier and less expensive to develop, and it allows imports in smaller quantities. LPG is also clean burning, has limited military diversion potential, and setting up LPG networks can be a first step toward the use of natural gas in the DPRK. Ultimately, natural gas pipelines and LNG terminals, shared with neighboring countries, can serve as a step toward economic development coupled with regional integration.

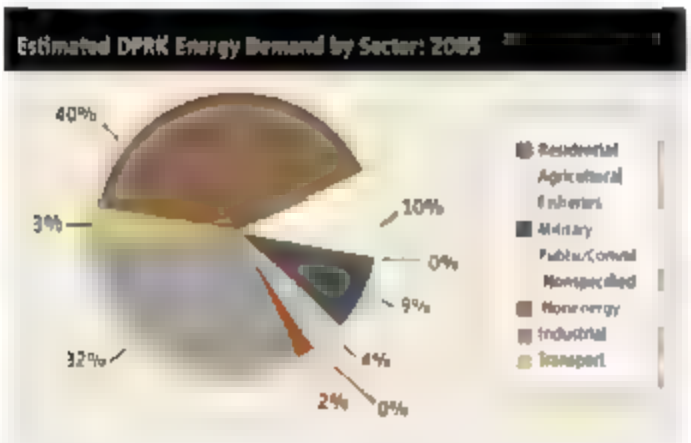

Energy demand. Comm, commercial. Further discussion of the estimates for this figure can be found in the supporting online material (*15*).

Activities in each of these seven categories can be implemented over a 3- to 5-year period at a total cost of about $100 to $150 million per year. We doubt that the DPRK can absorb more than this level of external assistance, until the institutional and physical obstacles to energy development are surmounted. We suggest a suite of options that lend flexibility and offer many ways to succeed rather than one or two single, brittle, and large-scale options that are almost certain (from past experience) to fail.

Which of these negotiation strategies North Korea would accept is unpredictable. We believe that other factors will drive DPRK negotiating strategy, including the need to strengthen domestic leadership positions and to improve their international position from being a weak state surrounded by strong neighbors, especially because diplomats leading the DPRK delegation will be flying blind with respect to technical and economic realities (with economic and energy planners, as well as agency officials, playing only minor roles) (*14*). However, it is essential to bring energy and economic agencies from the six parties into the ongoing negotiations from the outset if the coupled goals of DPRK nuclear disarmament and DPRK energy security are to be achieved.

References and Notes

1. "Joint Statement from the Third Session of the Fifth Round of the Six-Party Talks, 13 February 2007," www.nautilus.org/fora/security/07013Statement.html
2. P. Hayes, "The Beijing Deal is not the agreed framework" (Policy Forum Online 07-014A, Nautilus Institute, San Francisco, CA, 14 February 2007), www.nautilus.org/fora/security/07014Hayes.html
3. D. Von Hippel, "The DPRK energy sector: Current status and options for the future," Energy Paths Analysis/Methods Training Workshop, Vancouver, BC, Canada, 4 to 7 November 2003, www.nautilus.org/papers/regional/Hippel-dprk
4. D. Von Hippel, P. Hayes, T. Savage, *The DPRK Energy Sector: Estimated Year 2000 Energy Balance and Suggested Approaches to an Initial Redevelopment* (Nautilus Institute, San Francisco, CA, 2002); www.nautilus.org/energy/2005/beijingworkshop/datasets/DPRK_Energy_2000_revised.pdf
5. Details are available as supporting material on *Science* Online.
6. Washington, DC's energy consumption calculated from Energy Information Administration, table S1, www.eia.doe.gov/emeu/states/sep_sum/html/pdf/sum_btu_1.pdf
7. J. Williams *et al.*, "The wind farm in the cabbage patch," *Bull. Atom. Sci.* 55 (May/June), p. 40 (1999).
8. Korean (ROK) National Statistical Office, "Comparison of South and North Korean socio-economic data," from http://kosis.nso.go.kr/cgi-bin/wwi_999.cgi (in Korean).
9. J.Y. Yoon, "Analysis of present status and future supply-demand prospects for the DPRK power system."
10. M. Aden, "North Korean trade with China as reported in Chinese customs statistics: Recent energy trends and implications" (*15*).
11. S.-H. Lee, "Forest and other biomass production in the DPRK: Current situation and recent trends as indicated by remote sensing data" (*15*).
12. W. J. Chung, "Mineral resources in DPRK (*15*)."
13. D. Von Hippel, "Estimated DPRK military energy use: Analytical approach and draft updated results" (*14*).
14. For further analysis, see www.nautilus.org/fora-security/07043HayesVonHippel.pdf
15. DPRK Energy Experts Study Group meeting, Stanford University, 26 and 27 June 2006, www.nautilus.org/DPRKEnergyMeeting/Papers1.html.

Supporting Online Material
www.sciencemag.org/cgi/content/full/316/5829/1288/DC1

10.1126/science.1142090

PHYSICS

Watching Electrons Break Up

A basic relation between heat and charge transport in metals is violated in some materials, which may offer insights into the high-temperature cuprate superconductors

Piers Coleman

Electrons are surprisingly rugged particles that fiercely maintain their identity in metals. As they move, they conduct heat and electric charge in all directions in a precisely fixed ratio, a universal property of electricity called the Wiedemann-Franz law. On page 1320 of this issue, Tanatar *et al.* (*1*) show that under the right conditions, metals can exhibit a new type of electrical conductivity for which the Wiedemann-Franz law no longer holds. Under these conditions, conventional electrons appear to live alongside a fundamentally different kind of electricity in which electrons have broken apart and reformed into a new class of charge- and heat-carrying excitation. Such failures of accepted laws in science often signal new and interesting underlying causes, and these results may help us understand the mechanisms behind high-temperature superconductors and other unusual materials.

In the 19th century, physicists empirically discovered two important laws governing the thermal and electrical properties of dense matter: the Dulong-Petit law and the Wiedemann-Franz law. At that time, most scientists believed that Dulong and Petit's law stating that the specific heat of all materials is a constant was a fundamental law of nature. Yet it was the failure of the Dulong-Petit law at low temperatures in the 20th century that helped to usher in the era of quantum mechanics (*2*). Early on, physicists did not understand the mechanisms behind the Wiedemann-Franz law, yet it went on to survive, and we know it now to be a consequence of the discrete quantum nature of electrons in electrical current.

In a normal metal, the quantum motion of electrons is very highly organized (see the left panel of the figure) and might be likened to the organization of aircraft traffic near a major airport. Just as airplanes are stacked by altitude, each in its own slot, electrons are tightly stacked in velocity up to a maximum value called the Fermi velocity. Electron traffic is controlled by quantum physics and the "Pauli exclusion principle" which prevents more than two electrons per velocity slot and helps electrons protect their identity, even as they jostle one another inside the electron cloud. As long as this organization holds, the Wiedemann-Franz law is expected to remain intact.

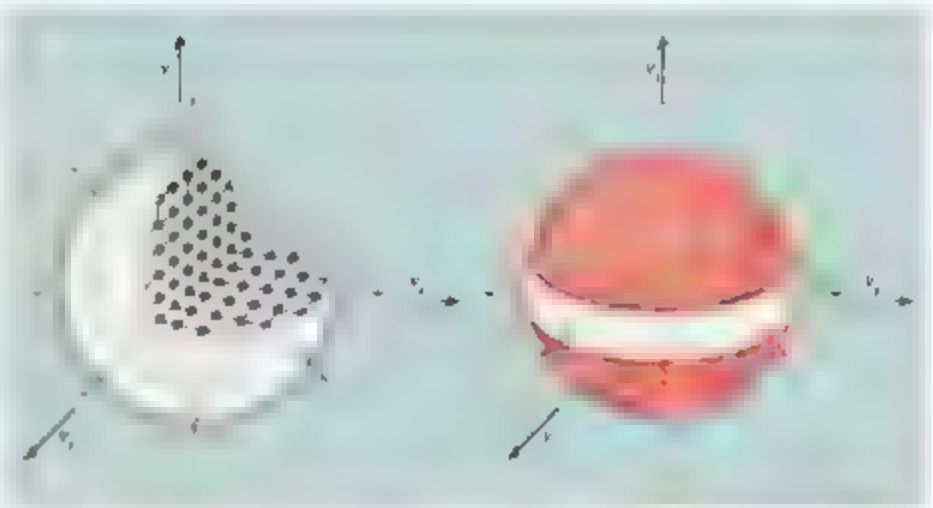

Electron flight patterns. (**Left**) Electrons in a conventional metal are highly organized swarm, in which each electron moves in its own specific velocity slot, filling each available slot up to a maximum, called the Fermi velocity. Excitations at the surface of this "Fermi sphere" carry heat and charge in a fixed universal ratio in all directions. (**Right**) In $CeCoIn_5$, well-defined electrons transport heat and charge in the x-y velocity plane, but transport in the z direction is far more turbulent. In these directions, electrons break up into new and as yet unidentified types of excitation that carry heat and charge in a different ratio from conventional electricity.

Today, physicists are seeking new ways to reorganize and control the motions of electrons inside dense matter and profoundly change their properties. One of the ideas being explored is to try reorganizing the electrons by increasing the strength of quantum fluctuations. These fluctuations are rooted in Heisenberg's uncertainty principle, which states that certain variables (such as energy and time, or position and momentum) can vary statistically as long as the product of the variations is constant. Thus, tightening the range of fluctuation in one variable will increase the fluctuations in another. Such fluctuations can be enhanced by tuning a metal to the brink of instability (via changes in temperature, composition, or applied fields), where it sits between one stable phase and another. Such a point of instability is called a quantum critical point (*3*–*5*), where the quantum fluctuations engulf the entire material. When this happens in a metal, the physics of the metal is found to change profoundly (*6*, *7*).

Tanatar *et al.* investigated whether electrons survive as well-defined particles in a metal that is tuned to such a quantum critical point—and to do so, they turned to the Wiedemann-Franz law. The material they chose to study is the metal $CeCoIn_5$ (*8*), which can be fine-tuned to a quantum phase transition by applying high magnetic fields (*9*). $CeCoIn_5$ is a layered "heavy fermion" metal in which the electron fluid is delicate and highly prone to instability. At low temperatures, $CeCoIn_5$ is a superconductor (*10*). When a magnetic field is applied, this material becomes a metal again, and just as it does so, it passes through a quantum critical point (*9*).

Tanatar *et al.* measured the heat and charge conductivity in different directions as the metal passes through this critical point. At high fields, they found that the material becomes a conventional metal, and the Wiedemann-Franz law is obeyed in all directions. But as the field is lowered, the temperature dependence of the resistance in this material changes profoundly, indicating that something has profoundly changed in the material. When they tuned the material to the quantum critical point, they found no change to the Wiedemann-Franz law when current flows parallel to the layers, but in directions perpendicular to the layers, the Wiedemann-Franz law was consistently found to be violated. By arranging conditions so the material

The author is at the Center for Materials Theory, Rutgers, The State University of New Jersey, Piscataway, NJ 08854, USA. E-mail: coleman@physics.rutgers.edu

CREDIT: ADAPTED BY K. NUEY/SCIENCE

approaches the quantum critical point. Tanatar *et al.* could literally "turn off" the Wiedemann-Franz law.

This failure of the Wiedemann-Franz law indicates a severe departure from our standard model of electricity at a quantum critical point. What is going on? Tanatar *et al.* propose an explanation inspired by high-temperature superconductors, in which x-ray measurements show that a continuous Fermi surface breaks up contiguous regions, separated by dead zones where well-defined electrons cease to exist (*10*). Tanatar *et al.* propose that at the quantum critical point, the Fermi surface of $CeCoIn_5$ breaks up into an annulus (see the right panel of the figure), supporting conventional charge and heat transport parallel to the planes of the crystal. But we still do not know what replaces the electron in the directions where the Wiedemann-Franz law fails.

It has taken more than 100 years to find a chink in the armor of the Wiedemann-Franz law, and this new discovery may herald a new understanding of how electricity can transform itself under extreme conditions. Some have suggested that in the fluctuating environment of quantum criticality, the electron actually breaks up into different components (*5*, *11*), it may even break up into separate spin and charge excitations (*12*, *13*). The idea that the electrons may break up into two different groups has also been advanced (*14*), but it is fair to say that no one anticipated this fascinating anisotropic separation into two components. Tanatar *et al.* can rule out some of these scenarios, but certainly not all. What is clear, however, is that at the quantum critical point, a new kind of electricity takes over, and we are only just beginning to understand its properties.

References and Notes

1. M. A. Tanatar *et al.*, *Science* **316**, 1320 (2007).
2. A. Pais, *Subtle Is the Lord: The Science and the Life of Albert Einstein* (Oxford Univ. Press, New York, 1982), chap. 20, pp. 389–401.
3. P. Coleman, A. Schofield, *Nature* **433**, 226 (2005).
4. A. J. Millis, *Phys. Rev. B* **48**, 7183 (1993).
5. Q. Si, S. Rabello, K. Ingersent, J. L. Smith, *Nature* **413**, 804 (2001).
6. H. von Löhneysen *et al.*, *Phys. Rev. Lett.* **72**, 3262 (1994).
7. N. D. Mathur *et al.*, *Nature* **394**, 39 (1998).
8. C. Petrovic *et al.*, *J. Phys. Cond. Mat.* **13**, 337 (2001).
9. J. Paglione *et al.*, *Phys. Rev. Lett.* **94**, 216602 (2005).
10. M. R. Norman *et al.*, *Nature* **392**, 157 (1998).
11. J. Custers *et al.*, *Nature* **424**, 524 (2003).
12. C. Pépin, *Phys. Rev. Lett.* **94**, 066402 (2005).
13. T. Senthil, S. Sachdev, M. Vojta, *Physica B* **359–361**, 9 [illegible].
14. S. Nakatsuji, D. Pines, Z. Fisk, *Phys. Rev. Lett.* **92**, 016401 [illegible].

15. The author thanks the NSF for support (grant DMR-0605935).

10.1126/science.1143504

IMMUNOLOGY

The Cutting Edge of T Cell Selection

The selection of T cells requires their exposure to a repertoire of peptides generated by an organelle whose structure is thymus-specific.

Michael J. Bevan

Why should a single cell type in a single organ of the body express a unique enzymatic component of a protein structure that is ubiquitously expressed? This is the puzzle posed by the study of Murata *et al.* on page 1349 of this issue (*1*), which shows that specific cells in the mouse thymus incorporate a distinct enzyme into their 20S proteasomes, the multicatalytic machine that degrades intracellular proteins to peptides. The answer to the puzzle lies in the special role played by these thymic cells in immune system development—that is, determining which immature T cells are selected to survive and populate peripheral lymphoid organs (spleen and lymph nodes), where they survey for unwanted pathogens and tumor cells.

The 20S proteasome is a barrel-shaped organelle composed of 14 different proteins in four stacks in the arrangement $\alpha(1-7)\beta(1-7)\beta(1-7)\alpha(1-7)$ (see the figure). Misfolded polypeptides in the cell interior are fed into the central bore of the proteasome, where three proteolytic components (β1, β2, and β5) cut them to pieces. The peptides pass out of the proteasome and transit into the endoplasmic reticulum, where a subset binds to the groove of nascent molecules called major histocompatibility (MHC) class I. The MHC-peptide complex folds into a mature structure that is transported to the cell surface, where the MHC molecule "presents" the peptide extracellularly. This process happens in all vertebrate cells, and in humans it is the means by which specific T cells (CD8$^+$ subtype) detect foreign antigens such as those encoded by a virus or by mutated self proteins.

MHC class I genes are enormously polymorphic, and each class I molecule has its own preferred peptide-binding motif to accommodate a different range of peptides 8 to 10 amino acids long (the polymorphism guards against a pathogen evolving away from producing sequences that bind MHC) (*2*). To ensure a best fit of the T cell receptor repertoire with foreign antigens outside the thymus, T cells within the thymus that bear receptors with low-binding affinity for one's own peptides (in the context of an MHC complex) are selected to survive. MHC class I molecules on the surface of thymus cortical epithelial cells select the CD8 T cell repertoire, whereas MHC class II molecules select the CD4 T cell repertoire (*3*).

Variation in the makeup and proteolytic specificity of thymus proteasomes has been noted previously (*4*). Murata *et al.* discovered a

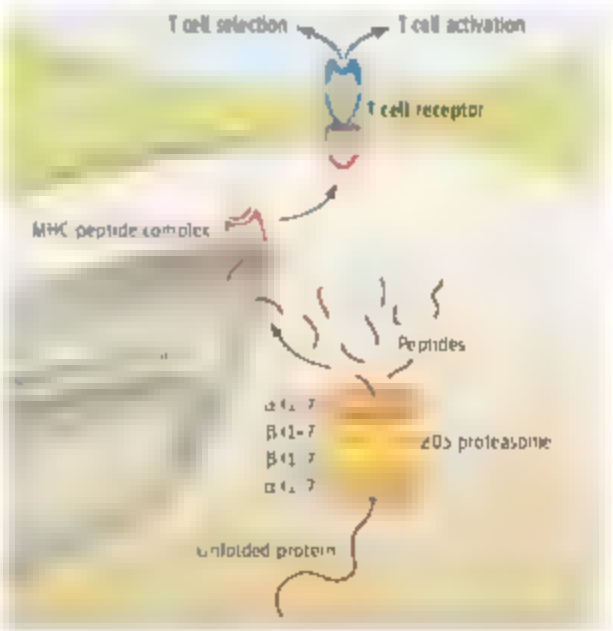

A degradation machine of its own. Proteasomes in the thymus contain a unique component that alters their proteolytic activity. This allows a range of peptides (bound to MHC molecules) to be expressed at the cell surface and function in T cell selection.

The author is at the Department of Immunology, Howard Hughes Medical Institute, University of Washington, Box 357370, Seattle, WA 98195, USA. E-mail: mbevan@u.washington.edu

CREDIT: K. HURVICH/SCIENCE

new catalytic proteasome subunit, designated β5t, expressed exclusively in mouse thymus cortical epithelial cells. It replaces the usual enzymatic component, with a resultant change in proteolytic specificity. In the "thymoproteasome," the chymotrypsin-like activity, which leaves hydrophobic residues at the C terminus of peptides, is dramatically reduced.

The peptide-binding motifs of many MHC class I molecules prefer a hydrophobic residue at the C terminus of bound peptides, raising the suspicion that the thymoproteasome may provide fewer peptides that fit snugly in class I grooves. The authors deleted the β5t-encoding gene in mice and found that although thymus architecture was normal and the development of CD4$^+$ T cells was not diminished, the number of mature CD8$^+$ T cells selected in the thymus decreased by 80%. Thus, the novel β5t component of the thymoproteasome enhances the selection of class I–restricted CD8$^+$ T cells. One obvious explanation for this result is that by decreasing the number of peptides with a hydrophobic C terminus, nascent MHC class I molecules become starved of snug-fitting peptides that stabilize the molecule for cell surface expression. This does not appear to be the case, however, because the expression level of class I molecules on the surface of normal and β5t-deficient epithelial cells is the same.

These new findings on proteasome specificity, MHC class I, and CD8$^+$ T cells are reminiscent of a previous analysis of lysosomal proteases and their effect on the selection of MHC class II–restricted CD4$^+$ T cells in the thymus (*5*). Most peripheral cells that express class II molecules use the enzyme cathepsin S, present in lysosomes, to assist in peptide presentation. In contrast, thymus cortical epithelial cells use lysosomal cathepsin L in place of cathepsin S. Deletion of the cathepsin L–encoding gene in mice reduced the efficiency of CD4$^+$ T cell selection without decreasing the overall level of class II molecule expression. In both cases—proteasomes, MHC class I, and CD8$^+$ T cells and the case of lysosomal proteases, MHC class II, and CD4$^+$ T cells—different cargoes of self peptides presented by MHC molecules in the thymus have a substantial impact on the selection of mature T cells.

The T cell receptor repertoire is not only molded by positive selection on MHC molecules presenting self peptides in the thymus, it is also subjected to negative selection to delete T cells with an affinity for self peptides that is high enough to potentially cause harmful autoimmune reactivity. It is assumed that low-affinity interaction between thymic epithelial cells bearing MHC–self peptide complexes and T cell receptors is required to positively select T cells for maturation, whereas an interaction with a high affinity leads to T cell deletion. In line with this, a number of MHC–peptide complexes have been defined that, on the basis of their affinity for the T cell receptor, can positively select but not delete T cells (*6*, *7*). It has been assumed that a T cell receptor repertoire with "not too high, not too low" affinity for self peptides can be selected without special rules for the peptides responsible for positive selection. However, if the thymus cortical epithelium expresses a unique range of self peptides as Murata *et al.* suggest, this raises the possibility that positive selection may be mediated by self antigens that are not seen outside the thymus (*8*). Such sequestration of the positively selecting peptide may provide a greater safety window between high and low affinity to better guard against activated T cells cross-reacting on self antigens and causing autoimmunity.

References

1. S. Murata *et al.*, *Science* **316**, 1349 (2007).
2. H.-G. Rammensee *et al.*, *Annu. Rev. Immunol.* **11**, 213 (1993).
3. A. W. Goldrath, M. J. Bevan, *Nature* **402**, 255 (1999).
4. A. Ito *et al.*, *Eur. J. Immunol.* **34**, 2681 (2004).
5. T. Nakagawa *et al.*, *Science* **280**, 450 (1998).
6. K. A. Hogquist *et al.*, *Cell* **76**, 17 (1994).
7. M. A. Daniels *et al.*, *Nature* **444**, 724 (2006).
8. P. Marrack, J. Kappler, *Science* **238**, 1073 (1987).

10.1126/science.1143806

ANTHROPOLOGY

Walking on Trees

Observations of modern orangutans suggest that human bipedalism may have evolved in the trees rather than on the ground

Paul O'Higgins and Sarah Elton

For decades, researchers have viewed standing upright and walking on the ground on two legs as defining features of the hominins (humans and our closest extinct relatives). However, we are beginning to learn that some apes in the Miocene (5 to 23 million years ago) not only had upright postures (*1*) but also incorporated bipedalism into their motion (*2*, *3*). Such movement may well have occurred in the trees. This raises the possibility that preadaptations for hominin bipedalism arose in arboreal settings rather than in terrestrial environments. On page 1328 of this issue, Thorpe and colleagues present compelling new evidence in support of this theory (*4*). Using observational data from modern orangutans they argue that hominin bipedal walking is not novel but rather a development of locomotor behaviors already established in the ancestor of great apes.

In modern orangutans, hand-assisted bipedalism with extended lower limbs in the small branches of the forest canopy allows movement on slender, springy supports. This enables the orangutans to access resources in the forest canopy that would otherwise be difficult to procure, or to cross between trees with minimum energy expenditure. These advantages might well have provided sufficient selective pressure for bipedal adaptations in arboreal habitats.

The orangutan model provides three scenarios for the emergence of modern great ape and human locomotor strategies from hand-assisted, straight-lower-limbed, arboreal bipedalism (see the figure). In the first, forest canopy fragmentation during the Miocene of Africa led to increased vertical climbing, rather than always crossing from tree to tree at canopy level. Thorpe *et al.* suggest that this climbing behavior, which is similar to knuckle walking, predisposed gorilla and chimpanzee ancestors to the independent acquisition of forms of knuckle walking. In the second scenario, orangutan ancestors in Southeast Asia became even more specialized in traversing at canopy level, the shrinking closed-canopy forest finally, hominins retained and further adapted preexisting arboreal bipedalism to exploit emerging, more open terrain between forested areas. This third scenario is consistent with the long forelimbs that are found in association with obviously bipedally adapted hindlimbs in various early hominins.

P. O'Higgins is at the Functional Morphology and Evolution Unit, Hull York Medical School, University of York, Heslington, York YO10 5DD, UK. E-mail: paul.ohiggins@hyms.ac.uk S. Elton is at the Functional Morphology and Evolution Unit, Hull York Medical School, University of Hull, Cottingham Road, Hull HU6 7RX, UK. E-mail: sarah.elton@hyms.ac.uk

It is necessary in a model such as this to simplify the nature and tempo of environmental change although Thorpe and colleagues do point out the probable fluctuations in forest coverage that occurred during the Miocene. Inevitably, past environments were complex, and there was no straightforward transition from forested to more open habitats. Primate adaptations and radiations were equally complex, and it has been argued (*5*) that apes diversified into a variety of environments well before any substantial Miocene forest shrinkage. Nonetheless, locomotion is strongly tied to habitat and therefore evolves in response to external pressures, whether they are caused by environmental change or by niche differentiation.

The work of Thorpe *et al.* reopens the debate about the origins of our own peculiar commitment to bipedal locomotion. To date, there is no consensus about the adaptive scenario that could have led to the adoption of terrestrial bipedalism. Many theories have been proposed, including the postural feeding hypothesis (*6*), a model (*7*) attributing bipedality to the social, sexual, and reproductive behavior of early hominins, in which bipedalism allowed better provisioning of offspring and enhanced reproductive fitness, the thermoregulatory hypothesis (*8*), where standing upright on two legs is argued to reduce the amount of the body directly exposed to sunlight, therefore allowing foraging during the hottest part of the day, and the appeasement model (*9*), which focuses on bipedal displays that allow for the relatively peaceful resolution of conflicts.

A similar lack of agreement is also evident in discussions about the locomotor behavior of the hominin ancestor. One possibility is that the common ancestor of humans and modern African apes knuckle walked on the ground (*10*), although it has been argued that the exact nature of knuckle walking differs among African great apes (*11*). Other proposed locomotor modes that could lead to adaptations for bipedalism include arboreal quadrupedalism (*12*), terrestrial quadrupedalism (*13*, *14*), climbing (*15*), and a hylobatian (gibbon-like) model (*16*) that suggests a small-bodied, arboreally bipedal ancestor of terrestrial bipeds.

Central to these debates is whether bipedalism arose in the trees and was taken to the ground, or whether it arose from an ancestor that was already terrestrial. The orangutan data presented by Thorpe and colleagues strongly suggest the former, and could also explain how hominin bipedality arose without needing to go through the stage of inefficient "bent-hip, bent-knee" bipedalism typical of modern chimpanzees. Crucially, the orangutan model also illustrates the way in which large-bodied primates could evolve straight-limbed bipedalism in arboreal contexts.

A number of fossils contemporary with the likely split of the chimpanzee-hominin and human clades, between 8 million and 8 million years ago, have been claimed to show anatomical evidence of upright posture and bipedal walking. These include *Sahelanthropus tchadensis*, *Orrorin tugenensis*, and two species of *Ardipithecus*. Although there is no general agreement on the locomotor and taxonomic affinities of these fossils (*17*), one possibility may well be that they are evidence of different ways of shifting from the ancestral type of hand-assisted arboreal bipedality proposed by Thorpe and colleagues. In later hominins, there is also evidence for locomotor diversity, within and between lineages. Limb proportions, for example, differ in *Australopithecus afarensis* and *Au. africanus* (*18*), and there is a range of foot morphologies in hominins from around the same time period (*19*). Thus, bipedal walking might have evolved independently in various early hominins. This could have occurred if multiple lineages originated from an earlier arboreal ancestor that used hand-assisted bipedalism. If that was the case, can anatomical evidence for bipedalism really be used as a crucial defining feature of hominins?

With the orangutan model, Thorpe and colleagues present a plausible and elegant argument in favor of the emergence of bipedalism in an arboreal rather than terrestrial context. In doing so, they have reinvigorated the debate over the emergence of behaviors preadaptive to bipedalism, and have shifted the focus back into the Miocene. A prediction of their model is that diversity of locomotor behaviors, including bipedalism and knuckle walking, could have arisen among descendants of an arboreally bipedal large ape. We must now question whether morphologies that indicate bipedalism can be used to identify hominins at the base of their radiation. This then raises the issue of whether

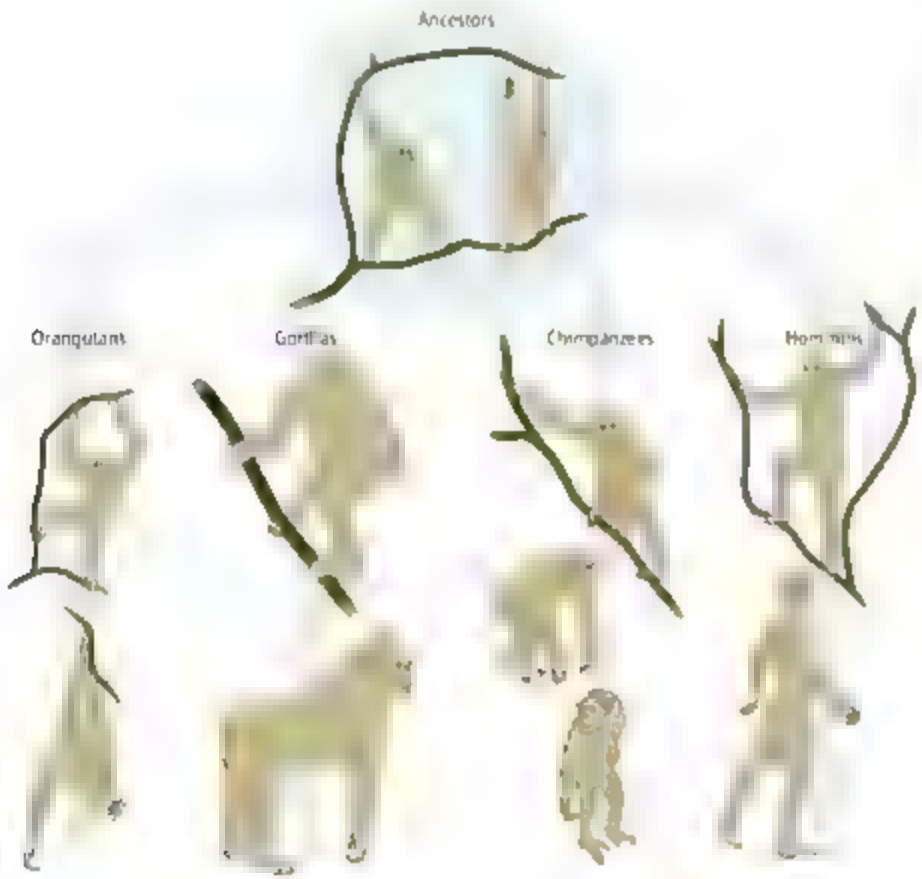

Learning the two-step. The locomotion of living great apes and humans derived from a large ancestral ape capable of hand-assisted arboreal bipedalism with extended lower limbs. Orangutan ancestors became arboreal specialists, moving mostly above-ground in tropical forests, whereas the ancestors of gorillas and chimpanzees, in response to changing and variable habitats, moved terrestrially in and out of trees, and thus independently acquired knuckle walking. Note the bent-hip, bent-knee bipedal posture of the chimpanzee, a necessary compromise that arose out of the biomechanical demands of vertical climbing. Hominins retained existing adaptations for extended-limb bipedalism and eventually became committed terrestrial bipeds.

we can unequivocally identify any traits that are truly diagnostic of early hominins (30)

References

1. L. M. MacLatchy, D. Gebo, R. Kityo, D. Pilbeam, *J. Hum. Evol.* **39**, 159 (2000)
2. L. Rook, L. Bondioli, M. Köhler, S. Moyà-Solà, R. Macchiarelli, *Proc. Natl. Acad. Sci. U.S.A.* **96**, 8795 (1999).
3. M. Köhler, S. Moyà-Solà, *Proc. Natl. Acad. Sci. U.S.A.* **94**, 11747 (1997)
4. S. R. S. Thorpe, R. L. Holder, R. H. Crompton, *Science* **316**, 1328 (2007)
5. P. Andrews, L. Humphrey, in *African Biogeography, Climate Change, and Early Hominid Evolution*, T. Bromage, F. Schrenk, Eds. (Oxford Univ. Press, Oxford, 1999), pp. 282–300
6. K. D. Hunt, *J. Hum. Evol.* **26**, 183 (1994)
7. C. O. Lovejoy, *Science* **211**, 341 (1981)
8. P. E. Wheeler, *J. Hum. Evol.* **21**, 107 (1991)
9. M. G. Jablonski, G. Chaplin, *J. Hum. Evol.* **24**, 259 (1993)
10. B. G. Richmond, D. R. Begun, D. S. Strait, *Yrbk. Phys. Anth. Appl.* **33**, 70 (2001)
11. M. Darroch, G. A. Macho, *J. Hum. Evol.* **36**, 171 (1999)
12. W. L. Straus, *Q. Rev. Biol.* **24**, 200 (1949)
13. D. L. Gebo, *Am. J. Phys. Anthropol.* **89**, 29 (1992)
14. E. E. Sarmiento, *Am. Mus. Novit.* **3091**, 1 (1994).
15. J. T. Stern, *Yrbk. Phys. Anthropol.* **18**, 59 (1975).
16. R. H. Tuttle, *Curr. Anthropol.* **15**, 389 (1974)
17. P. Andrews, T. Harrison, in *Interpreting the Past: Essays on Human, Primate and Mammal Evolution*, D. E. Lieberman, R. J. Smith, J. Kelley, Eds. (Brill Academic, Boston, 2005), pp. 103–121
18. B. G. Richmond, L. Aiello, B. A. Wood, *J. Hum. Evol.* **43**, 529 (2002)
19. W. E. H. Harcourt-Smith, L. C. Aiello, *J. Anat.* **204**, 403 (2004)
20. B. A. Wood, B. Richmond, *J. Anat.* **197**, 19 (2000)

10.1126/science.1143571

OCEAN SCIENCE

Burial at Sea

Insights into the mechanism that protects organic matter from degradation in the ocean will help scientists evaluate the Earth's carbon cycle

Jack J. Middelburg and Filip J. R. Meysman

Only about 0.4% of the carbon fixed by phytoplankton in the ocean surface is buried in oceanic sediments (see the figure). Yet, this burial has major consequences, because it links carbon pools that cycle fast (oceanic, atmospheric, and terrestrial) with sediment carbon pools that cycle on geological time scales. Burial of organic carbon in sediments represents a net carbon dioxide removal from, and oxygen (O_2) input into, the atmosphere. Without carbon burial, O_2 would not have accumulated in the atmosphere. Moreover, the small quantity of carbon transferred from surface to subsurface sediments supports prokaryotes that live deep in Earth's crust and that make up about 30% of the total living biomass on Earth (*1*).

It has been shown that the burial of organic matter in marine sediments is controlled by biological, chemical, and physical processes (*2*). However, explaining why some organic matter escapes mineralization, and what controls the mineralization rate, has proven to be a challenge. On page 1325 of this issue, Rothman and Forney (*3*) demonstrate that encapsulation of organic matter by clay materials—a process termed "physical exclusion"—plays a key role in determining the degradation rate of organic matter in marine sediments.

The degradability of organic matter is usually expressed in terms of a first-order rate constant *k*. Two decades ago, a synthesis of the available data revealed a clear trend: The reactivity decreases with increasing time scale following a power law (see the figure) (*4*). The challenge was to find a mechanism that could explain this pattern. The decrease in reactivity had to be a property of the organic matter and its relation with the environment. Boudreau and Ruddick (*5*) proposed a theory in which organic matter consists of a spectrum of reactive compounds, each with its own first-order rate constant *k*. However, this theory requires that one know the specific form of the reactivity distribution, a property that cannot be measured. Rothman and Forney now show that an inverse reactivity distribution is consistent with the power-law data. As a result, the new target is to find a proper explanation for the inverse reactivity distribution that underlies the power law.

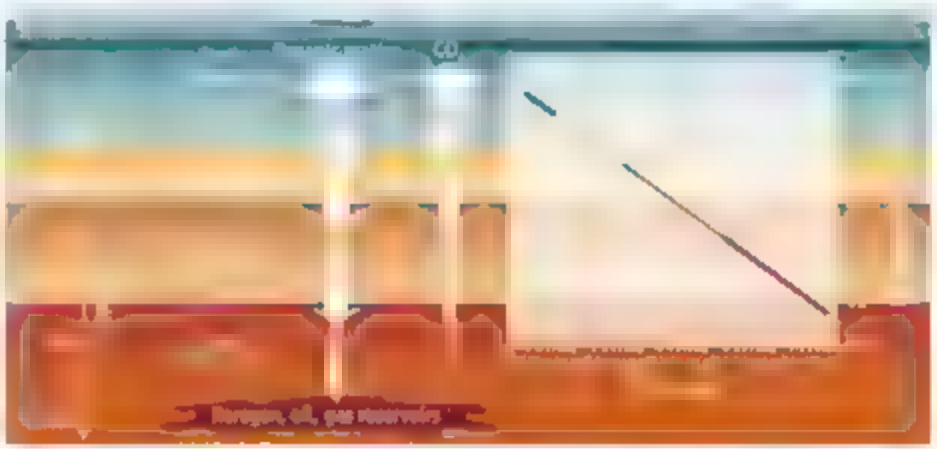

Carbon burial and degradation. Organic matter is transferred from the photic zone of the upper ocean to the sediments of the deep biosphere (**left**). During this transfer, organic matter is continuously degraded, yet the rate of degradation slows with time. Data from sediment cores, laboratory degradation experiments, and sediment traps show that the decay constant follows a power law with time (that is, with increasing depth in sediment) (*4*) (**right**). Rothman and Forney now propose a mechanistic model that explains this power law degradation behavior.

Three main factors govern organic matter degradation in sediments: the chemistry of the organic matter itself, the physical details of the sediment environment, and the biological agents that cause the breakdown of organic matter. Past explanations heavily favored either a chemical or a physical view, even though that the three factors often interact and their relative importance depends on the time scale (*2*, *6*).

In the strictly chemical view, organic matter consists of a range of molecules that differ in their chemical structure. These differences determine the kinetic rate by which they succumb to the attack of microbial enzymes, as a result, the more recalcitrant compounds are selectively preserved (*2*, *5*). In contrast, in the physical view, it is the environment that controls the rate at which organic matter degrades. One possible control mechanism is the availability of electron acceptors. When O_2 is present in the sediment, organic matter

The authors are at the Centre for Estuarine and Marine Ecology, Netherlands Institute of Ecology, 4401 NT Yerseke, Netherlands. E-mail: j.middelburg@nioo.knaw.nl; f.meysman@nioo.knaw.nl

tends to degrade more rapidly and the exposure time to O_2 thus seems to be crucial. In a second mechanism, the microbes or their digestive enzymes may be physically excluded from the organic material because the latter is enclosed in a mineral clay matrix.

In their model, Rothman and Forney focus on this physical-exclusion mechanism. They assume that organic matter consists of one chemical pool and propose a simple model for the behavior of digestive enzymes around a single microbe. When the enzymes diffuse away from the microbes, they are hindered by the physical sediment matrix. Fewer enzymes are found farther away from the microbe, where organic matter thus decays less rapidly. Limitation of enzyme supply to reactive organic matter eventually leads to the inverse reactivity distribution that explains the power law.

The model by Rothman and Forney provides a mechanistic underpinning of the empirical power law, adding confidence to predictions of organic matter degradation over time periods that are beyond experimental investigation (see the figure). Organic geochemists and microbial ecologists may find the underlying assumptions of the model too simplistic. However, the physical-exclusion hypothesis is supported by the compositional similarity of organic matter in sediments (*5*, *6*) and is a valuable first approach for linking microbes, enzymes, mineral particles, organic matter, and diffusion in sediments to a quantitative prediction of organic matter degradation over orders of magnitude. Such models are crucial for understanding and quantifying the turnover of prokaryotes that live deep in Earth's crust (*7*).

1. W. B. Whitman, D. C. Coleman, W. J. Wiebe, *Proc. Natl. Acad. Sci. U.S.A.* **95**, 6578 (1998).
2. B. J. Battage, *Chem. Rev.* **107**, 467 (2007).
3. D. H. Rothman, D. C. Forney, *Science* **316**, 1325 (2007).
4. J. J. Middelburg, *Geochim. Cosmochim. Acta* **53**, 1577 (1989).
5. B. P. Boudreau, B. R. Ruddick, *Am. J. Sci.* **291**, 507 (1991).
6. L. M. Mayer, *Mar. Chem.* **92**, 135 (2004).
7. J. F. Biddle *et al.*, *Proc. Natl. Acad. Sci. U.S.A.* **103**, 3846 (2006).

10.1126/science.1144001

ATMOSPHERIC SCIENCE

The Monsoon's Past

A sediment core from the Gulf of Guinea provides insights into changes in the African monsoon over the past 155,000 years

Philip A. Barker

Monsoons arise from the differential heating of land and oceans. Their strength and direction are governed by temperature and pressure differences between the land and ocean surfaces. Elucidating how the monsoon may have varied in the past therefore requires a suite of sea surface temperature and precipitation records from diverse oceanic and continental locations. On page 1393 of this issue, Weldeab *et al.* (*1*) report a new paleoclimate record from the Gulf of Guinea that contains evidence of oceanic conditions and continental monsoon precipitation over the past 155,000 years. The site is set to become important for understanding monsoon variation across West Africa, and the role of the tropical Atlantic in continental-scale climate forcing more generally.

The record, called core MD03-2707, is located in a region with limited upwelling from the deep ocean and with weak local currents. The site preserves a geographically integrated record that is largely unperturbed by local influences. This offshore location is thus of particular importance, because few long continental sedimentary records from West Africa are available.

Weldeab *et al.* have retrieved a high-resolution, well-dated geochemical record that spans the past 155,000 years and that they interpret as a proxy of monsoon changes at the millennial time scale (*1*). They use Ba/Ca ratios from planktonic foraminifera as evidence of freshwater discharge from the Congo River system. Ba concentrations are relatively high in the river as compared to the ocean. This and other cores from the region (*2*, *3*) show substantial changes in the rate of Congo discharge at millennial time scales. At present, the Congo discharges 1270 km^3 of fresh water per year (see the figure) (*4*) and also delivers key nutrients into the oceans, including silicon, whose biogeochemical cycle is emerging as an important climate feedback process (*5*). With greater discharges reconstructed for the past, the Congo's discharge would have variably seeded oceanic productivity.

While Ba/Ca ratios reveal river discharge, Mg/Ca ratios of foraminifera offer a proxy for sea surface temperatures in that vary independently of Ba/Ca, thereby enabling the role of sea surface temperatures on monsoon-driven runoff to be evaluated. Surprisingly, in the Gulf of Guinea, monsoon intensity and sea surface temperatures were decoupled for parts of the record. Enhanced freshwater inputs from the Congo were not

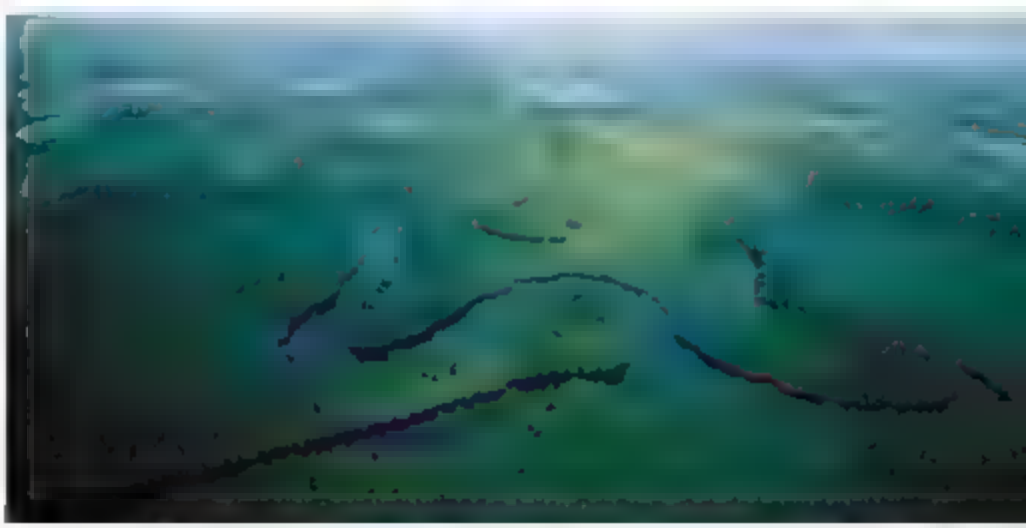

CREDIT: ROBERT CAPUTO/AURORA/GETTY IMAGES

Monsoon clues. This aerial view shows the Congo River winding through mangrove swamps near the mouth of the river. Today, the Congo River discharges 1270 km^3 of fresh water per year into the ocean. Weldeab *et al.* provide evidence that discharges have episodically been higher in the past, providing insights into changes in the African monsoon over the past 155,000 years.

The author is in the Department of Geography, Lancaster Environment Centre, Lancaster University, Lancaster LA1 4YQ, UK. E-mail: p.barker@lancaster.ac.uk

synchronous with interstadials (multimillennial warm periods within a broadly glacial period) in the Northern Hemisphere, but lagged sea surface temperatures by several thousand years during glacial-interglacial transitions. In contrast, sea surface temperatures changed at times when solar insolation received in tropical latitudes changed drastically as a result of changes in Earth's orbit.

These findings demonstrate the importance of considering both atmospheric and oceanic circulation systems that can force changes at different time scales in disparate locations. Consider, for example, the Younger Dryas (12,700 to 11,500 years ago), when Earth's climate system reverted back to near-glacial conditions during the period of post-glacial warming. During this time, Weldeab *et al.* observe a substantial stepwise reduction in Congo discharge, but the record does not show a similar reduction in sea surface temperature. This is in marked contrast to the Cariaco Basin record from the western equatorial Atlantic, where sea surface temperatures were low throughout the Younger Dryas (*6*, *7*). Instead of a direct control from sea surface temperatures, Weldeab *et al.* suggest that an atmospheric reorganization in the North Atlantic may have been propagated by meridional circulation systems to reduce monsoon intensity.

At the multimillennial time scale, discharge rates from the Congo Basin are found to be positively related to warmer episodes of the past 155,000 years. This result concurs well with findings from continental African sites—including Lake Bosumtwi, Ghana, a meteorite impact crater with sediments accumulated over the course of 1 million years that is the current focus of an International Continental Drilling Programme project.

The past 30,000 years from Lake Bosumtwi (*8*) have become a cornerstone of African paleoclimate research and offer a useful terrestrial comparator to the Congo discharge record. Reduced freshwater discharge occurred during the Last Glacial maximum, when large parts of Africa were relatively dry. Dry conditions persisted in most regions until about 15,000 years ago, when Congo discharge and the levels of many African lakes, including Bosumtwi, began to increase dramatically. DeMenocal *et al.* have hypothesized that the disproportionate intensification of monsoon precipitation after 15,000 years was triggered by a threshold response to rising insolation (*9*). Discharge from the Congo peaked around 10,500 years ago, at a time when Lake Bosumtwi was at its maximum and was overflowing.

More puzzling is the gradual and continuous decline in Congo discharge from the early Holocene maxima shown by the new data. This gradual transition differs from the much more abrupt shift from wet to dry conditions about 5000 years ago shown in many lake-level curves and offshore dust records (*9*). Vegetation dieback as the climate dried could increase erosion potential and therefore dust supply in a stepwise fashion. The more abrupt response shown by lake data might either be due to the sensitivities of the climate proxies used in the reconstructions or could indicate differences in the rate of precipitation decline between central equatorial Africa and neighboring regions.

Hydrological changes in the tropics amplify global climate changes through regulation of water vapor, change in heat transport, methane release from wetlands, and shifts in surface albedo. Spatial differences in hydrological variability will be unveiled as more sites like the Gulf of Guinea and high-resolution continental sites are investigated. There is abundant evidence of the tropics responding to changes driven from higher latitudes, but there are also suggestions from some sites that change in tropical regions may take the lead. For example, a shift toward greater aridity occurs in several African lakes 200 to 400 years before the well known cold interval at 8200 years before present (*8*) found in Greenland (*10*) and many northern temperate records. Similarly, well-dated continental records extending to before the Eemian interglacial (more than 135,000 years ago) are beginning to suggest a tropical lead out of glaciation through either generation of greenhouse gases from wetland expansion or strengthened meridional circulation (*11*).

Data of high temporal resolution from prized localities challenge the modeling community to resolve the climate dynamics behind ocean-continent interactions.

References

1. S. Weldeab, D. W. Lea, R. R. Schneider, N. Andersen, *Science* **316**, 1303 (2007).
2. E. Schefuß, S. Schouten, R. R. Schneider, *Nature* **437**, 1003 (2005).
3. F. Marret, J. Scourse, G. Versteegh, J. H. F. Jansen, R. Schneider, *J. Quat. Sci.* **16**, 761 (2001).
4. A. Dai, K. E. Trenberth, *J. Hydrometeorol.* **3**, 660 (2002).
5. D. J. Conley, *Global Biogeochem. Cycles* **16**, 1121 (2002).
6. K. A. Hughen, J. T. Overpeck, L. C. Peterson, S. Trumbore, *Nature* **380**, 51 (1996).
7. D. W. Lea, D. K. Pak, L. C. Peterson, K. A. Hughen, *Science* **301**, 1361 (2003).
8. J. M. Shanahan *et al.*, *Palaeogeogr. Palaeoclimatol. Palaeoecol.* **242**, 287 (2006).
9. P. deMenocal *et al.*, *Quat. Sci. Rev.* **19**, 347 (2000).
10. R. B. Alley *et al.*, *Geology* **25**, 483 (1997).
11. M. H. Trauth, A. L. Deino, A. G. N. Bergner, M. R. Strecker, *Earth Planet. Sci. Lett.* **206**, 297 (2003).

10.1126/science.1143451

PLANT SCIENCE

Infectious Heresy

J. Allan Downie

Rot a l symbiotic bacteria that fix nitrogen for legumes do so by secreting a specific nodule initiating factor. Two strains use an alternative strategy.

Leguminous plants, such as peas and soybeans, enter into a symbiotic relationship with soil bacteria called rhizobia. For years it has been the accepted wisdom that Nodulation (Nod) factors secreted by rhizobia enable them to infect a legume and initiate formation of nodules on the host plant's roots. Within these nodules, the bacteria convert free nitrogen to ammonia, which the plant uses for its growth. On page 1307 in this issue, Giraud *et al.* (*1*) provide evidence that overturns this orthodoxy. They determined that the genomes of two strains of legume-nodulating rhizobia do not contain genes that are necessary for the synthesis of Nod factors. This means that these bacteria must have an alternative way of initiating the dialogue that results in legume nodulation.

The symbiosis between legumes and rhizobia is an agriculturally important relationship because such legumes grow well without added nitrogen fertilizer. Nod factors activate a plant signaling pathway that induces oscillations in the concentration of intracellular calcium (called calcium spiking). Calcium spiking triggers the expression of genes that are required for nodule morphogenesis in roots (*2*). Nodulation is intimately linked with the establishment of threadlike structures that convey rhizobia into nodule cells (see the figure).

The two rhizobia (ORS278 and BTAi1) sequenced by Giraud *et al.* are unusual because they induce nodule formation on both stems and roots of some legumes. Stem nodulation can occur on some legumes that undergo periods of flooding, which enables

The author is in the Department of Molecular Microbiology, John Innes Centre, Norwich NR4 7UH, UK. E-mail: allan.downie@bbsrc.ac.uk

colonization of stems by rhizobia. Another oddity is that these strains engage in photosynthesis and contain a cluster of photosynthesis-related genes that are similar to those found in closely related photosynthetic bacteria. However, the real surprise is that neither strain contains *nodA* or *nodC* genes, which are essential for the synthesis of Nod factors. NodC produces chain oligomers from uridine 5′-diphosphate *N*-acetylglucosamine, and NodA transfers a long-chain acyl group onto the chain molecules to form a core Nod-factor structure which can then be modified by other *nod* gene products (*3*).

How do ORS278 and BTAi1 infect and induce development of nitrogen-fixing nodules on their hosts, the aquatic legumes *Aeschynomene sensitiva* and *Aeschynomene indica*? Not only are these bacteria unusual, but so are these legumes. To demonstrate this, Giraud *et al.* used a *nod*-gene containing *Bradyrhizobium* strain (ORS285), which nodulates other legumes in addition to *A. sensitiva*. Mutation of the *nod* genes in ORS285 does not affect nodulation of *A. sensitiva* but does block nodulation of the other legumes. This shows that unlike the other legumes, *A. sensitiva* can respond to a rhizobial signal other than Nod factor.

How does *A. sensitiva* induce nodule development without Nod-factor signaling? An important clue comes from recent work on legume mutants that spontaneously form nodules in the absence of any bacteria or Nod factors. Constitutive activation of lotus histidine kinase 1 (LHK1), a cytokinin hormone receptor (*4*) that is required for nodulation (*5*) in the legume *Lotus japonicus*, results in spontaneous formation of nodules in the absence of rhizobia or Nod factors. This activated cytokinin receptor appears to bypass several of the early steps in the Nod factor–activated signaling cascade, including the gene products required for calcium spiking (*4*). Other evidence supporting a nodulation role for cytokinins is that a strain of *Sinorhizobium meliloti* that lacks Nod factor but is genetically engineered to secrete a cytokinin, can initiate nodule morphogenesis (*6*). Also, treatment of certain legumes with cytokinins induces the expression of several genes that are expressed during normal nodule development (*7*).

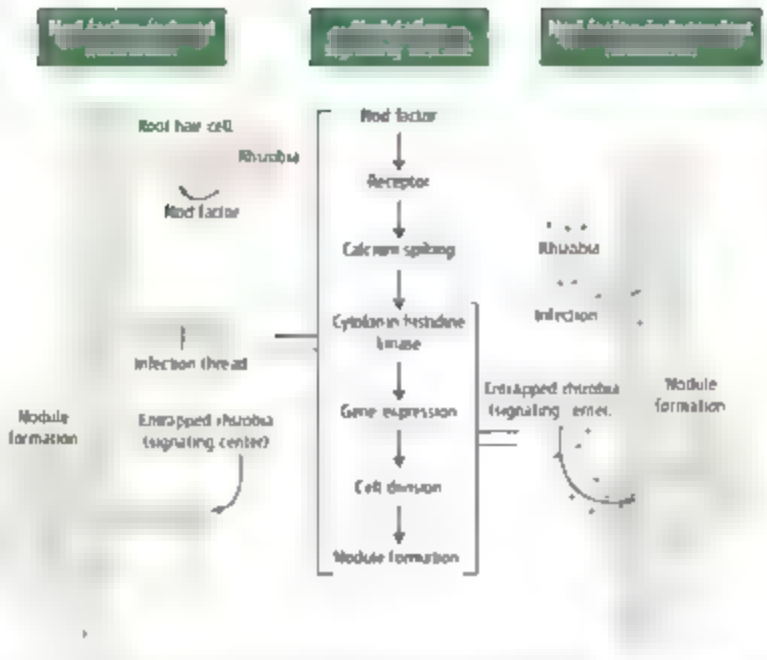

Getting, or not getting, the Nod. Nod factors produced by symbiotic bacteria infect the legume host and initiate the formation of nitrogen-fixing nodules (**left**). Nod factor–independent nodulation may result from rhizobial colonization through cracks in the root epidermis (**right**). Increased sensitivity to a cytokinin-like signal may allow part of the normal Nod-factor signaling cascade (**middle**) to be bypassed, leading to nodulation and infection in the absence of Nod factors.

To identify the signal that ORS278 and BTAi1 use to initiate nodulation, Giraud *et al.* screened for mutants of ORS278 that could not induce nodule formation in *A. sensitiva*. Although no mutants completely defective for nodulation were found, some were greatly impaired for nodulation. Several of these mutants had defective purine biosynthesis. Because plant cytokinins are derived from the purine adenine, this suggested that the bacterial mutants might produce smaller amounts of a cytokinin (or cytokinin precursor) that initiates nodulation. Supporting a possible role for such a signal during conventional nodulation is the observation that other rhizobia carrying mutations in purine biosynthesis are defective for infection of nodules in common legumes (*8*). Furthermore, proteins similar to a previously unrecognized plant cytokinin-activating enzyme, encoded by the rice *LONELY GUY* gene, may be present in agrobacteria (*9*). However, in the absence of a mutant that is completely nodulation defective, Giraud *et al.* cannot formally distinguish between a signal that activates the entire nodulation signaling pathway or a signal that bypasses the signaling pathway by stimulating production of a cytokinin.

If Nod factors are not required for nodulation in some legumes, why should the Nod factor–induced nodulation pathway be so predominant? Formation of nitrogen-fixing nodules requires rhizobial infection, and this requires entrapment of the bacteria. During "conventional" infection, Nod factors induce root-hair deformation, leading to bacterial entrapment. Subsequent growth of infection threads requires modification of Nod factors (as specified by *nod* genes), and probably increased concentrations of Nod factors. In some legumes, however, bacteria gain entry to roots through cracks in the epidermis, often at the sites where lateral roots emerge. In another well-studied stem-nodulating legume (*Sesbania rostrata*), this type of infection shows much less specificity for Nod-factor structure, although it does require some type of Nod factor (*10*). The mode of infection of *A. sensitiva* and *A. indica* by ORS278 and BTAi1 shows similarities to that seen in *S. rostrata*. Such entry through cracks may allow bacteria to accumulate and form a "signaling center" (*10*) that can induce nodulation and infection (see the figure). Nodule development could occur if a cytokinin-type signal accumulates in such a signaling center and bypasses the early Nod-factor signaling pathway. However, induction of infection-thread growth without Nod factors is highly unusual. Therefore, for both nodule and infection-thread development to occur in this system implies that *A. sensitiva* and *A. indica* may enhance intercellular colonization by bacteria and/or be unusually sensitive to some bacterially made signal. Whether this signal is a cytokinin or not remains to be established.

References

1. E. Giraud *et al.*, *Science* **316**, 1307 (2007).
2. G. E. D. Oldroyd, J. A. Downie, *Nat. Rev. Mol. Cell Biol.* **5**, 566 (2004).
3. H. P. Spaink, *Annu. Rev. Microbiol.* **54**, 257 (2000).
4. L. Tirichine *et al.*, *Science* **315**, 104 (2007).
5. J. D. Murray *et al.*, *Science* **315**, 101 (2007).
6. J. B. Cooper, S. R. Long, *Plant Cell* **6**, 215 (1994).
7. P. R. Gargantini *et al.*, *Planta* **48**, 843 (2006).
8. J. D. Newman, R. J. Diebold, B. W. Schultz, K. D. Noel, *J. Bacteriol.* **176**, 3286 (1994).
9. T. Kurakawa *et al.*, *Nature* **445**, 652 (2007).
10. S. Goormachtig, W. Capoen, M. Holsters, *Trends Plant Sci.* **9**, 1360 (2004).

10.1126/science.1143870

Large-Scale Spatial-Transmission Models of Infectious Disease

Steven Riley

During transmission of seasonal endemic diseases such as measles and influenza, spatial waves of infection have been observed between large distant populations. Also, during the initial stages of an outbreak of a new or reemerging pathogen, disease incidence tends to occur in spatial clusters, which makes containment possible if you can predict the subsequent spread of disease. Spatial models are being used with increasing frequency to help characterize these large-scale patterns and to evaluate the impact of interventions. Here, I review several recent studies on four diseases that show the benefits of different methodologies: measles (patch models), foot-and-mouth disease (distance transmission models), pandemic influenza (multigroup models), and smallpox (network models). This review highlights the importance of the household in spatial studies of human diseases, such as smallpox and influenza. It also demonstrates the need to develop a simple model of household demographics, so that these large-scale models can be extended to the investigation of long–time scale human pathogens, such as tuberculosis and HIV.

Outbreaks of directly transmitted infectious diseases of humans have the potential to become pandemics, causing extensive morbidity and mortality (*1*, *2*). Even when widespread transmission is averted, a multicountry outbreak can have a disproportionately large negative economic impact at a regional level (*3*). Similarly, in domestic animals, the need to maintain livestock movements against a background of epidemics is a major concern for policy-makers who are trying to control economically important pathogens (*4*). It would be unusual for naturally occurring disease emergence or nondeliberate disease importation to occur simultaneously at many locations. Therefore, infectious individuals are necessarily clustered in space during the initial phase of sustained transmission. If containment is possible, this initial clustering provides an opportunity to make effective use of limited resources for intervention.

Many types of host heterogeneity influence host-pathogen interactions at the scale of the individual, such as genetics, age, sexual activity, location, and typical movement patterns. Sometimes, these factors are important at larger scales and sometimes they are not (*5*). Consider heterogeneities in the location and movement of hosts during outbreaks of directly transmitted infectious diseases of humans. The vast majority of hosts spend a substantial proportion of their time at a single location: that is, at home or in the herd. When cases arise, their location is often reported rapidly. Furthermore, for many populations, accurate census data with which to examine spatial population distributions are available. For humans, an accurate estimate of population density is available for the entire Earth, up to a resolution of 1 km sq. (*6*). Typical movement patterns of hosts are also important. For directly transmitted pathogens, an infectious individual must be close to a susceptible individual for infection to occur. Therefore, the probability that an infectious individual from one home location infects a specific susceptible individual from another is influenced greatly by the journeys made away from home by both infectious and susceptible individuals during the period of infectiousness. For many populations, data sets from which typical movement patterns can be accurately inferred are now available (*7*, *8*).

Spatial models of infectious disease transmission provide the only plausible experimental system in which knowledge of the location of hosts and their typical movement patterns can be combined with a quantitative description of the infection process and disease natural history to investigate observed patterns and to evaluate alternative intervention options. As such, the use of these models will increase as spatially heterogeneous interventions are considered more frequently and as spatially resolved incidence data are made available for more pathogens (the best currently available data sets cover notifiable childhood diseases in developed countries). However, one problem is that these models can be seductive to policy-makers. Realistic population densities permit results to be presented as maps and movies, and although these formats are useful to describe spatiotemporal incidence patterns, their visual impact conveys credibility that may not be justified. Rather, the underlying structure of each transmission model should be appropriate for the infection process, the potential interventions, and most important, the specific hypotheses that are under consideration.

In this review, I highlight results from different diseases (Fig. 1) that use different methodologies (Fig. 2). I did not include more analytically sophisticated approaches (*11*), because they have only rarely been applied to the dynamics of infectious disease in realistically structured populations of animals (*4*, *12*).

Measles and Patch Models

Measles is a disease that requires government notification in England and Wales, for which district-level data are available for each bi-weekly period from 1948 onward. Two intriguing epidemiological features of this rich data set have been explained, with the help of patch models (or spatial metapopulation models) (Fig. 2): (i) the longer-than-expected period of fade-out after the start of mass vaccination in 1968 (*13*, *14*) and (ii) the apparent waves of infection observed before and after vaccination (*15*). In these studies, large amounts of detailed data and sophisticated descriptive statistics (e.g., wavelets) were used in conjunction with very simple (illustrative) models to demonstrate the plausibility of dynamical explanations. The example of spatial heterogeneity of transmission observed in (*15*) was illustrated with the use of 16 patches of two types (urban or semiurban) arranged in a line. A refined version of this methodology has been used to show that state-scale spatial patterns of excess human mortality attributed to pneumonia and influenza in the United States are consistent with human travel patterns (*16*). This latter study highlights the computational efficiency of patch models over individual-based approaches, that is, it was possible to include the transmission model within the incidental framework because solutions could be obtained so efficiently.

Patch models have also been used to investigate aspects of global disease spread (*8*, *9*, *16*), largely motivated by the 2002–2003 outbreak of severe acute respiratory syndrome (SARS). The availability of disease incidence data at the national level and the accuracy with which contemporary global travel is described by airline-ticket data (*17*) make this topic well suited to the use of computationally efficient patch models. For example, the observed size of country outbreaks of SARS during 2003 is largely consistent with model outcomes (*9*), although mainland China was not included, and temporal variation in the underlying rate of transmission was assumed to be the same in every country as that observed in Hong Kong and Singapore.

Similar studies have investigated the potential impact of reduced travel on the rate of international disease spread during an influenza pandemic (*8*, *16*). A theoretical model of 100 identical populations suggests that even the most stringent border controls (>99% effective) would delay global spread of a novel influenza strain by only a few weeks (*16*). This result is supported by a study of 52 globally connected cities (*8*), which was validated using travel and

Department of Community Medicine and School of Public Health, Faculty of Medicine, University of Hong Kong, Hong Kong, Special Administrative Region, People's Republic of China. E-mail: steven.riley@hku.hk

disease data from the 1968 1969 pandemic (*18*, *19*).

Foot-and-Mouth Disease and Distance Transmission

The 2001 foot-and-mouth disease (FMD) outbreak in the United Kingdom resulted in the slaughter of 4.2 million animals and produced a severe negative economic impact in the affected districts (*20*). During the outbreak and afterward, various stakeholder groups disagreed over the relative merits of spatial culling and vaccination strategies. Largely because updated case data were made available to researchers early in the course of the outbreak, statistical and mathematical models were developed rapidly enough to be of use in policy formulation while the outbreak was underway (*4*, *12*, *21*, *22*).

The availability of spatially resolved farm census data, with unique identifiers that were consistent with the case database, encouraged one research team to formulate a spatially explicit distance-transmission model (Fig. 2) of FMD, with farms as the individual units of infection (*21*). The infection kernel for FMD in the United Kingdom in 2001 was estimated directly from case data (*4*, *21*) and used in a distance-transmission model (Fig. 2) to assess the marginal benefits of refinements to culling strategies, such as reducing the average delay from report to culling of index premises (IPs) and additional preemptive culling of contiguous premises (*21*). Initial results using this spatially explicit approach helped to validate those from an earlier pair-correlation model (*4*), in which properties of an implicit spatial network were approximated with ordinary differential equations. This series of studies (*4*, *12*, *21*, *22*), conducted while the outbreak was in progress, demonstrates the potential benefits to policymakers of multiple research teams addressing similar questions using alternative methodologies.

The precise location of individual farms in distance-transmission models of FMD facilitated the investigation of highly structured spatial interventions that could not be considered in pair-correlation models, for instance, vaccination of a barrier region to protect large pools of susceptible farms (*21*), prophylactic vaccination of high-risk farms (*23*), reactive ring vaccination (*23*), preemptive vaccination of nearby farms thought to be most susceptible to infection (*23*), and vaccination of an annulus around infectious farms (*24*). However, the logistical implications of constantly revising a large vaccination queue would be substantial. Therefore, a more straightforward strategy was specified: to prioritize farms for vaccination based only on their proximity to IPs reported in the previous 10 days or to dangerous contacts of those IPs. This latter strategy was shown to be the most effective in terms of reducing the expected number of animals that would be culled (*24*).

Pandemic Containment and Groups

In the event of sustained human-to-human transmission of a novel strain of influenza, public health interventions should ideally attempt to contain the outbreak at the source. The transmission of influenza between individual human hosts occurs over much smaller distances than does the transmission of FMD between farms. Therefore, spatial multigroup models have an advantage over pure distance-transmission models when used to investigate influenza containment because they explicitly represent the actual locations (such as households, schools, and workplaces) in which interventions will be used to reduce transmission (Fig. 2). The household is particularly important because relatively static groups of hosts (families) spend prolonged periods together in this setting.

The basic reproductive number R_0 is used to quantify the transmissibility of an infectious disease and is defined as the average number of secondary cases generated by one typically infectious individual in an otherwise susceptible population (*76*). Two studies of influenza based on models that include a multigroup component suggest that the spatially targeted use of antivirals in rural Asia, in addition to other control measures, has a greater than 90% probability of containing pandemics with basic reproductive numbers $R_0 < 1.9$ (vaccination not included) (*26*) or $R_0 < 2.4$ (partial vaccination coverage included) (*27*). In addition to recent estimates of R_0 for influenza that fall in this range (*26*, *28*), these findings led to the addition of containment as an objective of the World Health Organization (*29*).

The results from these independent studies are difficult to compare, owing to the many interventions considered and to the principal objective of both, which was to demonstrate feasibility, rather than optimality. However, the two models simulated quite different spatial infection processes, as reflected by their assumed force of infection (FOI) (the hazard of infection experienced by susceptible individuals). In (*26*), although most individuals belonged to a household and to either a school or a workplace, only two-

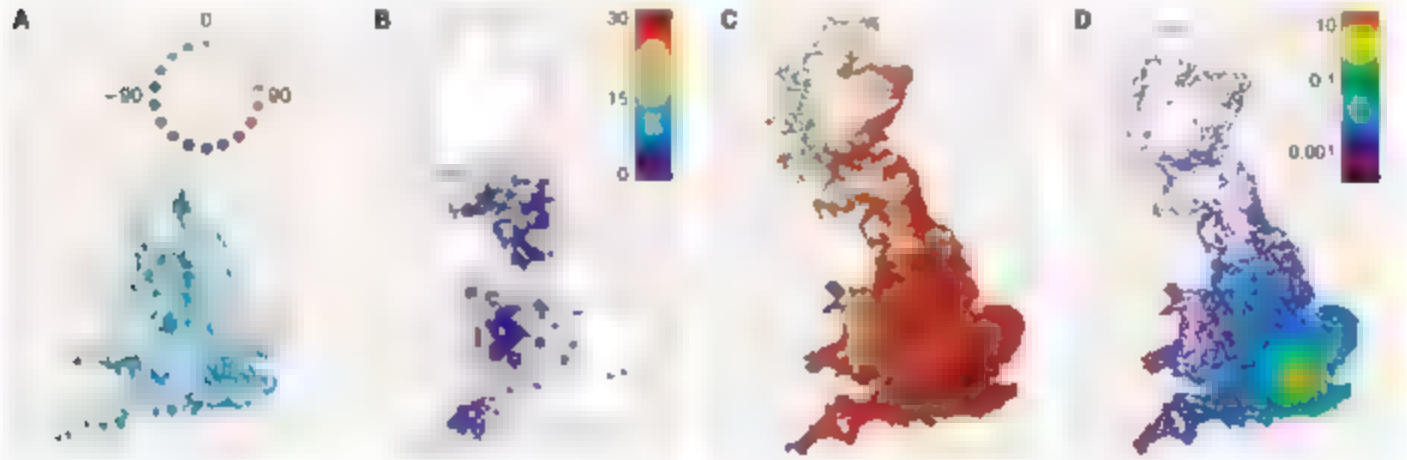

Fig. 1. Patterns of disease transmission in the United Kingdom. (**A**) Wavelet analysis of prevaccination measles epidemics in 954 locations in England and Wales [reproduced with permission from (*25*)] shows how London (black box) drove the epidemics in most of the country, with the exception of the Manchester-Liverpool urban concentration (upper left). (**B**) Simulations show the three high-risk areas [adapted with permission from (*21*)] for FMD in the United Kingdom in 2001. The key indicates the average number of cases in a 10-by-10–km square from 100 model realizations. (**C**) A novel strain of influenza [reproduced with permission from (*34*)] would spread rapidly though the United Kingdom during a global pandemic. Only 75 days after the arrival of the first cases from overseas, the intensity of red color shows the relative concentration of infectious individuals, and green indicates that the epidemic is already over in some small communities. (**D**) In contrast, even under a pessimistic transmission scenario, 75 days after 10 initial seeds became infectious with smallpox in London [adapted with permission from (*33*)], there would have been relatively few cases, and the degree of spatial correlation would still be striking (same key as in (B) but with 5-by-5–km squares).

thirds of the disease transmission occurred in these settings. The remaining third occurred randomly, as a function of the distance from infectious individuals. In contrast, individuals in the model used in (*27*) belonged to multiple groups. In addition to households, schools, and workplaces, The inclusion of these extra settings was an alternative to the distance-transmission component used in (*26*). Although both approaches require parameters for which there is little or no supporting empirical data, the model used in (*26*) could be viewed as more parsimonious because its conclusions are less sensitive to these uninformed parameters, and it made good use of the data that were available, such as spatially resolved population density and travel survey data.

Model design choices such as these can have a substantial impact on predictions of intervention efficacy. For example, in (*27*), targeted antiviral prophylaxis implicitly assumes that household clusters and small neighborhoods that are important in transmission could be easily identified, resulting in a relatively low upper bound of 1 million courses of treatment required for containment. Conversely, the spatial recruitment of households into the intervention processes proposed in (*26*) implicitly assumed a weaker correlation between antiviral distribution and transmission, resulting in the more conservative estimate that 3 million courses of treatment would be required to achieve containment.

Smallpox and Networks

Patch, distance kernel, and multigroup models can all be considered as special cases of spatial-network models, in which nodes represent individual hosts and arcs represent potentially infectious links. As networks, all of the model pathogen combinations described above would have high average numbers of arcs per node (i.e., a large neighborhood size) relative to their basic reproductive number R_0. However, for smallpox, intimate contact was almost always required for transmission to occur (*30*). Therefore, it is necessary to represent a substantial proportion of smallpox transmission as occurring over a static network with a relatively small neighborhood size. This approach was used (*31*) to show that for the United Kingdom, the additional benefits of geographically targeted regional vaccination would not outweigh the adverse effects of vaccinating many low-risk individuals. Specifically, contact tracing with isolation and vaccination alone would probably result in fewer deaths from a small initial cluster of cases in London than would occur if geographically targeted regional vaccination was used in addition to such a policy.

Perhaps the most innovative modeling approach to emerge from smallpox epidemiology (*27*) is the derivation of static contact networks from individual-based second-by-second microsimulations (*e.g.*, *33*), all of the people, locations, and journeys in the city of Portland, Oregon, were simulated explicitly. Simple rules were then used to construct static contact networks from dynamic networks of individuals and locations. For example, if two individuals were present in the same location for more than an hour, it was assumed that a social contact existed between the two. Because the intensity of contact was assumed to be similar in all locations, implicitly, people's behavior in supermarkets (with respect to disease transmission) was assumed to be the same as in the home. This uniformity of contact intensity is unrealistic and must have resulted in overly connected social networks. However, when good data are available on the relative transmissibility of respiratory pathogens in different social settings, the derivation of large spatial contact networks from microsimulations will provide a natural refinement of the distance-transmission approach described above.

Current Challenges

Some of the individual-based spatial models described above include age classes and house-

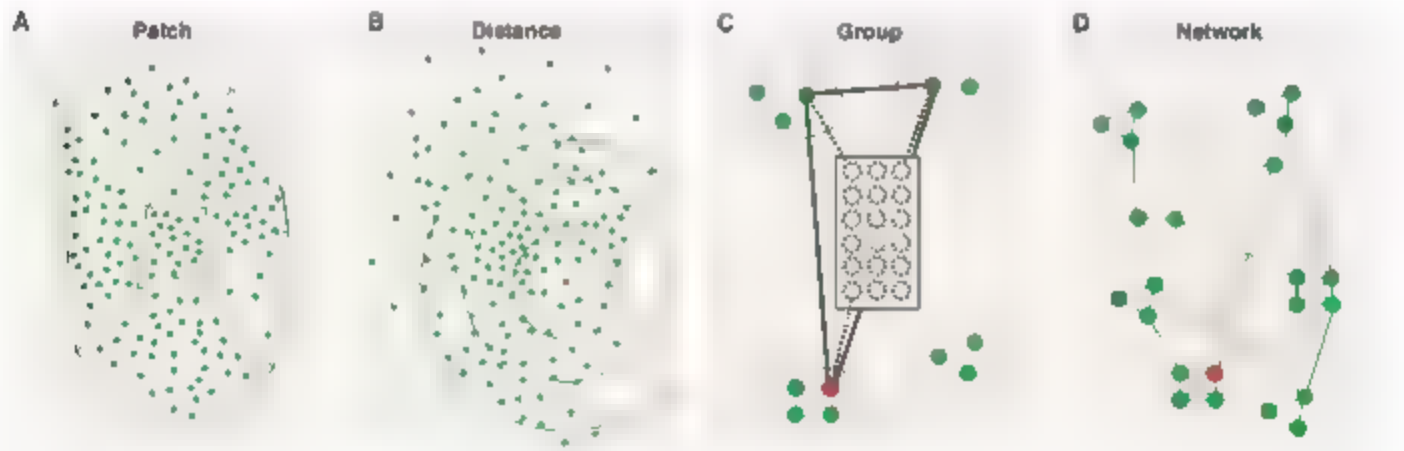

Fig. 2. Four common abstractions for the spatial transmission of infectious diseases. Differences between these approaches are best understood in terms of the FOI, which is location-specific in spatially explicit models. Red dots represent infectious individuals. (**A**) For patch transmission, all members of the same patch (residents of a town, for example) receive the same FOI, which is a function of the distance from their home patch to other patches and of the prevalence of infection in all patches. (**B**) Distance transmission is explicitly individual-based; that is, each farm is assigned a precise location. It is assumed that any given infectious individual can infect all susceptible individuals within range. The pairwise probability of infection is usually a monotonically decreasing function of distance, and the absolute FOI experienced by each susceptible individual because of a single infectious individual is low. (**C**) In a pure multigroup model, the FOI is determined entirely by group membership. For example, if an infectious individual shares a household with a susceptible individual (ovals), there is a high probability of transmission occurring between the two. However, if an infectious individual does not share a group with a particular susceptible individual, transmission between the two cannot occur. Spatial patterns of spread are determined by the locations of households and workplaces/schools (rectangle) and by the typical distribution of journeys between them. Dashed lines indicate group membership and solid lines indicate potentially infectious links between individuals. (**D**) Network transmission is similar to group transmission in that the FOI experienced by susceptible individuals is zero, unless they share an arc with an infectious individual. For directly transmitted respiratory pathogens, network transmission can be thought of as a refinement of an implicit group structure, in which it is assumed that not all members of a group are equally well connected; e.g., all colleagues at a workplace are not contacts. More than one component of transmission is included in some models. In general, computational requirements increase from (**A**) to (**D**). Patch models can be implemented effectively on a typical desktop computer because they do not explicitly represent individuals. For population sizes greater than 10 million, individual-based models have been implemented on clusters of large-memory personal computers (*26*, *31*, *34*). Detailed microsimulation models (*33*) have not yet been implemented at scales larger than a city.

role structure (*26*, *33*–*35*). However, none of them include demographic processes so that the birth, death, and aging of individuals are consistent with the formation and dissolution of households over time. Although these processes would introduce substantial additional complexity, spatially resolved census data and projections are available for many populations, which would allow the small number of parameters required by the additional demographic processes to be estimated independently of the transmission model. Demographic projections have already been incorporated with good effect into metapopulation models, such as those for HIV (*36*) and pertussis (*37*). I suggest that several human-pathogen interactions that exhibit spatial clustering at large scales and that are often transmitted within the household could be investigated with such an extension to current individual-based spatial models. For example, it may be possible to refine predictions of spatial patterns of zoonotic tuberculosis and HIV transmission in developing countries (*38*) and hence to consider the use of spatially heterogeneous household-based intervention strategies at different distance scales. The sensitivity of results from such models to the demographic processes that were used could be illustrated clearly with appropriate sensitivity analyses.

If one uses the network paradigm to critique models of directly transmitted infectious diseases, there is a desperate need for empirical evidence to inform basic choices of topology, such as average neighborhood size. For example, the model structures used in many recent studies of pandemic influenza (*26*, *27*, *34*, *35*, *39*) assume implicitly that neighborhood size outside the household is large; i.e., that a substantial proportion of the small number of secondary cases (basic reproductive number $R_0 < 2$, including household transmission) arises with low probability from brief contacts with many people. Although this assumption is appropriate because it is conservative with respect to the efficacy of group-based interventions, there is very little supporting empirical evidence. For example, I am not aware of any studies that have been able to infer reliable estimates (for any pathogen) of the infectivity and susceptibility of individuals in the home, relative to the workplace or school. Techniques that allow highly specific, non-invasive sampling for bacteria and viruses, coupled with intense empirical studies based in households, workplaces, and schools, could dramatically reduce these gaps in our knowledge. Detailed microsimulation models (*33*) could be used to obtain estimates of spatial-network topologies for different pathogens.

References and Notes

1. O. N. Bjørnstad, K. Sriamonaya, P. J. Edelstein, S. S. Morse, *Proc. Natl. Acad. Sci. U.S.A.* **102**, 13059 (2005).
2. J. C. Quinn, *Lancet* **348**, 99 (1996).
3. The World Bank, http://siteresources.worldbank.org/INTLAPHAIVEALMSPMAG/Resources/AP_Brief_avian-flu.pdf (accessed 28 November 2006) (2005).
4. N. M. Ferguson, C. A. Donnelly, R. M. Anderson, *Science* **292**, 1155 (2001); published online 12 April 2001 (10.1126/science.1060270).
5. S. A. Levin, B. Grenfell, A. Hastings, A. S. Perelson, *Science* **275**, 334 (1997).
6. J. E. Dobson, J. A. Bright, R. R. Coleman, R. C. Durfee, B. A. Worley, *Photogramm. Eng. Remote Sens.* **66**, 849 (2000).
7. D. Brockmann, L. Hufnagel, T. Geisel, *Nature* **439**, 462 (2006).
8. B. S. Cooper, R. J. Pitman, W. J. Edmunds, N. J. Gay, *PLoS Med.* **3**, e212 (2006).
9. L. Hufnagel, D. Brockmann, T. Geisel, *Proc. Natl. Acad. Sci. U.S.A.* **101**, 15124 (2004).
10. C. Viboud *et al.*, *Science* **312**, 447 (2006); published online 29 March 2006 (10.1126/science.1125237).
11. S. A. Levin, H. Darrell, *Philos. Trans. R. Soc. London Ser. B* **351**, 1615 (1996).
12. N. M. Ferguson, C. A. Donnelly, R. M. Anderson, *Nature* **413**, 542 (2001).
13. B. M. Bolker, B. T. Grenfell, *Proc. Natl. Acad. Sci. U.S.A.* **93**, 12648 (1996).
14. M. J. Keeling, B. T. Grenfell, *Science* **275**, 65 (1997).
15. B. T. Grenfell, O. N. Bjørnstad, J. Kappey, *Nature* **414**, 716 (2001).
16. T. D. Hollingsworth, N. M. Ferguson, R. M. Anderson, *Nat. Med.* **12**, 497 (2006).
17. International Airline Travel Association, www.iata.com (accessed 23 November 2006).
18. I. M. Longini, P. E. M. Fine, S. B. Thacker, *Am. J. Epidemiol.* **123**, 383 (1986).
19. L. A. Rvachev, I. M. Longini, *Math. Biosci.* **75**, 3 (1985).
20. Department for Environment Food and Rural Affairs (UK) www.defra.gov.uk/footandmouth (accessed 23 November 2006).
21. M. J. Keeling *et al.*, *Science* **294**, 813 (2001); published online 3 October 2001 (10.1126/science.1065973).
22. M. Woolhouse *et al.*, *Nature* **411**, 258 (2001).
23. M. J. Keeling, M. E. Woolhouse, R. M. May, G. Davies, B. T. Grenfell, *Nature* **421**, 136 (2003).
24. M. J. Tildesley *et al.*, *Nature* **440**, 83 (2006).
25. J. A. P. Heesterbeek, *Acta Biotheor.* **50**, 189 (2002).
26. N. M. Ferguson *et al.*, *Nature* **437**, 209 (2005).
27. I. M. Longini Jr. *et al.*, *Science* **309**, 1083 (2005); published online 3 August 2005 (10.1126/science.1115717).
28. C. L. Mills, J. M. Roberts, M. Lipsitch, *Nature* **432**, 904 (2004).
29. World Health Organization, www.who.int/csr/resources/publications/influenza/WHO_CDS_CSR_GIP_2005_5rev/en/index.html (accessed 28 November 2006) (2005).
30. F. Fenner, D. A. Henderson, I. Arita, Z. Jezek, I. D. Ladnyi, *Smallpox and Its Eradication* (World Health Organization, Geneva, Switzerland, 1988).
31. S. Riley, N. M. Ferguson, *Proc. Natl. Acad. Sci. U.S.A.* **103**, 12637 (2006).
32. N. M. Ferguson *et al.*, *Nature* **425**, 681 (2003).
33. S. Eubank *et al.*, *Nature* **429**, 180 (2004).
34. N. M. Ferguson *et al.*, *Nature* **442**, 448 (2006).
35. T. C. Germann, K. Kadau, I. M. Longini Jr., C. A. Macken, *Proc. Natl. Acad. Sci. U.S.A.* **103**, 5935 (2006).
36. R. M. Anderson, R. M. May, M. C. Boily, G. P. Garnett, J. T. Rowley, *Nature* **352**, 581 (1991).
37. H. W. Hethcote, *Math. Biosci.* **145**, 89 (1997).
38. B. G. Williams, E. Granich, L. S. Chauhan, N. S. Dharmshaktu, C. Dye, *Proc. Natl. Acad. Sci. U.S.A.* **102**, 9619 (2005).
39. J. T. Wu, S. Riley, C. Fraser, G. M. Leung, *PLoS Med.* **3**, e361 (2006).

40. I thank the Research Fund for the Control of Infectious Diseases of the Health, Welfare and Food Bureau of the Hong Kong Special Administrative Region Government for funding and three anonymous reviewers; R. Anderson, B. Cowling, N. Ferguson, C. Fraser, B. Grenfell, M. Keys, G. Leung, P. Riley, and J. Wu for comments on the manuscript.

10.1126/science.1134695

Seawater Chemistry and Early Carbonate Biomineralization

Susannah M. Porter

Organisms use a wide variety of minerals to make their skeletons, including silica, apatite, and several polymorphs of carbonate. In particular, aragonite and calcite. It is unclear however, why different taxa evolved to use one mineral rather than another. Lineages rarely switched their mineralogy after acquiring skeletons, suggesting that, for most taxa, ambient seawater chemistry does not strongly influence skeletal mineralogy (1). However, seawater chemistry may have [illegible] choice of skeletal mineralogy at the time skeletons first evolved [illegible]

This hypothesis was tested by assessing the ancestral mineralogy (aragonite versus calcite) of 21 metazoan taxa that evolved mineralization during a time [illegible] Ordovician (~550 to 444 million years ago) and comparing the resulting pattern with independent constraints on ocean seawater chemistry (Fig. 1 and tables S1 and S2). The record is thought to represent an independent acquisition of biomineralization in most [illegible] should alter the interpretations of the hypothesis. Alternative taxonomic interpretations (table S1) affect the degree of support for the pattern presented here but do not change it. Four taxa known to be polyphyletic were excluded (table S1).

Determining the primary mineralogy of ancient carbonate fossils is not straightforward because aragonite recrystallizes to calcite at Earth's surface pressures. As a result, formerly aragonitic skeletons are often preserved as calcite. Five well-accepted criteria were used to infer primary mineralogy [Supporting Online Material (SOM) text]: (i) presence of original aragonite, (ii) phylogenetic distribution of mineralogies in extant members of a group, (iii) quality of preservation of original microstructures in calcite, (iv) morphology of crystals replicated by secondary minerals, and (v) magnesium content. Evidence for primary mineralogy was drawn from the literature (table S1) and critically evaluated with respect to these criteria.

For 18 of the 21 taxa, primary mineralogy is known with at least some confidence. Of these, eight are highly likely ($N = 4$) or likely ($N = 4$) to have been aragonite, and 10 are highly likely to have been calcite (either high- or low-magnesium calcite). Mapping inferred skeletal mineralogies on first appearances of mineralization (FAMs) results in a striking pattern (Fig. 1A): Aragonite taxa systematically appeared earlier, with FAMs occurring in the Ediacaran Period from Nemakit-Daldynian Stage followed by calcite taxa, which began mineralizing in the Tommotian Stage or later.

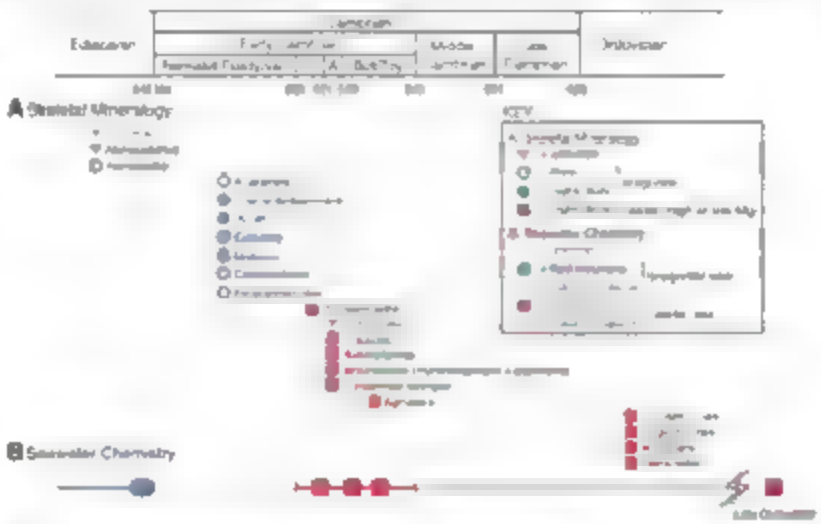

Fig. 1. First appearances of carbonate skeletons in animals (A) and constraints on seawater chemistry (B) during the Ediacaran through the Ordovician Periods. Fluid inclusion data are listed in table S2. Indirect evidence for seawater chemistry, reviewed in (2), refers to constraints from nonskeletal marine precipitates and from models of mid-ocean ridge hydrothermal brine fluxes. Because most taxa are fossilized in abundance, it is assumed that first appearances of skeletons in the fossil record closely approximate actual first appearances of skeletons. "Calcite sea" and "aragonite sea" refer to seawater that favors calcite and aragonite precipitation, respectively. Boundary age constraints are from the International Commission on Stratigraphy International Stratigraphic Chart (2007) (www.stratigraphy.org/cheu.pdf) and (11). Although there is uncertainty regarding the position of stage boundaries relative to some first appearances of skeletons, the sequence of taxa is unaffected (table S2). Ma, million years; T, Tommotian Stage; A, Aldabanian Stage; Bot/Toy, Botomian and Toyonian Stages.

Fluid inclusions in marine evaporite deposits provide the most definitive constraints on the Mg^{2+}/Ca^{2+} ratio of ancient seawater (4), which is thought to be the primary control on marine nonskeletal carbonate mineralogy (2, 5). These indicate that the Mg^{2+}/Ca^{2+} ratio of late Ediacaran seawater favored aragonite precipitation (4, 6), whereas the Mg^{2+}/Ca^{2+} ratio of Tommotian, Aldabanian through Toyonian seawater (4, 6, 7), as well as that of late Ordovician seawater (4, 8), favored calcite precipitation (Fig. 1B and table S2).

The close correspondence between the pattern of FAMs and the constraints on seawater chemistry (Fig. 1) suggests that selection of aragonite versus calcite was largely dictated by seawater chemistry at the time mineralized skeletons were first acquired in a clade. Mineralization of most animal skeletons is biologically controlled, occurring in an environment isolated from seawater (9). As a result, seawater chemistry does not have a direct influence on the mineralogy of most animal skeletons the way it does for biominerals that induce mineralization directly from seawater (9). However, seawater chemistry may have played an indirect role in determining skeletal mineralogy by affecting the physiological costs of biomineralization (1). Experimental and paleontological evidence suggests organisms have greater difficulty producing skeletons not favored by seawater chemistry (3, 10); thus, it is reasonable to posit that, when skeletons first evolved, natural selection favored the mineral easiest to precipitate (1). Once selected, however, taxa rarely switched mineralogies even though they may have been [illegible] affected when Mg^{2+}/Ca^{2+} ratios changed (2). Although initially optimal, skeletal mineralogy may since have presented a [illegible] evolutionary constraint.

References and Notes

1. A. H. Knoll, *Rev. Mineral. Geochem.* **54**, 329 (2003).
2. S. M. Stanley, L. A. Hardie, *Palaeogeogr. Palaeoclimatol. Palaeoecol.* **144**, 1 (1998).
3. S. Bengtson, S. Conway Morris, in *Origin and Early Evolution of the Metazoa*, J. H. Lipps, P. W. Signor, Eds. (Plenum, New York, 1992), pp. 447–481.
4. T. K. Lowenstein, M. N. Timofeeff, S. T. Brennan, L. A. Hardie, R. V. Demicco, *Science* **294**, 1086 (2001).
5. J. W. Morse, Q. Wang, M. Y. Tsio, *Geology* **25**, 85 (1997).
6. S. T. Brennan, T. K. Lowenstein, J. Horita, *Geology* **32**, 473 (2004).
7. O. Pokrovsky, J. Schott, *Chem. Geol.* **190**, 141 (2002).
8. V. M. Kovalevych, T. M. Peryt, W. Zang, S. V. Vovnyuk, *Terra Nova* **18**, 95 (2006).
9. S. Weiner, P. M. Dove, *Rev. Mineral. Geochem.* **54**, 1 (2003).
10. J. B. Ries, *Paleobiology* **31**, 445 (2005).
11. A. L. Maloof, G. P. Schrag, J. L. Crowley, S. A. Bowring, *Can. J. Earth Sci.* **42**, 2195 (2005).

12. This work benefited from discussions with S. Awramik, P. Baker, J. Boles, S. Carlson, J. Grotzinger, J. Kellogg, A. Knoll, T. Lowenstein, A. Maloof, J. Payne, J. Sorauf, F. Spera, M. Vendrasco, J. Weaver, S. Weiner, and G. Zempolich. Three anonymous reviewers offered helpful comments on earlier drafts. Supported by NASA grant no. EXB04-0000-0137.

Supporting Online Material

www.sciencemag.org/cgi/content/full/316/5829/1302/DC1
SOM Text
Tables S1 and S2
References

7 November 2006; accepted 27 February 2007
10.1126/science.1137284

Department of Earth Science, University of California at Santa Barbara, Santa Barbara, CA 93106, USA. E-mail: porter@geol.ucsb.edu

155,000 Years of West African Monsoon and Ocean Thermal Evolution

Syee Weldeab,[1]*† David W. Lea,[1] Ralph R. Schneider,[2] Nils Andersen[3]

A detailed reconstruction of West African monsoon hydrology over the past 155,000 years suggests a close linkage to northern high-latitude climate oscillations. Ba/Ca ratio and oxygen isotope composition of planktonic foraminifera in a marine sediment core from the Gulf of Guinea, in the eastern equatorial Atlantic (EEA), reveal centennial-scale variations of riverine freshwater input that are synchronous with northern high-latitude stadials and interstadials of the penultimate interglacial and the last deglaciation. EEA Mg/Ca-based sea surface temperatures (SSTs) were decoupled from northern high-latitude millennial-scale fluctuation and primarily responded to changes in atmospheric greenhouse gases and low-latitude solar insolation. The onset of enhanced monsoon precipitation lags behind the changes in EEA SSTs by up to 7000 years during glacial-interglacial transitions. This study demonstrates that the stadia-interstadia and deglacial climate instability of the northern high latitudes exerts dominant control on the West African monsoon dynamics through an atmospheric linkage.

The West African (WA) monsoon is an important component of the climate system because (i) it is part of the global monsoon system that regulates the moisture and heat budget of the atmosphere in low latitudes (*1*) and (ii) it is sensitive to climate processes in the northern high latitudes and tropical oceans (*1*, *2*) and, at a regional level, it is the main determinant of agricultural production in densely populated areas where the economy depends on subsistence agriculture. Thus, a deeper understanding of past WA monsoon dynamics and its controls is of pivotal importance to improving our knowledge of the monsoon system and assessing the impact of future climate change.

Previous studies of WA paleohydrology largely focused on the Holocene and the last deglaciation (*2*–*7*) and revealed alternating humid and dry conditions as reconstructed from lake-level fluctuations across the continent (*3*). These hydrological changes are thought to reflect the movement of the intertropical convergence zone (ITCZ) in close association with tropical SST and northern high-latitude climates (*2*–*4*). Because of the lack of a long, continuous, well-dated, and high-resolution record that includes independent and quantitative hydrological proxies, our understanding of the WA paleomonsoon and its teleconnections to global climate remains tenuous. To address these shortcomings, we present a 155,000-year reconstruction of WA monsoon precipitation variability at the centennial-to-millennial scale from marine sediment core MD03-2707 (02°30.11′N, 09°23.68′E; 1295 m water depth), which was recovered from the eastern part of the Gulf of Guinea in the EEA (Fig. 1).

Oceanographic setting and proxy records. The Gulf of Guinea is located in the eastern extension of the equatorial Atlantic warm tongue (*8*). In the upper 20 m of the water column, SST varies between 26° and 28.5°C (*8*). Freshwater input from the Sanaga and Niger rivers is the main factor determining modern sea surface salinity (SSS) variability in the eastern Gulf of Guinea (Fig. 1). The large volume of riverine runoff, combined with weak current and wind mixing (*9*, *10*), leads to markedly low SSS and a shallow halocline (20 to 30 m) (*8*) (Fig. 1). Our working hypothesis is that large-scale changes in past WA monsoon precipitation and riverine runoff are reflected in the isotopic composition of seawater and budget of dissolved Ba in Gulf of Guinea surface water, which as in turn archived in microfossils that accumulate in marine sediments. Because of the absence of coastal upwelling and strong local current mixing in the eastern part of the Gulf of Guinea (fig. S1), SST estimates likely reflect atmospheric conditions over the tropical Atlantic rather than advective signatures.

We measured Ba/Ca ratios, Mg/Ca ratios, and oxygen isotope composition ($\delta^{18}O$) in the tests (shells) of planktonic foraminifer *Globigerinoides ruber* (pink variety), which dwells in the upper 25 m of the water column, to infer past SSS and SST variation. MD03-2707 core sediment is 37.30 m long and covers the past 155,000 years (Fig. 2). The age model is described in (*16*). We applied Mg paleothermometry to obtain SST estimates using an established calibration equation (*11*). $\delta^{18}O$ in foraminiferal calcite ($\delta^{18}O_{calcite}$) is controlled by the calcification temperature and the $\delta^{18}O$ of seawater ($\delta^{18}O_{sw}$), which is controlled by salinity variation and continental ice volume. The $\delta^{18}O_{sw}$ is extracted by means of the Mg/Ca-based SST estimate with analyzed $\delta^{18}O$ and temperature-$\delta^{18}O_{calcite}$-$\delta^{18}O_{sw}$ equation (*12*). $\delta^{18}O_{sw}$ is calculated linearly to salinity (*13*). However, changes in the origin of surface water and changes in $\delta^{18}O$ of riverine runoff make the use of the modern $\delta^{18}O_{sw}$-SSS relationship to determine paleo-SSS estimates uncertain.

Ba/Ca in planktonic foraminiferal calcite (Ba/Ca_{foram}) provides an innovative tool to assess past variability in regional riverine runoff (*14*). Seawater Ba (Ba_{sw}) concentrations at oceanic sites influenced by riverine runoff have a notably high inverse correlation to salinity, with high Ba and low salinity at sites closest to the river mouth (figs. S4 and S5) because dissolved Ba is high in riverine water and Ba desorbs from suspended sediments in estuaries (*15*, *16*). Laboratory experiments on living planktonic foraminifera demonstrate that Ba incorporation in foraminiferal calcite varies linearly with changes in Ba_{sw} concentration, independent of temperature changes within ~7°C (*17*). Therefore, the variation of Ba/Ca_{foram} is controlled by the Ba_{sw} concentra-

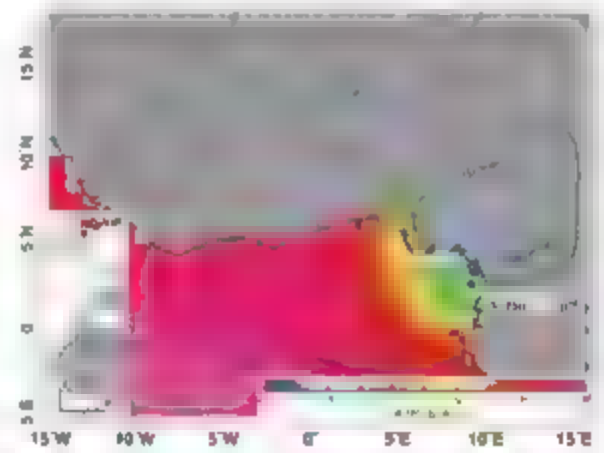

Fig. 1. Annual SSS in the Gulf of Guinea (*8*). Location of MD03-2707 (02°30.11′N, 09°23.68′E, 1295 m water depth) and drainage basin of Niger and Sanaga rivers (delineated by dotted line) are indicated. The Sanaga River, with an annual discharge of 77 km^3, drains a basin of 158,000 km^2 with the highest precipitation (10 mm/day) in the African continent (*23*); the catchment of the Niger River (2,400,000 km^2) integrates the largest part of WA monsoon area with annual runoff of almost 200 km^3 [data from Global Runoff Data Centre (http://grdc.bafg.de)]. Between June and September intense monsoon precipitation (~180 to 240 mm/month) prevails over the catchments of the Niger and Sanaga rivers (*23*), resulting in a large freshwater input into the eastern part of the Gulf of Guinea.

[1]Department of Earth Science and Marine Science Institute, University of California, Santa Barbara, CA 93106–9630, USA. [2]Institut für Geowissenschaften, Universität Kiel, Germany. [3]Leibniz-Labor für Altersbestimmung und Isotopenforschung, Universität Kiel, Germany.

*Present address: Leibniz Institut für Meereswissenschaften an der Universität Kiel (IFM-GEOMAR), Germany.

†To whom correspondence should be addressed. E-mail: sweldeab@ifm-geomar.de

tion, and the temporal variation of Ba/Ca_{foram} provides valuable insights into changes in riverine freshwater input. In order to obtain an estimate of the past runoff-induced SSS variations, as recorded by Ba/Ca_{foram}, we use the modern Ba/Ca_{sw}-salinity relationship obtained off the Congo River (*15*) and Ba/Ca_{sw}-Ba/Ca_{foram} partition coefficient (*17*) to obtain a Ba/Ca_{foram}-SSS relationship (Fig. 2). Although our approach is supported by the observation that Ba_{sw} concentration in three different estuaries (fig. S5) affected by runoff from three major tropical rivers shows a high and similar degree of linear correlation with salinity (*10*), the Ba/Ca_{foram}-based SSS estimates should be regarded as a first-order estimate, because the Ba/Ca_{foram}-salinity relationship in the Gulf of Guinea is not yet established.

Holocene WA monsoon history. The Ba/Ca record is the most direct proxy of riverine runoff. Variability of $\delta^{18}O$ in *G. ruber* generally follows that of Ba/Ca, although the $\delta^{18}O$ fluctuations are less pronounced (Fig. 3). The close correspondence between Ba/Ca and $\delta^{18}O_{sw}$ indicates that the latter was largely controlled by riverine runoff throughout the record. The largest and most abrupt Ba/Ca rise in the Gulf of Guinea record occurs at ~11,460 years before the present and marks the end of the Younger Dryas (YD) chronozone and the beginning of the Holocene epoch. The increase of Ba/Ca from 1.4 to 1.8 μmol/mol, equivalent to an SSS change from 27 to 34 practical salinity units (psu), occurred within a few decades (< 50 years) and points to an abrupt switch from relatively dry to extremely wet conditions and to a large northward expansion of the monsoonal rainfall front, as previously suggested by modeling studies (*18*, *19*) and paleoclimate data (*3*, *4*, *20*). The intensification of the monsoon in the earliest Holocene is consistent with Kutzbach's orbital forcing hypothesis, because perihelion occurred in early Northern Hemisphere summer at this time, resulting in enhanced summer insolation (*21*) and a seasonal warm tropical Atlantic (Fig. 3). Persistently high levels of Ba/Ca (~1.7 to 1.8 μmol/mol) for ~6,500 years suggest that intense monsoon precipitation and high riverine runoff continued throughout the early and middle Holocene, with a salinity minimum of 23 psu, which is just 2 psu higher than the salinity limit (21 psu) for *G. ruber* growth (*22*). Superimposed on the generally extreme wet conditions during the middle and early Holocene (11,460 to 5100 yr B.P.) are several centennial-scale Ba/Ca fluctuations, including a prominent event close to 8200 yr B.P.

After 5100 yr B.P. riverine Ba/Ca declined continuously, eventually attaining (at ~360 yr B.P.) an average value of 1 μmol/mol, which corresponds to an SSS estimate of 29 psu, which is equal to the modern annual SSS value at ~0 to 25 m water depth over the core site (*8*). The gradual decline of riverine freshwater input over the late Holocene, as indicated by Ba/Ca and $\delta^{18}O$, is most likely associated with a continuous southward retreat of the monsoonal rainfall front from its northernmost expansion (~23°N) during the early and mid-Holocene (~7,000 to ~5 N at the present (*23*). This finding is consistent with the results of terrestrial studies from the drainage basin of the Niger River (*24*, *25*), suggesting that weakening and gradual southward displacement of monsoon precipitation were accompanied by gradual changes in vegetation.

We hypothesize that, in the absence of large northern high-latitude ice-sheet instabilities, WA Holocene monsoon precipitation is linked to Northern Hemisphere low-latitude summer insolation and EEA SST. In fact, high riverine runoff in the early and middle Holocene, as indicated by high Ba/Ca, is accompanied by high SST and declining runoff occurred in parallel with decreasing SST throughout the late Holocene (Fig. 3). Furthermore, a comparison with other records of the global monsoon system indicates that the evolution of Holocene WA monsoon precipitation shares a close similarity with that of the Indian Ocean (*26*), the East Asian (EA) (*27*), and the South American monsoons (*28*), suggesting that declining Northern Hemisphere

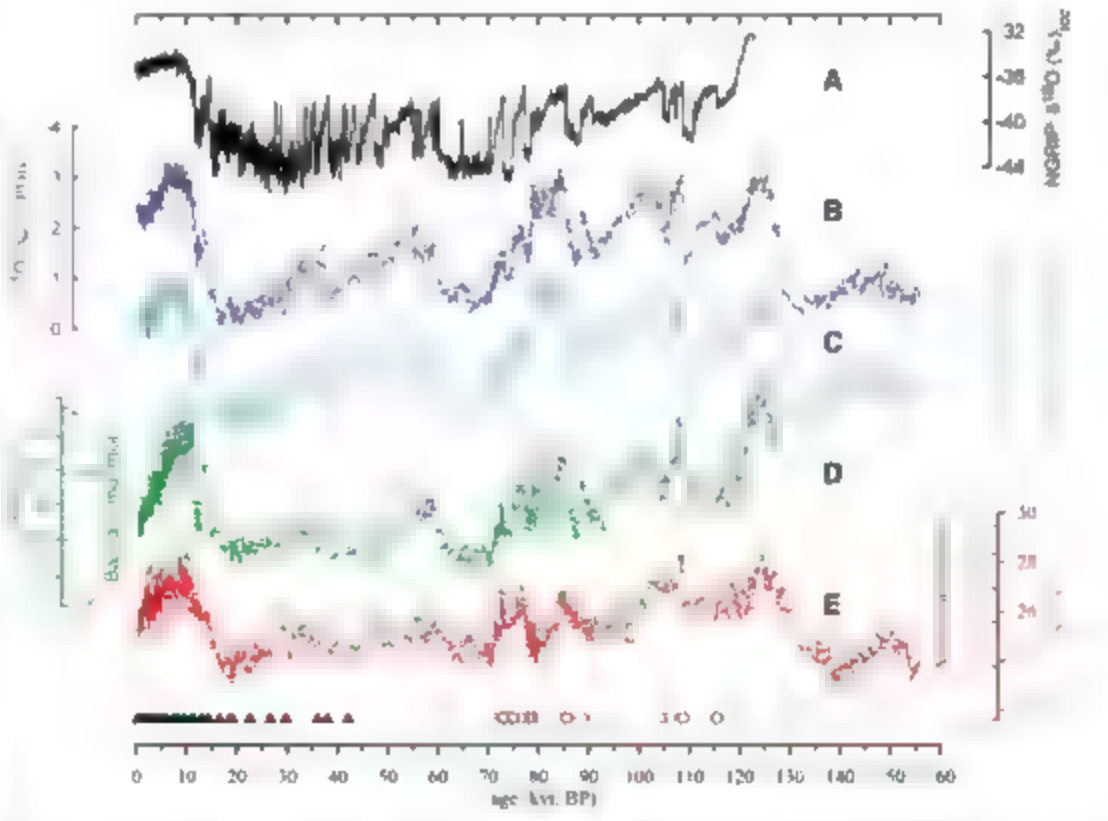

Fig. 2. Gulf of Guinea record based on trace element and $\delta^{18}O$ in tests of the shallow-dwelling planktonic foraminifer *G. ruber* (250 to 350 μm) from core MD03-2707. Proxy records in MD03-2707 are plotted versus calendar age [thousand years (kyr) B.P.] and compared with the $\delta^{18}O$ in ice ($\delta^{18}O_{ice}$) record of the NGRIP ice core (**A**) (*30*). $\delta^{18}O$ in the tests of *G. ruber* (**B**), $\delta^{18}O_{sw}$ (not corrected for changes in continental ice volume) (**C**), and Ba/Ca (μmol/mol) and Ba/Ca-based SSS estimates (**D**) are shown. PDB, Pee Dee belemnite; SMOW, standard mean ocean water. The Ba/Ca-based SSS estimate is calculated from the modern Ba_{sw}-salinity relationship obtained off the Congo River (*15*) and the partition coefficient for Ba incorporation in foraminifera of $D_{Ba} = 0.147$ [$Ba/Ca_{foram} = D_{Ba}\,(Ba/Ca_{sw})$] (*17*): SSS = [−7.47(Ba/Ca_{foram})] + 37.45; r^2 = 0.98; error estimate, ±0.41 psu (fig. S4). The Ba/Ca record between 122,000 and 127,500 yr B.P. might be slightly affected by diagenetic influence (*10*). (**E**) Mg/Ca (mmol/mol) and Mg/Ca-based SST estimates, where SST (°C) = 0.09^{-1}·ln[Mg/Ca(mmol/mol)/0.38] + 0.78 (*11*); SE estimate, ±1.2°C. Symbols along the *x* axis indicate age control points used for establishing the age model for MD03-2707 (*10*). Triangles indicate age control points as derived from a polynomial fit to individual calibrated ^{14}C-AMS ages (table S1 and fig. S3), and circles and diamonds are tie points obtained by the alignment of (i) the $\delta^{18}O$ record in (B) with the NGRIP $\delta^{18}O_{ice}$ record in (A) (*30*) and (ii) the benthic foraminiferal $\delta^{18}O$ record in MD03-2707 (fig. S2) with the "LR04" benthic foraminiferal $\delta^{18}O$ stack record (*49*), respectively (table S2).

summer solar insolation acted as a common control on the global monsoon system during the late Holocene (*29*).

Monsoon behavior during the last two deglaciations. Glacial Ba/Ca values are only slightly elevated over open-ocean Ba/Ca values (*15*), implying greatly reduced riverine runoff and SSS of ~32 psu (Figs. 2 and 3). Stable and low values give way to rising Ba/Ca after 16,430 yr B.P., indicating a gradual increase in runoff and precipitation. At 14,520 yr B.P., Ba/Ca rises sharply to peak values, corresponding to SSS of 26 psu during the Bølling-Allerød chronozone (B/A), indicating runoff levels similar to those of the early late Holocene (~4000 yr B.P.). At the onset of the YD (~12,930 yr B.P.), Ba/Ca drops abruptly to 1.1 μmol/mol, indicating a collapse of riverine runoff and a salinity increase to 29 psu, most likely as a result of sharply reduced monsoonal precipitation. Sustained low Ba/Ca values coincident with the YD chronozone (~12,930 to 11,460 yr B.P.) suggest that dry conditions in western Africa lasted for ~1400 years.

The records of riverine runoff proxies in the Gulf of Guinea closely correlate with the North Greenland Ice Core Project (NGRIP) $\delta^{18}O$ record (*30*) during the last deglaciation (Fig. 3). Periods of warm air temperature over Greenland were associated with periods of high riverine runoff in WA, whereas cold conditions were associated with reduced runoff. Within age model uncertainties of ~ 150 years, the onsets and terminations of the precipitation changes in the WA monsoon area during the B/A and YD are synchronous with the shift in the NGRIP record. This suggests a strong climate connection between northern high-latitude climate processes and WA monsoon precipitation, most likely due to synchronous latitudinal displacement of the polar front and the ITCZ.

In sharp contrast to the riverine runoff proxies, deglacial Mg/Ca ratios in the Gulf of Guinea record indicate a continuous SST rise from a glacial value of 24.1 ± 0.4°C (± 1 SD) between 23,000 and 19,000 yr B.P. to 27.2 ± 0.7°C between 11,000 and 8,500 yr B.P. This finding implies that deglacial air temperature instability over Greenland (*30*) was not matched by SST changes in the EEA. This observation, combined with SST reconstructions from the tropical western Atlantic (*31*), demonstrates that the YD did not leave a thermal imprint on the open-ocean equatorial Atlantic. Accordingly, the sharp YD cooling observed in the Cariaco Basin (*32*) reflects the sensitivity of this basin to northern high-latitude processes rather than a widespread open-ocean tropical Atlantic thermal event. It further implies that EEA SST was not the dominant control on deglacial WA monsoon precipitation variability. The continuous and gradual SST rise during the last deglaciation leads abrupt changes in monsoonal precipitation by ~2500 years. The penultimate deglacial is characterized by an even more pronounced lead-lag pattern, with gradually rising SST leading the rapid onset of monsoon intensification by ~7000 years. This finding that SST leads the deglacial monsoon onset by up to 7000 years suggests that regional SST rise was not the dominant control on deglacial WA monsoon evolution. Large-scale changes in atmospheric circulation linked to substantial reduction of the northern high-latitude ice sheets likely triggered the onset of monsoon intensification.

Glacial WA monsoon variability. Riverine runoff proxies suggest dry and relatively stable conditions during full glacial episodes in the WA monsoon area (Fig. 2). During the time intervals

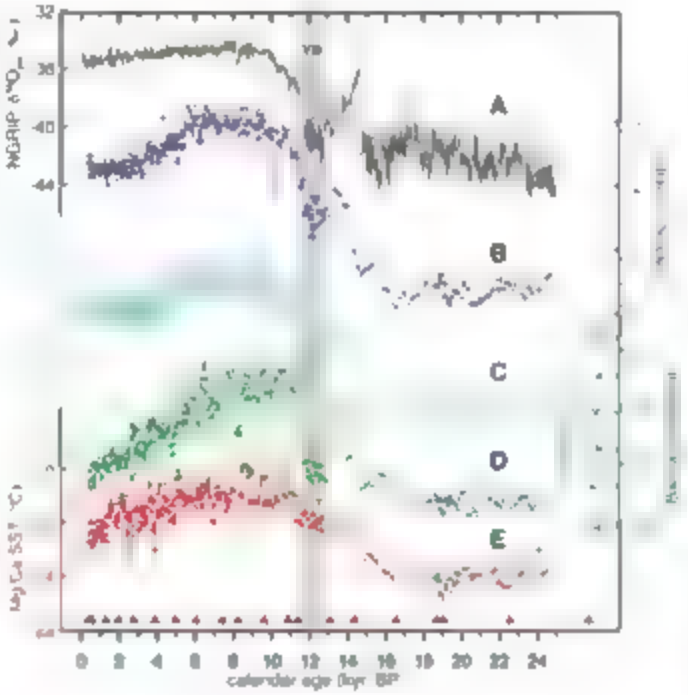

Fig. 3. Gulf of Guinea record over the past 25,000 years based on trace element and $\delta^{18}O$ in the tests of *G. ruber* from MD03-2707, in comparison with the $\delta^{18}O$ record of the NGRIP ice core (Greenland Ice Core Chronology 05) (*30*). (**A**) $\delta^{18}O$ in the tests of *G. ruber*. (**B**) $\delta^{18}O_{sw}$ (not corrected for changes in continental ice volume). (**C**) Ba/Ca and Ba/Ca-based SSS estimates. (**D**) and Mg/Ca-based SST estimates (**E**) are shown. Triangles along the *x* axis indicate age control points as derived from a polynomial fit to individual calibrated ^{14}C-AMS ages (table S1 and fig. S3). The gray bar marks the YD chronozone.

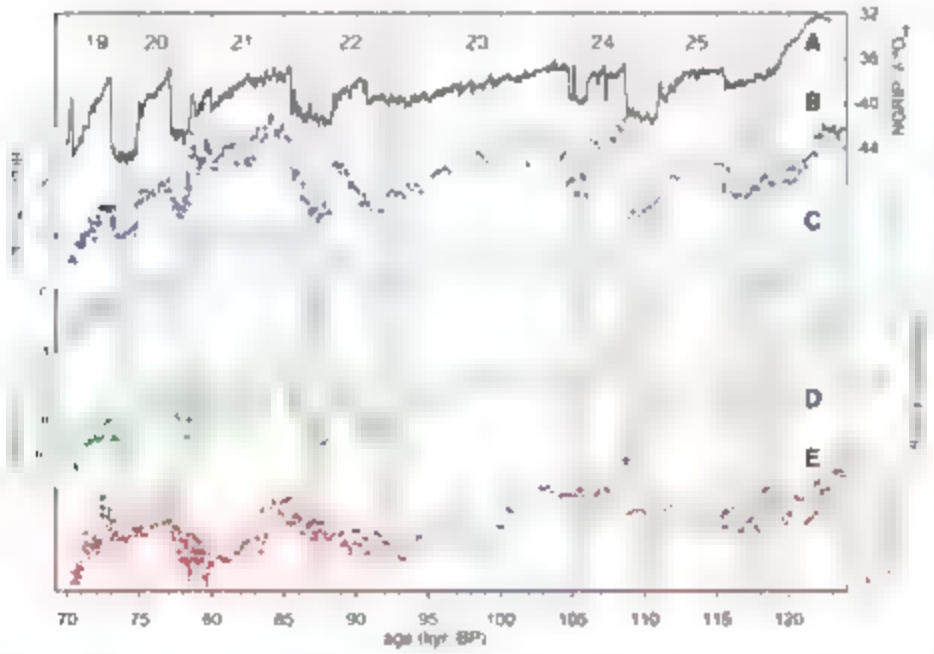

Fig. 4. Gulf of Guinea record covering the time interval from 65,000 to 123,000 yr B.P. based on trace element and $\delta^{18}O$ in the tests of *G. ruber* from MD03-2707, in comparison with $\delta^{18}O$ record of the NGRIP ice core (*30*). (**A**) $\delta^{18}O$ in the tests of *G. ruber*. (**B**) $\delta^{18}O_{sw}$. (**C**) Ba/Ca (μmol/mol) and Ba/Ca-based SSS estimates. (**D**) and Mg/Ca-based SST estimates (**E**) are shown. GIS identified in the $\delta^{18}O$ and Ba/Ca record of MD03-2707 are numbered ("19" to "25"), and associated GS are marked in gray.

from 19,000 to 5 ,000 and 6 ,,500 to 70,000 yr B.P [marine isotope stage 4 (MIS4)]. Ba/Ca ratios are markedly low and stable, ranging from 0.9 to 1.1 μmol/mol, which corresponds to an estimated SSS of 32 to 30 psu. Considering the effect of increasing continental ice volume on $\delta^{18}O_{sw}$ (*33*) from 42,000 through 19,000 yr B.P., the $\delta^{18}O_{sw}$ record corroborates the overall environmental conditions suggested by Ba/Ca, indicating low and stable riverine runoff and a severely weakened WA monsoon system. Starting at the beginning of the MIS4-MIS3 transition (62,000 yr B.P.), Ba/Ca gradually increases and peaks at 55,000 yr B.P. with a value of 1.5 μmol/mol, which corresponds to ~26.5 psu and suggests less saline surface water during early MIS3 relative to that of the late Holocene.

Unlike the last deglacial and penultimate interglacial (Fig. 4), glacial WA riverine runoff as recorded by Ba/Ca and $\delta^{18}O_{sw}$ did not fluctuate in concert with Greenland interstadials (GIS) and stadials (GS) (*30*). Assuming that our sample resolution sufficiently captures centennial- to millennial-scale hydrological changes in MIS3 and MIS2, the Gulf of Guinea record suggests that glacial boundary conditions dampened the response of the WA monsoon system to glacial GIS. This is in sharp contrast to the South American (*34*, *35*), Indian Ocean (*36*, *37*), and EA monsoon systems (*38*), which reveal strong coupling to the GIS events between 19,000 and 40,000 yr B.P.

We hypothesize that the extent to which the WA monsoon responds to suborbital extratropical forcing may depend on the initial summer position of the ITCZ that is determined by glacial and interglacial boundary conditions. During glacials and the second half of MIS3, the hydrological proxies suggest minimum runoff and severely reduced precipitation over WA. This is consistent with a wide-ranging southward ITCZ displacement over the Atlantic realm as evidenced by concomitant dry conditions in the Carioco basin (*39*) and wet conditions in northeastern Brazil (*35*). We argue that the seasonal northward migration of the oceanic ITCZ, which was positioned over the EEA during the glacials and late part of MIS3, did not extend north of the east-west trending WA coast, and that the ITCZ response to glacial GIS warming was dampened by the large thermal inertia of the ocean.

WA monsoon variability during the penultimate interglacial. Hydrological proxies in the Gulf of Guinea record indicate numerous millennial-scale fluctuations in riverine freshwater input during the penultimate interglacial (MIS5) (Fig. 4). Both Ba/Ca and $\delta^{18}O_{sw}$ suggest enhanced riverine runoff at time intervals that correlate to GIS 19 (twice), 18, 17, 16, and 15 runoff at the associated GIS (GIS 22 to GIS 25), as a result of diagenetic complications, Ba/Ca is not considered beyond 127,500 yr B.P. (*10*). Close examination also reveals that the relative amplitude of Ba/Ca and $\delta^{18}O$ changes in the Gulf of Guinea record correlating to GIS 19 and GIS 20 are less pronounced than those observed in the NGRIP record. We attribute this to the fact that both GIS 19 and GIS 20 occurred during the transition from interglacial (MIS5a) to glacial boundary conditions (MIS4), which, as argued above, appeared to dampen the WA monsoon response to extratropical influence. Some slight differences in the pattern of transitions also exist from stadial to interstadial and vice versa in the Gulf of Guinea record when compared with that of the NGRIP record (Fig. 4). GIS 23, for example, terminated abruptly as indicated by Ba/Ca in the MD03-2707 record; in the NGRIP record, the transition to GIS 22 is gradual. The role of EEA SST in modulating the WA monsoon precipitation during MIS5 (Fig. 4) was most likely secondary. This observation suggests that although the general conditions of millennial-scale WA monsoon precipitation during the MIS5 were set by northern high-latitude climate conditions, the amplitude and abruptness of WA precipitation changes appear to be modulated by internal variability of the monsoon system or were preconditioned by low-latitude summer insolation.

EEA SST forcings. Major changes in EEA SST are recorded at glacial terminations I and I., equivalent to SST increases of 3.1 ± 0.8°C and 3.7 0.5°C, respectively (Figs. 2 and 5). The EEA SST record is also in phase with midsummer solar insolation at 15°N (*29*) (fig. S6), suggesting that the EEA is thermally sensitive to Northern Hemisphere low-latitude summer radiation, either through a monsoonal feedback (*27*) or because Mg/Ca-based SST estimates are weighted toward the boreal summer. The effect of orbital forcing in the EEA SST changes is best exemplified by the SST rise at 40,000 to 155,000 yr B.P. when atmospheric greenhouse gases and their associated radiative forcings were low, as indicated in the Vostok record (*40*) (fig. S6). Apart from the large SST changes during terminations (i.e., the 100,000-year cycles) and those related to precessional variance in summer insolation, a feature that stands out is a cooling of 2°C between ~84,500 and 78,000 yr B.P. Comparison of EEA SST with the Vostok ice-core record (*40*) reveals that air temperature cooling over Antarctica and a decrease in atmospheric CO_2 also occurred at this time. This observation suggests that the decrease in EEA SST, as indicated by Mg/Ca, might relate to a broad-scale tropical cooling in response to greenhouse gas changes in the atmosphere. Major glacial-interglacial SST transitions in the EEA and elsewhere in the tropics (*41*, *43*) are paralleled by large changes in greenhouse gases as recorded in Antarctica ice cores (*40*). Radiative forcing associated with the increase in greenhouse gases during the glacial-interglacial transition has been estimated to give rise to an increase of 2° to 3°C in tropical SST (*44*) and ~4° to 6°C in air temperature over Antarctica (*40*). If this estimate is correct, the EEA SST increase at termination I and II was largely a consequence of radiative forcing corresponding to greenhouse gas increases. The abrupt increase of atmospheric methane associated with the intensified global monsoon (Fig. 5) would have also enhanced greenhouse

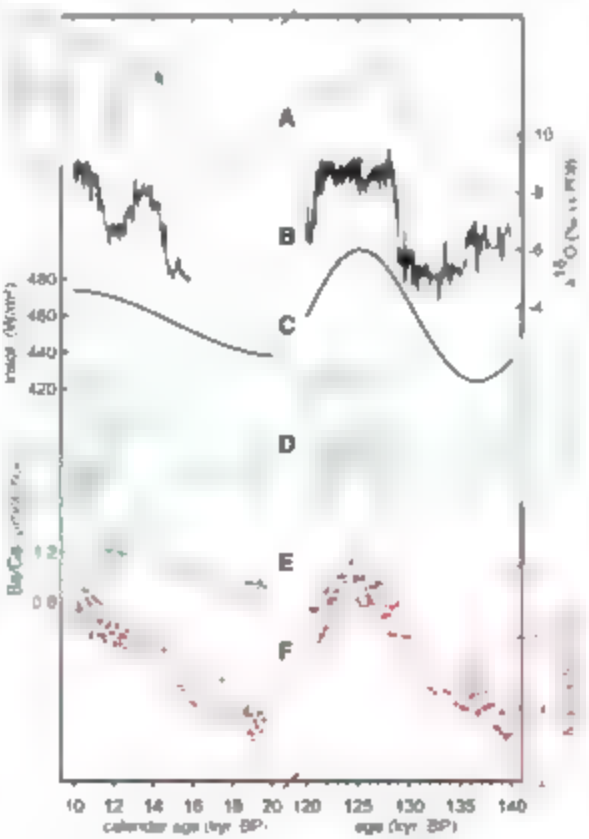

Fig. 5. Timing of deglacial onsets of the WA monsoon [as indicated by $\delta^{18}O_{sw}$ (**D**) and Ba/Ca (**E**)] and the Gulf of Guinea SST record during termination I and II (**F**), as compared with the EA monsoon record from Dongge Cave (**B**) (*27*, *46*), the midsummer solar insolation (Insol) at 15°N (*29*) (**C**), and changes in atmospheric methane concentration (**A**), as measured in the Greenland Ice Sheet Project 2 ice core (*47*) and in the Vostok ice core, Antarctica (*40*). ppbv, parts per billion per volume. The termination II Ba/Ca record is slightly affected by sedimentary contamination, and measurements older than ~127,000 yr B.P. are not shown (*10*). Abrupt monsoon WA and EA changes occurred late in the deglacial phase, whereas SSTs warmed relatively continuously and without abrupt shifts throughout the deglaciation. This observation suggests that the WA and EA monsoons acted in synchrony and supports the notion that the abrupt atmospheric methane increase associated with glacial terminations may have its source in monsoon areas (*46*, *48*).

forcing, thereby acting as a tropical feedback. Thus, EEA SST was mainly controlled by radiative forcing corresponding to the variation of atmospheric greenhouse gases (*40*) and orbital forcing (precession); submillennial ice-sheet instabilities in the northern high latitudes did not leave a strong imprint in the thermal evolution of the open-ocean tropical Atlantic, as has been previously observed in the Pacific (*45*). This strongly supports the general observation that thermal changes in the tropics primarily reflect greenhouse forcing and, to a lesser extent, orbital insolation changes.

WA monsoon in the context of the global monsoon system. The results of this study demonstrate the interplay and importance of several factors and forcings that govern the WA monsoon system at different time scales and boundary conditions. The role of low-latitude midsummer solar insolation and tropical SST in modulating the WA monsoon system is clearly evident, but millennial-scale extratropical influences can override ironical forcing. The major increase of deglacial WA monsoon precipitation coincides, within age model uncertainty, with the intensification of the EA monsoon (*27*, *46*) and rapid increase of atmospheric methane (*40*, *47*). This observation suggests that, during deglaciation, the WA and EA monsoons acted in synchrony and supports the notion that the abrupt atmospheric methane increase associated with glacial terminations may have its source in monsoon areas (*46*, *48*) (Fig. 5). However, the WA and EA monsoons responded differently to millennial-scale extratropical influence during the penultimate interglacial: The WA monsoon was weak during GIS events, while the EA monsoon largely followed insolation forcing (*27*). In contrast, during late MIS3 and MIS2 the WA monsoon did not vary strongly, while the EA monsoon varied in concert with GIS events. Land-ocean configuration and glacial-interglacial boundary conditions appear to exert constraints on how individual monsoon systems respond to millennial-scale northern high-latitude climate instabilities.

References and Notes

1. F. Gasse, *Quat. Sci. Rev.* **19**, 189 (2000).
2. P. deMenocal, J. Ortiz, T. Guilderson, M. Sarnthein, *Science* **288**, 2198 (2000).
3. F. Gasse, *Quat. Sci. Rev.* **19**, 189 (2000).
4. S. Weldeab, R. R. Schneider, M. Kölling, G. Wefer, *Geology* **33**, 981 (2005).
5. M. R. Talbot, T. Johannessen, *Earth Planet. Sci. Lett.* **110**, 23 (1992).
6. A. T. Adegbie, R. Schneider, D. Röhl, G. Wefer, *Palaeogeogr. Palaeoclimatol. Palaeoecol.* **197**, 323 (2003).
7. T. M. Shanahan *et al.*, *Palaeogeogr. Palaeoclimatol. Palaeoecol.* **242**, 287 (2006).
8. S. Levitus, T. P. Boyer, *World Ocean Atlas 1994* (National Oceanic and Atmospheric Administration, National Environmental Satellite Data, and Information Service, U.S. Department of Commerce, Washington D.C., 1994), vol. 4.
9. G. Gu, R. F. Adler, *J. Clim.* **17**, 3364 (2004).
10. Materials and methods are available as supporting material on Science Online.
11. P. S. Dekens, D. W. Lea, D. K. Pak, H. J. Spero, *Geochem. Geophys. Geosyst.* **3**, 1022 (2002).
12. R. E. Benns, N. Spero, J. Byrne, D. W. Lea, *Paleoceanography* **13**, 150 (1998).
13. G. A. Schmidt, *Paleoceanography* **14**, 482 (1999).
14. I. M. Hall, L.-H. Chan, *Paleoceanography* **19**, PA1017 (2004).
15. J. M. Edmond, K. D. Boyle, D. Drummond, B. Grant, T. Mielbeck, *Mem. J. Soc. Res.* **32**, 324 (1978).
16. M. Colley *et al.*, *Estuar. Coast. Shelf Sci.* **45**, 113 (1997).
17. D. W. Lea, H. Spero, *Paleoceanography* **9**, 445 (1994).
18. A. Ganopolski, C. Kubatzki, M. Claussen, V. Brovkin, V. Petoukhov, *Science* **280**, 1916 (1998).
19. Z. Liu, Y. Wang, R. Gallimore, M. Notaro, I. C. Prentice, *Geophys. Res. Lett.* **33**, L22709 (2006).
20. H. Kuhlmann, H. Meggers, T. Freudenthal, G. Wefer, *Geophys. Res. Lett.* **31**, L22204 (2004).
21. J. E. Kutzbach, Z. Liu, *Science* **278**, 440 (1997).
22. J. Byrne, W. W. Faber, C. Heinleben, *J. Foraminiferal Res.* **20**, 95 (1990).
23. J. E. Janowiak, P. Xie, *J. Clim.* **12**, 3335 (1999).
24. A. M. Lorrain, J. C. Duplessy, J. P. Caret, *Palaeogeogr. Palaeoclimatol. Palaeoecol.* **219**, 225 (2005).
25. U. Salzmann, P. Hoelzmann, I. Morozova, *Quat. Res.* **58**, 73 (2002).
26. D. Hartmann *et al.*, *Science* **309**, 1737 (2005).
27. D. Yuan *et al.*, *Science* **304**, 575 (2004).
28. G. H. Haug, K. A. Hughen, D. M. Sigman, L. C. Peterson, U. Röhl, *Science* **293**, 1304 (2001).
29. A. Berger, M. F. Loutre, *Quat. Sci. Rev.* **10**, 297 (1991).
30. R. K. Andersen *et al.*, *Nature* **431**, 147 (2004).
31. S. Weldeab, R. R. Schneider, M. Kölling, *Earth Planet. Sci. Lett.* **241**, 699 (2006).
32. D. W. Lea, D. K. Pak, L. C. Peterson, K. A. Hughen, *Science* **301**, 1361 (2003).
33. C. Waelbroeck *et al.*, *Quat. Sci. Rev.* **21**, 295 (2002).
34. R. G. Peterson, L. Stramma, *Prog. Oceanogr.* **26**, 1 (1991).
35. X. Wang *et al.*, *Nature* **432**, 740 (2004).
36. S. J. Burns, D. Hartmann, A. Matter, J. Kramers, A. A. Al-Subbary, *Science* **301**, 1365 (2003).
37. H. Schulz, U. von Rad, H. Erlenkeuser, *Nature* **393**, 54 [illegible].
38. L. Wang *et al.*, *Science* **294**, 2345 (2001).
39. L. C. Peterson, G. H. Haug, K. A. Hughen, U. Röhl, *Science* **290**, 1947 (2000).
40. J. R. Petit *et al.*, *Nature* **399**, 429 (1999).
41. D. W. Lea, D. K. Pak, H. J. Spero, *Science* **289**, 1719 (2000).
42. R. Sarmiento, R. Migam, S. Weldeab, A. Mackensen, P. D. Naidu, *Geophys. Res. Lett.* **32**, L24605 (2005).
43. R. R. Schneider, P. J. Müller, G. Ruhland, *Paleoceanography* **10**, 197 (1995).
44. D. W. Lea, *J. Clim.* **17**, 2170 (2004).
45. L. Stott, C. Poulsen, S. Lund, R. Thunell, *Science* **297**, 222 (2002).
46. M. J. Kelly *et al.*, *Palaeogeogr. Palaeoclimatol. Palaeoecol.* **236**, 20 (2006).
47. E. J. Brook, T. Sowers, J. Orchardo, *Science* **273**, 1087 (1996).
48. J. P. Severinghaus, T. Sowers, E. J. Brook, R. B. Alley, M. L. Bender, *Nature* **391**, 141 (1998).
49. L. Loulergue, M. E. Raymo, *Paleoceanography* **20**, PA1003 (2005).

50. We thank G. L. Paradis for mass spectrometry operation, T. Guilderson and P. Grootes for accelerator mass spectrometry (AMS)–^{14}C dating, N.-H. Conti, H. Gier, and H. Hecht for stable isotope measurements, Z. Liu for discussion, J. Dupak for sample preparation and discussion, and C. Kühlemann and E. Schefuß for shipboard help. R.R.S thanks Institut Français pour la Recherche et la Technologie Polaires for Calypso coring through European Union grant HPRI-2001-00120. S.W. has been funded by the Deutsche Forschungsgemeinschaft (postdoctoral fellowship grant We 2686/2-1) and D.W.L. by NSF (grants OCE0317611 and OCL050760R).

Supporting Online Material

www.sciencemag.org/cgi/content/full/316/5829/1303/DC1
Materials and Methods
Figs. S1 to S6
Tables S1 and S2
References

26 January 2007; accepted 17 April 2007
10.1126/science.1140461

Legumes Symbioses: Absence of *Nod* Genes in Photosynthetic Bradyrhizobia

Eric Giraud,[1]*† Lionel Moulin,[1] David Vallenet,[2] Valerie Barbe,[3] Eddie Cytryn,[4] Jean-Christophe Avarre,[1] Marianne Jaubert,[1] Damien Simon,[1] Fabienne Cartieaux,[1] Yves Prin,[1] Gilles Bena,[1] Laure Hannibal,[1] Joel Fardoux,[1] Mila Kojadinovic,[5] Laurie Vuillet,[1] Aurélie Lajus,[2] Stephane Cruveiller,[2] Zoe Rouy,[2] Sophie Mangenot,[3] Beatrice Segurens,[3] Carole Dossat,[3] William L. Franck,[6] Woo-Suk Chang,[6] Elizabeth Saunders,[7] David Bruce,[7] Paul Richardson,[8] Philippe Normand,[9] Bernard Dreyfus,[1] David Pignol,[5] Gary Stacey,[6] David Emerich,[6] André Vermeglio,[5] Claudine Médigue,[2] Michael Sadowsky[6]*†

Leguminous plants (such as peas and soybeans) and rhizobial soil bacteria are symbiotic partners that communicate through molecular signaling pathways resulting in the formation of nodules on legume roots and occasionally stems that house nitrogen-fixing bacteria. Nodule formation has been assumed to be exclusively initiated by the binding of bacterial host-specific lipochito-oligosaccharidic Nod factors, encoded by the *nodABC* genes, to kinase-like receptors of the plant. Here we show by complete genome sequencing of two symbiotic, photosynthetic, *Bradyrhizobium* strains, BTAi1 and ORS278, that canonical *nodABC* genes and typical lipochito-oligosaccharidic Nod factors are not required for symbiosis in some legumes. Mutational analyses indicated that these unique rhizobia use an alternative pathway to initiate symbioses, where a purine derivative may play a key role in triggering nodule formation.

Legume plants have developed symbiotic associations with specific soil bacteria, collectively referred to as the rhizobia, which allow plants to thrive and reproduce in nitrogen-poor environments. These plant-bacterial symbiotic associations typically result in the formation of root organs, termed nodules, in which the bacteria differentiate into nitrogen-fixing bacteroids. Initiation of nodule development involves molecular recognition between both symbiotic

partners (*1*–*4*). Flavonoid molecules exuded by plant roots induce expression of bacterial nodulation (*nod*) genes leading to the synthesis of Nod factors, rhizobial lipochito-oligosaccharide signal molecules. Synthesis of the Nod-factor chitin oligomer backbone requires the activity of three specific enzymes, encoded by the *nodABC* genes, which are present in all rhizobia characterized thus far. Nod factor signal molecules are recognized by plant kinases of the LysM-RLKs family, which, in turn, initiate a developmental program in the legume host resulting in the formation of the nodule structure. The ubiquitous presence of *nod* genes and Nod factors in all rhizobia led to the development of a universal "lock-and-key" hypothesis (*5*, *6*), which states that all symbiotic legumes and rhizobia have host nodulation determinants and homologs of the known nodulation genes, respectively.

The rhizobia belong to the alpha and beta subclasses of the Proteobacteria (*7*), and most species belong to the genera *Rhizobium*, *Bradyrhizobium*, *Mesorhizobium*, *Sinorhizobium*, and *Azorhizobium*. Among them, some photosynthetic *Bradyrhizobium* sp. strains specifically induce nodules on both the root and stem of the aquatic legume *Aeschynomene* (*8*). According to their host specificity within different species of *Aeschynomene*, two groups of photosynthetic *Bradyrhizobium* have been described (*8*). Group I strains contain the common nodulation genes *nodABC* and form nodules on all stem-nodulating *Aeschynomene* species (*9*), whereas nodulation ability in group II strains is restricted to a few species, including *A. sensitiva* and *A. indica*. The *nod* genes have not been detected in group II strains.

To unravel the genetic features contributing to the symbiotic properties of the stem-nodulating *Bradyrhizobium*, we determined the complete genomic sequences of two group II photosynthetic *Bradyrhizobium* strains, BTAi1 and ORS278 (*10*). We also performed a genome-wide screen for mutants unable to induce nodules on *Aeschynomene* plants.

General genome features. The photosynthetic *Bradyrhizobium* strains ORS278 and BTAi1 were isolated from stem nodules of two *Aeschynomene* species, *A. sensitiva* and *A. indica*, in Africa and North America, respectively. The ORS278 and BTAi1 strains were sequenced by Genoscope (France) and the U. S. Department of Energy (DOE) Joint Genome Institute (USA), respectively (see SOM). Manual annotation of both genomes was conducted using MaGe comparative genomic software (*11*).

The ORS278 genome consists of a single circular chromosome of 7,456,587 base pairs (bp); the BTAi1 genome contains both a large chromosome of 6,264,689 bp and a single circular 228,826-bp plasmid, pBTAi1. Chromosomes from ORS278 and BTAi1 are almost identical in G+C content, 65.5 and 64.9%, respectively. In contrast, the G+C content of plasmid pBTAi1 is 60.7%. The genomes of ORS278 and BTAi1 contain 6752 and 7729 predicted coding sequences (CDSs), respectively, of which 59 and 60.1% could be assigned putative functions (Table 1).

Comparative genomic analyses. BLAST analyses indicate that the genomes of BTAi1 and ORS278 share more genes with *B. japonicum* (4802) than with their closest photosynthetic neighbor, *Rhodopseudomonas palustris* (2563) (*12*). This agrees with phylogenies created using 16S ribosomal RNA sequences (*13*). A cross-comparison of the two photosynthetic *Bradyrhizobium* genomes identified a common pool of 1343 genes, whereas 1274 and 2133 genes were unique to ORS278 and BTAi1, respectively. Most of the 1343 genes in common were homogenously distributed on the genomes (Fig. 1), except for genes involved in photosynthesis, which were clustered in a 50-kb region. This region, designated the photosynthesis gene cluster (PGC), is common in purple photosynthetic bacteria. The organization of the PGC is identical in the BTAi1 and ORS278 strains and is highly conserved with the PGC in *R. palustris*. In addition, the G+C content (67%) of the *Bradyrhizobium* PGCs is similar to the rest of the genomes. *Bradyrhizobium* strains BTAi1 and ORS278 also have additional genes specialized in light perception and response, including three putative bacteriophytochromes (biliprotein photoreceptors) and two *kaiBC* circadian clock operons. Taken together, these data strengthen previous hypotheses that photosynthetic capacity is an ancestral trait in these *Bradyrhizobium* strains that was subsequently lost in most rhizobial lineages (*14*).

The large variation in genome sizes (1.6 Mb between ORS278 and *B. japonicum*, and 1 Mb between ORS278 and BTAi1), the overall low level of synteny (Fig. 2 and fig. S1), and the presence of numerous mobile genetic elements indicate that bradyrhizobia genomes are highly plastic. Indeed, the genomes of ORS278 and BTAi1 contain 21 and 29 putative horizontally acquired genomic islands (HAIs), respectively, displaying hallmarks of recent gene transfer events (Fig. 1 and tables S1 and S2). HAIs may confer functional advantages in the adaptation of these strains to their symbiotic or free-living ecological niches. Genes encode for important metabolic functions on HAIs, in both strains, including the following: (i) a ribulose 1,5-bisphosphate carboxylase (RuBisCO); (ii) enzymes involved in nitrogen metabolism, including urease; (iii) lipopolysaccharide (LPS) modification enzymes; (iv) a type II secretion system; (v) a chemotaxis operon; and (vi) a multidrug efflux pump. In addition, the BTAi1 genome contains a specialized HAI that is made up of all the genes necessary for CO_2 fixation, along with a hydrogenase gene cluster. Remarkably, this

Table 1. General features of *Bradyrhizobium* genomes. The distribution of CDSs for *B. japonicum* is derived from the original annotation (*29*). IS, insertion sequence.

Genome feature	*Bradyrhizobium* sp.		*B. japonicum*
	ORS278	BTAi1	USDA 110
Genome size (bp)	7,456,587	6,493,515	9,105,828
G+C content (%)	65.5	64.9	64.1
Ribosomal RNA operons	2	2	1
Transfer RNAs	50	52	50
Total protein-coding genes	6,752	7,729	8,317
Assigned function (%)	59	60.1	52.3
Conserved hypothetical (%)	27.7	31.8	30.1
Hypothetical (%)	13.3	8.1	17.6
Coding DNA (%)	90.5	91.0	91.3
Plasmid no. (size in bp)	0	1 (228,826)	0
IS elements (%)	0.5	1.4	2
Pseudogenes (%)	0.3	0.6	0

[1]Laboratoire des Symbioses Tropicales et Méditerranéennes, Unité mixte recherche (UMR) 113, Institut de Recherche pour le Developpement, Centre de Coopération Internationale en Recherche Agronomique pour le Developpement, AGRO Montpellier, Institut National de la Recherche Agronomique, Université Montpellier 2, 34 A-B-20, Campus de Baillarguet, 34398 Montpellier Cedex 5, France. [2]Genoscope, CNRS UMR 8030, Atelier de Génomique Comparative, 2 rue Gaston Crémieux, BP5706, 91057 Evry Cedex, France. [3]Genoscope, Centre National de Séquençage, 2 rue Gaston Crémieux, BP5706, 91057 Evry Cedex, France. [4]Department of Soil, Water and Climate, Biotechnology Institute, and Microbial and Plant Genomics Institute, University of Minnesota, 1991 Upper Buford Circle, 439 Bioscience Center, St. Paul, MN, 55108, USA. [5]Commissariat à l'Energie Atomique (CEA), Cadarache, Direction des Sciences du Vivant, Institut de Biologie Environnementale et Biotechnologie, Service de Biologie Végétale et de Microbiologie Environnementale, Laboratoire de Bioénergétique Cellulaire, DSV/IBEB/SBVME/LBC, UMR 6191 CNRS/CEA/Université Aix-Marseille, Saint-Paul-lez-Durance, F-13108, France. [6]National Center for Soybean Biotechnology, Division of Plant Sciences and Biochemistry, Department of Molecular Microbiology and Immunology, University of Missouri, Columbia, MO, 65211, USA. [7]Department of Energy (DOE) Joint Genome Institute, Los Alamos National Laboratory, Los Alamos, NM 87545, USA. [8]DOE Joint Genome Institute, Walnut Creek, CA 94598, USA. [9]Université Lyon1, CNRS, UMR 5557, Ecologie Microbienne, Lyon, F-69003, France.

*To whom correspondence should be addressed. E-mail: giraud@supagro.inra.fr (E.G.); sadowsky@umn.edu (M.S.)

†E.G. and M.S. coordinated the sequence annotation of the *Bradyrhizobium* ORS278 and BTAi1 genomes, respectively.

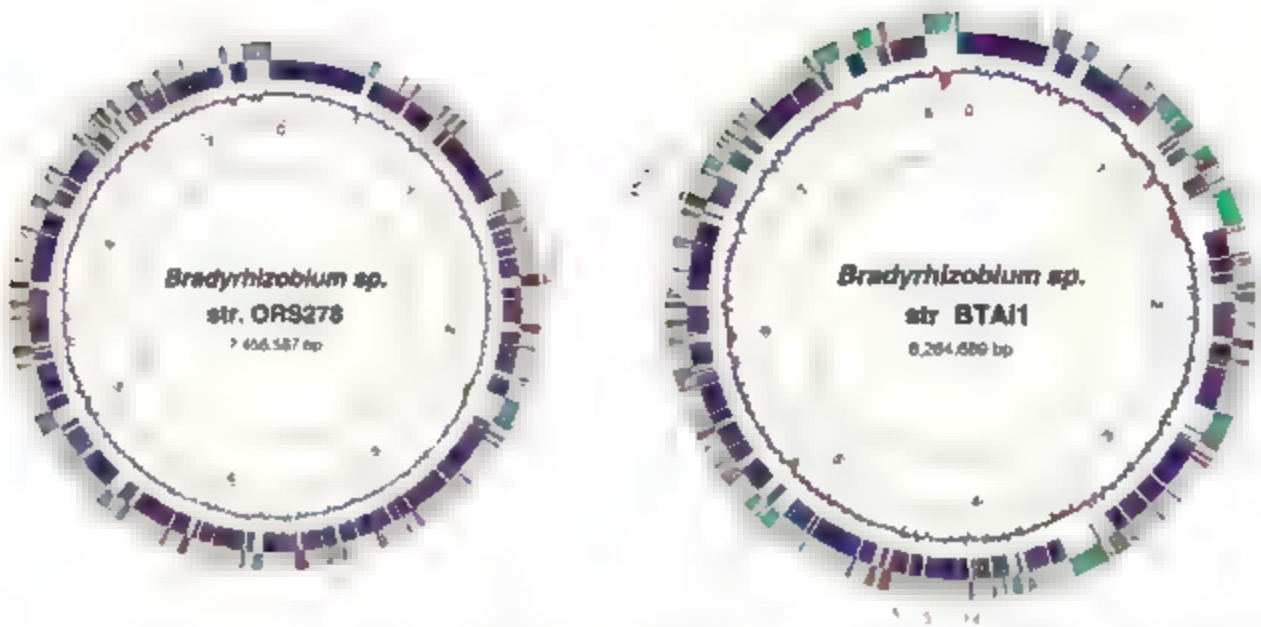

Fig. 1. Circular representation of the *Bradyrhizobium* strains ORS278 and BTAi1 chromosomes. Circles, from the inside out, show (1) GC skew (G+C/G−C using a 1-kb sliding window), (2) IS elements and transposases, (3) the coordinates in Mb beginning at 0 = oriC, and (4) GC deviation (mean GC content in a 1-kb window—overall mean GC). Regions with a GC deviation less than two times the standard deviation are highlighted in red. Circles 5 and 6 show the gene content comparison between the ORS278, BTAi1, and *B. japonicum* USDA110 genomes by using a similarity threshold of 40% identity and a ratio of 0.8 of the length of the smallest protein: blue, backbone genes found in all three strains; red, genes present in ORS278 and BTAi1, but absent from USDA110; cyan in (ORS278) show genes present in ORS278 and USDA110, but not in BTAi1, and in (BTAi1), genes present in BTAi1 and USDA110, but not in ORS278; green, genes specific to each strain. The different genomic islands identified in both chromosomes are highlighted by number. See tables S1 and S2.

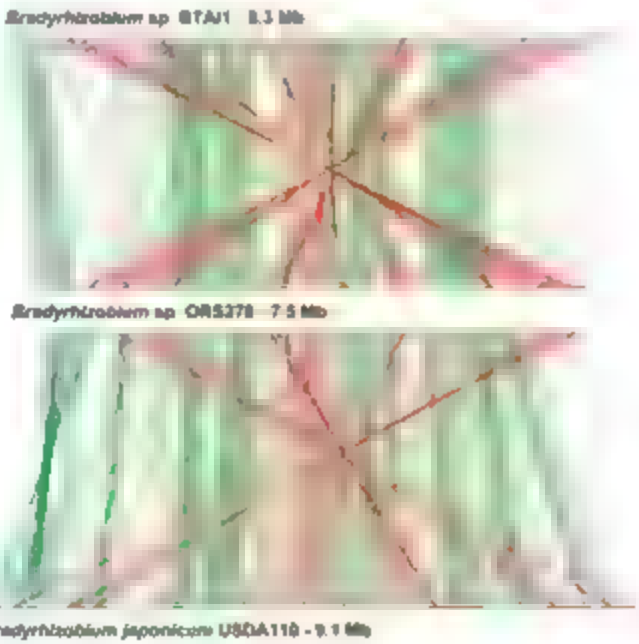

Fig. 2. Synteny plot between the three Bradyrhizobial chromosomes. This line plot (*11*) was obtained by using synteny results between *Bradyrhizobium* sp. BTAi1 and *Bradyrhizobium* sp. ORS278, as well as results obtained from comparison of *Bradyrhizobium* sp. ORS278 and *Bradyrhizobium japonicum* USDA110. Synteny groups containing a minimum of five homologous genes are drawn in green for colinear regions, and in red for inverted regions.

strain harbors three RuBisCOs, which assimilate CO_2, and three uptake hydrogenase complexes, one of which is plasmid-borne; the other two are in an HAI and close to the PGC. The presence of these elements suggests that these bacteria have an exceptional ability to fix CO_2 partly due to reducing power furnished by the photosynthetic activity and partly by the uptake hydrogenase enzymes, which potentially scavenge hydrogen produced during nitrogen fixation.

No symbiotic genes (*nod*, *nif*, or *fix*) were found on islands in the chromosomes of ORS278 and BTAi1 or on plasmid pBTAi1 (tables S1 and S2). Although the *nif* and *fix* genes are clustered in a 45-kb region of the BTAi1 and ORS278 genomes, there is no evidence that this region was acquired by lateral transfer. This is in contrast to all rhizobial genomes characterized to date (*15*–*27*), which have nodulation and nitrogen fixation genes clustered either on plasmids or in large chromosomal symbiotic islands, for example, as observed in *B. japonicum* USDA110 (see fig. S2).

Lack of canonical nodulation genes. BLAST analyses indicate that neither the BTAi1 nor the ORS278 genome contain homologs of NodA (acyl transferase) or NodC (oligomerization of *N*-acetyl-glucosamine), two of the three enzymes essential for the synthesis of lipochitooligosaccharide Nod factors in rhizobia. Although a homologous gene in both strains displayed a moderate level of amino acid identity (33 to 36%) to NodB from *Rhizobium galegae*, this homology was limited only to the polysaccharide deacetylase domain of NodB (Table 2), a motif found in other enzymes, including chitin deacetylases and endoxylanases. The low identity that these CDSs have to NodB and the absence of *nodA* and *nodC* gene homologs indicate that the canonical *nodABC* genes are absent in both the BTAi1 and ORS278 genomes. CDSs displaying some similarity to other Nod proteins are present in the genomes of both BTAi1 and ORS278 (Table 2); however, these homologs are well conserved in other nonsymbiotic prokaryotes.

Consistent with genomic information revealed by our analyses, two other observations

support our statement that ORS278 and BTAi1 are unique among rhizobia. First, infection of *A. sensitiva* by ORS278 (fig. S3) revealed the absence of Nod factor–mediated root-hair deformation that classically precedes the entry of rhizobia into legumes. Despite this, the nodules induced by ORS278 (*14*) on the stems and roots of *Aeschynomene* displayed the functional characteristics of classical nodules induced by other rhizobia, such as the synthesis of leghemoglobin, nitrogenase activity, and transfer of fixed N_2 into the plant. Second, the production of classical Nod factor–like compounds by strain ORS278 could not be shown when genistein was used as a *nod*-gene inducer and with a Nod factor isolation method currently shown to work with bradyrhizobia (*22*, *23*). To show more definitively that classical Nod factors are not involved in the *A. sensitiva* symbiosis, we examined the nodulation phenotype of a *nodB* mutant of the broader host-range *Bradyrhizobium* sp. strain ORS285 (group I). This strain nodulates both *A. sensitiva* and *A. afraspera*, whereas the ORS278 and BTAi1 strains do not nodulate *A. afraspera*. As shown in Fig. 3, this mutant failed to induce root and stem nodules on *A. afraspera*, although it maintained its ability to form nitrogen-fixing nodules on roots and stems of *A. sensitiva* with an efficiency similar to that of the wild-type strain. These observations and results demonstrate that the canonical common nodulation genes and, thus, typical lipochitooligosaccharide Nod factors are not required for the symbiotic interaction of the photosynthetic bradyrhizobia with *A. sensitiva*.

The absence of *nodABC* genes in *Bradyrhizobium* strains ORS278 and BTAi1 raises the question of the nature of the bacterial signal used to induce nodule formation on *A. indica* and *A. sensitiva* plants. Analysis of the ORS278 and BTAi1 genomes revealed several other genes involved in plant-microbe symbiotic and pathogenic interactions (table S3). These include genes involved in the following: (i) synthesis or degradation of phytohormones (*24*), (ii) modification of O-antigen (or LPS) (*25*, *26*), and (iii) biosynthesis of exopolysaccharides (*5*, *27*). Nevertheless, the symbiotic role of these candidate genes remains highly speculative, and we cannot rule out the possibility that the mechanism of interaction involves genes of unknown function.

Nodulation defective mutants. In order to identify new genes involved in the interaction between the group II photosynthetic bradyrhizobia and *A. sensitiva* and *A. indica* plants, a library of ORS278 transposon (Tn*5*) mutants was screened for strains unable to induce nodule formation on *A. sensitiva*. Of the 4500 mutants tested, 27 were found to be severely defective in symbiosis, most eliciting only a few pseudonodules on a small number of plants (Table 3). Some plants displayed an apparent nodulation-minus phenotype, and microscope examination often revealed a small number of pseudonodules. No completely nodulation-deficient mutant could be found; we tentatively attribute this phenotype to one or more factors: (i) there are redundant genes controlling this initial step in the symbiotic process, (ii) the appropriate mutation may be fatal in this bacterium, or (iii) the mutagenesis procedure used was not saturating, and an essential gene may have been missed.

The site of Tn*5* insertion in each of the 27 symbiosis-deficient mutants was determined, and none were found to have a mutation in a CDS that could encode the action of the Nod ABC proteins. Four classes of mutants were distinguished. Class I comprised 11 independent amino acid requiring (AA) auxotrophic mutants. Numerous AA auxotrophs of rhizobia were found to be defective in symbiosis (*28*–*31*), and generally, these have symbiotic capacity rescued with the addition of the missing amino acid(s). This suggests that the absence of symbiosis stems from a growth deficiency, rather than an alteration in the infection process (*30*, *32*). The single class II mutant had an insertion in *glnD*, a uridyltransferase uridylt-removing enzyme constituting the sensory component of the nitrogen regulation (ntr) system, similar to a *Rhizobium leguminosarum glnD* mutant impaired in cell

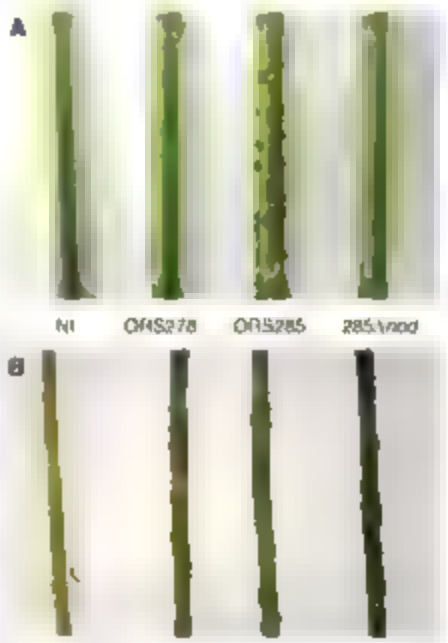

Fig. 3. Efficiency of stem nodulation by *Bradyrhizobium* sp. strains ORS278, ORS285, and the *nod* gene deletion mutant ORS285Δ*nodB* (285Δ*nod*) on *A. afraspera* (**A**) and *A. sensitiva* (**B**). The NI refers to the noninoculated control. The ORS285 Δ*nodB* mutant was obtained by homologous recombination as described (*14*) after insertion of the *lacZ-KanR* cassette (pKOK5) in the unique Xho I site of *nodB*. Plants were inoculated and cultivated as described (*14*).

Table 2. Coding sequences in the ORS278 and BTAi1 genomes showing similarities with known nodulation (Nod) proteins. Absent refers to no hits with ≥30% amino acid identity using the BLASTP algorithm. Brado and BBta refer to *Bradyrhizobium* sp. strains ORS278 and BTAi1, respectively. CDS with best BLASTP hits. Percent amino acid similarity to named species of the BLASTP hit. Acc no., GenBank accession numbers of the Nod protein. E value of the BLASTP hit. Abbreviations: *R.*, *Rhizobium* sp., *M.*, *Mesorhizobium* sp., *R. leg.*, *Rhizobium leguminosarum* bv. *viciae*; and *B.*, *Bradyrhizobium* sp.

Nod protein	*Bradyrhizobium* sp. strains							
	ORS278				BTAi1			
	CDS	Similarity (%)	Acc. no.	E value	CDS	Similarity (%)	Acc no.	E value
NodA	Absent				Absent			
NodB	Brado4564	33% to *R. galegae*	P50354	$2e^{-16}$	BBta4792	36% to *R. galegae*	P50354	$2e^{-16}$
NodC	Absent				Absent			
NodD	Brado3695	39% to *R.*	Q53061	$1e^{-54}$	BBta1932	38% to *R.*	Q53061	$1e^{-53}$
NodE	Absent				BBta0068	31% to *R. leg.*	P04684	$1e^{-47}$
NodG	Brado3311	66% to *M.*	P72332	$4e^{-86}$	BBta3818	65% to *M*	P72332	$2e^{-85}$
NodI	Brado0517	39% to *R. tropici*	Q933C0	$5e^{-37}$	BBta7658	39% to *R. tropici*	Q933C0	$4e^{-35}$
NodJ	Absent				Absent			
NodL	Brado2093	42% to *R. leg*	P08632	$2e^{-81}$	Absent			
NodM	Brado3763	78% to *B.*	Q9AQ10	$1e^{-277}$	BBta4166	76% to *B.*	Q9AQ10	$1e^{-269}$
NodP	Brado5192	75% to *B. elkanii*	BAB55898	$1e^{-132}$	BBta0328	73% to *R.*	P72338	$2e^{-125}$
NodQ	Brado5193	66% to *B. elkanii*	BAB55899	$5e^{-234}$	BBta0327	55% to *R.*	O07309	$2e^{-195}$

viably (*33*). Similarly, class III contained a single mutant with an insertion in a key enzyme (PyrF, orotidine 5′-phosphate decarboxylase) of the pyrimidine biosynthesis pathway.

In contrast, class IV contained 14 mutants that were affected in the biosynthesis of purines. The mutated genes (10) were scattered throughout the ORS278 genome, which indicated that there was no Tn*5* integration hotspot and that purines play a pivotal role in the symbiotic process. Symbiotically defective purine auxotrophs of several *Rhizobium* species have been previously reported (*34*–*36*). The intriguing finding that purine intermediates, such as 5-aminoimidazole-4-carboxamide riboside (AICAR), rather than purine itself can partially restore nodulation deficiency in purine mutants of *Rhizobium leguminosarum* or *R. etli* suggested that a purine precursor might act as a signal molecule during infection (*35*, *37*).

To further examine this, a ORS278 *purL* mutant, which only produced a few pseudonodules, was evaluated for its ability to normally nodulate *A. sensitiva* in the presence of the purine biosynthesis precursors AICAR, inosine monophosphate (IMP), and adenosine monophosphate (AMP) (fig. S4). In the absence of precursors, the mutant bacterium proliferated on the root surface, which indicated that the host plant can supply the required nutrient(s) for mutant growth. In addition, although cytological analysis showed that pseudonodules elicited by the *purL* mutant contained bundles of infection threads progressing intercellularly around the meristematic zone, the bacteria were not released into meristematic cells. In contrast, the symbiotic ability of the mutants was partially restored when the plant culture medium was supplemented with AICAR, IMP or AMP at 0.5 mM. Treatment of plants with these compounds allowed the mutant to proliferate in meristematic cells, and plants had normal size nodules.

Similar observations were obtained using *purH* and *purB* mutants, except that the partial rescue of the *purH* mutant was observed only in the presence of IMP and AMP and the nodulation phenotype of the *purB* mutant was only rescued in the presence of AMP. Taken together, these data suggest that a purine derivative, which may be a cytokinin-like molecule, plays a key role in the formation of nodules on *A. sensitiva*, and presumably *A. indica*, by the photosynthetic bradyrhizobia. This hypothesis is consistent with previous observations that (i) several *Bradyrhizobium* strains were shown to produce cytokinin compounds (*38*, *39*); (ii) a Nod factor deficient *Sinorhizobium* strain carrying a constitutive transzeatin secretion (*tzs*) gene involved in cytokinin production induced nodule-like structures on alfalfa plants (*40*); and (iii) a plant cytokinin-receptor was shown to play a key role in the activation of nodule organogenesis in *Lotus japonicus* (*41*, *42*). We were unable to identify a homolog to the *tzs* gene in the ORS278 or BTAi1 genomes, this suggests that these two strains may use a different pathway for cytokinin production. This is likely the case, as *B. japonicum* USDA110, which produces cytokinin molecules (*39*), also lacks a *tzs* homolog.

Our data show that nodulation of some legumes by rhizobia occurs in the absence of the *nodABC* genes and lipochito-oligosaccharidic Nod factors, which indicates that other signaling strategies can trigger nodule organogenesis in some legumes. The *nodABC* genes have been identified in all the rhizobia thus far characterized, consisting of hundreds of symbiotically distinct strains isolated worldwide. This indicates that the nodulation of legumes in the absence of canonical *nod* genes is likely an unusual phenomenon. However, such a discovery is highly significant and raises several interesting questions. Is the first recognition step initiated by Nod factor simply bypassed in some legume plants, especially those allowing infection via crack entry? What is the signal molecule(s) directly triggering nodule organogenesis in *Aeschynomene*? Is there any relation between the molecular mechanism used by photosynthetic bradyrhizobia and other symbiotic organisms, such as *Frankia* which induces nodulation on nonleguminous plants? Our discovery should stimulate research on plant-bacteria interactions by providing insight into the diversity and evolution of symbiotic strategies used by both partners.

Table 3. *Bradyrhizobium* sp. strain ORS278 mutants affected in symbiosis with *Aeschynomene sensitiva*. Mini-transposon mTn*5*-GN*m* (*43*) containing a *gusA* reporter gene and the *nptII* gene encoding neomycin resistance, was used for the construction of the insertion mutants. After mutagenesis, the mutants were selected on YM-modified rich medium (*34*) containing kanamycin (50 μg/ml) and nalidixic acid (35 μg/ml). Each of the 9500 mutants was initially individually tested on one *A. sensitiva* plant. Mutants having an alteration in their nodulation efficiency were retested using three plants per mutant, and subsequently tested again in a third analysis with six additional plants. The localization of the site of Tn*5* insertion in symbiotically deficient mutants was ascertained as previously described (*44*). Mutant number describes the number of independent mutants identified in the corresponding CDS. Phenotype shows the number of plants not nodulated (−), number of plants having pseudonodules (PN), and number of plants having classical nodules (+).

CDS	Gene	Function	Mutant no.	Phenotype
		Amino acid auxotrophs		
Brado0374	*leuC*	Leucine biosynthesis	5	9−, 1PN
Brado0365	*leuD*	Leucine biosynthesis	2	8−, 2PN
Brado3572	*hom (metL)*	Homoserine biosynthesis	1	4−, 2PN, 4+
Brado0430	*proA*	Proline biosynthesis	1	9−, 1PN
Brado6238	*gltB*	Glutamate biosynthesis	2	8−, 2PN
		Nitrogen regulation system		
Brado0530	*glnD*	Nitrogen regulation system	1	8−, 2PN
		Pyrimidine or purine biosynthesis		
Brado0160	*pyrF*	Pyrimidine biosynthesis	1	4−, 6PN
Brado3260	*purF*	Purine biosynthesis	1	5−, 5PN
Brado6088	*purD*	Purine biosynthesis	2	5−, 5PN
Brado2785	*purL*	Purine biosynthesis	3	6−, 4PN
Brado3344	*purM*	Purine biosynthesis	1	8−, 2PN
Brado1206	*purE*	Purine biosynthesis	1	2−, 8PN
Brado2830	*purB*	Purine biosynthesis	2	9−, 1PN
Brado0338	*purH*	Purine biosynthesis	1	9−, 1PN
Brado5935	*purA*	Purine biosynthesis	1	8−, 2PN
Brado3165	*guaB*	Purine biosynthesis	1	2−, 8PN
Brado3317	*gmk*	Purine biosynthesis	1	7−, 3PN

References and Notes

1. X. Perret, C. Staehelin, W. J. Broughton, *Microbiol. Mol. Biol. Rev.* **64**, 180 (2000).
2. J. Cullimore, J. Dénarié, *Science* **302**, 575 (2003).
3. R. Geurts, E. Fedorova, T. Bisseling, *Curr. Opin. Plant Biol.* **8**, 346 (2005).
4. G. Starey, M. Libbenb, I. Brechenmacher, J. Wan, G. Bi May, *Curr. Opin. Plant Biol.* **9**, 110 (2006).
5. W. J. Broughton, S. Jabbouri, X. Perret, *J. Bacteriol.* **182**, 5641 (2000).
6. M. Patriarca, A. Downie, *Nature* **425**, 569 (2003).
7. L. Moulin, A. Munive, B. Dreyfus, C. Boivin-Masson, *Nature* **411**, 948 (2001).
8. L. Giraud, D. Fleischman, *Photosynth. Res.* **82**, 115 (2004).
9. C. Chaintreuil, C. Boivin, B. Dreyfus, E. Giraud, *FEMS Microbiol. Lett.* **194**, 83 (2001).
10. Materials and methods are available as supporting material on *Science* Online.
11. D. Vallenet *et al.*, *Nucleic Acids Res.* **34**, 53 (2006).
12. Two genes were considered orthologs when their products satisfy the bi-directional best hit (BBH) criterion, based on BLAST comparisons with an identity threshold of 40% over more than 80% of the length of the smallest protein.
13. J. P. W. Young, H. L. Downer, B. D. Eardly, *J. Bacteriol.* **173**, 2271 (1991).
14. E. Giraud, L. Hannibal, J. Fardoux, A. Vermeglio, B. Dreyfus, *Proc. Natl. Acad. Sci. U.S.A.* **97**, 14795 (2000).
15. C. Freiberg *et al.*, *Nature* **387**, 394 (1997).
16. T. Kaneko *et al.*, *DNA Res.* **7**, 331 (2000).
17. F. Galibert *et al.*, *Science* **293**, 668 (2001).
18. M. A. Barnett *et al.*, *Proc. Natl. Acad. Sci. U.S.A.* **98**, 9883 (2001).

19. T. Kaneko *et al.*, *DNA Res.* **9**, 189 (2002).
20. V. Gonzalez *et al.*, *Proc. Natl. Acad. Sci. U.S.A.* **103**, 3834 (2006).
21. J. P. Young *et al.*, *Genome Biol.* **7**, R34 (2006).
22. P. Roche, F. Jerouge, C. Ponthus, J. C. Promé, *J. Biol. Chem.* **266**, 10933 (1991).
23. J. Dénarié and F. Maillet, personal communication.
24. A. Costacurta, J. Vanderleyden, *Crit. Rev. Microbiol.* **21**, 1 (1995).
25. F. Jerouge, J. Vanderleyden, *FEMS Microbiol. Rev.* **26**, 17 (2002).
26. W. D'Haeze, M. Holsters, *Trends Microbiol.* **12**, 555 (2004).
27. J. A. Leigh, D. L. Coplin, *Annu. Rev. Microbiol.* **46**, 307 (1992).
28. J. Dénarié, B. Bergeron, in *Symbiotic Nitrogen Fixation*, P. S. Nutman, Ed. (Cambridge Univ. Press, Cambridge, 1975), pp. 47–61.
29. M. M. Meade, S. R. Long, G. B. Ruvkun, S. E. Brown, F. M. Ausubel, *J. Bacteriol.* **149**, 114 (1982).
30. M. J. Sadowsky, K. Rastas, P. R. Sims, H. Bursey, O. P. S. Verma, *Arch. Microbiol.* **144**, 334 (1986).
31. J. S. So *et al.*, *Mol. Gen. Genet.* **207**, 15 (1987).
32. E. J. Palmiano, R. Tate, M. Goodwin, *Microbiol. Mol. Biol. Rev.* **66**, 703 (2002).
33. A. Schlüter, M. Mohlen, M. Kramer, R. Defar, U. B. Priefer, *Microbiology* **146**, 2967 (2000).
34. C. E. Pankhurst, E. A. Schwinghamer, *Arch. Microbiol.* **100**, 219 (1974).
35. K. D. Noel, K. J. Dietzold, J. R. Cava, H. A. Bindi, *Arch. Microbiol.* **149**, 499 (1988).
36. M. Collavino, P. M. Riccillo, O. H. Grasso, M. Crespo, M. Aguilar, *Mol. Plant Microbe Interact.* **18**, 742 (2005).
37. J. D. Newman, K. J. Dietzold, B. W. Schultz, K. D. Noel, *J. Bacteriol.* **176**, 3286 (1994).
38. D. B. Sturtevant, B. J. Taller, *Plant Physiol.* **89**, 1247 (1989).
39. L. Boivin *et al.*, *Appl. Microbiol. Biotechnol.* **74**, 874 (2007).
40. J. B. Cooper, S. R. Long, *Plant Cell* **6**, 215 (1994).
41. J. D. Murray *et al.*, *Science* **315**, 101 (2007).
42. L. Tirichine *et al.*, *Science* **315**, 104 (2007).
43. W. G. Reeve *et al.*, *Microbiology* **145**, 1307 (1999).
44. M. A. Jacobs *et al.*, *Proc. Natl. Acad. Sci. U.S.A.* **100**, 14339 (2003).
45. We thank [illegible] technical help, S. Sylla and F. Ndoye for providing *Aeschynomene* seeds, and the DOE's Joint Genome Institute production sequencing team. The sequencing work on ORS278 was performed at Genoscope, Evry, France and supported by the Consortium National de la Recherche en Génomique (CNRG) and INRIA (ACI IMPBio2004). A portion of the BTAi1 sequencing work was performed under the auspices of the U.S. Department of Energy's Office of Science, Biological and Environmental Research Program, by the University of California, Lawrence Livermore National Laboratory, Lawrence Berkeley National Laboratory, and Los Alamos National Laboratory. This work was supported, in part, from grants from the French Agence Nationale de la Recherche (ANR Blanc), and grant 2004-35604-14708 from the National Research Initiative of the Cooperative State Research, Education, and Extension Service, U.S. Department of Agriculture (USDA) (to D.E., M.S., and G.S.). Sequences of the entire genomes of *Bradyrhizobium* sp. ORS278 and BTAi1 have been submitted to the EMBL database under accession number CU234118, and to the GenBank database under accession numbers CP000494 (chromosome) and CP000495 (plasmid), respectively. Expert annotation data and comparative analysis results are publicly available via the MaGe interface in the RhizoScope relational database (https://www.genoscope.cns.fr/agc/mage). Strain BTAi1 has been deposited in the American Type Culture Collection under accession number BAA 1182.

Supporting Online Material

www.sciencemag.org/cgi/content/full/316/5829/1307/DC1
Materials and Methods
Figs. S1 to S4
Tables S1 to S3

4 January 2007; accepted 12 April 2007
10.1126/science.1139548

REPORTS

Quantum Register Based on Individual Electronic and Nuclear Spin Qubits in Diamond

M. V. Gurudev Dutt,[1]* L. Childress,[1]* L. Jiang,[1] E. Togan,[1] J. Maze,[1] F. Jelezko,[2] A. S. Zibrov,[3] P. R. Hemmer,[3] M. D. Lukin[1]†

The key challenge in experimental quantum information science is to identify isolated quantum mechanical systems with long coherence times that can be manipulated and coupled together in a scalable fashion. We describe the coherent manipulation of an individual electron spin and nearby individual nuclear spins to create a controllable quantum register. Using optical and microwave radiation to control an electron spin associated with the nitrogen-vacancy (NV) color center in diamond, we demonstrated robust initialization of electron and nuclear spin quantum bits (qubits) and transfer of arbitrary quantum states between them at room temperature. Moreover, nuclear spin qubits could be well isolated from the electron spin, even during optical polarization and measurement of the electronic state. Finally, coherent interactions between individual nuclear spin qubits were observed and their excellent coherence properties were demonstrated. These registers can be used as a basis for scalable, optically coupled quantum information systems.

Quantum registers are controllable quantum systems composed of several qubits. They form fundamental building blocks for quantum information science and can be connected into useful communication and computation systems, for example, via quantum optical channels (*1*–*9*). A useful register must support high-fidelity local operations between its qubits as well as permit excellent isolation of the qubits from each other and from the external environment. Over the past few years, quantum registers consisting of a few interacting trapped ions with exceptional coherence properties have been implemented experimentally (*10*, *11*), and the first steps toward optical interconnections have been taken (*12*, *13*). We report on the realization of a quantum register in a room-temperature solid by means of controlled manipulation of individual electron and nuclear spins.

Our approach makes use of coherent manipulation of the electron spin associated with individual nitrogen-vacancy (NV) centers in diamond (*14*–*18*). The NV center has a long-lived spin triplet as its electronic ground state (*14*) that can be initialized, manipulated, and measured using microwave and optical excitation (Fig. 1A) (*15*). In pure samples, the electron spin acts as a sensitive magnetic probe of the local environment. The electron spin dynamics is governed by interactions with spin-½ ^{13}C nuclei (present in 1.1% natural abundance) in the diamond lattice (Fig. 1B). Although such a nuclear spin environment normally causes dephasing of electron spin qubits (*19*, *20*), we show that if properly controlled it also provides a very useful resource. Certain proximal nuclei, by virtue of their stronger hyperfine interaction and enhanced magnetic moment, can be distinguished from each other and from the rest of the environment (*21*), allowing us to individually address single nuclear spins and to use the resulting electron-nuclear coupled systems as few-qubit registers.

Although nuclear spins are well known for their long coherence times (*22*), conventional techniques for probing them require the use of macroscopic spin ensembles to obtain measurable signals (*23*, *24*). Coherent oscillations of a single nuclear spin were observed in (*25*), using a thermal state of a ^{13}C nuclear spin that was inextricably coupled by strong contact interactions with the nearest-neighbor NV electron spin. In contrast, we demonstrate a high degree of polarization (corresponding to an effective spin temperature below 1 μK) and control over an isolated nuclear spin that is coupled nonlocally to the electron spin. This results in coherence times

[1]Department of Physics, Harvard University, Cambridge, MA 02138, USA. [2]Physikalisches Institut, Universität Stuttgart, Pfaffenwaldring 57, D-70550 Stuttgart, Germany. [3]Department of Electrical and Computer Engineering, Texas A&M University, College Station, TX 77843, USA.

*These authors contributed equally to this work.
†To whom correspondence should be addressed. E-mail: lukin@fas.harvard.edu

that are at least three orders of magnitude longer, and allows independent control over the electron and nuclear spin qubits, which is essential for scalable applications.

Individual nuclear spins in the diamond lattice can be manipulated by combining control over an NV electronic spin with a coherent mapping between electron and nuclear spin states. Consider a system involving an NV electron spin interacting with a single proximal ^{13}C nuclear spin (Fig. 1C). When the electron is in the $m_s = 0$ state, the hyperfine interaction vanishes. When the electron is in the $m_s = -1$ state, the hyperfine interaction introduces a splitting ω_I between the nuclear spin states $|\uparrow\rangle$, $|\downarrow\rangle$. Hence, we can selectively flip the electron spin state conditional on the nuclear spin. If we apply a weak magnetic field perpendicular to the nuclear spin quantiza-

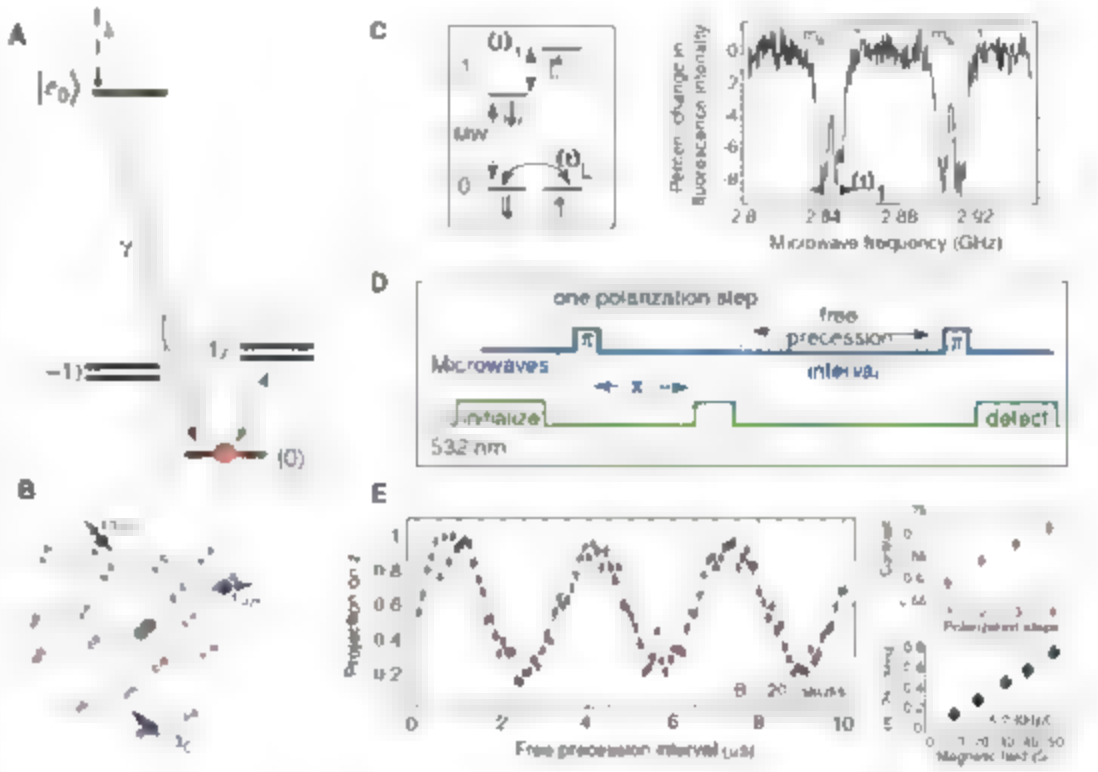

Fig. 1. Isolating, addressing, and reading out single electron and nuclear spins in the register. (**A**) Level diagram for the coupled spin system formed by the NV electron spin and a nearby ^{13}C nuclear spin. Optical transitions of the NV center are used to polarize and measure the electron spin state of the NV. (**B**) Illustration of the ^{13}C environment near the NV center that is used to create the register. (**C**) A single electron spin transition $|0\rangle \leftrightarrow |-1\rangle$ is addressed with resonant microwaves (MW), and hyperfine structure associated with the ^{13}C spin states $|\uparrow\rangle$, $|\downarrow\rangle$ can be resolved within this transition. (**D**) Experimental pulse sequence. As described in the text, we create and measure the nuclear spin polarization in $|\downarrow\rangle$ via the electron spin. (**E**) Nuclear free precession in a ~20-G magnetic field. Top right inset: By increasing the number of polarization steps, a higher contrast for the nuclear free precession signal is obtained. Four polarization steps were used for the data shown. Bottom right inset: Observed Larmor frequency as a function of magnetic field, approximately oriented along $\hat{x} - (\hat{z}/4)$, where $\hat{z}$ is the NV axis.

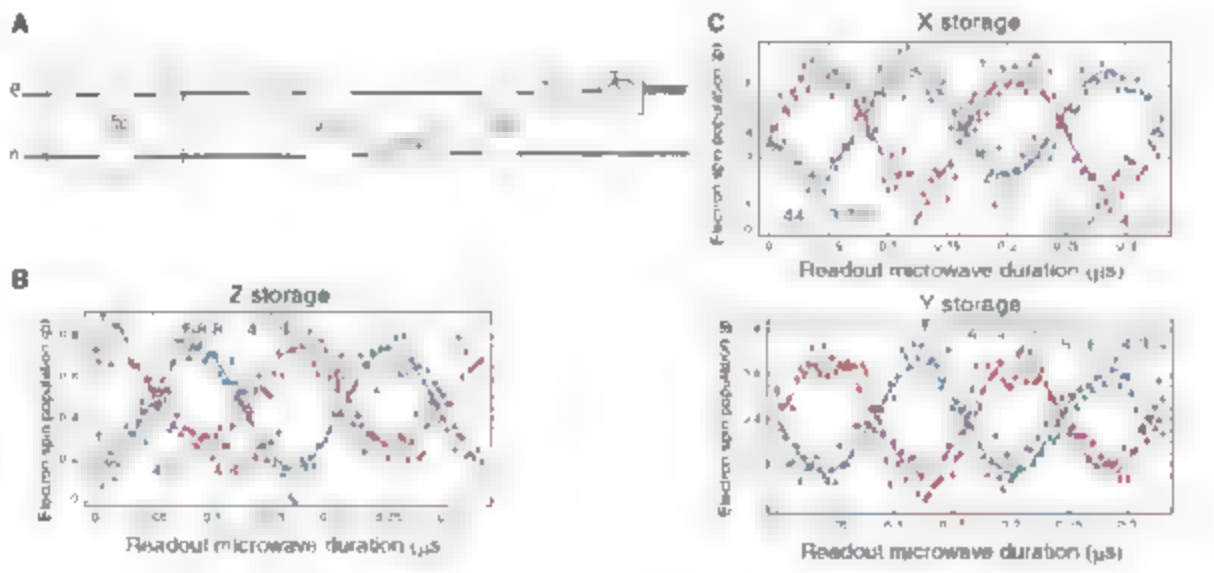

Fig. 2. Storage and retrieval of electron spin coherence in a single nuclear spin. (**A**) Experimental sequence. A single nuclear spin is prepared in the state $|\downarrow\rangle$, after which an electron spin state is created by appropriate microwave pulses $R_\phi(\theta)$, where θ is the rotation angle and $\phi = (0, \pi/2)$ is the phase of the qubit rotation relative to the storage step. The electron spin state is then mapped onto the nuclear spin and is mapped back after an interval $(2N + 1)\pi_I$. The resulting electron spin state is read out by driving electron spin nutations with $R_\phi(\theta_2)$, where θ_2 is varied. (**B** and **C**) Observed electron spin nutations after storage of different electron spin states. X storage refers to storage of the electron spin state $(1/\sqrt{2})(|0\rangle \pm |1\rangle)$, Y storage is $(1/\sqrt{2})(|0\rangle \pm i|1\rangle)$, and Z storage measures the population storage, $\{|0\rangle, |1\rangle\}$. The total time is $3\pi_I \sim 2.4\ \mu s > T_{2e}^*$ between creation of the electron spin state and measurement.

tion axis, the nuclear spin precesses at the Larmor frequency ω_L when the electron spin is in the $m_s = 0$ state. When the electron spin is in $m_s = 1$ the large hyperfine splitting ω_A prevents Larmor precession. By selectively driving a π pulse on one hyperfine transition $|0, \downarrow\rangle \leftrightarrow |1, \downarrow\rangle$, and then waiting for a time $\tau = \pi/\omega_L$ (denoted as π_L), we can map a nuclear spin superposition onto the electron spin: $|0\rangle \otimes (\alpha|\downarrow\rangle + \beta|\uparrow\rangle) \rightarrow |\downarrow\rangle \otimes (\alpha|1\rangle + \beta|0\rangle)$ (Fig. 2D). This mapping gate (*Map*) allows complete control over the specific, individual nuclear spins because of their unique hyperfine splitting and Larmor frequencies.

The present experiments were carried out with the use of a setup described in (*27*). The nuclear spin is polarized by first preparing the electron spin state $|0\rangle$ by means of optical pumping with 532-nm light (*15*, *16*), mapping the initial incoherent mixture of nuclear spin states onto the electron spin, and then applying a pulse of 532-nm light sufficient to repolarize the electron spin into $|0\rangle$. Ideally, this pumping step results in the system being prepared in the state $|0, \downarrow\rangle$. In practice it can be repeated several times to further increase nuclear spin polarization. After a variable precession time, the nuclear spin state can be measured by mapping it onto the electron spin, which exhibits state-selective fluorescence. The observed contrast of $C \sim 70\%$ achievable with four pumping steps (Fig. 1E) indicates that we prepare and read out the nuclear spin state with an overall fidelity $F = (1 + C)/2$ (*10*) greater than 85% (*26*). The enhancement of the gyromagnetic ratio ($\gamma_n/2\pi$) = 15.2 kHz/G over the bare ^{13}C nuclear spin arises from interactions with the proximal electron spin, yielding a unique "chemical shift" (*28*) for the specific nuclear spin, depending on its relative position from the NV center (*27*). This is the key physical mechanism allowing for isolation of individual nuclear spin qubits and control of few-qubit registers.

Having established a procedure to reliably initialize and read out individual nuclear spins in the electron environment, we carried out a nontrivial quantum operation with the two-qubit register: storage and retrieval of an arbitrary electronic qubit in a nuclear qubit with high fidelity. This operation is particularly important in light of proposed protocols for quantum information processing (*6*, *9*). The experimental procedure is illustrated in Fig. 2A. After polarizing the nuclear spin, we created an electron spin state in one of three bases: $\{X_0 = (|\uparrow\rangle + |\downarrow\rangle)/\sqrt{2}, Y_0 = (|\uparrow\rangle + i|\downarrow\rangle)/\sqrt{2}, Z_{0,1} = \{|0\rangle, |1\rangle\}\}$. The electron spin was then stored in the nuclear spin via the inverse mapping gate (Map^{-1}), where it was allowed to remain for a time $(2V + 1)\pi_L$ before retrieval via the gate *Map*. We then observed the retrieved coherence (for X or Y storage) or population (for Z storage) by driving electron spin rotations and recording their contrast relative to rotations of a fully polarized electron spin. The overall fidelity of the memory is $F = (1 + C)/2$, where $\langle C \rangle$ is the average contrast for the six measurements, we find $F = 75 \pm 13\%$ (*26*), which exceeds the classical limit (*27*) of $F_c = \frac{2}{3}$.

To investigate the degree of independent control over the two coupled qubits, we studied the nuclear spin evolution under the optical excitation used to polarize and measure the electron spin qubit (Fig. 3). We prepared a nuclear spin state $(|\uparrow\rangle + |\downarrow\rangle)/\sqrt{2}$ or $|\uparrow\rangle$ by initializing into $|\downarrow\rangle$ and allowing the spin to precess for either $\pi_L/2$ or π_L. A pulse of 532-nm light was then applied, which could dephase or depolarize the nuclear spin state, resulting in reduced contrast of the nuclear free precession signal (Fig. 3A). As we increased the duration of the 532-nm light pulse, we found that the nuclear spin precession signal decayed much more slowly than did the electron spin. In particular, hardly any nuclear spin dephasing was visible for light pulses of ~140 ns (dashed line in Fig. 3B) sufficient to completely polarize the electron spin. Furthermore, the illuminated nuclear spin decay depended on the magnetic field (Fig. 3C). Whereas a few scattered photons completely decohered the electron spin, at low magnetic fields the nuclear precession was unaffected by a large number ($\sim 10^3$) of scattered optical photons. This insensitivity is critical for optical scaling (*7*, *9*) because many optical cycles may be required to establish entanglement between the registers (*12*, *13*).

The dephasing under optical illumination shown in Fig. 3 can be qualitatively understood as arising from different nuclear Larmor precession rates in the ground and optically excited electronic states. The nuclear gyromagnetic ratio is strongly enhanced by hyperfine interactions with the electron spin, which depends on the electron spatial distribution (*27*). Excited electron orbital states can thus lead to different nuclear gyromagnetic ratios. Under optical illumination, the system makes transitions between orbital states with different nuclear spin precession rates. To estimate the resulting nuclear spin dephasing, we suppose that optical excitation induces transitions at a rate $1/\tau_e$, much faster than the difference of the state-dependent nuclear spin precession frequencies $\delta\omega$. After each transition, the nuclear spin picks up a small random phase $\phi \sim \delta\omega\tau_e$. Variations in this random phase give rise to dephasing at a rate $\sim \delta\omega^2\tau_e$, much smaller than the illuminated electron spin dephasing rate $\sim 1/\tau_e$. Because $\delta\omega$ is proportional to the magnetic field for states with $m_s = 0$, it may be possible to almost completely decouple electron and nuclear spins by switching the magnetic field to zero during free evolution.

Finally, we explored the coherence properties of the nuclear spin quantum memory. In contrast to the electron spin, which dephases on a time scale $T_2^* \sim 1$ μs for this NV center, the nuclear spin free precession signal persisted out to ~0.5 ms ($T_{2n}^* = 494 \pm 30$ μs in Fig. 4A). Characteristic collapses and revivals in the data correspond to coherent interactions between individual nuclear spins. The nuclear spins can be decoupled using a Hahn echo (or spin-echo) sequence (*23*), which consists of $(\pi/2)_x$-τ-π_y-τ'-$(\pi/2)_{x'}$ where $(\pi)_y$ represents a pulse that flips the nuclear spin, and τ and τ' are durations of free evolution (Fig. 4C). We accomplished the nuclear π-pulse by exciting the system into the $m_s = 1$ manifold, where the large hyperfine splitting rapidly introduces a phase between the nuclear spin states. Viewed in the orthogonal $m_s = 0$ eigenbasis, this constitutes the

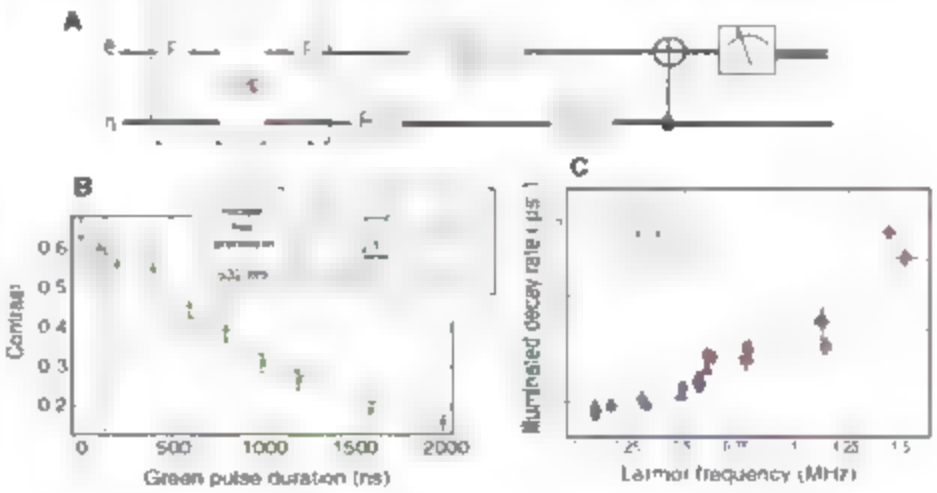

Fig. 3. Probing the isolation of a nuclear spin qubit under optical illumination. (**A**) Experimental sequence as explained in text. (**B**) Decay of illuminated nuclear spin free precession. When illuminated by approximately half the saturation intensity at 532 nm for the NV optical transition, the nuclear spin signal decays on a time scale of 1.5 ± 0.1 μs. For comparison, the polarization rate for the electron spin (under the same conditions) is 140 ± 6 ns, shown by the dashed lines. (**C**) Illuminated decay rate as a function of magnetic field. The decay rate does not depend strongly on whether we apply green light when the nuclear spin is in its polarized state $|\uparrow\rangle$ (red points) or in a superposition state $(1/\sqrt{2})(|\uparrow\rangle + |\downarrow\rangle)$ (blue points), as illustrated in the inset. The data are fitted to the function $(a + b\omega_L)^2$.

population nutations required to effect a π_n pulse (*36*). As shown in Fig. 4D, the spin echo sequence extended the coherence time far beyond the values obtained from free evolution. Specifically, we observed no evidence of echo decay on the time scales accessible in our present experiments, limited by long averaging times, which suggests that T_2 of our nuclear spin qubit is well above 20 ms.

These results can be understood by considering the interactions between the observed ^{13}C nuclear spin (I_1) with other ^{13}C nuclear spins I_2. Let us first consider only one nearby spin I_2. The Hamiltonian in the secular approximation is given by $H = \omega_1^{\,1} I_{1,z} + \omega_1^{\,2} I_{2,z} + \beta I_{1,z} I_{2,z}$, where $\omega_1^{\,2}$ are the Larmor frequencies of the two spins, and β is the effective dipole-dipole coupling between nuclei (*26*). As a result of the different Larmor frequencies caused by the different interactions with the NV electronic spin, these nuclear spins are not involved in flip-flop processes with each other or with the rest of the nuclear spin environment. Thus, the nuclear interaction only results in energy shifts $\pm\beta/4$ of I_1 that depend on the state of I_2, leading to the observed coherent modulation in the free precession (Fig. 4A) for $\beta/2\pi \sim 7.2$ kHz. Interactions with the next nearest spin I_3 will similarly result in free precession collapse (and revival) on a longer time scale, etc. (fig. S1). This theoretical model predicts that the nuclear interactions introduce only some energy shifts that are easily refocused by the spin-echo sequence. The resulting nuclear spin coherence is greatly enhanced relative to the electron spin (*21*), consistent with the much weaker interactions of I_1 with the surrounding environment. Further confirmation of the theoretical model comes from the observed dependence of the coherent coupling (modulation) rate on the orientation of the magnetic field (Fig. 4B), which illustrates the anisotropic character of the electron-mediated nuclear dipole-dipole interaction (*26*).

These observations indicate that controlled manipulation of a few coupled nuclear spin qubits is possible in a room-temperature solid-state system, with coherence times that can approach seconds when advanced nuclear magnetic resonance techniques are used (*23*). In addition to the direct coupling between the nuclear spins demonstrated here, the number of distinct controllable nuclear spins in the register can be increased by selecting NV centers with a few proximal ^{13}C spins (*21*), or by creating NV centers through controlled implantation of $I = \frac{1}{2}$ ^{15}N ions (*36*). Such registers provide a starting point for a realization of a quantum network in which qubits can be encoded and manipulated in nuclear spins via magnetic resonance techniques (*23*), whereas long-range entanglement between electron spins at arbitrary locations can be created optically (*6, 9, 29*) with techniques now explored for atoms and ions (*12, 13*). Recently, the relatively broadened lines and spin-dependent optical transitions required for realization of these techniques were demonstrated in diamond (*30, 31*). Few-qubit registers can provide powerful tools for scalable quantum information systems even in the presence of realistic noise and losses that affect the long-range entanglement (*6, 7, 9*). Beyond specific applications in quantum information science, our measurements show that the electron spin can be used as a sensitive local magnetic probe that allows for a remark-

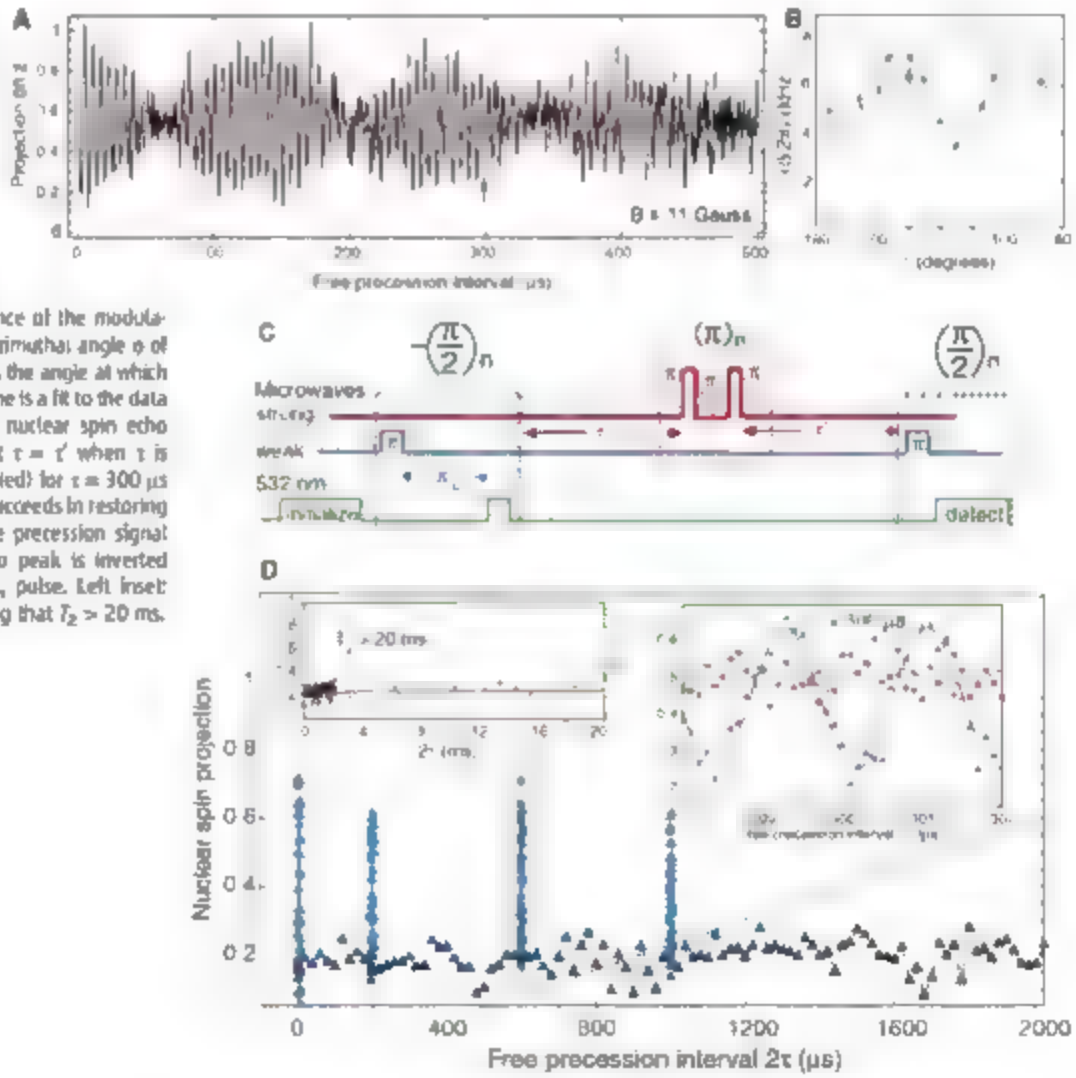

Fig. 4. Coherent dynamics of coupled nuclear spin qubits. **(A)** Long-time precession signal of a single nuclear spin in a magnetic field of 11 G. The data were fitted to the function $a + b\cos(\omega_L \tau)\cos(\beta\tau/2)\exp[-(\tau/T_{2n}^*)^2]$, where $\omega_L \sim 2\pi(172)$ kHz is the Larmor frequency, $\beta \sim 2\pi(7.2)$ kHz is the strength of the interaction with the nearby proximal nucleus, and T_{2n}^* is the dephasing time. **(B)** Dependence of the modulation frequency (blue points) on the azimuthal angle ϕ of the magnetic field. The arrow denotes the angle at which the data in (A) were taken. The solid line is a fit to the data (*26*). **(C)** Experimental sequence for nuclear spin echo (*26*). **(D)** Main plot: Echo signal at $\tau = \tau'$ when τ is varied. Right inset: Echo data (τ varied) for $\tau = 300$ μs (blue points) showing that the echo succeeds in restoring the coherence even though the free precession signal (red points) has vanished. The echo peak is inverted because we initially apply a $(-\pi/2)_n$ pulse. Left inset: Long-time echo signal, demonstrating that $T_2 > 20$ ms.

able degree of control over individual nuclear spins.

References and Notes

1. J. I. Cirac, P. Zoller, H. Mabuchi, H. J. Kimble, *Phys. Rev. Lett.* **78**, 3221 (1997).
2. A. Steane, D. Lucas, *Fortschr. Phys.* **48**, 839 (2000).
3. H. J. Briegel, W. Dür, J. I. Cirac, P. Zoller, *Phys. Rev. Lett.* **81**, 5932 (1998).
4. D. Gottesman, I. Chuang, *Nature* **402**, 390 (1999).
5. L. Duan, B. Blinov, D. Moehring, C. Monroe, *Quant. Inf. Comp.* **4**, 165 (2004).
6. S. C. Benjamin, D. E. Browne, J. Fitzsimons, J. J. L. Morton, *N. J. Phys.* **8**, 141 (2006).
7. L. Childress, J. M. Taylor, A. Sørensen, M. D. Lukin, *Phys. Rev. Lett.* **96**, 070504 (2006).
8. P. van Loock *et al.*, *Phys. Rev. Lett.* **96**, 240501 (2006).
9. L. Jiang, J. M. Taylor, A. S. Sorensen, M. D. Lukin, http://arxiv.org/abs/quant-ph/0703029 (2007).
10. D. Leibfried *et al.*, *Nature* **438**, 639 (2005).
11. H. Häffner *et al.*, *Nature* **438**, 643 (2005).
12. B. Blinov, D. L. Moehring, L. M. Duan, C. Monroe, *Nature* **428**, 153 (2004).
13. P. Maunz *et al.*, http://arxiv.org/abs/quant-ph/0608047 (2006).
14. J. Wrachtrup, S. Y. Kilin, A. P. Nizovtsev, *Opt. Spectrosc.* **91**, 429 (2001).
15. F. Jelezko, T. Gaebel, I. Popa, A. Gruber, J. Wrachtrup, *Phys. Rev. Lett.* **92**, 076401 (2004).
16. T. Gaebel *et al.*, *Nature Phys.* **2**, 408 (2006).
17. R. Hanson, F. Mendoza, R. J. Epstein, D. D. Awschalom, *Phys. Rev. Lett.* **97**, 087601 (2006).
18. R. J. Epstein, F. M. Mendoza, Y. K. Kato, D. D. Awschalom, *Nat. Phys.* **1**, 94 (2005).
19. J. R. Petta *et al.*, *Science* **309**, 2180 (2005); published online 1 September 2005 (10.1126/science.1116955).
20. F. H. L. Koppens *et al.*, *Nature* **442**, 766 (2006).
21. L. Childress *et al.*, *Science* **314**, 281 (2006); published online 13 September 2006 (10.1126/science.1131871).
22. B. Kane, *Nature* **393**, 133 (1998).
23. L. M. K. Vandersypen, I. L. Chuang, *Rev. Mod. Phys.* **76**, 1037 (2004).
24. C. Negrevergne *et al.*, *Phys. Rev. Lett.* **96**, 170501 (2006).
25. F. Jelezko *et al.*, *Phys. Rev. Lett.* **93**, 130501 (2004).
26. See supporting material on *Science* Online.
27. S. Massar, S. Popescu, *Phys. Rev. Lett.* **74**, 1259 (1995).
28. J. Rabeau *et al.*, *Appl. Phys. Lett.* **88**, 023113 (2006).
29. M. D. Lukin, P. R. Hemmer, *Phys. Rev. Lett.* **84**, 2818 (2000).
30. P. Tamarat *et al.*, *Phys. Rev. Lett.* **97**, 083002 (2006).
31. C. Santori *et al.*, *Phys. Rev. Lett.* **97**, 247401 (2006).

32. We thank P. Cappellaro, J. Doyle, N. Khaneja, C. Marcus, A. Mukherjee, J. Taylor, and J. Wrachtrup for many stimulating discussions and experimental help, and S. Prawer for providing high-purity diamond samples. Supported by NSF (CAREER and Physics at the Information Frontier), the Army Research Office, the Packard and Hertz Foundations, Deutsche Forschergemeinschaft grant SFB/TR21, and the European Commission (F.J.).

Supporting Online Material

www.sciencemag.org/cgi/content/full/316/5829/1312/DC1
Materials and Methods
SOM Text
Figs. S1 and S2
References

11 January 2007; accepted 11 April 2007
10.1126/science.1139831

Functional Quantum Nodes for Entanglement Distribution over Scalable Quantum Networks

Chin-Wen Chou, Julien Laurat, Hui Deng, Kyung Soo Choi, Hugues de Riedmatten,* Daniel Felinto,† H. Jeff Kimble‡

We demonstrated entanglement distribution between two remote quantum nodes located 3 meters apart. This distribution involves the asynchronous preparation of two pairs of atomic memories and the coherent mapping of stored atomic states into light fields in an effective state of near maximum polarization entanglement. Entanglement is verified by way of the measured violation of a Bell inequality, and it can be used for communication protocols such as quantum cryptography. The demonstrated quantum nodes and channels can be used as segments of a quantum repeater, providing an essential tool for robust long-distance quantum communication.

In quantum information science (*1*), distribution of entanglement over quantum networks is a critical requirement for metrology (*2*), quantum computation (*3*, *4*), and communication (*5*, *6*). Quantum networks are composed of quantum nodes for processing and storing quantum states, and quantum channels that link the nodes. Substantial advances have been made with diverse systems toward the realization of such networks, including ions (*6*), single trapped atoms in free space (*7*, *8*) and in cavities (*9*), and atomic ensembles in the regime of continuous variables (*10*).

An approach of particular importance has been the seminal work of Duan, Lukin, Cirac, and Zoller (DLCZ) for the realization of quantum networks based on entanglement between single photons and collective excitations in atomic ensembles (*11*). Critical experimental capabilities have been achieved, beginning with the generation of nonclassical fields (*12*, *13*) with controlled waveforms (*14*) and extending to the creation and retrieval of single collective excitations (*15*–*17*) with high efficiency (*18*, *19*). Heralded entanglement with quantum memories, which is the cornerstone of networks with efficient scaling, was achieved between two ensembles (*20*). More recently, conditional control of the quantum states of a single ensemble (*21*–*23*) and of two distant ensembles (*24*) has also been implemented; the quantum states are likewise required for the scalability of quantum networks based on probabilistic protocols.

Our goal is to develop the physical resources that enable quantum repeaters (*5*), thereby allowing entanglement-based quantum communication tasks over quantum networks on distance scales much larger than those set by the attenuation length of optical fibers, including quantum cryptography (*25*). For this purpose, heralded number-state entanglement (*20*) between two remote atomic ensembles is not directly applicable. Instead, DLCZ proposes the use of pairs of ensembles (L_i, D_i) at each quantum node i, with the sets of ensembles (U_i, D_i) separately linked in parallel chains across the network (*11*). Relative to the state of the art in our previous work (*20*), the DLCZ protocol requires the capability for the independent control of pairs of entangled ensembles between two nodes.

In our experiment, we created, addressed, and controlled pairs of atomic ensembles at each of two quantum nodes, thereby demonstrating entanglement distribution in a form suitable both for quantum network architectures and for entanglement-based quantum communication schemes (*26*). Specifically, two pairs of remote ensembles at two nodes were each prepared in an entangled state (*20*), in a heralded and asynchronous fashion (*24*), thanks to the conditional control of the quantum memories. After a signal indicating that the two chains are prepared in the desired state, the states of the ensembles were coherently transferred to propagating fields locally at the two nodes. The fields were arranged such that they effectively contained two photons, one at each node, whose polarizations were entangled. The entanglement between the two nodes was verified by the violation of a Bell inequality. The effective polarization-entangled state, created with favorable scaling behavior, was thereby compatible with entanglement-based quantum communication protocols (*11*).

The architecture for our experiment is shown in Fig. 1. Each quantum node L (left) and R (right), consists of two atomic ensembles, U (up) and D (down), or four ensembles altogether, namely (LU, LD) and (RU, RD), respectively. We first prepared each pair in an entangled state, in which one excitation is shared coherently, by using a pair of coherent weak write pulses to induce spontaneous Raman transitions $|g\rangle \rightarrow |e\rangle \rightarrow |s\rangle$ (bottom left, Fig. 1). The Raman fields ($|L_{Ge}\rangle$, $|L_{gs}\rangle$) from (LU, RU) were

Norman Bridge Laboratory of Physics 12-33, California Institute of Technology, Pasadena, CA 91125, USA.

*Present address: Group of Applied Physics, University of Geneva, Geneva 1211, Switzerland.

†Present address: Departamento de Física, Universidade Federal de Pernambuco, Recife-PE, 50670-901, Brazil.

‡To whom correspondence should be addressed. E-mail: hjkimble@caltech.edu

combined at the 50-50 beamsplitter BS_U, and the resulting fields were directed to single-photon detectors. A photoelectric detection event in either detector indicated that the two ensembles were prepared. The remote pair of D ensembles, (LD, RD), was prepared in an analogous fashion.

Conditioned upon the preparation of both ensemble pairs (LU, LD) and (RU, RD), a set of read pulses was triggered to map the stored atomic excitations into propagating Stokes fields in well-defined spatial modes through $|s\rangle \rightarrow |e\rangle \rightarrow |g\rangle$ with the use of a collective enhancement (11) (bottom left, Fig. 1). This generated a set of four fields denoted by $(2_{LU}, 2_{RU})$ for ensembles (LU, RU) and by $(2_{LD}, 2_{RD})$ for ensembles (LD, RD). In the ideal case and neglecting higher-order terms, the mapping results in a quantum state for the Field 2 fields given by

$$|\Psi\rangle_{2_{LU}2_{RU}2_{LD}2_{RD}} = \frac{1}{\sqrt{2}}\left(|0\rangle_{2_{LU}}|1\rangle_{2_{RU}} + e^{i\eta_U}|1\rangle_{2_{LU}}|0\rangle_{2_{RU}}\right)\otimes\left(|0\rangle_{2_{LD}}|1\rangle_{2_{RD}} + e^{i\eta_D}|1\rangle_{2_{LD}}|0\rangle_{2_{RD}}\right) \quad (1)$$

Here, $|n\rangle_k$ is the n-photon state for mode k, where $k \in \{2_{LU}, 2_{RU}, 2_{LD}, 2_{RD}\}$, and η_U and η_D are the relative phases resulting from the writing and reading processes for the U and D pair of ensembles, respectively (20). The + signs for the combinations of states L, D result from the unitarity of the transformation by the beamsplitters (BS_U, BS_D). The extension of Eq. 1 to incorporate various nonidealities is given in the supporting online material (SOM) text.

Apart from an overall phase, the state $|\Psi\rangle_{2_{LU}2_{RU}2_{LD}2_{RD}}$ can be rewritten as follows

$$|\Psi\rangle_{2_{LU}2_{RU}2_{LD}2_{RD}} = \frac{1}{2}\left(|0\rangle_{2_{LU}}|1\rangle_{2_{RU}}|0\rangle_{2_{LD}}|1\rangle_{2_{RD}} + e^{i\eta_U}|1\rangle_{2_{LU}}|0\rangle_{2_{RU}}|0\rangle_{2_{LD}}|1\rangle_{2_{RD}} + e^{i\eta_D}|0\rangle_{2_{LU}}|1\rangle_{2_{RU}}|1\rangle_{2_{LD}}|0\rangle_{2_{RD}} + e^{i(\eta_U+\eta_D)}|1\rangle_{2_{LU}}|0\rangle_{2_{RU}}|1\rangle_{2_{LD}}|0\rangle_{2_{RD}}\right) \quad (2)$$

where $|\psi\rangle_{2_L}$ denotes $|0\rangle_{2_L} - |1\rangle_{2_L}$. If only coincidences between both nodes L,R are registered, the first two terms (i.e., with $e^{i\eta_U}$, $e^{i\eta_D}$) do not contribute. Hence, as noted by DLCZ, excluding such cases leads to an effective density matrix equivalent to the one for a maximally entangled state of the form of the last term in Eq. 2. Notably, the absolute phases η_U and η_D do not need to be independently stabilized. Only the relative phase $\eta = \eta_U - \eta_D$ must be kept constant, leading to 1/2 unit of entanglement for two quantum bits (i.e., 1/2 ebit).

The experimental demonstration of this architecture for implementing the DLCZ protocol relies crucially on the ability to carry out efficient parallel preparation of the (LU, RU) and (LD, RD) ensemble pairs, as well as the ability to stabilize the relative phase η. The first requirement is achieved by the use of real-time control, as described in Feinto *et al.* (24) in a simpler case. As shown in Fig. 1, we implemented control logic that monitors the outputs of Field 1 detectors. A detection event at either pair triggers electro-optic intensity modulators (IM) that gate off all laser pulses traveling toward the corresponding pair of ensembles, thereby storing the associated state. Upon receipt of signals indicating that the two pairs of ensembles, (LU, RU) and (LD, RD), have both been independently prepared, the control logic triggers the retrieval of the stored states by simultaneously sending a strong read pulse into each of the four ensembles. Relative to the case in which no logic is implemented, this process resulted in a 19-fold enhancement in the probability of generating this overall state from the four ensembles (SOM text).

The second requirement, stability of the relative phase η, could be accomplished by active stabilization of each individual phase η_{LU}, η_{RD}, as in (24). Instead of implementing this challenging technical task (which ultimately would have to be extended across longer distances of ensembles), our setup exploits the passive stability between two independent polarizations propagating in a single interferometer to prepare the two ensemble pairs (27). No active phase stabilization is thus required. In practice, we found that the passive stability of our system was sufficient for operation overnight without adjustment. Additionally, we implemented a procedure that deterministically sets the relative phase to zero.

We also extended the original DLCZ protocol (Fig. 1) by combining fields $(2_{LU}, 2_{LD})$ and $(2_{RU}, 2_{RD})$ with orthogonal polarizations on polarizing beamsplitters PBS_L and PBS_R to yield fields 2_L and 2_R, respectively. The polarization encoding opens the possibility of performing additional entanglement purification and thus superior scalability (28, 29). In the ideal case, the resulting state would now be effectively equivalent to a maximally entangled state for the polarization of two photons

$$|\Psi^+\rangle_{2_L,2_R} = \frac{1}{\sqrt{2}}\left(|H_{2_L}\rangle|V_{2_R}\rangle + e^{i\eta}|V_{2_L}\rangle|H_{2_R}\rangle\right) \quad (3)$$

where H and V stand for the state of a single photon with horizontal and vertical polarization, respectively. The sign of the superposition in Eq. 3 is inherited from Eq. 1 and is determined by the particular pair of heralding signals recorded by (D_{1a}, D_{1b}) and (D_{1c}, D_{1d}). The entanglement in the polarization basis is well suited for entanglement-based quantum cryptography (11, 25), including security verifica-

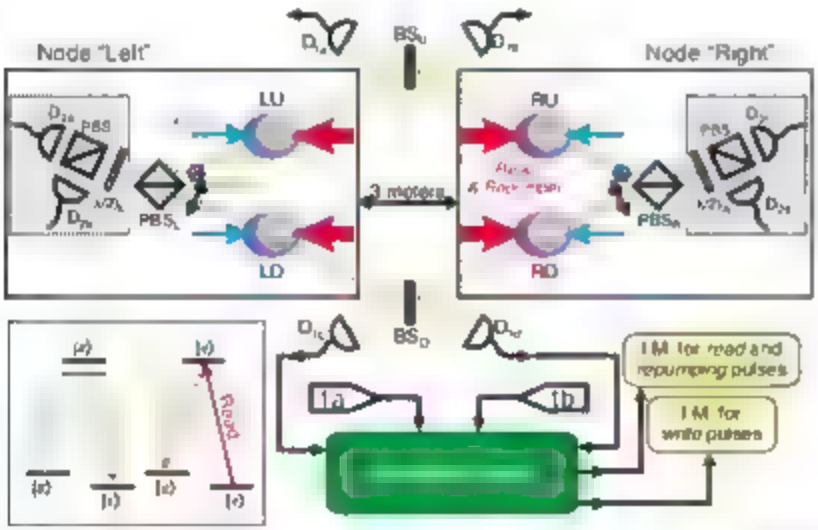

Fig. 1. Setup for distributing entanglement between two quantum nodes (L,R) separated by 3 m. The inset at the bottom left shows the relevant atomic levels for the $6S_{1/2}$ – $6P_{3/2}$ transition in atomic cesium, as well as the associated light fields. The ensembles are initially prepared in $|g\rangle$. Weak write pulses then induce spontaneous Raman transitions $|g\ (F = 4)\rangle \rightarrow |e\ (F = 4)\rangle \rightarrow |s\ (F = 3)\rangle$ resulting in the emission of anti-Stokes fields (Field 1, near the $|e\rangle \rightarrow |s\rangle$ transition along with the storage of collective excitations in the form of spin flips shared among the atoms (11). With this setup, a photo-detection event at either detector D_{1a} or D_{1b} indicates entanglement between the collective excitation in LU and RU, and a photo-detection event at either detector D_{1c} or D_{1d} indicates entanglement between the collective excitation in LD and RD (20). Two orthogonal polarizations in one fiber beamsplitter implement BS_U and BS_D, yielding excellent relative path stability. A heralding detection event triggers the control logic to gate off the light pulses going to the corresponding ensemble pair (U or D) by controlling the intensity modulators (IM). The atomic state is thus stored while waiting for the second ensemble pair to be prepared. After both pairs of ensembles U,D are entangled, the control logic releases strong read pulses to map the states of the atoms to Stokes Field 2 fields through $|s\rangle \rightarrow |e\rangle \rightarrow |g\rangle$. Fields 2_{LU} and 2_{LD} are combined with orthogonal polarizations on the polarizing beamsplitter PBS_L to yield field 2_L. Fields 2_{RU} and 2_{RD} are combined with orthogonal polarizations on the polarizing beam splitter PBS_R to yield field 2_R. If only coincidences between fields 2_L and 2_R are registered, the state is effectively equivalent to a polarization maximally entangled state.

tion by way of the violation of a Bell inequality as well as for quantum teleportation (11).

As a first step to investigate the joint states of the atomic ensembles, we recorded photoelectric counting events for the ensemble pairs (LU,RU) and (LD,RD) by setting the angles for the half-wave plates ($\lambda/2$)$_{L,R}$ shown in Fig. 1 to 0°, such that photons reaching detectors D_{2u} and D_{2d} come only from the ensemble pair U, and photons reaching detectors D_{2u} and D_{2c} come only from the ensemble pair D. Conditioned upon detection events at D_{2u} or D_{2d} (or at D_{1c} or D_{1d}), we estimated the probability that each ensemble pair (U,D) contains only a single shared excitation as compared with the probability for two excitations by way of the associated photoelectric statistics. In quantitative terms, we determined the ratio (20)

$$h_X^{(2)} = \frac{P_{X,11}}{P_{X,01}P_{X,10}} \quad (4)$$

where $P_{X,mn}$ is the probability to register m photodetection events in mode 2_{LX} and n events in mode 2_{RX} ($X = \{U,D\}$), conditioned on a detection event at D_1. A necessary condition for the two ensembles (LX, RX) to be entangled is that $h_X^{(2)} < 1$, where $h_X^{(2)} = 1$ corresponds to the case of independent (unentangled) coherent states for the two fields (20). Figure 2 shows the measured $h_X^{(2)}$ versus the duration τ_M (where M stands for memory) that the state is stored before retrieval. For both U and D pairs, $h^{(2)}$ remains well below unity for storage times $\tau_M < \sim 10$ μs. For the U pair, the solid line in Fig. 2 provides a fit by the sample expression $h^{(2)} = 1 - A\exp[-(\tau_M/\tau)^2]$. The fit gives $A = 0.94 \pm 0.01$, where the error is SD, and $\tau = 22 \pm 2$ μs, providing an estimate of a coherence time for our system. A principal cause for decoherence is an inhomogeneous broadening of the ground state levels by residual magnetic fields (30). The characterization of the time dependence of $h^{(2)}$ constitutes an important benchmark of our system (SOM text).

We next measured the correlation function $E(\theta_L,\theta_R)$, defined by

$$E(\theta_L,\theta_R) = \frac{C_{ac} + C_{bd} - C_{ad} - C_{bc}}{C_{ac} + C_{bd} + C_{ad} + C_{bc}} \quad (5)$$

Here, C_{jk} gives the rates of coincidences between detectors D_{2j} and D_{2k} for Field 2 fields, where $j,k \in \{a,b,c,d\}$, conditioned upon heralding events at detectors D_{1a},D_{1b} and D_{1c},D_{1d} from Field 1 fields. The angles of the two half-wave plates ($\lambda/2$)$_L$ and ($\lambda/2$)$_R$ are set at $\theta_L/2$ and $\theta_R/2$, respectively. As stated above, the capability to store the state heralded in one pair of ensembles and then to wait for the other pair to be prepared markedly improves the various coincidence rates C_{jk} by a factor that increases with the duration τ_M that a state can be preserved (24) (SOM text).

Figure 3 displays the correlation function E as a function of θ_R, for $\theta_L = 0°$ (Fig. 3A) and $\theta_L = 45°$ (Fig. 3B). Relative to Fig. 2, these data are taken with increased excitation probability (higher wing power) to validate the phase stability of the system, which is evidently good. Moreover, these four-fold coincidence fringes in Fig. 3A provide further verification that predominantly one excitation is shared between a pair of ensembles. The analysis provided in the SOM text with the measured cumulative $h^{(2)}$ parameter for this set of data, $h^{(2)} = 0.12 \pm 0.02$, predicts a visibility of $V = 78 \pm 3\%$, in good agreement with the experimentally determined $V = 79\%$. Finally, one of the fringes is inverted with respect to the other in Fig. 3B, which corresponds with the two possible signs in Eq. 3.

As for $\theta_L = 45°$, the measurement is sensitive to the square of the overlap ξ of photon wavepackets for fields $2_{L,R}$; we may infer $\xi_{L,R} = 0.83$ from the reduced fringe visibility ($V = 55\%$) in Fig. 3B relative to Fig. 3A. [illegible] reduction is attributed to a nonideal overlap. An independent experimental characterization of interference in this setup has shown an overlap $\xi = 0.90$, which confirms that the reduction can be principally attributed to the nonideal overlap. Other possible causes include imperfect phase alignment $\eta \neq 0$ and imbalance of the effective-state coefficients (SOM text).

With the measurements from Figs. 2 and 3 in hand, we verified entanglement unambiguously

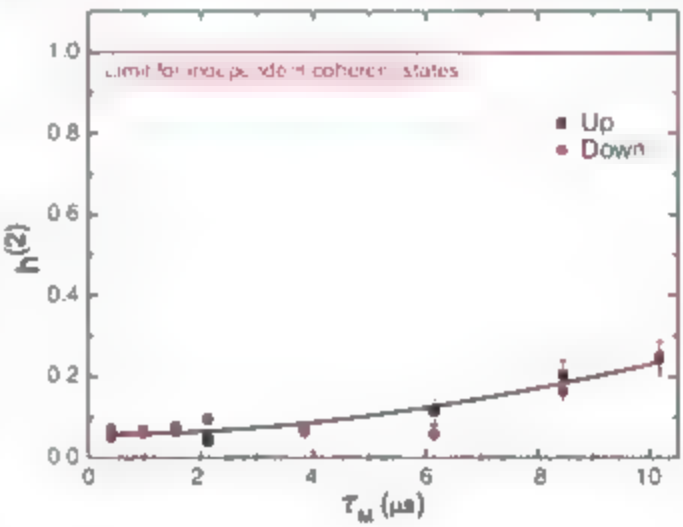

Fig. 2. Suppression $h^{(2)}$ of the probabilities for each ensemble to emit two photons compared with the product of the probabilities that only one photon is emitted, as a function of the duration τ_M that the state is stored before retrieval. The solid line gives a fit for the U pair. Error bars indicate SD.

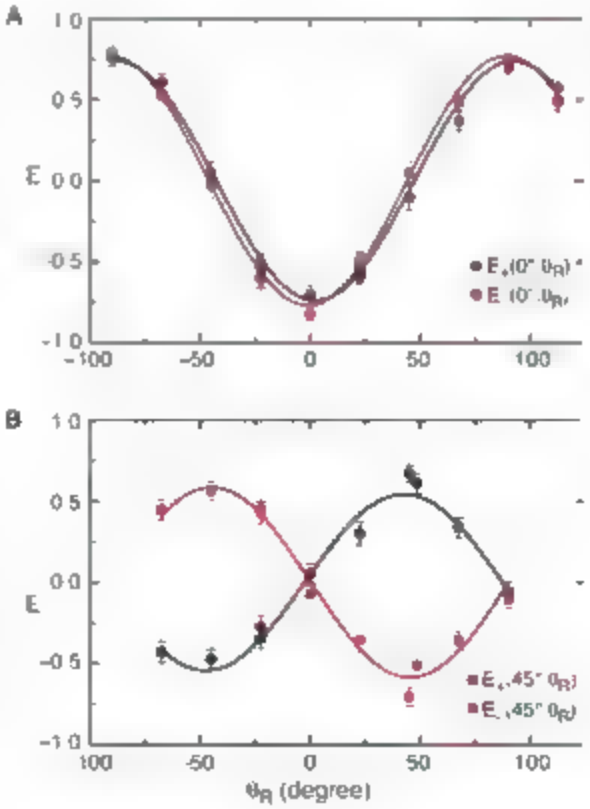

Fig. 3. Measured correlation function $E(\theta_L,\theta_R)$ as a function of θ_R with θ_L fixed at (A) 0° and (B) 45°. The excitation probabilities for the ensembles are increased by ~1.5 times relative to Fig. 2, with each point taken for 30 min at a typical coincidence rate of 400 per hour for each fringe. Error bars indicate SD.

by way of the violation of a Bell inequality (*31*). For this purpose, we chose the canonical values $\theta_L = \{0°, 45°\}$ and $\theta_R = \{22.5°, -22.5°\}$ and constructed the Clauser-Horne-Shimony-Holt (CHSH) parameters

$$S_+ = |E(0°, 22.5°) + E(0°, -22.5°) + E(45°, 22.5°) - E(45°, -22.5°)| \quad (6)$$

$$S_- = |E(0°, 22.5°) + E(0°, -22.5°) + E(45°, 22.5°) - E(45°, -22.5°)| \quad (7)$$

for the two effective states $\psi_{2_L 2_R}$ of Eq. 3. For local realistic hidden-variable theories, $S_\pm \leq 2$ (*31*). Figure 4 shows the CHSH parameters $S_\pm$ as functions of the duration τ_M up to which one pair of ensembles holds the prepared state, in the excitation regime of Fig. 2. As shown in the SOM text, the requirements for minimization of higher-order terms are much more stringent in this experiment with four ensembles than with simpler configurations (*31*).

Figure 4, A and B, gives the results for our measurements of S_+ with binned data. Each point corresponds to the violation obtained for states generated at $\tau_M = 3n\tau_M^0$ ($3\tau_M^0$ is marked by the thick horizontal lines in Fig. 4). Strong violations are obtained for short memory times (for instance, $S_+ = 2.55 \pm 0.14 > 2$ and $S_- = 2.36 \pm 0.13 > 2$ for the second bin), demonstrating the presence of entanglement between fields 2_L and 2_R. Therefore, these fields can be exploited to perform entanglement-based quantum communication protocols, such as quantum key distribution with, at minimum, security against individual attacks (*11*, *32*).

As can be seen in Fig. 4, the violation decreases with increasing τ_M. The decay is largely due to the time-varying behavior of $h^{(2)}$ (Fig. 2 and SOM text). In addition to this decay, the S_+ parameter exhibits modulation with τ_M. We explored different models for the time dependence of the CHSH parameters, but thus far have found no satisfactory agreement between model calculations and measurements. Nevertheless, the density matrix for the ensemble over the full memory time is potentially useful for tasks such as entanglement concentration, as shown by Fig. 4, C and D, in which cumulative data are given. Each point at memory time τ_M gives the violation obtained by taking into account all the states generated from 0 to τ_M. Overall significant violations are obtained, namely $S_+ = 2.21 \pm 0.04 > 2$ and $S_- = 2.24 \pm 0.04 > 2$ at $\tau_M \sim 10\ \mu s$.

In our experiment, we were able to generate excitation-number entangled states between remote locations, which are well suited for scaling purposes, and, with real-time control, we were able to operate them as if they were effectively polarization-entangled states, which can be applied to quantum communications such as quantum cryptography. Measurements of the suppression of $h^{(2)}$ of two-excitation components versus storage time explicitly demonstrate the major source that causes the extracted polarization entanglement to decay, emphasizing the critical role of multi-excitation events in the experiments aiming for a scalable quantum network. The present scheme, which constitutes a functional segment of a quantum repeater in terms of quantum state encoding and channel control, allows the distribution of entanglement between two quantum nodes. The extension of our work to longer chains involving many segments becomes more complicated and is out of reach for any current system. For long-distance communication, the first quantity to improve is the coherence time of the memory. Better cancellation of the residual magnetic fields and switching to new trap schemes should improve this parameter to ~ 0.1 s by using an optical trap (*30*), thereby increasing the rate of preparing the ensembles in the state of Eq. 1 to 100 Hz. The second challenge that would immediately appear in an extended chain would be the increase of the multi-excitation probability with the connection stages. Recently, Jiang *et al.* (*28*) have theoretically demonstrated the prevention of such growth in a similar setup, but its full scalability still requires very high retrieval and detection efficiency and photon-number resolving detectors. These two points clearly show that the quest of scalable quantum networks is still a theoretical and experimental challenge. The availability of our first functional segment opens the way for fruitful investigations.

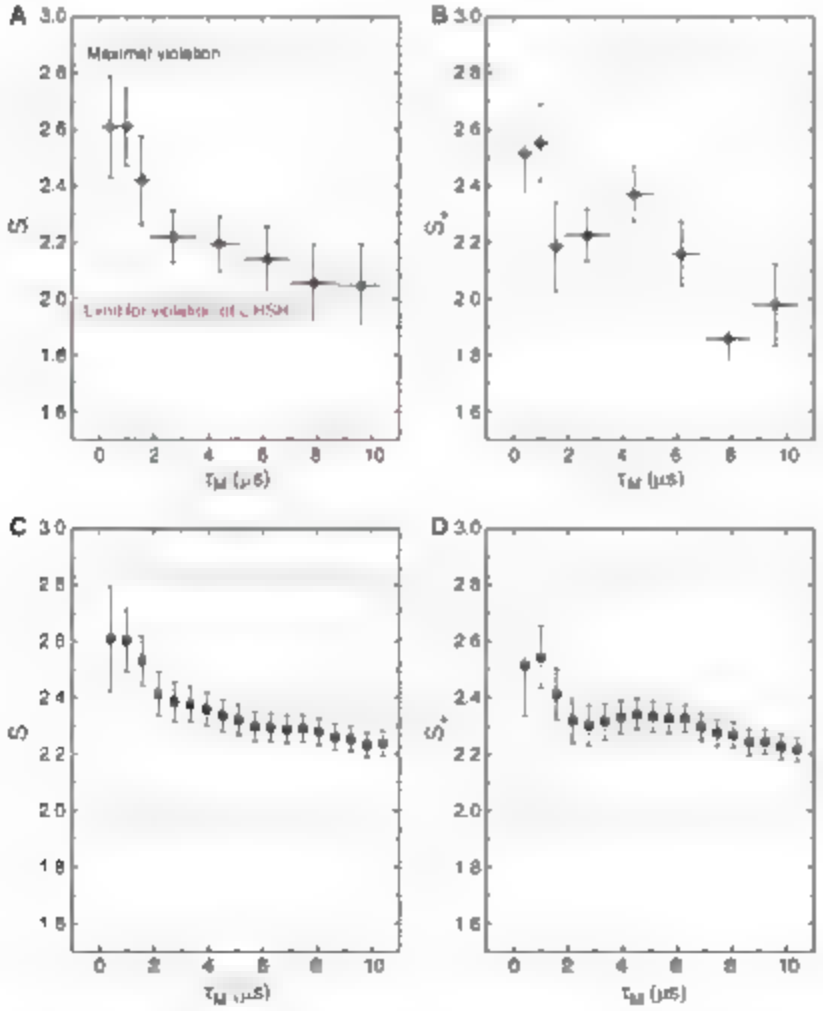

Fig. 4. Measured CHSH parameters $S_\pm$ for the two possible effective states in Eq. 3, as functions of duration τ_M for which the first ensemble pair holds the prepared state. The excitation probabilities are kept low for high correlation (as in Fig. 2). (**A** and **B**) Binned data. The horizontal solid lines indicate the size of the bins used. (**C** and **D**) Cumulative data. The coincidence rate for these measurements is about 150 per hour for each effective state. Error bars indicate SD.

References and Notes

1. P. Zoller *et al.*, *Eur. Phys. J. D* **36**, 203 (2005).
2. V. Giovannetti, S. Lloyd, L. Maccone, *Science* **306**, 1330 (2004).
3. J. I. Cirac, P. Zoller, H. J. Kimble, H. Mabuchi, *Phys. Rev. Lett.* **78**, 3221 (1997).
4. L.-M. Duan, M. J. Kimble, *Phys. Rev. Lett.* **92**, 127902 (2004).
5. H.-J. Briegel, W. Dür, J. I. Cirac, P. Zoller, *Phys. Rev. Lett.* **81**, 5932 (1998).
6. B. B. Blinov, D. L. Moehring, L.-M. Duan, C. Monroe, *Nature* **428**, 153 (2004).
7. J. Volz *et al.*, *Phys. Rev. Lett.* **96**, 030404 (2006).
8. J. Beugnon *et al.*, *Nature* **440**, 779 (2006).

9. A. D. Boozer, A. Boca, R. Miller, T. E. Northup, H. J. Kimble, *Phys. Rev. Lett.* in press; preprint available at http://xxx.lanl.gov/abs/quant-ph/0702248.
10. J. F. Sherson *et al.*, *Nature* **443**, 557 (2006).
11. L.-M. Duan, M. Lukin, J. I. Cirac, P. Zoller, *Nature* **414**, 413 (2001).
12. A. Kuzmich *et al.*, *Nature* **423**, 731 (2003).
13. C. H. van der Wal *et al.*, *Science* **301**, 196 (2003).
14. V. Balić, D. A. Braje, P. Kolchin, G. Y. Yin, S. E. Harris, *Phys. Rev. Lett.* **94**, 183601 (2005).
15. C.-W. Chou, S. V. Polyakov, A. Kuzmich, H. J. Kimble, *Phys. Rev. Lett.* **92**, 213601 (2004).
16. M. D. Eisaman *et al.*, *Nature* **438**, 837 (2005).
17. T. Chanelière *et al.*, *Nature* **438**, 833 (2005).
18. J. Laurat *et al.*, *Opt. Express* **14**, 6912 (2006).
19. R. Thompson, J. Simon, H. Loh, V. Vuletić, *Science* **313**, 74 (2006).
20. C.-W. Chou *et al.*, *Nature* **438**, 828 (2005).
21. H. de Riedmatten *et al.*, *Phys. Rev. Lett.* **97**, 113603 (2006).
22. D. N. Matsukevich *et al.*, *Phys. Rev. Lett.* **97**, 013601 (2006).
23. S. Chen *et al.*, *Phys. Rev. Lett.* **97**, 173004 (2006).
24. D. Felinto *et al.*, *Nat. Phys.* **2**, 844 (2006).
25. A. K. Ekert, *Phys. Rev. Lett.* **67**, 661 (1991).
26. Materials and methods are available as supporting material on Science Online.
27. C.-W. Chou, thesis, California Institute of Technology, Pasadena, CA (2006); http://etd.caltech.edu/etd/available/etd-05252006-165918/unrestricted/thesis.pdf).
28. L. Jiang, M. Taylor, M. D. Lukin, *Quant. Phys.* in press; preprint available at http://xxx.lanl.gov/abs/quant-ph/0609236.
29. Z. B. Chen, B. Zhao, J. Schmiedmayer, *W. Pan Quant. Phys.* in press; preprint available at http://xxx.lanl.gov/abs/quant-ph/0609152.
30. D. Felinto, C.-W. Chou, H. de Riedmatten, S. V. Polyakov, H. J. Kimble, *Phys. Rev. A* **72**, 053809 (2005).
31. J. F. Clauser, A. Shimony, *Rep. Prog. Phys.* **41**, 1881 (1978).
32. C. A. Fuchs, M. Grassl, K. B. Griffiths, C. S. Niu, A. Peres, *Phys. Rev. A* **56**, 1163 (1997).

33. We gratefully acknowledge critical discussions with S. J. van Enk. This research is supported by the Disruptive Technologies Office and by the NSF. J.L. acknowledges financial support from the European Union (Marie Curie fellowship). H.D. acknowledges support as Fellow of the Center for the Physics of Information at the California Institute of Technology.

Supporting Online Material

www.sciencemag.org/cgi/content/full/1140300/DC1
Materials and Methods
SOM Text
Figs. S1 to S3
Table S1
References

23 January 2007; accepted 27 March 2007
Published online 5 April 2007
10.1126/science.1140300
Include this information when citing this paper.

Anisotropic Violation of the Wiedemann-Franz Law at a Quantum Critical Point

Makariy A. Tanatar[1,2*†] Johnpierre Paglione,[2,3*] Cedomir Petrovic,[4] Louis Taillefer[1,5‡]

A quantum critical point transforms the behavior of electrons so strongly that new phases of matter can emerge. The interactions at play are known to fall outside the scope of the standard model of metals, but a fundamental question remains: Is the basic concept of a quasiparticle—a fermion with renormalized mass—still valid in such systems? The Wiedemann-Franz law, which states that the ratio of heat and charge conductivities in a metal is a universal constant in the limit of zero temperature, is a robust consequence of Fermi-Dirac statistics. We report a violation of this law in the heavy-fermion metal $CeCoIn_5$ when tuned to its quantum critical point, depending on the direction of electron motion relative to the crystal lattice, which points to an anisotropic destruction of the Fermi surface.

Discovered in 1853, the Wiedemann-Franz (WF) law (1) has stood as a robust empirical property of metals, whereby the thermal conductivity κ of a sample is related to its electrical conductivity σ through a universal ratio. In 1927, Sommerfeld (2) used quantum mechanics, applying to electrons the new Fermi-Dirac statistics, to derive the following theoretical relation:

$$\frac{\kappa}{\sigma T} = \frac{\pi^2}{3}\left(\frac{k_B}{e}\right)^2$$

where T is the absolute temperature, k_B is Boltzmann's constant, and e is the charge of the electron. The extremely good agreement between the theoretical constant $L_0 = \frac{\pi^2}{3}\left(\frac{k_B}{e}\right)^2$ and the empirical value played a pivotal role in establishing the quantum theory of solids. In 1957, Landau went on to show that, even in the presence of strong interactions, electrons in a metal can still be described as weakly interacting fermions ("quasiparticles") with renormalized mass (3). This is the essence of what became known as Fermi-liquid (FL) theory, the "standard model" of metals. In the limit of zero temperature, the WF law survived unchanged because it does not depend on mass. (Eq. 1 is only a law at $T \to 0$, as only in that limit is energy conserved in collisions.) It has since been shown that the WF law remains valid as $T \to 0$ for arbitrary strong scattering, disorder, and interactions (4). It is built into the fabric of matter, valid down to the quanta of conductance, respectively equal to $\frac{\pi^2}{3}\frac{k_B^2 T}{h}$ for heat and $\frac{e^2}{h}$ for charge (5).

In the past decade, however, departures from FL theory have been observed in *d*- and *f*-electron metals when tuned to a quantum critical point (QCP), a zero-temperature phase transition between distinct electronic ground states (6). These typically show up as an anomalous temperature dependence of properties at the QCP, for example, a specific heat coefficient that never saturates, growing as $C/T \sim \log(1/T)$ (7), and an electrical resistivity that grows linearly with T (8). Quantum criticality also appears to be linked to the emergence of exotic forms of superconductivity (9, 10) and nematic (11) electronic states of matter.

To determine whether Landau quasiparticles survive at a QCP, we have measured the transport of heat and charge in $CeCoIn_5$, a heavy-fermion metal with a QCP tuned by magnetic field H. In its phase diagram (Fig. 1), the QCP is located on the border of superconductivity and marks the end of a FL regime at $H = H_c = 5.0$ T, where the electrical resistivity obeys the FL form $\rho = \rho_0 + AT^2$ (12). A power-law fit to the A coefficient yields $A \sim (H - H_c)^{-\alpha}$, with α a 4/3 and H_c 5.0 ± 0.1 T (13). At H_c, C/T never saturates (14). The same phenomenology is found at the field-tuned QCP of $YbRh_2Si_2$ (with $\alpha \approx 1$) (15).

In Fig. 2, we show how the thermal and electrical resistivities in the $T = 0$ limit behave in $CeCoIn_5$ as the field is tuned toward H_c. These are extrapolations to $T = 0$ of the low-temperature thermal resistivity, defined as $w = L_0 T/\kappa$, and electrical resistivity ρ, for current directions parallel ($J \parallel c$) and perpendicular ($J \perp c$) to the tetragonal axis of the crystal lattice. The raw data and their extrapolation are shown in detail in (4). For $H = 10$ T, far away from H_c, $w(T)$ and $\rho(T)$ converge as $T \to 0$ for both current directions. However, very close to the QCP, for $H = 5.3$ T, they only converge for in-plane transport. In other words, transport along the c axis violates the WF law, with w_c extrapolating to a distinctly larger value than ρ_c as $T \to 0$. In the supporting material (4), we show that extrapolations are not needed to conclude on a violation of the WF law, as the difference data, $w_c(T) - \rho_c(T)$ versus T, shows a rigid T-independent shift from field to field. The normalized Lorenz ratio, $\frac{L}{L_0} = \frac{\kappa\rho}{L_0 T} = \frac{\rho}{w}$, is also seen to approach unity at 10 T but not at 5.3 T.

Our observation of a violation of the WF law at a QCP is characterized by three distinctive

[1]Département de Physique et RQMP, Université de Sherbrooke, Sherbrooke, Canada. [2]Department of Physics, University of Toronto, Toronto, Canada. [3]Department of Physics, University of California, San Diego, CA 92093, USA. [4]Condensed Matter Physics and Materials Science Department, Brookhaven National Laboratory, Upton, NY 11973, USA. [5]Canadian Institute for Advanced Research, Toronto, Canada.

*These authors contributed equally to this work.
†Present address: Institute of Surface Chemistry, National Academy of Sciences of Ukraine, Kyiv, Ukraine.
‡To whom correspondence should be addressed. E-mail: louis.taillefer@physique.usherbrooke.ca

features. (i) charge conduction is essentially unperturbed, (ii) heat conduction becomes less efficient, so that $L < L_0$, and (iii) the violation is qualitatively anisotropic, present in one direction and absent in the other.

The constancy of charge conduction distinguishes this from the two known instances of WF violation. The first occurs in the case of superconductivity, where σ immediately goes to infinity as H drops below H_{c2}, whereas κ drops gradually so that $L/L_0 = 0$. The second instance occurs in the other limit ($\sigma \to 0$), realized in the crossover from a metal to an insulator. In this limit, a violation has been observed in cuprates as the Mott insulating state is approached (4). The case of $CeCoIn_5$ is neither one of superfluid condensation nor one of charge localization, but that of a good metal violating the WF law. The fact that it is a downward violation, $L(T \to 0) < L_0$, seems inconsistent with the possibility of neutral fermionic excitations such as those predicted to emerge at a heavy-fermion QCP (16). Instead, we will argue that the Fermi surface is destroyed, anisotropically.

At the $T \to 0$ limit, the WF law holds as long as there is a step in the Fermi distribution function, that is, as long as a sharp Fermi surface exists. This step is proportional to the renormalization parameter Z, the defining property of a Landau quasiparticle (17). In standard FL theory, Z is a measure of how strongly the quasiparticle mass m^* is enhanced by electron interactions, with $Z \sim 1/m^*$. The anisotropic violation seen in $CeCoIn_5$ thus suggests that a sharp Fermi surface does not exist in the c direction but does exist in the plane. This is consistent with the observation of de Haas–van Alphen oscillations in $CeCoIn_5$ for $H \parallel c$ (18), because these result from coherent electron orbits in the plane. In other words, Z must be a function of polar angle, $Z = Z(\theta)$, whereby $Z \to 0$ over a region around the "poles" (c axis) and $Z > 0$ in a region around the "equator" (basal plane), which provides evidence of anisotropic zeros in the Z parameter of a metal, due to a QCP.

An anisotropic destruction of the Fermi surface is reminiscent of what occurs in the pseudogap state of underdoped high-temperature superconductors, where photoemission studies have revealed a Fermi surface broken into small arcs (19), shrinking to points along "nodal" directions ($\varphi = \pi/4$) as $T \to 0$ (20). This angle-dependent destruction may be caused by strong antiferromagnetic (AF) correlations, it certainly is predominant at points connected by the AF ordering vector. By analogy, the unusual destruction of the Fermi surface in $CeCoIn_5$ may be caused by spin fluctuations with a unusual character, a scenario which is consistent with both the known fluctuation spectrum and the finite-temperature properties discussed below.

Having focused on the $T = 0$ limit, we now examine how quantum criticality unfolds as a function of T. The electrical resistivity of $CeCoIn_5$ at the QCP is plotted up to 15 K (Fig. 3) for both current directions. ρ_c shows a purely linear T dependence from 0.4 $\mu\Omega$ cm at 25 mK all the way to 40 $\mu\Omega$ cm at 16 K. This 100-fold increase in resistivity extends by one order of magnitude the range over which criticality has so far been observed to persist in any material, proving beyond doubt that the power law is an intrinsic property of electrons scattered by critical fluctuations. ρ_a is qualitatively different. Its linear T dependence is seen only above 4 K or so, crossing over to a $T^{3/2}$ dependence below $\approx$ 1 K (21).

A comparison of heat and charge conductivities reveals information about the momentum dependence of inelastic scattering. This was discussed in detail in the context of our study of $CeRhIn_5$ (22), the antiferromagnetic cousin of $CeCoIn_5$ with a Néel ordering temperature $T_N = 3.8$ K. The main piece of information that can be extracted directly is the characteristic temperature T_{sf} of magnetic fluctuations, defined as the temperature below which the WF law is restored, i.e., $\kappa(T) = \rho(T)/LT$. T_{sf} is the magnetic analog of the Debye temperature, the characteristic temperature for the scattering of electrons by phonons, Θ_D. In $CeRhIn_5$, $T_{sf} \approx 8$ K (22), in good agreement with the onset of AF correlations seen with neutron scattering. In $CeCoIn_5$, the same approach applied to in-plane transport yields a field-dependent $T_{sf} \approx 4$ K at H_c and rising to match that of $CeRhIn_5$ at high field (21). This allows us to understand the strange behavior of ρ_a. The linear-T regime above T_{sf} arises from fluctuations without preferred spatial correlations, effectively scattering electrons on the whole Fermi surface and making it uniformly "hot." (A T-linear resistivity is also found in conventional metals when $T > \Theta_D$.) Below T_{sf}, the emergence of AF correlations peaked at certain q vectors in the plane leads to "hot spots" and the higher $T^{3/2}$ power law at low T. The fact that ρ_c remains linear down to the lowest temperatures suggests that $T_{sf} \to 0$ in this case, that no interplane correlations build up, and that the Fermi surface remains hot over large regions (away from the plane). [In our phonon analog, this would imply $\Theta_D \to 0$, a quantum melting of the three-dimensional (3D) solid into stacks of solid sheets separated by nonviscous liquid or gas.

Whereas the $T = 0$ intercepts are different, the linear T dependence of the c-axis electrical resistivity is paralleled by the thermal resistivity (Fig. 3, inset): $w(T)$ is perfectly linear down to the lowest T. Not only is $w_c \sim T$ but also the slope of w_c is roughly equal to that of ρ_c—a confirmation that T_{sf} indeed vanishes in this direction. This indicates that the usual $(1 - \cos\theta)$ vertex, which makes small-angle scattering ineffective in degrading a charge current, is not working in $CeCoIn_5$. It may be unimportant because inelastic scattering is dominated by large-q processes, as one would expect from AF fluctuations, or it may be inoperative for some special reason, as in the "Kondo breakdown" model (23).

At this instance of anisotropic quantum criticality, given that Z and T_{sf} exhibit the same anisotropy ($Z, T_{sf} \to 0$ along the c axis and Z, $T_{sf} > 0$ in the basal plane), it is tempting to suggest that (i) a vanishing energy scale, $Z \to 0$, and it

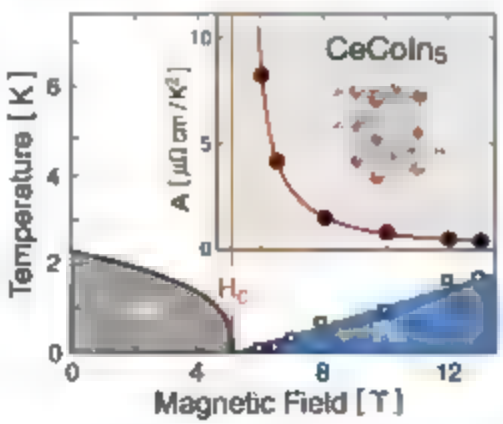

Fig. 1. Phase diagram of $CeCoIn_5$. Magnetic field–temperature phase diagram for a field perpendicular to the basal plane of the tetragonal crystal lattice (shown in inset) i.e., $H \parallel c$, as determined from in-plane resistivity measurements (10). The QCP is located at $H = H_c = 5.0$ T (vertical red line). FL behavior, $\rho = \rho_0 + AT^2$, is obeyed in the blue wedge, ending at H_c. The coefficient A, proportional to the square of the electron effective mass, diverges at H_c as a power law. Below H_c, superconductivity (SC) sets in.

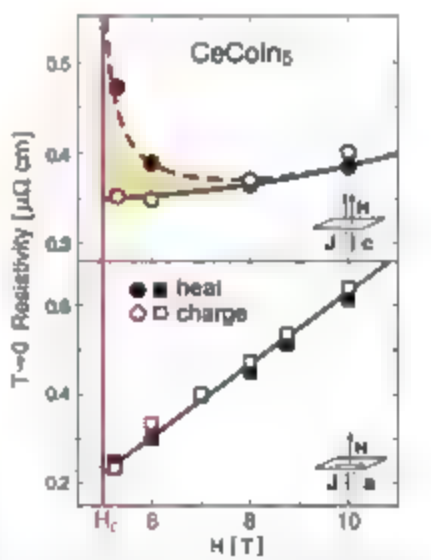

Fig. 2. Violation of the WF law. Residual resistivities extrapolated to $T = 0$ as a function of magnetic field, for heat (solid symbols) and charge (open symbols) transport. For in-plane transport (**bottom**), the two resistivities track each other as a function of field, thereby obeying the WF law at all fields. For inter-plane transport (**top**), the electrical resistivity ρ_c is flat as $H \to H_c$, whereas the thermal resistivity increases, thereby causing a violation of the WF law at the QCP, with a Lorenz number $L < L_0$.

WF law violation are all related, and (ii) a good indicator for their joint occurrence is a linear-T resistivity. Returning to our comparison with cuprates, a similar connection between $\rho \sim T$ and $Z = 0$ appears to exist there as well. Indeed, a recent measurement of the tazimuthal anisotropy of the in-plane scattering rate $\Gamma(\phi)$ in an overdoped cuprate (*36*) revealed that $\Gamma \propto T$ at $\phi = 0$, where the Fermi surface is eventually destroyed (at lower doping), and $\Gamma \sim T^2$ at $\phi = \pi/4$, where it survives.

It is instructive to compare our findings with the properties of other materials and theories of quantum criticality. A $T^{3/2}$ resistivity is observed in $CeIn_3$ near the pressure-tuned QCP where its AF order vanishes (*6*). $CeIn_3$ is the cubic parent compound of tetragonal $CeRhIn_5$ and, along with the increase in c/a ratio, the ordering temperature drops from $T_N = 10$ K in the former to $T_N = 3.8$ K in the latter. However, they still have comparable T_{SF} (assuming that in $CeIn_3$ $T_{SF} \cong T_N$). $CeCoIn_5$ encounters a further stretch of the c/a ratio, and long-range AF order is no longer stabilized. However, it can still be viewed as a layered version of $CeIn_3$, with similar in-plane correlations and scattering. In this sense, the $T^{3/2}$ dependence observed in $CeCoIn_5$ can be viewed as the result of AF fluctuations that are characteristic of the parent compound. Theoretically, a $T^{3/2}$ resistivity is expected for AF critical fluctuations in 3D from the so-called quantum spin density wave (SDW) model (*17*, *25*, *26*). In this scenario, critical scattering is peaked at "hot spots" connected by the AF wave vectors (*24*). As $T \to 0$, one would expect the Fermi surface to remain sharp everywhere else and thus the WF law to prevail, as found here for in-plane currents.

A T-linear resistivity is observed at the composition-tuned QCP of $CeCo(In_{1-x}Sn_x)_5$ (*7*) and field-tuned QCP of $YbRh_2Si_2$ (*12*), where AF order is thought to disappear. In these cases, the power law is linear in both high-symmetry

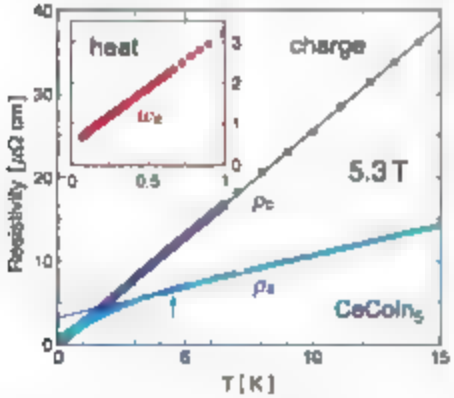

Fig. 3. Anisotropic quantum criticality. Electrical resistivity at the QCP (at $H = 5.3$, $T \cong H_{c2}$) for in-plane (ρ_a) and inter-plane (ρ_c) current directions. $\rho_c(T)$ remains linear over a 100-fold increase in magnitude. By contrast, ρ_a is linear only above a characteristic fluctuation temperature $T_{SF} \cong 4$ K (arrow) (*18*). (**Inset**) Thermal resistivity ($w_c = L_0 T/\kappa_c$) at the QCP, for inter-plane transport. w_c is perfectly linear down to the lowest temperature.

directions (*19*, *27*). The fact that a linear power is inconsistent with the SDW model for AF fluctuations in 3D prompted the proposal of a 2D version (*28*) and of an alternate theory, where critical scattering is local in space and therefore present at all wave vectors (*29*). These scenarios would lead to a more extreme breakdown of FL theory, because the Fermi surface is "hot" not only at certain specific spots but everywhere. It was argued in (*8*) that the specific heat data on (Ge-doped) $YbRh_2Si_2$, which shows a C/T that exceeds the $\log(1/T)$ dependence at low temperature, may be an indication of such enhanced breakdown. In $CeCoIn_5$, the fact that it is in the direction where $\rho \sim T$ that the WF law is violated is certainly consistent with this picture. Clearly, it would be interesting to test the WF law in $YbRh_2Si_2$.

Bringing together our findings for $T \to 0$ and $T > 0$, a picture of qualitative anisotropy emerges, not present in either the SDW model or the local criticality model, at least in their current forms. The characteristic spin fluctuation temperature T_{SF} vanishes at the QCP for transport along the c axis but not in the plane. As a result, the breakdown of FL theory is extreme in the c direction ($\rho_c \sim T$ and $w_c \sim T$ down to the lowest temperatures and the $T = 0$ Fermi surface is blurred, that is, the quasiparticle Z parameter vanishes, in regions around the c-axis direction).

A possible origin for this anisotropic criticality is an anisotropic spin fluctuation spectrum. First, an AF instability is present in all three $CeMIn_5$ compounds (M = Co, Rh, Ir), as shown by the fact that magnetic ordering can be induced by Cd doping (*30*). Second, a magnetic field does tune the magnetism. In $CeRhIn_5$ under pressure (where it becomes in many ways more similar to $CeCoIn_5$, e.g., by developing superconductivity with the same T_c), a magnetic field stabilizes long-range magnetic order (*31*, *32*). In $CeCoIn_5$, it is the magnetic fluctuations that are tuned by a magnetic field (*21*), with T_{SF} starting at a value equivalent to that of $CeRhIn_5$ at high fields and then lowered to a minimum at H_{c2}. Third, the AF fluctuations in $CeCoIn_5$ have strongly anisotropic character (*33*), with magnetic moments well coupled in-plane but weakly coupled interplane. This is consistent with the helical ordering of moments in $CeRhIn_5$, commensurate in-plane and incommensurate along the c axis. Therefore, it seems natural to link this uniaxial anisotropy with the observed anisotropy in T_{SF}, power laws, and $Z(\theta)$. What is not yet known is whether a scenario of AF critical fluctuations can indeed cause a violation of the WF law at $T = 0$.

However, the AF scenario is not the only candidate for the anisotropic quantum criticality of $CeCoIn_5$. The "Kondo breakdown" model proposed recently (*23*, *34*), a type of deconfined QCP where the hybridization between conduction and f electrons goes to zero, captures some of the key signatures: absence of magnetic order in the phase diagram, strong anisotropy, multiple energy scales, and a T-linear behavior of both charge and heat resistivities. Proximity to a Pomeranchuk instability of the Fermi surface can also cause anisotropy in electronic liquids (*7*). Recent calculations show that the transport decay rate at such a QCP has a linear T dependence everywhere on the Fermi surface except at "cold" points, resulting in a $T^{3/2}$ dependence of the resistivity (*35*).

References and Notes

1. G. Wiedemann, R. Franz, *Ann. Phys.* **89**, 497 (1853).
2. A. Sommerfeld, *Naturwissenschaften* **15**, 825 (1927).
3. L. D. Landau, *Sov. Phys. JETP* **3**, 920 (1957).
4. Additional data, analysis, and discussion are available as supporting material on *Science* Online.
5. L. G. C. Rego, G. Kirczenow, *Phys. Rev. B* **59**, 13080 (1999).
6. P. Coleman, A. J. Schofield, *Nature* **433**, 226 (2005).
7. H. von Löhneysen *et al.*, *Phys. Rev. Lett.* **72**, 3262 (1994).
8. J. Custers *et al.*, *Nature* **424**, 524 (2003).
9. M. D. Mathur *et al.*, *Nature* **394**, 39 (1998).
10. S. S. Saxena *et al.*, *Nature* **406**, 587 (2000).
11. F. Levy, I. Sheikin, B. Grenier, A. D. Huxley, *Science* **309**, 1343 (2005).
12. R. A. Borzi *et al.*, *Science* **315**, 214 (2007).
13. J. Paglione *et al.*, *Phys. Rev. Lett.* **91**, 246405 (2003).
14. A. Bianchi *et al.*, *Phys. Rev. Lett.* **91**, 257001 (2003).
15. P. Gegenwart *et al.*, *Phys. Rev. Lett.* **89**, 056402 (2002).
16. P. Coleman, J. B. Marston, A. J. Schofield, *Phys. Rev. B* **72**, 245111 (2005).
17. P. Coleman, C. Pépin, Q. Si, R. Ramazashvili, *J. Phys. Cond. Mat.* **13**, R723 (2001).
18. A. McCollam, S. R. Julian, P. M. C. Rourke, D. Aoki, J. Flouquet, *Phys. Rev. Lett.* **94**, 186401 (2005).
19. M. R. Norman *et al.*, *Nature* **392**, 157 (1998).
20. A. Kanigel *et al.*, *Nat. Phys.* **2**, 447 (2006).
21. J. Paglione *et al.*, *Phys. Rev. Lett.* **97**, 106606 (2006).
22. J. Paglione *et al.*, *Phys. Rev. Lett.* **98**, 216602 (2005).
23. I. Paul, C. Pépin, M. R. Norman, *Phys. Rev. Lett.* **98**, 026402 (2007).
24. M. Abdel-Jawad *et al.*, *Nat. Phys.* **2**, 821 (2006).
25. A. J. Millis, *Phys. Rev. B* **48**, 7183 (1993).
26. T. Moriya, T. Takimoto, *J. Phys. Soc. Jpn.* **64**, 960 (1995).
27. A. Neubert *et al.*, *Physica B (Amsterdam)* **230**, 587 (1997).
28. A. Rosch, A. Schröder, O. Stockert, H. von Löhneysen, *Phys. Rev. Lett.* **79**, 159 (1997).
29. Q. Si, S. Rabello, K. Ingersent, J. L. Smith, *Nature* **413**, 804 (2001).
30. L. D. Pham, T. Park, S. Maquilon, J. D. Thompson, Z. Fisk, *Phys. Rev. Lett.* **97**, 056404 (2006).
31. T. Park *et al.*, *Nature* **440**, 65 (2006).
32. G. Knebel, D. Aoki, D. Braithwaite, B. Salce, J. Flouquet, *Phys. Rev. B* **74**, 020501 (2006).
33. Y. Kawasaki *et al.*, *J. Phys. Soc. Jpn.* **72**, 2308 (2003).
34. T. Senthil, M. Vojta, S. Sachdev, *Phys. Rev. B* **69**, 035111 (2004).
35. L. Del Anna, W. Metzner, *Phys. Rev. Lett.* **98**, 136402 (2007).

36. We thank D. G. Hawthorn, R. W. Hill, F. Ronning, and M. Sutherland for experimental assistance, and P. C. Canfield, Y. B. Kim, C. Pépin, A. M. Tremblay, A. Rosch, and M. F. Smith for useful discussions. L.T. acknowledges support from the Canadian Institute for Advanced Research, a Canada Research Chair, the Natural Sciences and Engineering Research Council of Canada, the Canada Foundation for Innovation, and Le Fonds Québecois de Recherche sur la Nature et la Technologie. Part of this research was carried out at the Brookhaven National Laboratory, which is operated for the U.S. Department of Energy by Brookhaven Science Associates (DE-AC02-98CH10886).

Supporting Online Material

www.sciencemag.org/cgi/content/full/316/5829/1320/DC1
Materials and Methods
Figs. S1 to S11
References

2 February 2007; accepted 19 April 2007
10.1126/science.1140762

Mars: A New Core-Crystallization Regime

Andrew J. Stewart,[1] Max W. Schmidt,[1]* Wim van Westrenen,[2] Christian Liebske[1]

The evolution of the martian core is widely assumed to mirror the characteristics observed for Earth's core. Data from experiments performed on iron-sulfur and iron-nickel-sulfur systems at pressures corresponding to the center of Mars indicate that its core is presently completely liquid and that it will not form an outwardly crystallizing iron-rich inner core, as does Earth. Instead, planetary cooling will lead to core crystallization following either a "snowing-core" model, whereby iron-rich solids nucleate in the outer portions of the core and sink toward the center, or a "sulfide inner-core" model, where an iron-sulfide phase crystallizes to form a solid inner core.

For Mars, the presence of a metallic core dominated by Fe, Ni, and S is well established by martian meteorite geochemistry (*1*–*3*). However, because of the absence of seismic data and direct samples from the martian mantle, the composition, thermal evolution, and physical state of the core are hotly debated. The Mars Global Surveyor mission has allowed detailed refinement of the geophysical data available for the planet. Precise determinations of the moment of inertia (*4*) and solar tidal deformation (*5*) have provided strong constraints on structural models of the planet, requiring a core radius of 1520 to 1840 km, as compared with a mean planetary radius of 3390 km. The same data also indicate that the present-day metallic core is not completely solid (*4*, *5*) and are consistent with a range of possibilities between an entirely liquid and a highly solidified core with only a small outer liquid region (*6*). The evolution of the physical state of the martian core is particularly important, in view of the recent identification (*7*, *8*) of highly magnetized highland rocks in the southern hemisphere, indicating the presence of a strong transient magnetic field in the Noachian period (~ 4 billion years ago), generated by the flow of metallic liquid in the martian core. The mechanism that caused the subsequent cessation of the magnetic field is one of the fundamental unknowns about the evolution of the martian interior (*9*) and depends critically on the physical state of the core.

The core-mantle boundary of Mars occurs at ~23 GPa (*10*) and ~1800 K (*11*). High-pressure experiments performed on the Fe-S system at such conditions (*12*) indicate relatively low eutectic melting temperatures throughout the planet (*11*, *13*, *14*), as compared with calculated temperature profiles (termed areotherms). This implies that at least the outer core is in a liquid state (*10*). Here we present an experimental study of high-temperature phase relations in the Fe-S and (Fe,Ni)-S systems extending to pressures that exist at the center of Mars, estimated to be near 40 GPa and 2200 K, thereby experimentally constraining the physical state of the entire martian core.

Using high-pressure multianvil devices, we investigated the Fe-rich portions of the binary Fe-S and pseudobinary (Fe,Ni)-S systems at 23 and 40 GPa. Experiments at 23 GPa were performed in a traditional uniaxial multianvil device with static lateral confinement (*15*), whereas a spherical multianvil device (*16*, *17*) equipped with sintered diamond anvils was used for experiments at 40 GPa (*18*).

Recovered run products were sectioned, polished, and investigated by electron microprobe analysis. The results (table S1) show that the Fe-S system preserved its eutectic behavior as observed at 25 GPa (*12*) up to 40 GPa (Fig. 1). At 40 GPa, the eutectic melting temperature of the Fe-S system was found to be 1520 K, which is 800 K lower than that of pure Fe melting at that pressure (*20*) and only 200 K higher than the eutectic temperature at 23 GPa. The eutectic melt composition shifted from 16 weight % (wt %) S at 23 GPa to 12 wt % at 40 GPa. No new phases were observed in the system. At subsolidus temperatures, Fe is found to coexist with $Fe_{3-x}S_2$ rather than Fe_3S (*21*). We consider this an artifact in subsolidus experiments because of the short run durations and low temperatures involved; recently, thermally equilibrated subsolidus experiments by Seagle *et al.* (*22*) observed stable coexistence of Fe and Fe_3S at pressures up to 80 GPa. The effect of Ni on the binary Fe-S system was evaluated by replacing 36 wt % of Fe by Ni (Fe:Ni = 16:9). This addition of Ni had no effect on the phases observed or the eutectic nature of the system, as compared to the Fe-S system. Ni appears to substitute for Fe in all phases. Nevertheless, the presence of Ni lowered the eutectic temperatures at both 23 and 40 GPa by ~125 K, which widens the liquidus loop slightly by increasing the S content of the eutectic melt by 1 wt %. Assuming that eutectic temperatures vary linearly with Ni content, a cosmochemical abundance of Ni (~8 wt %) (*9*) will lower the eutectic temperature by ~30 K, which thus has only a minor effect on the S content of the eutectic composition. The solubility of S in the solid Fe metal phase increases with pressure to 25 GPa (*12*). However, solubilities at 23 and 40 GPa in our Ni-bearing samples were similar (1.6 and 1.8 wt % S, respectively).

Using our data reaching pressures at the center of Mars with previous lower-pressure studies, we are able to draw a temperature-pressure diagram for the entire range of martian conditions (Fig. 2). By comparing liquidus intersections (temperatures

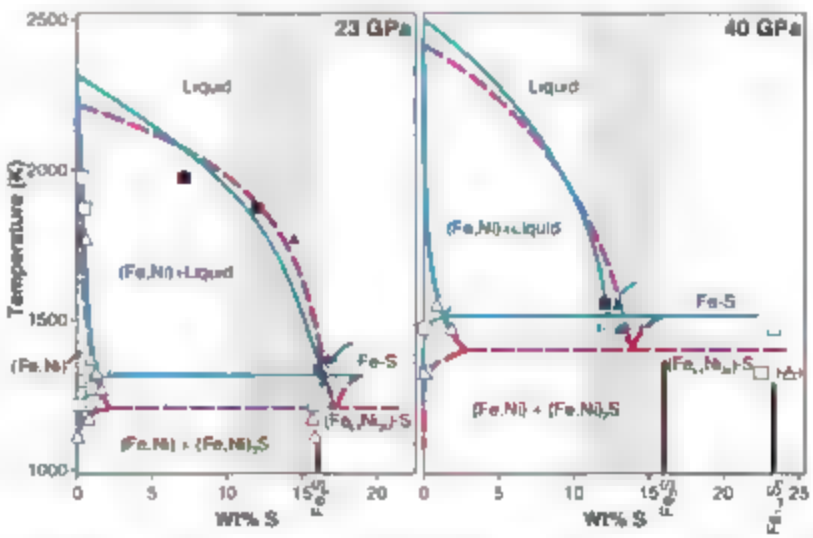

Fig. 1. Fe-S and (Fe,Ni)-S phase diagrams at 23 (**left**) and 40 (**right**) GPa. Fe-S results, squares; (Fe,Ni)-S results, triangles; liquid phases, black symbols; solids, white symbols. The resulting phase boundaries for Fe-S (solid blue lines) and (Fe,Ni)-S (dashed red lines) are shown. Thick black vertical lines indicate the composition of stable sulfide phases, as indicated along the *x* axis. Temperatures for melting of pure Fe are from Boehler (*20*). Pure Fe-Ni melting temperatures at both pressures are based on the melting depression from pure Fe of roughly 80 K observed at 1 atm for $Fe_{64}Ni_{36}$. The gray shaded region represents the estimated bulk martian core composition (*3*, *9*). Error bars (1σ) represent analytical variation and are indicated when larger than the symbol.

[1]Institute for Mineralogy and Petrology, Eidgenössische Technische Hochschule Zurich, CH 8092 Zurich, Switzerland. [2]Faculty of Earth and Life Sciences, Vrije Universiteit, 1081 HV Amsterdam, Netherlands.

*To whom correspondence should be addressed. E-mail: max.schmidt@erdw.ethz.ch

below which solids will begin to crystallize) of various estimated core S contents to anadiabatic estimates, we observed that the anadiabats lie at higher temperatures, with the exception of the 10.6 wt % S estimate (though only near the core/mantle boundary). This observation indicates a complete absence of crystallization in most, if not all, of the present-day martian core.

Although it is not evident that crystallization of the martian core has begun, Mars continues to cool, and the core will undoubtedly solidify in the geological future. The mechanisms of core crystallization will critically depend on the effect of pressure on crystallization temperatures in the (Fe,Ni)-S system, the corresponding phase compositions, and particularly on the bulk S concentration of the martian core. Estimates of such S contents, obtained by comparing the chemical compositions of martian meteorites with those of other primitive meteorites, range from 10.6 to 16.2 wt % (*1*–*3*). These concentrations encompass the eutectic melt compositions at various core pressures. Liquidus temperatures of core melts are thus substantially lowered, as compared with the melting temperature of pure Fe.

For the martian core, two different crystallization regimes can be envisaged, depending on whether the bulk core composition lies on the left- or right-hand side (i.e., the Fe- or S-rich composition, relative to the eutectic) of the (Fe,Ni)-S pseudobinary phase diagram at core pressures. For example, assuming a bulk S content of the martian core of 10.6 wt % (*2*), the onset of crystallization of an Fe-rich alloy with minor amounts of dissolved S will occur once the actual anadiabatic falls below ~970 K (Fig. 1). Interpolation of liquidus temperatures for this S content between 33 and 40 GPa indicates that the slope of the liquidus temperature as a function of pressure is negative. However, any adiabatic anadiabat must have a positive temperature-pressure (dT/dP) slope (Fig. 2), which implies that the crystallization of core melts with S contents lower than the eutectic compositions (e.g., 14 wt %) must begin at the core-mantle boundary.

To evaluate possible consequences for the evolution of the core under these conditions, the densities of coexisting solid and liquid phases were approximated with equations of states for γ-Fe (*23*), the Fe polymorph expected to be stable at martian core conditions, and Fe-S liquid with 10 wt % S (*24*, *25*). The calculations show that γ-Fe is denser than the coexisting liquid, having a density that increases from 9.4 to 10.3 g/cm^3 across core pressures at 2050 K (*23*), as compared with a coexisting Fe-S liquid with a maximum density of 6.9 to 7.7 g/cm^3 across core pressures over the temperature range from 773 to 2123 K (*24*). Thus, any solid Fe-rich phase crystallizing from the S-bearing liquid should sink within that liquid, leading to the snowing-core hypothesis (Fig. 3A). A similar Fe snowing-core regime has been previously proposed for the core of Ganymede (*26*). In an equilibrium situation, these solid Fe-Ni droplets would redissolve while sinking, but their fate also depends on the kinetics of re-melting, and the vigor of convection. The functionality of convective currents bringing the solid precipitates deep into the core along colder downwellings can be imagined to provide much faster descent times than those allowable by Stokes law. As core temperatures decrease with time, it is possible that an inner Fe-Ni core will form as a metastable sedimentary agglomerate of sinking Fe-rich solids (Fig. 3A). The liquid portion of the core will then become progressively enriched in S, until finally the core will complete its crystallization from a eutectic liquid crystallizing both (Fe,Ni) and $(Fe,Ni)_3S$.

A second crystallization regime for the martian core arises if the bulk S content is toward the higher end of current estimates (i.e., on the S-rich side of the eutectic composition at core pressures). Although our data set is limited in this compositional range, the dT/dP slope of the liquidus on this side of the eutectic composition is steeper, because the eutectic composition moves away from the bulk composition as pressure increases. As a result, crystallization will first occur at high pressures. Unlike Earth, such martian core melts would have compositions on the S-rich side of the eutectic and thus first crystallize an inner core of $(Fe,Ni)_3S$ (Fig. 3B). The equation of state for Fe_3S (*22*) indicates a density increasing from 7.7 to 8.2 g/cm^3 over the martian core pressure range, with no substantial variation in density between 1600 and 2100 K in the same pressures (*22*). The densities calculated above for an Fe-S liquid with 10 wt % S (6.5 to 7.7 g/cm^3) provide maximum values of densities for all liquids with >10 wt % S, as increasing S contents will decrease the density. Hence, the crystallizing $(Fe,Ni)_3S$ would remain at the center of the core. Removing $(Fe,Ni)_3S$ from the liquid core will cause the residual liquid compositions to evolve toward the high-pressure eutectic, finally forming a crystallizing outer martian core composed of (Fe,Ni) and $(Fe,Ni)_3S$, with an inner core composed of $(Fe,Ni)_3S$.

Our data demonstrate that present-day Mars has a molten core and that a solid inner core can be excluded from the Early Noachian period (~4

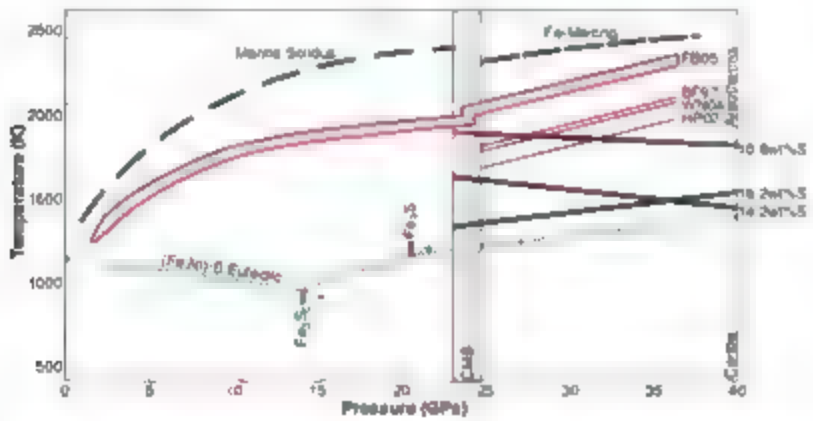

Fig. 2. Effect of pressure on the Fe-S and (Fe,Ni)-S systems. Eutectic melting temperatures for (Fe,Ni)-S with Fe/Ni of 10.6:1 are shown as a dotted blue line. Eutectic temperature inflections around 14 and 20 GPa are due to the stabilization of Fe_3S_2 and Fe_3S above these pressures. Temperatures for liquidus-loop intersections (i.e., first crystallization) presented in Fig. 1 for core S contents of 10.6 (*2*), 14.2 (*3*), and 16.2 (*1*) wt % are presented as solid black lines. The 16.2 wt % curve has a positive slope because its S content is higher than the eutectic. The anadiabat estimated by Fei and Bertka in 2005 (*10*) (F805) is presented along with calculated estimates (*11*) for the core anadiabat, based on core/mantle boundary temperature determinations by Bertka and Fei in 1997 (BF97) (*3*), Williams and Nimmo in 2004 (WN04, (*11*)), and Hauck and Phillips in 2002 (HP02) (*14*). The pressure of the core/mantle boundary (CMB), the mantle solidus, and the melting curve of pure Fe (*10*) are given for reference.

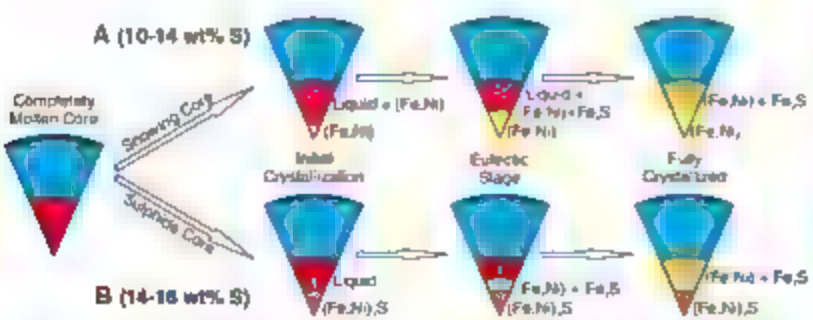

Fig. 3. Cross section through Mars, illustrating two possible crystallization regimes for the martian core. Solid (Fe-Ni), yellow; solid Fe_3S, orange; liquid sulfide, red; mantle, blue; crust, black (not drawn to scale). (**A**) Snowing-core hypothesis. (**B**) Sulfide inner-core hypothesis.

billion years ago), when the highly magnetized highland rocks of the southern hemisphere formed (*7*, *8*). This implies that the Noachian magnetic field was generated by very vigorous convection, unlike any thick or thin-shell dynamo models applied to present Earth and Mercury (*27*, *28*). In the absence of solid core formation, the cessation of magnetic field generation must have been caused by a dramatic change in the liquid core convection regime. Such a change could be related to a decrease (with time) of radiogenic heat production from potassium decay in the core, or to the termination of surface tectonics (*29*). With the onset of large-scale core crystallization, the release of latent heat, gravitational energy, and compositionally driven convection may provide enough energy to initiate increased convection within the liquid portion of the core. It is possible that this convection, over time, can reestablish a dynamo, resulting in the generation of a second period with a strong global martian magnetic field.

References and Notes

1. C. Sanloup, A. Jambon, P. Gillet, *Phys. Earth Planet. Inter.* **112**, 43 (1999).
2. K. Lodders, B. Fegley Jr., *Icarus* **126**, 373 (1997).
3. H. Wänke, G. Dreibus, *Philos. Trans. R. Soc. London Ser. A* **325**, 545 (1988).
4. P. Sahl, G. Schubert, E. Spohn, *J. Geophys. Res.* **110**, E12006 (2005).
5. C. F. Yoder, A. S. Konopliv, D. N. Yuan, E. M. Standish, W. M. Folkner, *Science* **300**, 299 (2003).
6. D. J. Stevenson, *Nature* **412**, 214 (2001).
7. M. H. Acuña *et al.*, *Science* **284**, 790 (1999).
8. J. E. P. Connerney *et al.*, *Science* **284**, 794 (1999).
9. S. C. Solomon *et al.*, *Science* **307**, 1214 (2005).
10. Y. Fei, C. Bertka, *Science* **308**, 1120 (2005).
11. J.-P. Williams, P. Nimmo, *Geology* **32**, 97 (2004).
12. J. Li, Y. Fei, H. K. Mao, K. Hirose, S. R. Shieh, *Earth Planet. Sci. Lett.* **193**, 509 (2001).
13. C. M. Bertka, Y. Fei, *J. Geophys. Res. B* **102**, 5251 (1997).
14. S. A. Hauck II, J. Phillips, *J. Geophys. Res.* **107**, 5052 (2002).
15. D. Walker, *Am. Mineral.* **76**, 1092 (1991).
16. K. Kanda, S. Endo, *Rev. Sci. Instrum.* **41**, 1178 (1970).
17. E. Ito, A. Kubo, T. Katsura, M. Akaogi, T. Fujita, *Geophys. Res. Lett.* **22**, 821 (1995).
18. G. Van Platen, in *Modern Very High Pressure Techniques*, R. H. Wentorf, Ed. (Butterworths, Washington, DC, 1962), pp. 126–136.
19. Materials and methods are available as supporting material on *Science* Online.
20. R. Boehler, *Nature* **363**, 534 (1993).
21. Y. Fei, J. Li, C. M. Bertka, C. T. Prewitt, *Am. Mineral.* **85**, 1830 (2000).
22. C. T. Seagle, A. J. Campbell, D. L. Heinz, G. Shen, V. Prakapenka, *J. Geophys. Res.* **111**, B06209 (2006).
23. J. M. Besson, M. Nicol, *J. Geophys. Res.* **95**, 21717 (1990).
24. P. S. Balog, B. A. Secrist, D. C. Rubie, D. J. Frost, *J. Geophys. Res.* **108**, 2124 (2003).
25. C. Sanloup *et al.*, *Geophys. Res. Lett.* **27**, 811 (2000).
26. S. A. Hauck, J. M. Aurnou, A. J. Dombard, *J. Geophys. Res.* **111**, E09008 (2006).
27. M. H. Heimpel, J. M. Aurnou, F. M. Al-Shamali, N. Gómez Perez, *Earth Planet. Sci. Lett.* **236**, 542 (2005).
28. A. Sakuraba, M. Kono, *Phys. Earth Planet. Inter.* **111**, 105 (1999).
29. F. Nimmo, D. J. Stevenson, *J. Geophys. Res.* **105**, 11969 (2000).

30. We gratefully thank E. Ito for his insight into multianvil design, as well as his hospitality in Japan. We also thank A. Jackson for a helpful discussion of the snowing-core model and two reviewers for their helpful comments on the manuscript. This work was supported by the Swiss National Science Foundation (grants 2100-066903-01/1 and 200020-103729/1).

Supporting Online Material

www.sciencemag.org/cgi/content/full/316/5829/1327/DC1

Figs. S1 to S3
Table S1
References

29 January 2007; accepted 11 April 2007
10.1126/science.1140549

Physical Model for the Decay and Preservation of Marine Organic Carbon

Daniel H. Rothman[1]* and David C. Forney[1,2]

Degradation of marine organic carbon provides a major source of atmospheric carbon dioxide whereas preservation in sediments results in accumulation of oxygen. These processes involve the slow decay of chemically recalcitrant compounds and physical protection. To assess the importance of physical protection, we constructed a reaction-diffusion model in which organic matter differs only in its accessibility to microbial degradation but not its intrinsic reactivity. The model predicts that organic matter decays logarithmically with time t and that decay rates decrease approximately as $0.2 \times t^{-1}$ until burial. Analyses of sediment-core data are consistent with these predictions.

Nearly half of Earth's primary production of organic carbon occurs in the oceans (*1*). Once fixed, this reduced carbon immediately enters the marine food chain, where nearly all of it—about 99.9‰—is eventually oxidized back to CO_2 via heterotrophic metabolism (*2*). The remainder escapes degradation and is immobilized in sediments (*2*–*4*). Whereas degradation rates influence atmospheric and oceanic concentrations of CO_2 at short time scales, burial rates influence O_2 concentrations at long (geologic) time scales (*3*, *4*). Moreover, the impact of this slow leak from the biological to the geological carbon cycle extends well beyond O_2. For example, the burial of organic carbon is a natural form of carbon sequestration (*5*) that can lead to the formation of petroleum (*6*), and O_2 accumulated as a consequence of burial must have preceded the evolution of complex life dependent on aerobic metabolism (*7*).

A fundamental understanding of the rates of decay and burial has been elusive, however. A central problem is that there appears to be no single rate that characterizes the microbial decay of organic matter (*8*, *9*). Indeed, a pronounced slowdown in respiration rates, as organic matter falls through the water column and degrades in sediments, has been unambiguously documented at time scales ranging from days to millions of years (*10*, *11*). However, the mechanisms responsible for this slowdown and their relation, if any, to the small fraction of organic matter that is preserved in sediments remain unresolved.

Many hypotheses have been proposed. Roughly speaking, these appeal to either chemistry or physics. The chemical scenarios typically ascribe the slowdown to changes in the chemical composition of organic matter. In probably the simplest such formulation, intrinsically highly reactive "labile" organic carbon is consumed first and then followed by less reactive compounds. The most recalcitrant organic compounds, for example algaenans, are then "selectively preserved" (*12*, *13*). An alternative hypothesis suggests that recalcitrance is ultimately not traceable to biosynthesis. It instead results from random repolymerization and condensation of a small set of unselective set of incompletely degraded but enzymatically depolymerized compounds, which, over time, constitute an increasingly large fraction of the remaining organic matter (*14*).

The physical scenarios attribute the slowdown and burial to some form of physical protection. This reasoning is born in part from observations showing a strong correlation between the concentrations of organic carbon and clay particles (*14*) or mineral surface area (*15*–*17*) in sediments, suggesting that some physical property of the sediments themselves is promoting the preservation of organic matter. Further evidence of physical protection comes from observations indicating that the chemical composition of organic matter changes little as it sinks to the sea floor (*18*), and from experiments suggesting that when apparently recalcitrant organic matter is physically separated from its mineral matrix, it becomes "labile" and is rapidly consumed (*19*).

Both chemical and physical mechanisms must play a role, but they have not received similar attention in quantitative models. Whereas intrinsic reactivity is commonly invoked (*8*, *9*, *20*), explicit consideration of physical mechanisms has been rare (*21*). To address this, we construct a

[1]Department of Earth, Atmospheric, and Planetary Sciences, Massachusetts Institute of Technology, Cambridge, MA 02139, USA. [2]Department of Mechanical Engineering, Massachusetts Institute of Technology, Cambridge, MA 02139, USA.

*To whom correspondence should be addressed. E-mail: dhr@mit.edu

theoretical model that purposely assumes an extreme case in which the chemical composition of organic matter is uniform. Degradation and preservation rates instead derive only from the physics of diffusion-limited reactions in porous media. As we show below, this simple theory provides predictions that are quantitatively consistent with a variety of observations, thereby suggesting that physical mechanisms play an important role in setting both degradation and preservation rates.

Our model assumes that organic matter is randomly distributed on the mineral surfaces of a porous medium populated by randomly distributed heterotrophic bacteria (Fig. 1). We assume that the typical bacterial spacing $r_b \sim n^{-1/3}$ associated with the bacterial number density n is much greater than the typical pore size of the porous medium, consistent with images obtained by microscopy (*22*). Spatial averaging of the porous medium at a scale greater than the pore size but less than r_b then provides a continuum approximation in which each microbe is embedded in a smooth porous medium characterized by its void fraction (porosity) ϕ.

The decay of a particular parcel of organic matter is assumed to be limited by its accessibility to hydrolytic enzymes. "Accessibility" is associated with grain boundaries. It is interpreted physically as the frequency f with which a mineral surface encounters a diffusing enzyme. We assume that f is proportional to the concentration c of functional enzymes in the pore fluid near the mineral surface, and that enzymes lose their functionality at rate α. Otherwise, c is conserved and diffuses within pores with diffusivity D. Averaged over lengths much greater than a pore size, the volume-averaged concentration $\bar{c} = \phi c$ of active enzymes therefore evolves according to the reaction-diffusion equation

$$\partial \bar{c}/\partial t = \bar{D}\nabla^2 \bar{c} - \alpha \bar{c} \quad (1)$$

where $\bar{D}$ is the effective diffusivity in the porous aggregate.

A complete treatment of this problem would require coupling the diffusion of c to the diffusion of organic matter hydrolyzed by its contact with c, along with the consumption of hydrolysate by bacteria (*21*). It would also include coupling the production of enzymes to energy gained from hydrolysate. We simplify our analysis, however, by assuming that the decay of organic matter is rate-limited by hydrolysis, and that the bacterial population density and the flux of enzymes emanating from each microbe is constant. We then set local decay rates $k \propto f$ and assume that the appropriate solution of Eq. 1, $c(r) \propto e^{-\beta r}/r$, where r is the distance from the nearest microbe and $\beta = (\alpha/\bar{D})^{1/2}$, suffices to determine f from the relation $f \propto c$. These assumptions correspond to a quasistatic limit in which enzymes diffuse much faster than microbes, hydrolysis is diffusion-limited, and the porosity ϕ is constant. They also imply that decreases in hydrolysate production represent a decreasing surplus. Although such excess solubilization suggests inefficiency at early times, it is consistent with previous model calculations (*21*) and observations of effluxes of dissolved organic matter from marine sediments (*23*) and sinking organic aggregates (*24*).

These simplifications allow us to express the temporal decay of the total concentration of organic matter $g(t)$, as a continuous (*20*) superposition of first-order reactions (*8*, *9*) weighted by the concentration $p(k,t)\,dk$ of organic matter associated with rate k at time t. Our formulation depends on two phenomenological parameters: a characteristic concentration $g_0 \propto g(0)$ arising from the requirement that $g(0) = \int p(k,0)\,dk$, and a minimum reaction rate k_{min} associated with the typical distance (r_b) between microbes. Assuming that k_{min} is much smaller than the (maximum) reaction rate adjacent to microbes, we obtain the approximation (supporting online text)

$$g^*(\tau) \approx \int_{\tau}^{\infty} \frac{1}{k^*} e^{-k^*} dk^* = E_1(\tau), \quad \tau > \tau_{min} \quad (2)$$

where $\tau = k_{min}t$, $k^* = k/k_{min}$, $g^*(k_{min}t) = g(t)/g_0$, and $\tau_{min} = k_{min}t_{min}$ is the dimensionless time associated with the initiation of observable decay at dimensional time $t = t_{min}$ (i.e., in a core-top sample). Equation 2 is a special case of the reactive continuum models introduced by Boudreau and Ruddick (*20*). Its particular form, which defines the exponential integral $E_1(\tau)$ (*25*), derives from its connections to the reaction-diffusion dynamics of Eq. 1.

For $\tau \ll 1$, an asymptotic expansion of Eq. 2 predicts that $g^*(\tau)$ decays logarithmically (*25*),

$$g^*(\tau) \approx \gamma - \ln \tau, \quad \tau_{min} \le \tau \ll 1 \quad (3)$$

where $\gamma \approx 0.5772\ldots$ is Euler's constant. The characteristic time $\tau \sim 1$ (i.e., $t \sim k_{min}^{-1}$) marks the termination of the logarithmic decay. Because subsequent decay proceeds slowly, as $e^{-\tau}/\tau$ (*25*), we interpret $t \sim k_{min}^{-1}$ as the approximate time of burial and the effective cessation of degradation. Consequently $g(k_{min}^{-1}) \sim g_0 E_1(1)$ approximates the burial concentration and $g_0/g(t) \ge g_{max}$, where g_{max} is the observed concentration at $t = t_{max}$ approximates the burial efficiency. Assuming $\tau_{max} \gg \tau_{min}$ implies $e^{-\tau_{max}} \ll \tau_{min}$. In τ_{max} and decreasing (supporting online text)

$$\frac{g_0}{g_{max}} \approx \frac{1}{\ln k_{max}/k_{min}} \approx \frac{\beta}{k_{max}} \quad (4)$$

The second relation derives from $k_{min} \propto r_b^{-2}$ and the assumption that $k_{max} \propto \beta$. Equation 4 approximates burial efficiency (neglecting the factor of $E_1(1) \approx 0.22$) by the ratio of the diffusion length β^{-1} to the typical distance between microbes r_b.

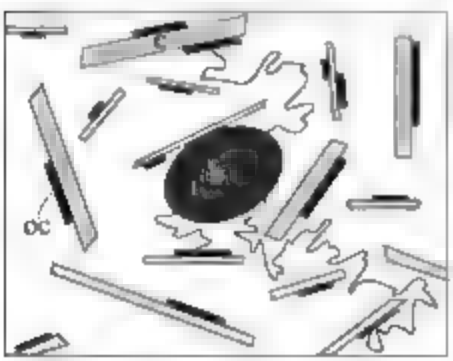

Fig. 1. Schematic illustration of the main features of our model. In a porous medium characterized by its porosity ϕ, organic carbon (oc) is associated with the surface area of clay (c) and other minerals. Extracellular enzymes are emitted from randomly distributed bacteria (b), diffuse through the medium, and hydrolyze organic matter upon contact. For simplicity, diffusive paths show only first encounters of enzymes with solid surfaces; later encounters occur until enzymes become inactive, at a specified rate α. Except for the random distribution of bacteria, each of these features is contained in a more detailed model proposed by Vetter *et al.* (*21*).

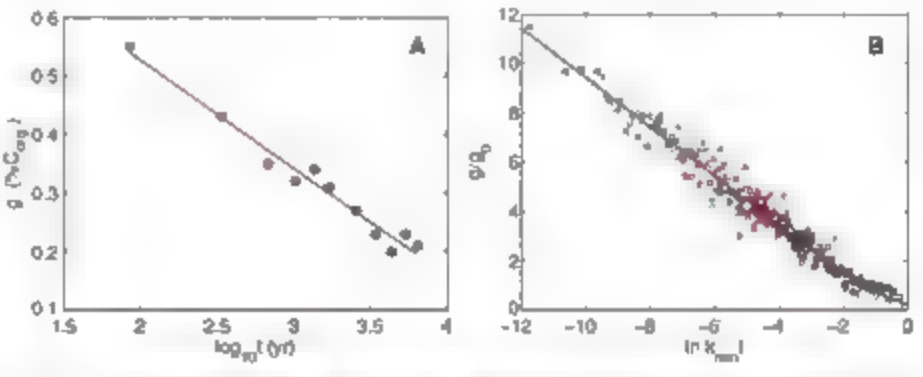

Fig. 2. (**A**) Concentration (weight %) of organic carbon (filled circles) from Pacific–Antarctic Ridge sediment core 7812-05 of Reimers and Suess (*32*). The theoretical curve (smooth line) corresponds to Eq. 2 with $\log_{10} k_{min} = -5.1$ (year^{-1}) and $g_0 = 0.08$ (%C_{org}). (**B**) Rescaling of 23 cores (287 points total) with respect to dimensionless axes $\ln k_{min}t$ and g/g_0. Each core corresponds to a different k_{min}, g_0 pair. Different colors and symbols correspond to different cores. Red corresponds to cores underlying anoxic environments.

bacterial spacing r_b. In conjunction with the first relation, it also shows that as r_b increases (with β and k_{min} constant), k_{min} decreases exponentially, reflecting the longer degradation times associated with lower microbial population densities and less efficient burial.

To test these predictions, we assembled a database of 23 published analyses of dated sediment cores that span a wide range of environmental settings, from the deep ocean to shallow waters, and from aerobic to anoxic conditions at the sediment-water interface (table S1). Each data set provides measurements of the bulk concentration g_i of particulate organic carbon at time t_i, where t_i is obtained by dividing depth by the average accumulation rate F_1 of the overlying sediment. A least-squares fit of each core to Eq. 2 provides a comparison between theory and observation along with estimates of the parameters k_{min} and g_0 (supporting online text).

Figure 2A shows data from a single core beneath oxygenated waters. In this case the fit, which is generally good, yields a value of k_{min} that is much less than the inverse of the time associated with the base of the core. Thus, the resulting theoretical curve is nearly identical [illegible] decay of Eq. 3. Figure 2B shows the data from all 23 cores after rescaling the g and t axes by the estimates of g_0 and k_{min}, respectively, that derived from each fit. The data generally show a reasonable fit to Eq. 2, including some evidence of diminishing decay rates near $t \sim k_{min}^{-1}$.

Figure 3A displays the 23 estimates of the fitted parameters k_{min} and g_0. One sees that the cores underlying anoxic waters are associated with higher burial concentrations ($\propto g_0$) and earlier terminations (i.e., higher k_{min}). The otherwise apparent disarray of the data, however, masks the relation between k_{min} and g_0 predicted by Eq. 4. Figure 3B compares this prediction to each of the g_0, k_{min} pairs of Fig. 3A. The good fit derives from the consistency of the degradation data with the theoretical model of Eq. 2.

Figure 3B also shows that the variation of g_0/g_{max} is not large and that there is a tendency for both oxic and anoxic cores to cluster around the mean $\langle g_0/g_{max} \rangle$. Thus, in Fig. 3C, where we plot the burial flux Fg_0 versus the flux to the sea floor Fg_{max}, we find a good fit to a straight line with a slope of unity in logarithmic coordinates. Although anoxia appears to have little influence on burial efficiency (26) (Fig. 3B), it is associated with a higher burial flux (Fig. 3C), which is in turn proportional, on average, to the flux to the sea floor. Insertion of the constant of proportionality $\langle g_0/g_{max} \rangle \cong 0.18$, into Eq. 4 then yields the mean $\langle \beta r_b \rangle \cong 5.6$, with all values of βr_b between 2.2 and 11.5. The narrow range of $\beta r_b = (\alpha \bar{D})^{1/2} r_b$ might be related to the apparent constancy of bacterial abundance with respect to fluid volume (27). If we assume $\bar{D} \approx \phi D$ (28), this range is also consistent with the natural variation of the dimensional constants α, r_b, D, and ϕ (21), but it suggests that $\beta r_b \gg 5.6$ is atypically large. We therefore hypothesize that the effective diffusivity $\bar{D} \ll \phi D$, because of sorption of enzymes to mineral surfaces (9, 29), shielding of organic matter (16) in clay-rich microenvironments (22), or both.

Finally, we return to the slowdown of respiration rates discussed in the introduction. Middelburg *et al.* (10, 11) have shown that the phenomenological effective rate $k(t) = -d\ln g/dt$ is well fit by the power law $k = 0.21 \times t^{-0.69}$ (11). This fit holds over nearly 10 orders of magnitude and includes water-column sediment trap data in addition to analyses of sea-floor sediments. Figure 4 shows a similar analysis with the 23 cores in our database. Here, rather than numerically estimating $d\ln g/dt$ from noisy data, we calculate it analytically from Eq. 2. Conversion back to dimensional variables then yields

$$k(t) = \frac{1}{t}\left\{ \frac{e^{-k_{min}t}}{\Gamma(1/3, k_{min}t)} \right\} \approx 0.23 \; t^{-0.67} \quad (5)$$

The approximation is obtained by averaging the logarithm of the slowly varying factor in parentheses over $\ln t$, between the average minimum and maximum values of $\ln k_{min}t$ (−6.95 and −3.19, respectively). Its excellent correspondence to Middelburg's expression is notable, not only because it is derived without any free parameters, but also because it indicates that our analysis may also apply to the decay of organic matter as it sinks, accompanied by ballast minerals (30), to the sea floor.

The picture that emerges is one in which the decay and preservation of marine organic matter are strongly influenced by physical constraints. In our model, physical protection (2, 15, 19) manifests itself as spatially varying reactivity that decays rapidly with distance from the nearest microbe, with a characteristic length scale (β^{-1}) that depends on the active lifetime of enzymes.

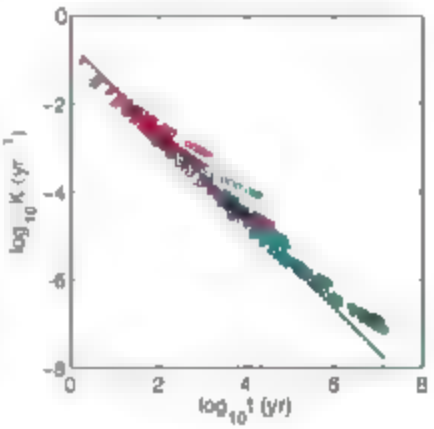

Fig. 4. The effective time-dependent reactivity $k(t) = -d\ln g/dt$. Symbols, k computed from Eq. 5, with estimates of k_{min} obtained from the fits of Fig. 2. Symbols and colors in both figures correspond to the same cores. Straight line, the theoretical approximation $k \cong 0.23 \times t^{-2/3}$ of Eq. 5, obtained without any free parameters. The rightward trends away from the line represent the slowing of rates as t approaches k_{min}^{-1}.

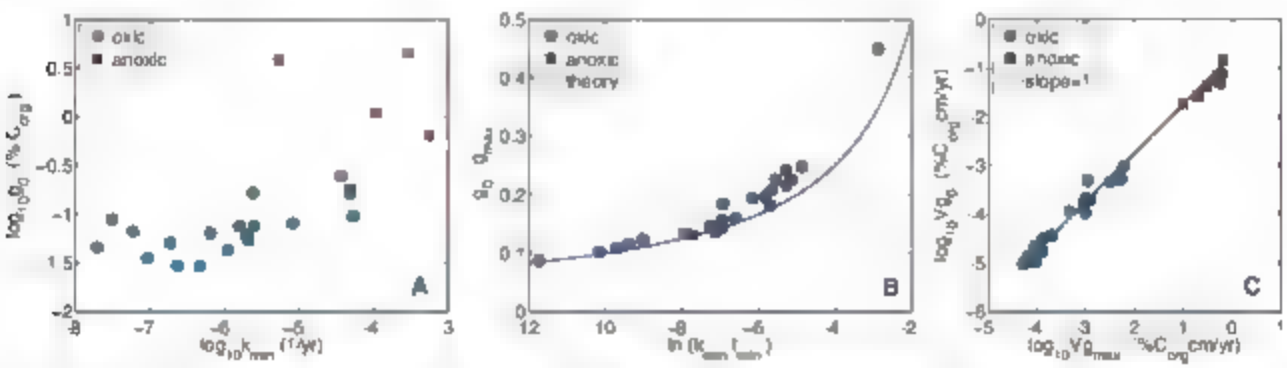

Fig. 3. (**A**) The 23 k_{min}, g_0 pairs used to rescale the data of Fig. 2B. The cores underlying anoxic waters (red squares) are associated with higher k_{min} and g_0. (**B**) The same k_{min}, g_0 pairs plotted with dimensionless rescaled axes g_0/g_{max} and $\ln k_{min}/k_{min}$. The vertical axis is proportional to burial efficiency. The smooth curve is the theoretical prediction of Eq. 4, which contains no free parameters. (**C**) Log-log plot of the sediment fluxes Vg_0 versus Vg_{max}, where Vg_0 is proportional to the burial flux of organic carbon and Vg_{max} is an estimate of the flux to the sea floor. The straight line corresponds to $g_0 = g_0/g_{max} g_{max}$, where $\langle g_0/g_{max} \rangle = 0.18$ is the mean burial efficiency multiplied by $E_3(1) \cong 0.22$. The correlation between log Vg_0 and log Vg_{max} is only marginally improved (from $r = 0.97$ to $r = 0.99$) by the common factor of the sedimentation rate V. See fig. S1 for a plot of g_0 versus g_{max}.

and their effective diffusivity. Because this mechanism appears to be general, it seems likely that it should apply to other contexts, such as soils (37), where finely divided media restrict microbial motility.

References and Notes

1. C. B. Field, M. J. Behrenfeld, J. T. Randerson, P. Falkowski, *Science* **281**, 237 (1998).
2. J. I. Hedges, R. G. Keil, *Mar. Chem.* **49**, 81 (1995).
3. H. D. Holland, *The Chemistry of the Atmosphere and Oceans* (Wiley, New York, 1978).
4. R. A. Berner, *The Phanerozoic Carbon Cycle: CO_2 and O_2* (Oxford Univ. Press, New York, 2004).
5. D. P. Schrag, *Science* **315**, 812 (2007).
6. P. H. Abelson, *Annu. Rev. Earth Planet. Sci.* **6**, 325 (1978).
7. A. H. Knoll, *Life on a Young Planet* (Princeton Univ. Press, Princeton, NJ, 2003).
8. B. B. Jørgensen, *Geomicrobiol. J.* **1**, 29 (1978).
9. R. A. Berner, *Early Diagenesis: A Theoretical Approach* (Princeton Univ. Press, Princeton, NJ, 1980).
10. J. J. Middelburg, *Geochim. Cosmochim. Acta* **53**, 1577 (1989).
11. J. J. Middelburg, T. Vlug, F. J. W. A. van der Nat, *Global Planet. Change* **8**, 47 (1993).
12. E. W. Engelen, J. W. de Leeuw, S. Derenne, C. Largeau, *Geochim. Cosmochim. Acta* **53**, 3103 (1989).
13. J. M. de Leeuw, C. Largeau, *Organic Geochemistry*, M. H. Engel, S. A. Macko, Eds. (Plenum Press, New York, 1993), pp. 23–72.
14. E. T. Peltzer, C. M. Berkowitz, J. S. Gaffney, J. J. Walsh, *Org. Geochem.* **4**, 63 (1982).
15. L. M. Mayer, *Geochim. Cosmochim. Acta* **58**, 1271 (1994).
16. L. M. Mayer, *Chem. Geol.* **114**, 347 (1994).
17. R. G. Keil, E. Tsamakis, C. Fuh, J. Giddings, J. I. Hedges, *Geochim. Cosmochim. Acta* **58**, 879 (1994).
18. J. I. Hedges *et al.*, *Nature* **409**, 801 (2001).
19. R. G. Keil, D. B. Montluçon, F. G. Prahl, J. I. Hedges, *Nature* **370**, 549 (1994).
20. B. P. Boudreau, B. R. Ruddick, *Am. J. Sci.* **291**, 507 (1991).
21. V. Vetter, J. Deming, P. Jumars, B. Krieger-Brockett, *Microb. Ecol.* **36**, 75 (1998).
22. B. Ransom, D. Bennett, R. Baerwald, K. Shea, *Mar. Geol.* **138**, 1 (1997).
23. D. J. Burdige, W. M. Berelson, K. H. Coale, J. McManus, K. S. Johnson, *Geochim. Cosmochim. Acta* **63**, 1507 (1999).
24. D. C. Smith, M. Simon, A. L. Alldredge, F. Azam, *Nature* **359**, 139 (1992).
25. C. M. Bender, S. A. Orszag, *Advanced Mathematical Methods for Scientists and Engineers* (McGraw-Hill Book Company, New York, 1978).
26. J. M. Betts, H. D. Holland, *Paleogeogr. Paleoclimatol. Paleoecol.* **97**, 5 (1991).
27. J. L. Schmidt, J. W. Deming, P. A. Jumars, R. G. Keil, *Cont. Shelf Res.* **43**, 976 (1998).
28. S. Kirkpatrick, *Rev. Mod. Phys.* **45**, 574 (1973).
29. A. D. Steen, C. Arnosti, C. Nesi, N. V. Blough, *Mar. Chem.* **101**, 266 (2006).
30. R. A. Armstrong, C. Lee, J. I. Hedges, S. Honjo, S. G. Wakeham, *Deep-Sea Res. II* **49**, 219 (2002).
31. J. I. Hedges, J. M. Oades, *Org. Geochem.* **27**, 319 (1997).
32. C. Reimers, E. Suess, *Mar. Chem.* **13**, 141 (1983).

33. We thank D. Fike, H. Hartman, J. M. Hayes, A. E. Lobkovsky, L. M. Mayer, F. M. M. Morel, R. E. Summons, and J. S. Weitz for helpful discussions. This work was supported by NSF Biocomplexity Grant EAR-0420592.

Supporting Online Material

www.sciencemag.org/cgi/content/full/316/5829/1325/DC1

Fig. S1
Table S1
References

30 November 2006; accepted 19 April 2007
10.1126/science.1138211

Origin of Human Bipedalism As an Adaptation for Locomotion on Flexible Branches

S. K. S. Thorpe,[1]* R. L. Holder,[2] R. H. Crompton[3]*†

Human bipedalism is commonly thought to have evolved from a quadrupedal terrestrial precursor, yet some recent paleontological evidence suggests that adaptations for bipedalism arose in an arboreal context. However, the adaptive benefit of arboreal bipedalism has been unknown. Here we show that it allows the most arboreal great ape, the orangutan, to access supports too flexible to be negotiated otherwise. Orangutans react to branch flexibility like humans running on springy tracks, by increasing knee and hip extension, whereas all other primates do the reverse. Human bipedalism is thus less an innovation than an exploitation of a locomotor behavior retained from the common great ape ancestor.

A fundamental question in human evolution is how modern humans and their ancestors (hominins) became terrestrial bipeds. The acquisition of habitual terrestrial bipedalism is generally taken to mark the separation of the hominins from the panins (chimpanzees, bonobos, and their ancestors, which form the rest of the hominine subfamily). It is widely held (*1*) that because the panins and the more distantly related gorillines (gorillas) move on the ground by quadrupedal horizontal-trunked knuckle-walking, pre-bipedal hominins must also have passed through a terrestrial knuckle-walking phase. Numerous hypotheses have competed to explain how this happened (see, for example, review in (*2*)). However, it has become apparent that before 2 to 3 million years ago (Ma), early hominins occupied woodland environments, not open or even bush-savannah environments [such as sites including Allia Bay (*3*), Aramis (*4*), Asaa Issie (*5*), and now Lacetoli (*6*)] and that although hominin hindlimbs rapidly became adapted for terrestrial bipedalism, they retained long grasping forelimbs, which are more obviously relevant in an arboreal context (*3*). Both facts are more consistent with an arboreal origin for bipedalism. Indeed, bipedal adaptations may antedate generally accepted dates for the genetic separation of the hominins and panins (*7*). Here we argue that hand-assisted bipedalism allows the most arboreal great ape, the orangutan, to move on flexible supports that are otherwise too small to access. This selective advantage would equally have benefited the common crown-hominoid ancestor (the ancestor of living apes), so that hand-assisted arboreal bipedality is both kinematically and ecologically a more parsimonious precursor to hominin bipedality than is terrestrial quadrupedalism.

In the trees, pronograde (horizontal) postures are much less dominant in panin and gorilline locomotion than they are on the ground, but ortho-grade (upright) postures are common to many types of arboreal gait (*8*). For example, it has been argued that patterns of motion and muscle activity in vertical climbing (such as climbing up and down tree trunks) may have been exaptive (prepared the body) for the adoption of terrestrial bipedalism (*9*). Although the trunk is orthogrhighly in vertical climbing, maximum joint extension in the hindlimbs falls well short of the full extension seen in human bipedalism, as indeed is the case in knuckle-walking. Overall, both behaviors seem to be highly unlikely precursors for habitual human bipedalism (*10*). Building on an early observation (*11*) that orangutan morphology is in many aspects strikingly like that of hominins, we proposed that "orthograde clambering," which is most frequent in orangutans but seen in all apes, was a kinematically more parsimonious precursor for bipedalism (*10*). Although the trunk is orthograde in this behavior, body weight is predominantly borne by the forelimbs suspending from supports above the head. All apes also exhibit brief bouts of arboreal bipedalism (*12*), but in panins and gorillines the hindlimbs are flexed rather than straight as they are in the bipedalism of humans and orangutans (compare, for example, the orangutan and chimpanzee in Fig. 1, A and D).

Despite the universal presence of arboreal bipedality in the apes, it is difficult to envisage selective pressures for bipedal locomotion in an arboreal context. In chimpanzees, postural bipedalism is associated with arboreal feeding on relatively stable branches >10 cm in diameter, in a

[1]School of Biosciences, University of Birmingham, Edgbaston, Birmingham B15 2TT, UK. [2]Department of Primary Care and General Practice, University of Birmingham, Edgbaston, Birmingham B15 2TT, UK. [3]School of Biomedical Sciences, University of Liverpool, Sherrington Buildings, Ashton Street, Liverpool L69 3GE, UK.

*These authors contributed equally to this work.
†To whom correspondence should be addressed. E-mail: rhcrump@liv.ac.uk

similar manner to their foraging from the ground for fruit on low branches (*13*). Given the static nature of bipedal posture, energetic costs, safety risk, and hence selective pressures are likely to be weaker on it than on bipedal locomotion. Large stable branches are also relatively unchallenging. However, predictions suggest that locomotion on slender unstable branches should be dominated either by orthograde suspension (which increases stability by placing the center of mass (COM) of the body directly under the support (*14*) (Fig. 1C)] or by "compliant" quadrupedalism [which involves substantial increases in elbow and knee flexion, smaller vertical excursions of the COM, and longer contact times as compared to those in other mammals traveling at dynamically similar speeds, to maximize stability and efficiency (*15*), and is similar to the posture in Fig. 1B but with greater fore- and hindlimb flexion].

An alternative hypothesis is that bipedal locomotion might confer substantial selective advantages on arboreal apes (including crown hominoids and pantolomines), because their long prehensile toes can grip multiple small branches and thus maximize stability, while freeing one or both limbs for balance and weight transfer. We tested this hypothesis by determining the impact of support flexibility on orthograde suspension, quadrupedalism, and bipedalism in the Sumatran orangutan (*Pongo abelii*), the only species of great ape to retain a predominantly arboreal lifestyle (Fig. 1). Although orangutans may have refined their arboreal adaptations since their evolutionary separation from other great apes, recent studies have shown that the mechanics of orangutan bipedalism are more similar to those of modern humans than are those of pygmy and gorillas (*16*). Orangutan locomotion is thus an important model for reconstructing the early evolution of bipedalism (*17*).

During a year-long field study of wild Sumatran orangutans in the Gunung Leuser National Park (3°4′ N, 97°39′ E), we obtained 2811 observations of orangutan locomotor bouts, including information on support diameter (a correlate of flexibility) and whether single or multiple supports were used. We performed a backward-elimination log-linear analysis of these variables (table S1). Log-linear analysis is designed for analysis of the categorical variables often acquired in observational fieldwork, and it works by comparing observed frequencies to theoretically expected values predicted by the models. The backward-elimination process begins with the most complicated model (in this case, a three-way association between locomotion, number of supports, and support diameter) and iteratively seeks the most important associations, deleting those that have least effect on the model [see (*18*) for full methods]. The final model derived with this method (Tables 1 to 3) shows that the modality of orangutan locomotion was associated with both the diameter of supports used and with their number. Bipedalism was strongly associated with locomotion on multiple supports (Table 2) and with locomotion on the smallest support diameters (Table 3, <4 cm, and combinations including <4 cm). In contrast, quadrupedalism was more associated with locomotion on single (Table 2) large (Table 3) supports, whereas orthograde suspension tended to be positively associated with the middle-diameter supports (4 to 10 cm).

Our results are consistent with the prediction that bipedalism allows orangutans to move on multiple supports that are more slender, and hence more detectable, than does quadrupedalism or even orthograde suspension (Table 3). This confirms our hypothesis that bipedal locomotion can confer selective advantages on arboreal apes and contradicts predictions that unstable supports are always best navigated using suspensory locomotor modes (*14*) or compliant quadrupedalism (*15*).

In 75% of the observed bipedal bouts in our study, orangutans used their hands for stabilization, and in ~90% of bipedalism on single and multiple supports, they used extended hindlimbs. The latter contrasts further with the flexed-limb gait of monkeys and other apes, including pygmy and gorillas, which adopt the same hindlimb posture in bipedalism as in quadrupedalism and which have limited balancing extensor force capacity at the hip and knee (*17*). However, straight-limbed bipedality is characteristic of normal modern human walking, where it reduces the joint moments required to exert locomotor forces and enables energy savings by pendulum-like transformations between potential and kinetic energies (*18*). Straight-limbed bipedality in orangutans must similarly reduce required joint moments, but the extent to which it may otherwise enable energy savings is yet to be demonstrated.

Locomotion on flexible branches is safer if supported from above as well as from below. The advantage of hand-assisted bipedality is that the hand assistance ensures maximum safety while the bipedalism enables an unloaded hand to reach out for feeding, weight transfer, or balance in the

Fig. 1. Key positional behaviors in orangutans and a comparison with the chimpanzee. (**A**) Assisted bipedalism. (**B**) quadrupedalism, and (**C**) orthograde suspension in Sumatran orangutans. (**D**) Assisted bipedalism in a chimpanzee.

Table 1. Associations between locomotion, support flexibility, and the number of supports used by orangutans. DF, degrees of freedom.

Log-linear model expressions (variable relationships)†	Partial χ^2	DF	Standardized χ^2 (χ^2/DF)‡
Locomotion × support diameter	186.02	12	15.50
Number of supports × support diameter	515.93	6	85.99
Locomotion × number of supports	36.05	2	18.03

†Likelihood ratio χ^2 = 8.91, DF = 6, P = 0.18, n = 932 observations. A significance value of P = 1 for the likelihood ratio χ^2 indicates a perfect fit of the model's predicted cell counts to the observed cell counts, but values >0.05 are significant. ‡The relative importance of associations is indicated by the rank of the standardized χ^2 values.

peripheral branches, where the majority of preferred foods are situated and where primates must cross between tree crowns. Effective gap-crossing behaviors are highly advantageous for primates, because crossing rather than circumventing gaps in the canopy can dramatically reduce the energetic costs of travel, especially where a change of height within the tree would otherwise be required. Hand-assisted locomotor bipedality adopted under these strong selective pressures, seems the most likely evolutionary precursor of straight-limbed human walking. This proposal is in accord with the conclusions of a comprehensive assimilation of studies of fossil morphology, computer modeling, human skeletal development, and experimental studies of human exercise physiology (*19*), suggesting that, despite differences from humans in body form (such as the retention of long arms), the best-known early hominin, *Australopithecus afarensis*, would have been a quite efficient upright biped, over short distances.

We therefore speculate that from the generalized orthogrady underlying straight-limbed bipedality and orthograde clambering of the hypothetical common ancestor of the great apes, the locomotor repertoire of African apes diversified as a response to forest canopy fragmentation events during the Miocene, while in Southeast Asia orangutan ancestors became more specialized for, and restricted to, shrinking closed-canopy forest that could be traversed at canopy level. In Africa, forest fragmentation alternated with reclosure and reexpansion of gallery forest, mosaic woodland, and rainforest environments (*2*). In both pongines and gorillines, the height range and frequency of vertical climbing locomotion must have increased to facilitate access to preferred foods in the main and emergent canopy and, usually also to fallback terrestrial food sources (*20*) but at different times (*2*) and in different forest types. Although the characteristic hindlimb and forelimb joint excursions in vertical climbing are markedly different from those in straight-limbed bipedalism, they are actually kinematically similar to those in knuckle-walking quadrupedalism (*10*). Both use relatively extended elbows but flexed knees, shoulders, and hips (movies S1 to S3). Adaptations to vertical climbing in the pongines and gorillines would therefore have increased the likelihood of quadrupedal knuckle-walking becoming selected as the least inefficient locomotion for crossing between trees on the ground. Selection for forelimb and hindlimb force over the wide, but relatively flexed, ranges of motion necessary for safe (*21*) and effective vertical climbing may then have compromised existing adaptations for stiff-legged arboreal bipedality (compare Fig. 1, A and D) and hence efficiency in terrestrial and arboreal bipedalism. In contrast, hominins, retaining existing adaptations for straight-legged bipedalism, sacrificed canopy access by maximizing hip and knee force over small but relatively extensive ranges of motion (*17*, *22*) to exploit the potential of the continuous stable terrestrial milieu for rapid bipedalism.

This hypothesis provides an adaptive context for morphological adaptations to orthogrady, such as lateral stiffness of the lumbar spine, found in crown hominoids between 9 and [illegible] Ma (*Devapithecus laetamus* and *Dryopithecus* (*23*)] and from 16.7 Ma (*23*) to as much as 21 Ma (*24*) in fossils assigned to *Afropithecus* (*24*) [or *Ugandapithecus major* (*25*)]. It further explains the universal presence in living apes of features adaptive for vertical trunk (orthograde) posture and highly abducted postures of the forelimb (*26*). Our hypothesis is consonant with paleoenvironmental evidence that both proto-hominins close to the chimpanzee/human divergence (such as *Orrorin* and *Ardipithecus*) and unquestionable hominins [*Australopithecus anamensis* as early as ~4 Ma and *Australopithecus afarensis*] lived in relatively wooded habitats (*3*, *6*, *27*). It helps resolve the apparent paradox that *Australopithecus anamensis* and *Australopithecus afarensis* combine (*3*) hindlimb features adaptive for terrestrial bipedalism (such as an ankle joint that allows parasagittal motion of the leg over the stance foot) with the retention of long, highly abductable forelimbs adaptive for reaching for arboreal supports (rather perhaps than for suspension per se (*12*, *26*)). It further explains the apparent adaptations for bipedality evidenced in protohominins dating to 6 to 7 Ma, which is close to or even antedating accepted dates for hominin-panin divergence (*7*). These include claims for a cranium placed directly above the vertebral column in *Sahelanthropus tchadensis* (*28*), but see (*29*), habitual and marked hip extension in *Orrorin tugenensis* (*27*); and morphological features of the proximal pedal phalanx of the >5-Ma Aramis protohominin assigned to *Ardipithecus ramidus kadabba* (*4*), which imply the early evolution of a propulsive role for the toes in bipedality.

Contrary to the hypothesis that quadrupedal knuckle-walking as in pongines or gorillines was the ancestral African ape locomotor behavior from which hominin bipedalism evolved (*1*), we suggest that in locomotor diversification within the

Table 2. Contingency table for model interaction: locomotion × no. of supports. Entries show row % and (column %). For example, 69.2% of all quadrupedalism was on one support, and 41.5% of all locomotion on one support was quadrupedalism. Standardized cell residuals (SCRs) are in italics. These indicate by their sign whether an interaction is more (positive values) or less (negative values) common than predicted by the model and, by their size, to what degree. SCRs greater than ±2.0 indicate a lack of fit.

	No. of supports		Total
	1	>1	
Quadrupedalism	69.2 (41.5)	30.8 (28.9)	(36.6)
	1.9‡	*−2.4*	
Bipedalism	29.1 (6.0)	70.9 (22.9)	(12.6)
	−4.4	*5.5*	
Orthograde suspension	63.1 (52.5)	36.9 (48.2)	(50.9)
	0.6	*−0.7*	
Total	61.1	38.9	

Table 3. Contingency table for model interaction: locomotion × diameter. For an explanation of Table 3, see legend of Table 2. Diameter classifications include single and multiple support use; therefore, the diameter classification "<4 cm" combines bouts where only one support of <4 cm was used and bouts in which more than 1 support of <4 cm was used.

Support diameter (cm)	Quadrupedalism	Bipedalism	Orthograde suspension	Total
<4	16.3 (7.0)	22.4 (28.2)	61.2 (19.0)	(15.8)
	−4.1	*3.4*	*1.8*	
4–10	20.4 (18.2)	12.5 (32.5)	67.1 (43.0)	(32.6)
	−4.7	*0*	*4*	
10–20	51.4 (32.0)	6.1 (11.1)	42.5 (19.0)	(22.7)
	3.6	*−2.6*	*1.7*	
>20	80.2 (27.3)	4.3 (4.3)	15.5 (3.8)	(12.4)
	7.8	*−2.5*	*−5.3*	
<4, 4–10	28.7 (8.5)	19.8 (17.1)	51.5 (11.0)	(10.8)
	1.3	*2.1*	*0.1*	
4–10, 10–20	52.5 (6.2)	5.0 (1.7)	42.5 (3.6)	(4.3)
	1.7	*−1.3*	*−0.7*	
<4, 10–20	25.0 (0.9)	50.0 (5.1)	25.0 (0.6)	(1.3)
	−0.7	*3.7*	*−1.3*	
Total	36.6	12.6	50.9	

African ape clade: it is the gorillas and gorillines that unsuspected, and the hominins that were conservative.

References and Notes

1. B. G. Richmond, D. S. Strait, *Nature* **404**, 382 (2000).
2. J. Kingdon, *Lowly Origins* (Princeton Univ. Press, Princeton, NJ, 2003).
3. C. V. Ward, M. G. Leakey, A. Walker, *Evol. Anthropol.* **7**, 197 (1999).
4. Y. Haile-Selassie, *Nature* **412**, 178 (2001).
5. T. D. White *et al.*, *Nature* **440**, 883 (2006).
6. K. Kovarovic, P. Andrews, *J. Hum. Evol.*, in press (available at http://dx.doi.org/doi:10.1016/j.jhevol.2007.01.001; doi: 10.1016/j.jhevol.2007.01.001).
7. N. Patterson, D. J. Richter, S. Gnerre, E. S. Lander, D. Reich, *Nature* **441**, 1103 (2006).
8. K. D. Hunt *et al.*, *Primates* **37**, 363 (1996).
9. J. G. Fleagle *et al.*, *Symp. Zool. Soc. London* **48**, 359 (1981).
10. R. H. Crompton *et al.*, *Cour. Forschinst. Senckenb.* **243**, 155 (2003).
11. J. T. Stern, *Yrbk. Phys. Anthropol.* **19**, 59 (1975).
12. S. K. S. Thorpe, R. H. Crompton, *Am. J. Phys. Anthropol.* **131**, 384 (2006).
13. K. D. Hunt, *J. Hum. Evol.* **26**, 183 (1994).
14. M. Cartmill, K. Milton, *Am. J. Phys. Anthropol.* **47**, 249 (1977).
15. E. Larney, S. Larsen, *Am. J. Phys. Anthropol.* **125**, 42 (2004).
16. S. K. S. Thorpe, R. H. Crompton, *Am. J. Phys. Anthropol.* **127**, 58 (2005).
17. S. K. S. Thorpe, R. H. Crompton, M. M. Gunther, R. F. Ker, R. McN. Alexander, *Am. J. Phys. Anthropol.* **110**, 179 (1999).
18. R. McN. Alexander, *Principles of Animal Locomotion* (Princeton Univ. Press, Princeton, NJ, 2003).
19. C. V. Ward, *Yrbk. Phys. Anthropol.* **45**, 185 (2002).
20. R. W. Wrangham, N. L. Conklin-Brittain, K. D. Hunt, *Int. J. Primatol.* **19**, 949 (1998).
21. H. Pontzer, R. W. Wrangham, *J. Hum. Evol.* **46**, 317 (2004).
22. R. C. Payne *et al.*, *J. Anat.* **208**, 709 (2006).
23. M. Pickford, B. Senut, D. Gommery, in *Late Cenozoic* [illegible] *Bishop*, P. Andrews, P. Banham, Eds. (Geological Society, London, 1999), pp. 27–38.
24. M. M. Young, L. MacLatchy, *J. Hum. Evol.* **46**, 163 (2004).
25. D. Gommery, B. Senut, M. Pickford, I. Kiura, *Ann. Paleontol.* **86**, 187 (2007).
26. C. V. Ward, in *Handbook of Paleoanthropology Vol. 2: Primate Evolution and Human Origins*, W. Henke, I. Tattersall, Eds. (Springer Heidelberg, Germany, 2007), pp. 1011–1030.
27. B. Senut, in *Human Origins and Environmental Backgrounds*, H. Ishida, R. H. Tuttle, M. Pickford, N. Ogihara, M. Nakatsukasa, Eds. (Springer, Heidelberg, Germany, 2006), pp. 199–208.
28. C. P. E. Zollikofer *et al.*, *Nature* **434**, 755 (2005).
29. M. Pickford, *Anthropologie* **69**, 193 (2005).

30. We thank the Indonesian Institute of Science, Indonesian Nature Conservation Service, and Leuser Development Programme for granting permission and giving support for research in the Leuser Ecosystem. R. McN. Alexander, T. M. Blackburn, S. Bunting, T. Rees, N. Jeffery, E. E. Vereecke, A. Walker, A. Wilson, and B. Wood commented on the manuscript. R. Savage developed the animation (fig. S1). Studies of captive animals were hosted by the North of England Zoological Society. This research was supported by grants from the Leverhulme Trust, the Royal Society, the L.S.B. Leakey Foundation, and the Natural Environment Research Council.

Supporting Online Material

www.sciencemag.org/cgi/content/full/316/5829/1328/DC1
Table S1
Movies S1 to S3

5 February 2007; accepted 18 April 2007
10.1126/science.1140799

Genome-Wide Association Analysis Identifies Loci for Type 2 Diabetes and Triglyceride Levels

Diabetes Genetics Initiative of Broad Institute of Harvard and MIT, Lund University, and Novartis Institutes for BioMedical Research*†

New strategies for prevention and treatment of type 2 diabetes (T2D) require improved insight into disease etiology. We analyzed 386,731 common single-nucleotide polymorphisms (SNPs) in 1464 patients with T2D and 1467 matched controls, each characterized for measures of glucose metabolism, lipids, obesity, and blood pressure. With collaborators (FUSION and WTCCC/UKT2D), we identified and confirmed three loci associated with T2D: one in a noncoding region near *CDKN2A* and *CDKN2B*, one in an intron of *IGF2BP2*, and one in an intron of *CDKAL1*, and replicated associations near *HHEX* and in *SLC30A8* found by a recent whole-genome association study. We identified and confirmed association of a SNP in an intron of glucokinase regulatory protein (GCKR) with serum triglycerides. The discovery of associated variants in unsuspected genes and outside coding regions illustrates the ability of genome-wide association studies to provide potentially important clues to the pathogenesis of common diseases.

Type 2 diabetes, obesity, and cardiovascular risk factors are caused by a combination of genetic susceptibility, environment, behavior, and chance. Whole-genome association studies (WGAS) offer a new approach to genic discovery, unbiased with regard to presumed functions or locations of causal variants. This approach is based on Fisher's theory for additive effects at common alleles (*1*): human heterozygosity being substantially attributable to common ancestral variants (*2*); and the hypothesis that variants influencing common, late-onset diseases of modernity may not have been subject to purifying selection, and has been made possible by genomic advances such as the human genome sequence, SNP and HapMap databases, and genotyping arrays (*3*).

We studied 1464 patients with T2D and 1467 controls from Finland and Sweden, each characterized for 18 clinical traits: anthropometric measures, glucose tolerance and insulin secretion, lipids and apolipoproteins, and blood pressure. The samples were both population-based (1022 T2D cases and 1075 euglycemic controls, matched on gender, age, body mass index, and region of origin) and family-based (326 sibships discordant for T2D: 442 cases and 392 euglycemic controls; tables S1 and S2).

Genotyping of 500,568 SNPs was attempted in each sample. Overall call rate for passing SNPs was 99.2%. After filtering rare and monomorphic variants (n = 69,696 SNPs) and applying stringent quality-control filters, high-quality genotypes for 386,731 common SNPs were obtained (*4*). To extend the set of putative causal alleles tested for association, we developed 284,968 additional multimarker (haplotype) tests based on these SNP genotypes (*5*, *6*). The 671,699 allelic tests capture (correlation coefficient $r^2 \geq 0.8$) 78% of common SNPs in HapMap CEU (*3*).

Each SNP and haplotype test was assessed for association to T2D and each of 18 traits with the software package PLINK (http://pngu.mgh.harvard.edu/purcell/plink/). For T2D, a weighted meta-analysis was used to combine results for the population-based and family-based subsamples (*4*). For quantitative traits, multivariable linear or logistic regression with or without covariates was performed (*4*). Association results for each SNP, haplotype test, and phenotype are available (www.broad.mit.edu/diabetes/).

In genome-wide analysis involving hundreds of thousands of statistical tests, modest levels of bias imposed on the null distribution can overwhelm a small number of true results. We used three strategies to search for evidence of systematic bias from unrecognized population structure, the analytical approach, and genotyping artifacts (*7*, *8*). First, we examined the distribution of *P*-values in the population-based sample, observing a close match to that expected for a null distribution (genomic inflation factor λ_{GC} = 1.05 for T2D). Second, we calculated association statistics using EIGENSTRAT, an independent method based on principal components analysis (*9*); *P*-values for T2D derived with the two methods were nearly identical (r^2 = 0.95; Fig. 1A). Third, 114 SNPs from the extreme tail of *P*-values for T2D were genotyped with an independent technology. Genotype concordance was 99.5%, indicating that even the extreme tail of low *P*-values is not substantially contaminated by genotyping artifacts.

*To whom correspondence should be addressed. David Altshuler (Broad Group Thomas E. Hughes E-mail: altshuler@molbio.mgh.harvard.edu (D.A.); tef group@med.lu.se (L.G.); thomas.e.hughes@novartis.com (T.E.H.).
†All authors with their contributions and affiliations appear at the end of this paper.

Although the observed *P*-value distribution closely matches expectation over most of its range ($1.0 > P > 0.0$), an excess of low *P*-values is observed (Fig. 1B and table S3). To evaluate the significance of this excess, we generated 1000 permuted whole-genome analyses in which phenotype data were randomized within matched case-control groups (*4*). For *P*-values between 0.01 and 0.001, 6370 SNPs were observed, as compared to an average of 5917 [95% confidence interval (CI): 5714 to 6128] in permuted scans ($Z = 4.3$, $P < 0.001$). For $P < 10^{-4}$, 125 SNPs were observed, compared to 94 [95% CI: 61 to 121] in permuted scans ($Z = 2.4$, $P < 0.02$). These observations support a model in which there are few common variants with large effects, but a substantial number with modest effects of the sort that generate *P*-values between 0.01 and 10^{-7} in 3000 samples.

Given this distribution, and because WGAS are hypothesis generating, we sought replication in independent samples. An initial set of 107 SNPs (table S4) was selected on the basis of our study ($n = 89$) and by comparison of our results with WGAS of T2D ($n = 18$) by Wellcome Trust Case Control Consortium (WTCCC) (*10*) and Finland United States Investigation of NIDDM Genetics (FUSION) (*11*). Each SNP was genotyped in 10,850 additional subjects (T2D and controls, from Sweden, Poland, and the United States (table S1) and analyzed for association to T2D under the same genetic model as the scan (*4*).

These results, with those from FUSION (*11*) and WTCCC UKT2D (*10*, *12*), identify SNPs at three previously unknown loci as influencing risk of T2D with $P < 10^{-10}$ (Table 1 and tables S4 and S5).

A SNP on chromosome 9p (rs10811661), 125 kb from the nearest annotated genes (*CDKN2A*/*CDKN2B*), was selected on the basis of strong association to T2D in our WGAS (rank #51) (Table 1, Fig. 2A). Combined analysis of data from our scan and replication samples provides strong evidence for association (odds ratio (OR) = 1.20, 95% CI 1.07 to 1.36, $P = 5.4 \times 10^{-5}$). Independent evidence of association for the same SNP phenotype, and genetic model was obtained by WTCCC UKT2D ($P = 10^{-7}$) and FUSION ($P = 0.001$) (*10*, *12*). No association with measured quantitative metabolic traits was observed in our scan or replication samples.

An intriguing aspect of this association is its location far from any annotated gene. The region of association is limited to a 9-kb region flanked by strong recombination hot-spots, in which there are multiple conserved noncoding sequences but no known genes or microRNAs. A member of the cyclin-dependent kinase (CDK)–inhibitor 2A (*CDKN2A*) locus plays a role in pancreatic islet regenerative capacity (*13*).

SNPs in the second intron of *IGF2BP2* were selected for replication on the basis of joint analysis of the three scans (*10*, *12*) (Fig. 2B). Evidence was weak in our initial scan ($P = 0.034$ for rs4402960), but pronounced in the replication samples ($P = 5.5 \times 10^{-6}$, Table 1). Strong evidence was obtained for the same SNP, phenotype, and genetic model by WTCCC UKT2D ($P = 10^{-5}$) and FUSION ($P = 10^{-4}$) (*10*, *12*). These SNPs showed no association to measured quantitative metabolic traits in our scan or replication samples.

Insulin-like growth factor 2 binding protein 2 (IGF2BP2) belongs to a family of three mRNA binding proteins with affinity for leader elements in the untranslated regions of *IGF-2* transcripts. Family members bind with weak sequence specificity and are implicated in transport of RNA targets to enable protein synthesis at specific locations in the cell (*14*). The IGFBP homolog is necessary for pancreas development in *Xenopus* (*15*), and *IGF2BP3* transgenic mice exhibit islet ductal pancreatic metaplasia (*16*).

We selected a SNP in a 90-kb intron within *CDKAL1* (rs7754840) for replication on the basis of nominal association in our scan, WTCCC (*10*), and FUSION (*11*) (Table 1). Analysis of the scan and replication samples (Fig. 2C) supports association under the same phenotype and genetic model (OR = 1.08, 95% CI 1.03 to 1.14, combined $P = 0.0024$; Table 2), as does evidence from WTCCC UKT2D (*10*, *12*) ($P = 10^{-5}$) and FUSION (*11*) ($P = 0.01$) (Table 1). The risk allele was nominally associated with reduced insulin secretion in controls from our scan ($P = 0.01$ for insulinogenic index).

CDKAL1 is homologous to CDKSRAP1, an inhibitor of cyclin-dependent kinase CDK5. CDK5 transduces glucotoxicity signals in pancreatic beta cells (*17*). As with the other variants, how SNPs in CDKAL1 might influence risk of T2D awaits further investigation.

Common variation in an intron of *TCF7L2* has been reproducibly associated with T2D (*18*). In our WGAS, *TCF7L2* was the third-ranked association (Fig. 2D, $P < 3 \times 10^{-6}$) and was among the top results in each of the three other wels-powered whole-genome scans of T2D (*10*, *11*, *19*) (Table 1). The consistency of these findings suggests that TCF7L2 is the single largest effect of a common SNP on T2D risk in European populations. Associations in *KCNJ11* (*20*) and *PPARG* (*21*) were not strongly observed in any single scan, but across the three scans provided $P < 10^{-10}$ and $P < 10^{-6}$, respectively (Table 1).

In 2007, Sladek *et al.* (*19*) reported four previously unknown associations to T2D in a WGAS, two with particularly strong evidence of replication (*HHEX* and *SLC30A8*). We confirm association at *HHEX* (Table 1, Fig. 2E) in our scan (OR = 1.15, $P = 0.01$) and in replication genotyping ($P = 10^{-3}$), as do WTCCC UKT2D ($P = 10^{-6}$) (*10*, *12*) and FUSION ($P = 0.03$) (*11*). At the zinc transporter *SLC30A8*, our data were less compelling ($P = 0.90$ in our scan and $P = 0.01$ in replication samples), but convincing evidence was obtained by WTCCC UKT2D (*10*, *12*) ($P = 10^{-3}$) and FUSION ($P = 10^{-5}$) (*11*). We observed no evidence for association to *LOC387761* ($n = 7401$, OR = 1.00, $P = 0.93$ for rs7480010) and *EXT2-ALX4* ($n = 7401$, OR = 1.06, $P = 0.12$ for rs3740878), nor was evidence obtained by WTCCC (*10*) or FUSION (*11*).

We observed intriguing replication signals at additional loci (*10*, *11*). For example, rs17044137 in *FLJ39370* was associated with T2D in our scan (OR = 1.27, $P = 3.7 \times 10^{-4}$) and replication (OR = 1.09, $P = 3.1 \times 10^{-3}$), but not in WTCCC (*10*) or FUSION (*11*) (Table 1). Similarly, rs6698181 in *PAX4* demonstrated evidence in our scan and replication samples ($P = 5.3 \times 10^{-5}$), and in FUSION (*11*) ($P = 10^{-3}$), but not WTCCC (*10*) ($P = 0.93$). Genotyping in more samples is needed to resolve these and other hypotheses.

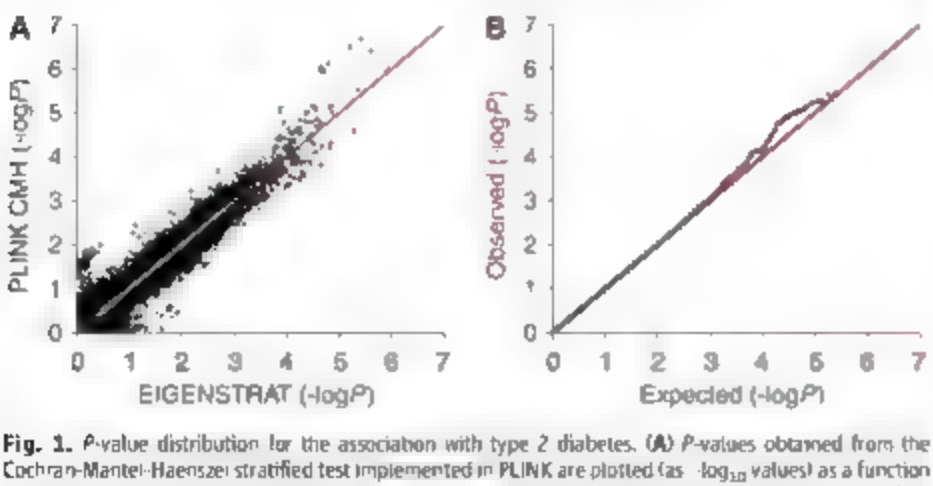

Fig. 1. *P*-value distribution for the association with type 2 diabetes. (**A**) *P*-values obtained from the Cochran-Mantel-Haenszel stratified test implemented in PLINK are plotted (as $-\log_{10}$ values) as a function of the corresponding *P*-value computed by EIGENSTRAT in the population-based case/control sample ($n = 2097$). These distributions are strongly correlated ($r^2 = 0.95$). (**B**) P-P plot for the combined (*Z* score) association analysis of type 2 diabetes in the population-based case/control sample and the discordant sibships ($n = 2,931$). The *P*-values for the corresponding *Z* scores are plotted (as $-\log_{10}$ values) as a function of *P*-values from the expected (uniform) null distribution. The observed distribution matches the expected distribution closely and shows an excess in the tail at $P < 10^{-3}$.

Table 1. Association results for type 2 diabetes. Odds ratios (OR), 95% confidence intervals (CI), and *P*-values are given for SNPs from Diabetes Genetics Initiative (DGI) scan, replication samples, and data from the WTCCC/UKT2D (*10, 12*) and FUSION (*11*) studies. Proxies include: for rs7754840, rs10946398 (r^2 = 1, WTCCC/UKT2D); for rs7903146, rs7901695 (r^2 = 0.92, WTCCC/UKT2D); and for rs5219, rs5215 (r^2 = 0.99, WTCCC/UKT2D).

SNP	Chr.	Risk allele*	Nearest gene	DGI							WTCCC/UKT2D[#]		FUSION[#]		All studies		Sample size for 80% power[¶]
				Genome scan			Replication[‡]		Combined								
				Freq.[†]	OR	*P*-value	OR	*P*-value[§]	OR (95%CI)	*P*-value	OR	*P*-value	OR	*P*-value	OR (95%CI)	*P*-value	
					n = 2931		*n* = 10,850		*n* = 13 781		*n* = 13 965		*n* = 4808		*n* = 32 554		
Novel loci																	
rs10811661	9	T	*CDKN2B*	0.83	1.37 (1.18–1.59)	3.6×10^{-5}	1.16 (1.09–1.27)	2.2×10^{-5}	1.20 (1.12–1.28)	5.4×10^{-8}	1.19 (1.11–1.28)	4.9×10^{-7}	1.20 (1.07–1.36)	2.2×10^{-3}	1.20 (1.14–1.25)	7.8×10^{-15}	~3400
rs4402960	3	T	*IGF2BP2*	0.29	1.14 (1.01–1.28)	0.034	1.18 (1.12–1.25)	5.5×10^{-9}	1.17 (1.11–1.23)	1.7×10^{-8}	1.11 (1.05–1.16)	1.6×10^{-4}	1.18 (1.08–1.28)	2.4×10^{-4}	1.14 (1.11–1.18)	8.9×10^{-16}	4300
rs1470579	3	C	*IGF2BP2*	0.30	1.12 (1.00–1.26)	0.052	1.19 (1.12–1.26)	2.1×10^{-9}	1.17 (1.11–1.23)	1.3×10^{-8}	-	-	-	-	-	-	-
rs7754840	6	C	*CDKAL1*	0.31	1.17 (1.04–1.31)	7.5×10^{-3}	1.06 (1.00–1.12)	0.024	1.08 (1.03–1.14)	2.4×10^{-3}	1.16 (1.10–1.22)	1.3×10^{-8}	1.12 (1.03–1.22)	9.5×10^{-3}	1.12 (1.08–1.16)	4.1×10^{-11}	~4800
Previously published loci																	
rs1111875	10	C	*HHEX*	0.53	1.15 (1.04–1.29)	0.01	1.13 (1.04–1.23)	6.0×10^{-3}	1.14 (1.06–1.22)	1.7×10^{-4}	1.13 (1.07–1.19)	4.6×10^{-6}	1.10 (1.01–1.19)	0.025	1.13 (1.08–1.17)	5.7×10^{-10}	~4200
rs13266634	8	C	*SLC30A8*	0.65	1.01 (0.90–1.31)	0.92	1.12 (1.02–1.23)	0.014	1.07 (1.00–1.16)	0.047	1.12 (1.05–1.18)	7.0×10^{-5}	1.18 (1.09–1.29)	6.8×10^{-5}	1.12 (1.07–1.16)	5.3×10^{-8}	~5400
rs7903146	10	T	*TCF7L2*	0.26	1.33 (1.17–1.50)	5.4×10^{-6}	1.40 (1.32–1.49)	3.9×10^{-15}	1.38 (1.31–1.46)	2.3×10^{-21}	1.37 (1.25–1.49)	6.7×10^{-11}	1.34 (1.21–1.49)	1.4×10^{-8}	1.37 (1.31–1.43)	1.0×10^{-48}	~800
rs5219	11	T	*KCNJ11*	0.47	1.14 (1.03–1.28)	0.012	1.14 (1.08–1.21)	2.6×10^{-6}	1.15 (1.09–1.21)	1.0×10^{-7}	1.15 (1.05–1.25)	1.3×10^{-3}	1.11 (1.02–1.21)	0.014	1.14 (1.10–1.19)	6.7×10^{-11}	~3700
rs1801282	3	C	*PPARG*	0.86	1.02 (0.87–1.19)	0.83	1.11 (1.02–1.19)	6.2×10^{-3}	1.09 (1.01–1.16)	0.019	1.23 (1.09–1.41)	1.3×10^{-3}	1.20 (1.07–1.33)	1.4×10^{-3}	1.14 (1.08–1.20)	1.7×10^{-6}	7900
Interesting for follow-up																	
rs17044137	4	A	*FLJ39370*	0.23	1.27 (1.11–1.44)	3.7×10^{-4}	1.09 (1.03–1.17)	3.1×10^{-3}	1.13 (1.06–1.19)	4.1×10^{-5}	1.01 (0.92–1.11)	0.90	1.02 (0.89–1.17)	0.79	-	-	
rs6698181	1	T	*PKN2*	0.29	1.17 (1.04–1.32)	7.6×10^{-3}	1.09 (1.03–1.16)	9.7×10^{-4}	1.11 (1.05–1.16)	5.3×10^{-5}	1.00 (0.92–1.09)	0.93	1.21 (1.06–1.37)	4.1×10^{-3}	-	-	-

*Alleles are indexed to the forward strand of NCBI Build 35. †Frequency of risk allele based on controls in DGI genome scan. ‡rs1111875 and rs13266634 genotyped in 0.5- and Polish replication samples (*n* = 4470). §Replication *P*-value is one-tailed for additive model; all other *P*-values reported are additive and two-tailed. ||Results reported for same SNP or proxy with r^2 > 0.95 in HapMap-CEU for FUSION and WTCCC except for *TCF7L2*: different SNPs selected based on genotyping platform (FUSION) or lowest *P*-value (FUSION,WTCCC/UKT2D). ¶Sample size required for 80% power (nominal α = 0.05) calculated with the pooled OR estimate from DGI, FUSION, WTCCC studies (*n* > 32,000), assuming an equal number of cases and controls, allele frequency in controls (DGI genome scan), and T2D prevalence of 10% (consistent with estimates in adults from the population-based Botnia PPP study in Finland).

For validated loci, variability in significance across studies may appear surprising, and suggestive of heterogeneity. However, formal tests for heterogeneity in effect size were not significant ($P > 0.05$). Moreover, in a simulated association study of 1500 cases and 1500 controls, allele frequency of 30%, and an OR of 1.20 per copy, the median P-value was 10^{-4}, but 5% of simulations P-values were >0.025 and 5% of P-values were $<10^{-7}$. Thus, substantial variability in rank and significance is expected when power is modest, particularly if a SNP is selected based on the study with an extreme P-value.

We also performed genome-wide analyses for 18 clinical traits (table S2). The distribution of P values was similar to that observed for T2D, with close match to expectation under the null hypothesis and a modest excess of signals in the tail (table S3). We observed strong evidence ($P < 10^{-4}$ rank in the top 100) for six previously reported common variants that influence lipid levels (table S3).

A previously unknown association with triglycerides was observed for rs780094 ($P = 3.7 \times 10^{-8}$), explaining 1% of residual variance in triglyceride levels (Fig. 2F, fig. S1A). This single SNP was tested in 9217 individuals from the Malmö Diet and Cancer Study, Cardiovascular Arm (MDC-CVA); the association replicated ($P = 8.7 \times 10^{-8}$) (Table 2, fig. S1B). The association was observed by FUSION ($P = 10^{-4}$ controls, $P = 10^{-5}$ cases) (*11*).

SNP (Rs780094) is in a large block of LD spanning 416 kb and 16 genes. The SNP resides, however, within a highly plausible biological candidate gene glucokinase regulatory protein (*GCKR*). GCKR regulates glucokinase (GCK), the first glycolytic enzyme. Adenovirus-mediated overexpression of *GCKR* in mouse liver increased GCK activity and lowered fasting blood glu-

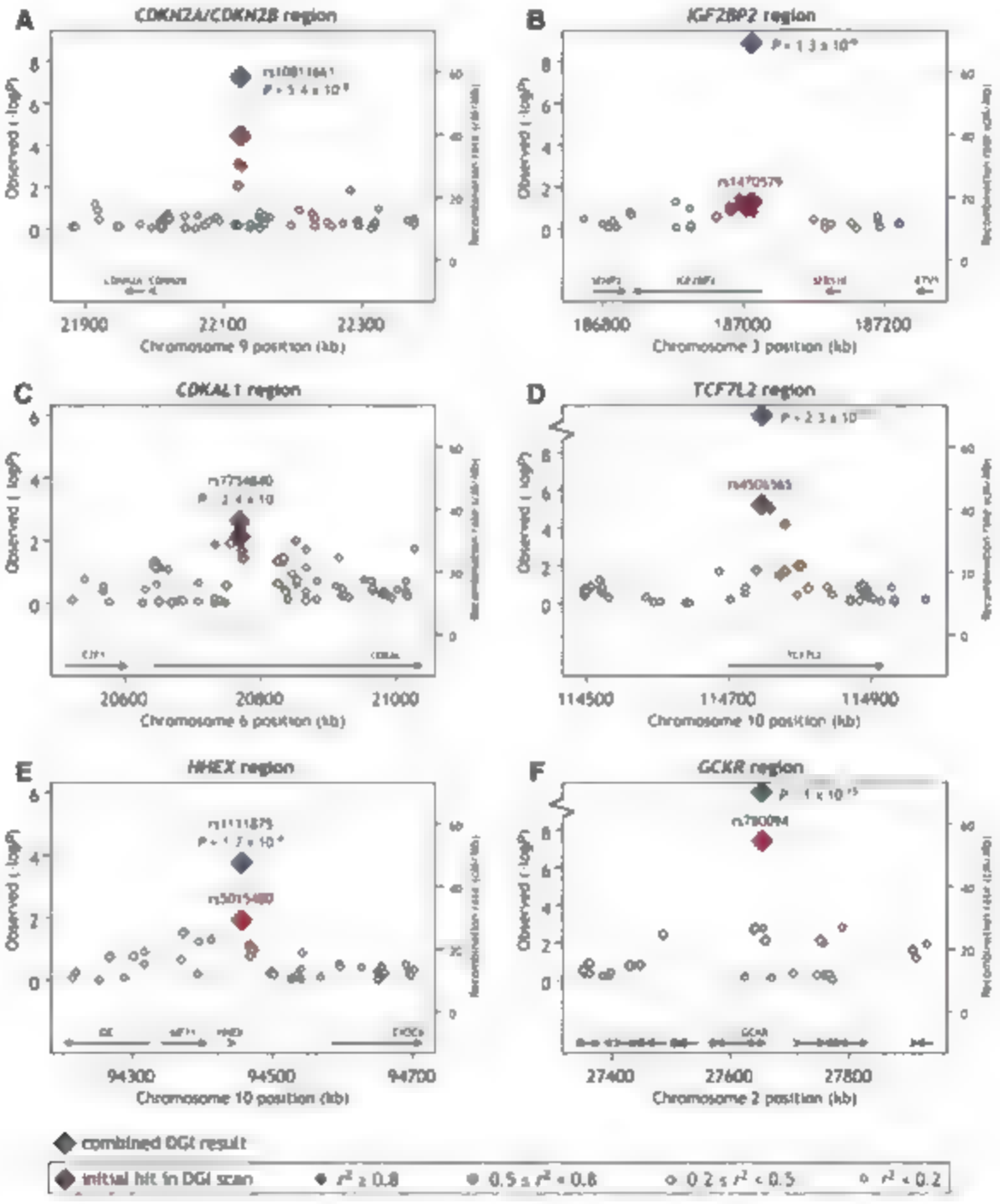

Fig. 2. Regional plots of six confirmed associations. For each of the (**A**) *CDKN2A/CDKN2B* (**B**) *IGF2BP2*, (**C**) *CDKAL1*, (**D**) *TCF7L2*, (**E**) *HHEX* regions associated with T2D, and (**F**) *GCKR* region associated with triglyceride levels, all genotyped SNPs in the DGI genome scan are plotted with their P-values (as $-\log_{10}$ values) as a function of genomic position (with NCBI Build 35). In each panel, the SNP with the most significant association in the DGI combined analysis is listed (blue diamond) and its initial P-value in the genome scan (red diamond). Estimated recombination rates (taken from HapMap) are plotted to reflect the local LD structure around the associated SNPs and their correlated proxies (red, $r^2 \geq 0.8$; orange, $0.5 \leq r^2 < 0.8$; gray, $0.2 \leq r^2 < 0.5$; white, $r^2 < 0.2$). Gene annotations were taken from the University of California Santa Cruz genome browser.

Table 2. Associations results for lipid/apolipoprotein traits in the top 100 of the DGI genome scan.

Trait	Previously reported SNP	Locus	SNP in genome scan*	Sample size	Minor allele†	Frequency	Residual variance explained (%)‡	*P*-value	Rank for trait
Novel locus									
TG	–	*GCKR*	rs780094	2659	T	0.35	1.2	3.7×10^{-8}	1
TG	–	*GCKR*	rs780094	5217§	T	0.35	0.5	8.7×10^{-8}	–
Previously published loci									
LDL-C	rs4420638	*APOE* cluster	rs4420638	2601	G	0.22	2.1	3.4×10^{-13}	1
LDL-C	rs693 (C7673T)	*APOB*	rs693	2600	A	0.49	1.0	7.1×10^{-7}	4
HDL-C	rs1800775 (C-629A)	*CETP*	rs1800775	2623	C	0.47	2.1	2.5×10^{-13}	1
HDL-C	rs328 (Ser447x)	*LPL*	rs17482753 ($r^2 = 1$)	2624	T	0.10	0.9	3.6×10^{-5}	24
HDL-C	rs1800588 (C-514T)	*LIPC*	rs261332 ($r^2 = 0.92$)	2628	A	0.18	0.7	3.4×10^{-5}	23
TG	rs328 (Ser447x)	*LPL*	rs17482753 ($r^2 = 1$)	2652	T	0.10	1.0	4.9×10^{-7}	2
TG	rs2286788 (T1259C)	*APOA5*	rs481843 ($r^2 = 0.52$)	2649	T	0.11	0.7	3.3×10^{-5}	28
apoB	rs693 (C7673T)	*APOB*	rs693	1448	A	0.45	1.1	9.4×10^{-5}	40
apoA-I	rs1800775 (C-629A)	*CETP*	rs1800775	1451	C	0.44	1.6	2.7×10^{-6}	1

*r^2 between proxy and previously reported SNP based on HapMap-CEU. †Minor allele is ordered to the forward strand of NCBI Build 35. ‡Residual after adjustment of lipid/apolipoprotein levels for age, age², sex, diabetes status, and geographic region. §Replication in Malmö Diet and Cancer Study—Cardiovascular Arm.

cose (22), overexpression of GCK in liver led to lowered blood glucose and increased triglyceride levels (23, 24).

On the basis of these findings, we examined measures of glucose homeostasis. In both our scan and replication samples, the T allele of rs780094 trended toward association to lower glucose (P = 0.10, P = 0.02 respectively), less insulin resistance (HOMA-IR P = 0.05 and P = 0.01), and lower risk of T2D (P = 0.20, P = 0.13). The association of higher triglycerides with lower blood glucose reverses the correlation normally seen in humans, but is consistent with overexpression studies of GCKR and GCK in mouse models.

In summary, we carried out WGAS for T2D and related clinical traits. With collaborators we provide compelling evidence for associations at three previously unknown loci with risk of T2D, the first replications of two additional T2D loci, and a previously unknown association to triglyceride levels. Including long-recognized associations, our data provide strong support for 15 common variants as influencing T2D and lipid levels in European populations. The annotations of the new T2D genes suggest a primary role of the pancreatic beta cell, but much additional work will be required to develop and test this hypothesis.

Our results have general implications for genome-wide association studies of common diseases. The modest effect of each SNP demonstrates that large sample sizes will be required to discover and validate genetic risk factors for common disease. Although the eight T2D variants discussed in this report each conveys a substantial population attributable risk (5 to 27% at each locus), each contributes very modestly to overall variance in diabetes risk (0.04 to 0.8%, 2.3% combined across the eight SNPs). Thus, many more variants remain to be found as risk factors for T2D, and many questions remain about the balance between common and rare variants, SNPs and copy-number alterations, main effects and epistasis. Additional associated variants may be found in or near these loci, as has been the case for other examples (25–31).

The most notable aspect of this and other such studies may be the generation of new hypotheses. Before this work, few would have argued that these genes and noncoding genomic regions were a high priority for T2D research. Now, on the basis of their validated relationship to disease, it is evident that they should be explored and understood. The ability to discover etiological factors that fall outside previous biological hypotheses is a major motivation for unbiased genome-wide approaches and is well supported by these and other emerging data from genome-wide association studies.

References and Notes

1. R. A. Fisher, *Trans. R. Soc. Edinb.* **52**, 399 (1918).
2. M. Kimura, *T. Ote. Genetics* **78**, 199 (1971).
3. The International HapMap Consortium, *Nature* **437**, 1299 (2005).
4. Materials and methods are available as supporting material on *Science* Online.
5. L. Peltonen *et al.*, *Nat. Genet.* **38**, 863 (2006).
6. P. I. W. de Bakker *et al.*, *Nat. Genet.* **37**, 1217 (2005).
7. C. D. Campbell *et al.*, *Nat. Genet.* **37**, 868 (2005).
8. D. G. Clayton *et al.*, *Nat. Genet.* **37**, 1243 (2005).
9. A. L. Price *et al.*, *Nat. Genet.* **38**, 904 (2006).
10. The Wellcome Trust Case Control Consortium, *Nature* in press.
11. L. J. Scott *et al.*, *Science* **316**, 1341 (2007).
12. E. Zeggini *et al.*, *Science* **316**, 1336 (2007).
13. J. Krishnamurthy *et al.*, *Nature* **443**, 453 (2006).
14. F. C. Nielsen, Nielsen-Christiansen, *Scand. J. Clin. Lab. Invest. Suppl.* **234**, 93 (2001).
15. F. M. Spagnolo, A. H. Bonarrico, *Dev. Biol.* **292**, 447 (2006).
16. M. Wagner *et al.*, *Gastroenterology* **124**, 1901 (2003).
17. M. Ueda, J. M. Rakstadis, J. F. Halpern, *J. Biol. Chem.* **281**, 28858 (2006).
18. S. F. Grant *et al.*, *Nat. Genet.* **38**, 320 (2006).
19. R. Sladek *et al.*, *Nature* **445**, 881 (2007).
20. E. H. Rani *et al.*, *Diabetologia* **41**, 1511 (1998).
21. S. S. Deeb *et al.*, *Nat. Genet.* **20**, 284 (1998).
22. E. D. Stoltzberg *et al.*, *Diabetes* **50**, 1313 (2001).
23. R. M. O'Doherty, D. L. Lehman, S. Telemaque-Potts, C. B. Newgard, *Diabetes* **48**, 2022 (1999).
24. T. Ferre, E. Riu, F. Bosch, A. Valera, *FASEB J.* **10**, 1213 (1996).
25. R. B. Graham *et al.*, *Proc. Natl. Acad. Sci. U.S.A.* **104**, 6758 (2007).
26. J. Muller *et al.*, *Nat. Genet.* **38**, 1055 (2006).
27. M. Li *et al.*, *Nat. Genet.* **38**, 1049 (2006).
28. R. H. Ouet *et al.*, *Science* **314**, 1461 (2006).
29. J. P. Hugot *et al.*, *Nature* **411**, 599 (2001).
30. C. A. Hasman *et al.*, *Nat. Genet.* **39**, 638 (2007).
31. L. K. Kotowski *et al.*, *Am. J. Hum. Genet.* **78**, 410 (2006).

32. We are indebted to all participants in the studies for their support and contributions. This work was supported by Novartis Institutes for BioMedical Research (D.A.), with additional support from The Richard and Susan Smith Family Foundation/American Diabetes Association Pinnacle Program Project Award (D.A., M.N., M.J.D.). We thank our colleagues from the UK T2D study and the FUSION study for sharing data before publication and for close and enjoyable collaboration. We thank P. Donnelly for sharing results before publication on behalf of the WTCCC. The following are supported by NIH Research Career Awards: J.C.F. (K23 DK65978-04), M.N.I. [National Institute of Diabetes and Digestive and Kidney Diseases (NIDDK) K24 DK067768], NIH Research Service Award (R.S.), and a NIH Training grant award (E.K.S.). G.L. is supported by March of Dimes research grant (6-FY04-61). S.K.'s work is supported by grants from the Doris Duke Charitable Foundation, the Juvenile Diabetes Research Foundation, and NIH (grant K23-HL083102). M.J.D., D.A., S.P., and P.I.W.d.B. acknowledge support from NIH/National Heart, Lung, and Blood Institute (grant U01 HG004171). D.A. is a Burroughs Wellcome Fund Clinical Scholar in Translational Research, and a Distinguished Clinical Scholar of the Doris Duke Charitable Foundation. L.G., T.T., B.I., M.R.J., and the Botnia Study are principally supported by the Sigrid Juselius Foundation, the Finnish Diabetes Research Foundation, the Folkhälsan Research Foundation, and Clinical Research Institute HUCH Ltd; work in Malmö, Sweden, was also funded by a Jämé grant from the Swedish Research Council (349-2006-237). We thank H. Hilden, H. Perttunen-Nio, and S. Mahan for technical assistance. We thank the Botnia and Skara research teams for clinical contributions and colleagues at Massachusetts General Hospital, Harvard, Broad, and Novartis for helpful discussions. We thank J. Avruch, M. Fishman, E. Lander, R. Ulton, and E. Scolnick for support and helpful comments on the manuscript.

Diabetes Genetics Initiative of Broad Institute of Harvard and MIT, Lund University, and Novartis Institutes of BioMedical Research

Writing team: Richa Saxena[1–3] (team leader), Benjamin F. Voight,[1–3,5] Valeriya Lyssenko,[7] Noël P. Burtt,[1] Paul I. W. de Bakker,[1–3] Hong Chen,[8] Jeffrey J. Roix,[8] Sekar Kathiresan,[1–3,9] Joel N. Hirschhorn,[1,4,9–11] Mark J. Daly,[1–3,9] Thomas E. Hughes,[8] Leif Groop,[7,12] David Altshuler[1–3] (Chair)

Project management: Noël P. Burtt,[1] Leif Groop,[7,12] Thomas E. Hughes,[8] David Altshuler[1–3]

Study design: Richa Saxena[1–4] and Valeriya Lyssenko[5] (Team Leaders), Peter Almgren,[5] Paul I. W. de Bakker,[1–4] Noël P. Burtt,[1] Jose C. Florez,[1–4] Hong Chen,[6] Joanne Meyer,[6] Joel N. Hirschhorn,[1,4,7–11] Mark J. Daly,[1–4,12] Thomas E. Hughes,[6] Lund Group,[5,13] David Altshuler[1–4] (Chair)

Clinical characterization and phenotypes: Valeriya Lyssenko[5] and Richa Saxena[1–4] (Team Leaders), Peter Almgren,[5] Kristin Ardlie,[1] Kristina Bengtsson Boström,[14] Noël P. Burtt,[1] Hong Chen,[6] Jose C. Florez,[1–4] Bo Hvinden,[14,15] Sekar Kathiresan,[1,4,5] Guillaume Lettre,[1,8,9–11] Jill Lindblad,[16] Helen M. Lyon,[1,8,9–11] Olle Melander,[5] Christopher Newton-Cheh,[1–4,7] Peter Nilsson,[17] Marju Orho-Melander,[5] Lennart Råstam,[18] Elizabeth K. Speliotes,[1,4,8,9–11] Marja-Riitta Taskinen,[19] Tiinamaija Tuomi,[4,20] Benjamin F. Voight,[1–4,7] David Altshuler,[1–4] Joel N. Hirschhorn,[1,4,8,9–11] Thomas E. Hughes,[6] Lund Group[5,13] (Chair)

DNA sample QC and diabetes replication genotyping: Candace Guiducci[1] and Valeriya Lyssenko[5] (Team Leaders), Anna Berglund,[5] Joyce Carlson,[1,2] Lauren Gianniny,[1] Rachel Hackett,[1] Liselotte Hall,[16] Johan Holmkvist,[5] Esa Laurila,[5] Marju Orho-Melander,[5] Marketa Sjögren,[5] Maria Sterner,[16] Aarti Surti[1] Margareta Svensson,[5] Malin Svensson,[5] Ryan Tewhey,[1] Noël P. Burtt[1] (Chair)

Whole genome scan genotyping: Brendan Blumenstiel[1] (Team Leader), Melissa Parkin,[1] Matthew DeFelice,[1] Candace Guiducci,[1] Ryan Tewhey,[1] Rachel Barry,[1] Wendy Brodeur,[1] Noël P. Burtt,[1] Jody Camarata,[1] Nancy Chia,[1] Mary Fava,[1] John Gibbons,[1] Bob Handsaker,[1] Claire Healy,[1] Kieu Nguyen,[1] Casey Gates,[1] Carrie Sougnez,[1] Diane Gage,[1] Marcia Nizzari,[1] David Altshuler[1–4] Stacey B. Gabriel[1] (Chair)

GCKR replication genotyping and analysis Malmö Diet and Cancer Study: Sekar Kathiresan[1,4,5] (Team Leader), Candace Guiducci,[1] Aarti Surti,[1] Noël P. Burtt,[1] Olle Melander,[5] Marju Orho-Melander[5] (Chair)

Statistical analysis: Benjamin F. Voight[1–4] and Paul I. W. de Bakker[1–4] (Team Leaders), Richa Saxena,[1–4] Valeriya Lyssenko,[5] Peter Almgren,[5] Noël P. Burtt,[1] Hong Chen,[6] Cung-Wei Chen,[4] Qicheng Ma,[1] Hemang Parikh,[1] Deborah Richardson,[6] Darrell Ricke,[1] Jeffrey C. Barrett,[1] Lund Group,[5,13] Shaun Purcell,[1,4] David Altshuler,[1–4] Mark J. Daly[1–4] (Chair)

[1]Broad Institute of Harvard and Massachusetts Institute of Technology (MIT), Cambridge, MA 02142, USA. [2]Center for Human Genetic Research, Massachusetts General Hospital, Boston, MA 02114, USA. [3]Department of Medicine, Massachusetts General Hospital, Boston, MA 02114, USA. [4]Department of Molecular Biology, Massachusetts General Hospital, Boston, MA 02114, USA. [5]Department of Medicine, Harvard Medical School, Boston, MA 02115, USA. [6]Department of Genetics, Harvard Medical School, Boston, MA 02115, USA. [7]Department of Clinical Sciences, Diabetes and Endocrinology Research Unit, University Hospital Malmö, Lund University, Malmö, Sweden. [8]Diabetes and Metabolism Disease Area, Novartis Institutes for BioMedical Research, 100 Technology Square, Cambridge, MA 02139, USA. [9]Department of Pediatrics, Harvard Medical School, Boston, MA 02115, USA. [10]Division of Endocrinology, Children's Hospital, Boston, MA 02115, USA. [11]Division of Genetics, Children's Hospital, Boston, MA 02115, USA. [12]Department of Medicine, Helsinki University Hospital, University of Helsinki, Helsinki, Finland. [13]Skaraborg Institute, Skövde, Sweden. [14]Malmska Municipal Health Center and Hospital, Jakobstad, Finland. [15]Folkhälsan Research Center, Helsinki, Finland. [16]Department of Clinical Sciences, Community Medicine Research Unit, University Hospital Malmö, Lund University, Malmö, Sweden. [17]Department of Clinical Sciences, Medicine Research Unit, University Hospital Malmö, Lund University, Malmö, Sweden. [18]Clinical Chemistry, University Hospital Malmö, Lund University, Malmö, Sweden. [19]Department of Psychiatry, Massachusetts General Hospital, Harvard Medical School, Boston, MA 02115, USA.

Supporting Online Material

www.sciencemag.org/cgi/content/full/1142358/DC1
Materials and Methods
Figs. S1 and S2
Tables S1 to S6
References

9 March 2007; accepted 20 April 2007
Published online 26 April 2007
10.1126/science.1142358
Include this information when citing this paper.

Replication of Genome-Wide Association Signals in UK Samples Reveals Risk Loci for Type 2 Diabetes

Eleftheria Zeggini,[1,2]* Michael N. Weedon,[3,4]* Cecilia M. Lindgren,[1,2]* Timothy M. Frayling,[3,4]* Katherine S. Elliott,[2] Hana Lango,[1,4] Nicholas J. Timpson,[2,5] John R. B. Perry,[3,4] Nigel W. Rayner,[1,2] Rachel M. Freathy,[3,4] Jeffrey C. Barrett,[2] Beverley Shields,[4] Andrew P. Morris,[2] Sian Ellard,[4,6] Christopher J. Groves,[3] Lorna W. Harries,[4] Jonathan L. Marchini,[7] Katharine R. Owen,[1] Beatrice Knight,[4] Lon R. Cardon,[2] Mark Walker,[8] Graham A. Hitman,[9] Andrew D. Morris,[10] Alex S. F. Doney,[10] The Wellcome Trust Case Control Consortium (WTCCC),† Mark I. McCarthy,[1,2]‡§ Andrew T. Hattersley[3,4]‡

The molecular mechanisms involved in the development of type 2 diabetes are poorly understood. Starting from genome-wide genotype data for 1924 diabetic cases and 2938 population controls generated by the Wellcome Trust Case Control Consortium, we set out to detect replicated diabetes association signals through analysis of 3757 additional cases and 5346 controls and by integration of our findings with equivalent data from other international consortia. We detected diabetes susceptibility loci in and around the genes *CDKAL1*, *CDKN2A/CDKN2B*, and *IGF2BP2* and confirmed the recently described associations at *HHEX/IDE* and *SLC30A8*. Our findings provide insight into the genetic architecture of type 2 diabetes, emphasizing the contribution of multiple variants of modest effect. The regions identified underscore the importance of pathways influencing pancreatic beta cell development and function in the etiology of type 2 diabetes.

The pathophysiological bases of type 2 diabetes (T2D) remain unclear despite its growing global importance (*1*). Candidate gene and positional cloning efforts have suggested many putative susceptibility variants, but unequivocal replications are so far limited to variants in just three genes, *PPARG*, *KCNJ11*, and *TCF7L2* (*2*–*4*).

Improved understanding of the correlation between genetic variants [linkage disequilibrium (LD)], allied to advances in genotyping technology, have enabled systematic searches for disease-associated common variants on a genome-wide scale. The Wellcome Trust Case Control Consortium (WTCCC) recently completed such a genome-wide association (GWA) scan in 1924 T2D cases and 2938 population controls from the United Kingdom, using the Affymetrix GeneChip Human Mapping 500 k Array Set (*5*). The strongest association signals genome-wide were observed for single-nucleotide polymorphisms (SNPs) in *TCF7L2* [For example, for rs7901695, odds ratio (OR) = 1.37, 95% confidence interval (CI) = 1.25–1.49, and $P = 6.7 \times 10^{-13}$.] The other known T2D susceptibility variants were detected with effect sizes consistent with previous reports (*2*, *3*).

Here, we describe how integration of data from the WTCCC scan and our own replication studies with similar information generated by the Diabetes Genetics Initiative (DGI) (*6*) and the Finland United States Investigation of NIDDM Genetics (FUSION) (*7*) has identified seven additional susceptibility variants for T2D.

In the WTCCC study, analysis of 490,032 autosomal SNPs in 16,179 samples yielded 459,448 SNPs that passed initial quality control (*5*). We considered only the 393,453 autosomal SNPs with minor allele frequency (MAF) exceeding 1% in both cases and controls and no extreme departure from Hardy-Weinberg equilibrium ($P < 10^{-4}$ in cases or controls) (*8*). This T2D-specific data set shows no evidence of substantial confounding from population substructure and genotyping biases (*8*).

To distinguish true associations from those reflecting fluctuations under the null or residual errors arising from aberrant allele calling, we first submitted putative signals from the WTCCC study to additional quality control, including cluster-plot visualization and validation genotyping on a second platform (*8*). Next, we attempted replication of selected signals in up to 3757 additional cases and 5346 controls (replication sets RS1 to RS3). RS1 comprised 2022 cases and 2037 controls from the U.K. Type 2 Diabetes Genetics Consortium collection (UKT2DGC) all from Tayside, Scotland). RS2 included 632 additional T2D cases and 1750 population controls from the Exeter Family Study of Child Health (EFSOCH). A subset of SNPs were typed in RS3, comprising a further 1103 cases and 1569 controls from the UKTDGC (table S1).

The first wave of validated SNPs sent for replication was selected from the 30 SNPs, in nine distinct chromosomal regions (excluding *TCF7L2*), which had, in the WTCCC scan alone,

attained the most extreme ($P < 10^{-5}$) significance values on Cochran-Armitage tests of association. Genotyping of 31 representative SNPs generated evidence of replication ($P < 0.05$) for three of these nine regions (Table 1 and table S2).

Rs8050136 [mapping to the *FTO* (fat mass and obesity-associated) gene region on chr 6] was among a cluster of SNPs generating the strongest evidence for association outside *TCF7L2* in the original scan: risk allele OR = 1.27 (1.16–1.37), $P = 2.0 \times 10^{-8}$ (fig. S1). This SNP showed strong replication [OR = 1.22 (1.12–1.32), $P = 5.4 \times 10^{-7}$]. As we recently reported (9), this effect on T2D risk is mediated through a primary effect on adiposity, and adjustment for body mass index (BMI) abolishes the T2D association.

Replication was also obtained for SNPs within the *CDKAL1* locus on chromosome 6, including rs9465871 and rs10946398. Although rs9465871 generated the stronger signal in the WTCCC scan, replication at this SNP was modest ($P = 0.023$). The replication signal at rs10946398 was more striking (OR = 1.14 (1.07–1.22), $P = 8.4 \times 10^{-5}$) (Table 1 and table S2). Consistent evidence of association is provided by the DGI ($P = 4.1 \times 10^{-4}$ at rs7754840) and FUSION groups ($P = 9.5 \times 10^{-3}$ at rs7171253) (Table 1 and table S3) (6, 7), both SNPs being strong ($r^2 > 0.99$) proxies for rs10946398. Across all studies, combined evidence for association at *CDKAL1* is compelling ($P = 4.3 \times 10^{-11}$).

All associated SNPs map to a large (90 kb) intron within *CDKAL1* (Fig. 1). Flanking recombination hotspots define a 208 kb interval likely to contain the etiological variant(s). *CDKAL1* [cyclin-dependent kinase 5 (CDK5) regulatory subunit associated protein 1 like 1] encodes a 579-residue, 65-kD protein of unknown function. We have detected expression of *CDKAL1* mRNA in human pancreatic islet and skeletal muscle (fig. S2). CDKAL1 shares considerable protein domain and amino acid homology with CDK5 regulatory subunit associated protein 1 (CDK5RAP1), a known inhibitor of CDK5 activation. CDK5 has been implicated in the regulation of pancreatic beta cell function through formation of p35:CDK5 complexes that down-regulate insulin expression (*10*, *11*).

The third replicated association maps to the *HHEX* (hematopoietically expressed) gene region on chromosome 10. This gene showed strong association in the WTCCC scan [rs5015480 risk allele OR = 1.22 (CI, 1.17–1.33), $P = 5.4 \times 10^{-8}$] and is a powerful biological candidate (*12*, *13*). We could not optimize a replication assay for rs5015480 but observed evidence for replication at a perfect proxy, rs1111875 [risk allele OR = 1.06 (CI, 1.01–1.15), $P = 0.03$] (Table 1, tables S2 and S3). Both DGI and FUSION studies showed modest but consistent association signals generating strong, combined evidence ($P = 5.7 \times 10^{-10}$) for a role in T2D susceptibility (Table 1 and table S3). A fourth genome-wide association scan, in French subjects, recently yielded independent evidence for a T2D signal in this region (*14*). The signal resides within an extended (295 kb) region of LD containing not only *HHEX* [highly expressed in fetal and adult pancreas (fig. S2)] but also the genes encoding kinesin-interacting factor (*KIF11*) and insulin-degrading enzyme (*IDE*) (fig. S3). *IDE* represents a second strong biological candidate given postulated effects on both insulin signaling and islet function and data from rodent models (*15*–*17*).

Of the remaining regions selected in the first wave, none showed any evidence of replication in U.K. samples (table S2), and for none was there strong support from the DGI and FUSION scans.

The relatively strict thresholds imposed for SNP selection in the first wave (i.e., point-wise

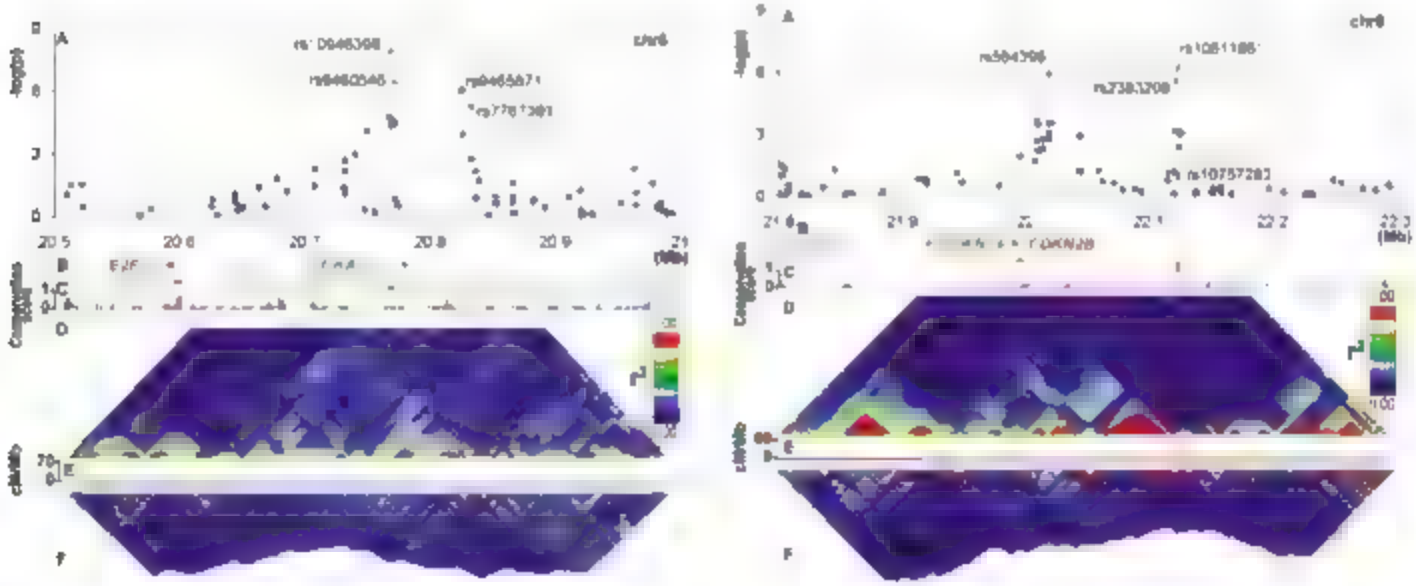

Fig. 1. (left) Overview of *CDKAL1* signal region. **(A)** Plot of −log(*P* values) for T2D (Cochran-Armitage test for trend) against chromosome position in Mb. Blue diamonds represent primary scan results and pink triangles denote meta-analysis results across all UK samples. **(B)** Genomic location of genes showing intron and exon structure (NCBI Build 35). Pink triangles show position of replication SNPs relative to gene structure. **(C)** MULTIZ (*24*) vertebrate alignment of 17 species showing evolutionary conservation. **(D)** GoldSurfer2 (*25*) plot of linkage disequilibrium (r^2) for SNPs genotyped in WTCCC scan (passing T2D-specific quality control) in WTCCC T2D cases. **(E)** Recombination rate given as cM/MB. Red boxes represent recombination hotspots (*26*). **(F)** GoldSurfer2 plot of linkage disequilibrium (r^2) for all HapMap (haplotype map of the human genome) SNPs across the region (HapMap CEU data) (*27*). **Fig. 2. (right)** Overview of chr9 signal region. Panel layout as in Fig. 1.

[1]Oxford Centre for Diabetes, Endocrinology and Metabolism, University of Oxford, Churchill Hospital, Oxford, OX3 7LJ, UK. [2]The Wellcome Trust Centre for Human Genetics, University of Oxford, Roosevelt Drive, Oxford, OX3 7BN, UK. [3]Genetics of Complex Traits, Institute of Biomedical and Clinical Science, Peninsula Medical School, Magdalen Road, Exeter EX2 7LD, UK. [4]Diabetes Genetics Group, Institute of Biomedical and Clinical Science, Peninsula Medical School, Barrack Road, Exeter EX2 5DW, UK. [5]Medical Research Council Centre for Causal Analyses in Translational Epidemiology, Bristol University, Canynge Hall, Whiteladies Rd, Bristol, BS2 8PR, UK. [6]The Molecular Genetics Laboratory, Royal Devon and Exeter NHS Foundation Trust, Old Pathology Building, Barrack Road, Exeter EX2 5DW, UK. [7]Department of Statistics, University of Oxford, 1 South Parks Road, Oxford, OX1 3TG, UK. [8]Diabetes Research Group, School of Clinical Medical Sciences, Newcastle University, Framlington Place Newcastle upon Tyne NE2 4HH, UK. [9]Centre for Diabetes and Metabolic Medicine, Barts and The London, Royal London Hospital, Whitechapel, London, E1 1BB, UK. [10]Diabetes Research Group, Division of Medicine and Therapeutics, Ninewells Hospital and Medical School, Dundee DD1 9SY, UK.

*These authors contributed equally to this work.
†Membership of the WTCCC is listed at the end of this paper.
‡These authors contributed equally to this work.
§To whom correspondence should be addressed. E-mail: mark.mccarthy@drl.ox.ac.uk

Table 1 Confirmed T2D susceptibility variants. Representative SNPs are shown for each signal with ORs and 95% CIs reported (for the Cochran-Armitage 1 df test) with respect to the risk allele (denoted in bold, with the ancestral allele underlined where known). SNPs selected for inclusion are those with the strongest evidence for association in the U.K. data sets (except in the case of *TCF7L2* where, to maximize consistency across the data sets, rs7901695 is presented). In the case of *HHEX*, the U.K. meta-analysis combines data from rs5015480 and rs1111875 (r^2 = 1 in HapMap CEU). Because DGI and FUSION had not typed the identical SNPs in all samples, results shown for those studies feature the SNP generating the strongest association. In all cases, these were SNPs in strong LD (minimum r^2 0.95, except *TCF7L2*) and with consistent direction of effect with the SNP reported in the U.K. data (see table S3 for details). The use of different SNPs may result in slightly different estimates of *P* values and OR between the three studies. Combined estimates of the ORs were calculated by weighting the logORs of each study by the inverse of their variance.

rs	chr	position	A1	A2	Region	WTCCC 1924 cases 2938 controls OR (95% CI)	P_{add}	Replication meta-analysis 3757 cases 5346 controls OR (95% CI)	P_{add}	All UK sample meta-analysis 5681 cases 8284 controls OR (95% CI)	P_{add}	DGI 6529 cases 7252 controls OR (95% CI)	P_{add}	FUSION 2376 cases 2432 controls OR (95% CI)	P_{add}	All combined 14,586 cases 17,968 controls OR (95% CI)	P_{add}
rs8050136	16	52373776	**A**	C	*FTO*	1.27 (1.16–1.37)	2.0×10^{-8}	1.22 (1.12–1.32)	5.4×10^{-7}	1.23 (1.18–1.32)	7.3×10^{-16}	1.03 (0.91–1.17)	0.25	1.11 (1.02–1.20)	0.017	1.17 (1.12–1.22)	1.3×10^{-12}
rs10946398	6	20769013	A	**C**	*CDKAL1*	1.20 (1.10–1.31)	2.5×10^{-5}	1.14 (1.07–1.22)	8.3×10^{-5}	1.16 (1.10–1.22)	1.3×10^{-8}	1.08 (1.03–1.14)	2.4×10^{-3}	1.12 (1.03–1.22)	9.5×10^{-3}	1.12 (1.08–1.16)	4.1×10^{-11}
rs5015480	10	94455539	**C**	T	*HHEX*	1.22 (1.12–1.33)	5.4×10^{-6}	–	–	1.13 (1.07–1.19)	4.6×10^{-5}	1.14 (1.06–1.22)	1.7×10^{-4}	1.10 (1.01–1.19)	0.025	1.13 (1.08–1.17)	5.7×10^{-10}
rs1111875	10	94452862	C	**T**	*HHEX*	–	–	1.08 (1.01–1.15)	0.020								
rs10811661	9	22124094	**C**	T	*CDKN2B*	1.22 (1.09–1.37)	7.6×10^{-4}	1.18 (1.08–1.28)	1.7×10^{-4}	1.19 (1.11–1.28)	4.9×10^{-7}	1.20 (1.12–1.28)	5.4×10^{-8}	1.20 (1.07–1.36)	2.2×10^{-3}	1.20 (1.14–1.25)	7.8×10^{-15}
rs564398	9	22019547	C	**T**	*CDKN2B*	1.16 (1.07–1.27)	3.2×10^{-4}	1.12 (1.05–1.19)	8.6×10^{-4}	1.13 (1.08–1.19)	1.3×10^{-6}	1.05 (0.94–1.17)	0.5	1.13 (1.01–1.27)	0.039	1.12 (1.07–1.17)	1.2×10^{-7}
rs4402960	3	186994389	**G**	T	*IGF2BP2*	1.15 (1.05–1.25)	1.7×10^{-3}	1.09 (1.01–1.16)	0.018	1.11 (1.05–1.16)	1.6×10^{-4}	1.17 (1.11–1.23)	1.7×10^{-9}	1.18 (1.08–1.28)	2.4×10^{-4}	1.14 (1.11–1.18)	8.6×10^{-10}
rs13266634	8	118253964	**C**	T	*SLC30A8*	1.12 (1.02–1.23)	0.020	1.12 (1.04–1.19)	1.2×10^{-3}	1.12 (1.05–1.18)	7.0×10^{-5}	1.07 (1.00–1.16)	0.047	1.18 (1.09–1.29)	7.0×10^{-5}	1.12 (1.07–1.16)	5.3×10^{-8}
rs7901695	10	114744078	**C**	T	*TCF7L2*	1.37 (1.25–1.49)	6.7×10^{-11}	–	–	–	–	1.38 (1.31–1.46)	2.3×10^{-31}	1.34 (1.21–1.49)	1.4×10^{-8}	1.37 (1.31–1.43)	1.0×10^{-48}
rs5215	11	17365206	C	**T**	*KCNJ11*	1.15 (1.05–1.25)	1.3×10^{-3}	–	–	–	–	1.15 (1.09–1.21)	1.0×10^{-7}	1.11 (1.02–1.20)	0.014	1.14 (1.10–1.19)	5.0×10^{-11}
rs1801282	3	12368125	**C**	G	*PPARG*	1.23 (1.09–1.41)	1.3×10^{-3}					1.09 (1.01–1.16)	0.019	1.20 (1.07–1.33)	1.4×10^{-3}	1.14 (1.08–1.20)	1.7×10^{-6}

$P < 10^{-5}$) help to limit false discovery, but many genuine susceptibility variants will fail to reach them. We initiated a second wave of replication based around SNPs for which the WTCCC scan generated more modest evidence for association (Cochran-Armitage $P = 10^{-2}$ to 10^{-5}). We prioritized the 3367 SNPs in this range using additional criteria: (i) evidence of association in DGI and FUSION (6, 7); (ii) presence of multiple, independent ($r^2 < 0.4$) associations within the same locus; and (iii) biological candidacy (*8*, *18*).

Analysis of the 56 SNPs, representing 49 putative signals, selected for this "second wave" of replication (table S4) yielded two further regions implicated in T2D susceptibility. A cluster of SNPs on chromosome 9 (represented by rs10811661) generated a promising signal in all three scans. Replication was observed in UK samples [rs10811661: OR = 1.18 (CI, 1.08 to 1.28), $P = 1.7 \times 10^{-4}$], as well as DGI ($P = 2.2 \times 10^{-5}$) and FUSION follow-up studies (rs2383208, $P = 9.7 \times 10^{-3}$). A second signal from the WTCCC scan located ~100 kb 5′ [rs564398, OR = 1.16 (CI, 1.07 to 1.27), $P = 3.2 \times 10^{-4}$], was weakly supported in the FUSION scan but not the DGI scan (Table 1 and table S3), and was replicated in the U.K. RS samples [OR = 1.12 (CI, 1.05 to 1.19), $P = 8.6 \times 10^{-4}$] (Table 1 and table S3).

These two association signals are separated by a recombination hotspot (*19*) between rs10811661 and rs564398 (a 0.057, $r^2 < 0.001$) (Fig. 2). Across all studies, the combined evidence for association is stronger for the 3′ ($P = 7.8 \times 10^{-15}$) than for the 5′ ($P = 1.2 \times 10^{-7}$) peak (Table 1). The 3′ signal maps to sequence with no characterized genes, whereas the recombination interval enclosing the 5′ signal includes the full coding sequences of *CDKN2B* and *CDKN2A* (encoding $p15^{INK4b}$ and $p16^{INK4a}$, respectively). *CDKN2A* is a known tumor suppressor and its product, $p16^{INK4a}$ inhibits CDK4 (cyclin-dependent kinase 4), a powerful regulator of pancreatic beta cell replication (*19*–*21*). Overexpression of *Cdkn2a* leads to decreased islet proliferation in aging mice (*22*). *Cdkn2b* overexpression is also causally related to islet hypoplasia and diabetes in murine models (*23*). Both *CDKN2B* and *CDKN2A* display high levels of expression in pancreatic islets and pituitary (fig. S2).

A fifth replicated association lies within the *IGF2BP2* gene on chromosome 3. We observed some evidence of association for SNPs in this region in the WTCCC scan (*5*) [e.g., rs4402960: OR = 1.15 (CI, 1.05 to 1.25), $P = 1.7 \times 10^{-3}$]. Consistent associations in the DGI and FUSION scans (*6*, *7*) and the biological candidacy of the gene [a known regulator of insulin-like growth factor 2 (IGF2) translation] prompted replication. We obtained only modest evidence for replication at rs4402960 (OR = 1.09 (CI, 1.01 to 1.16), $P = 0.018$; Table 1 and table S4), but combined evidence across all studies ($P = 8.6 \times 10^{-16}$) establishes this as a genuine T2D signal (Table 1 and table S3). The associated SNPs map to a 97-kb region spanning the promoter and first 3 exons of *IGF2BP2* (fig. S4).

Most of the remaining 50 "second-wave" SNPs can be discounted as susceptibility variants based on their failure to replicate (table S4), although some merit further consideration. One such example is rs9369425, located 57 kb downstream of the *LEG4* (vascular endothelial growth factor A) gene on chromosome 6 (fig. S5). Evidence for association in the WTCCC scan [OR = 1.16 (CI, 1.06 to 1.27), $P = 8.6 \times 10^{-4}$] is supported by nominal replication in U.K. samples [OR = 1.08 (CI, 1.01 to 1.15), $P = 0.03$] and by DGI scan results [1.17 (1.04 to 1.32), $P = 4.4 \times 10^{-3}$]. Although no signal is apparent in the FUSION study, this does not allow us to reject the association. For 80% power to detect an OR of 1.11 ($\alpha = 0.05$), more than 3000 case-control pairs are needed.

In the French genome-wide scan (*14*), variants in both the *HHEX* and *SLC30A8* genes were implicated in T2D susceptibility. Because the associated SNPs in *SLC30A8* are poorly captured on the Affymetrix chip ($r^2 < 0.01$), the WTCCC scan was not informative for this locus. However, we genotyped rs13266634 independently and obtained replication of the finding: risk allele OR = 1.12 (CI, 1.05 to 1.18), $P = 7.0 \times 10^{-5}$ in all UK data] and across all three studies ($P = 5.3 \times 10^{-8}$) (Table 1 and table S4).

The present analysis has contributed to identification of several confirmed T2D susceptibility loci. One of these (*FTO*) exerts its primary effect on T2D risk through an impact on adiposity (*9*). Some of the other signals was attenuated by adjustment for BMI or waist circumference (tables S5 to S7). One of the remaining four loci (*HHEX/IDE*) represents a strong replication of findings recently reported (*14*). The other three loci (near *CDKAL1*, *IGF2BP2*, and *CDKN2A/B*), all showing extensive replication across the three studies, represent previously unknown T2D susceptibility loci.

Across the four T2D scans completed (*5*–*7*, *14*), *TCF7L2* clearly emerges as the largest association signal. On current evidence, all other confirmed loci display more modest effect sizes (between 1.10 and 1.25 per allele). Extensive resequencing and fine-mapping will be required to define the full spectrum of etiological variation at each locus, and these may yet identify variants with greater impact. Our findings offer clear lessons for the design of future studies. Robust identification of variants with such effect sizes is only feasible with large-scale sample sets (13,965 individuals were typed in the present study). Further, the exchange of data between groups (providing data on up to 32,554 samples) was key to the rapid and unequivocal identification of the signals we report.

As a result of the four GWA studies reported to date (*5*–*7*, *14*), the number of genuine, replicated T2D susceptibility signals has climbed from three to nine (adding *HHEX/IDE*, *SLC30A8*, *CDKAL1*, *CDKN2A/B*, *IGF2BP2*, and *FTO*). However, these loci explain only a small proportion of the observed familiality (the sibling relative risk, λ_s, attributable to all loci in the U.K. samples, is only ~1.07). We expect additional loci to be revealed by further rounds of replication initiated by more systematic meta-analysis of these and other scans. Our study provides an important validation of the genome-wide indirect association mapping approach and a demonstration of the value of aggressive data-sharing efforts. It also generates insights into T2D pathogenesis, emphasizing the likely importance of pathways involved in pancreatic beta cell development, regeneration, and function. In-depth physiological and functional studies are now needed to establish the precise mechanisms involved.

References and Notes

1. M. Stumvoll, B. J. Goldstein, T. W. van Haeften, *Lancet* **365**, 1333 (2005).
2. G. Altshuler *et al.*, *Nat. Genet.* **26**, 76 (2000).
3. A. L. Gloyn *et al.*, *Diabetes* **52**, 568 (2003).
4. S. F. Grant *et al.*, *Nat. Genet.* **38**, 320 (2006).
5. Wellcome Trust Case Control Consortium, *Nature*, in press.
6. Diabetes Genetics Initiative, *Science* **316**, 1331 (2007); published online 26 April 2007 [10.1126/science.1142358].
7. L. Scott *et al.*, *Science* **316**, 1341 (2007); published online 26 April 2007 [10.1126/science.1142382].
8. Materials and methods are available as supporting material on Science Online.
9. T. M. Frayling *et al.*, *Science* **316**, 889; 10.1126/science.1141634 (2007).
10. M. Uhrda, J. M. Rakotalis, J. P. Haberer, *J. Biol. Chem.* **281**, 28858 (2006).
11. F. Y. Wei *et al.*, *Nat. Med.* **11**, 1104 (2005).
12. A. Cobry, M. Mendelsohn, *Genome Dev.* **19**, 187 (2005).
13. R. Bort, P. Martinez-Barbera, K. S. Beddington, *Int. J. Dev. Biol.* **49**, 797 (2004).
14. R. Saxena *et al.*, *Nature* **445**, 881 (2007).
15. H. Cakmaz-Kadar *et al.*, *Hum. Mol. Genet.* **9**, 2149 (2000).
16. K. A. Jetha, R. A. Kahn, *Biochem. Biophys. Res. Commun.* **231**, 167 (1997).
17. W. Ferris *et al.*, *Am. J. Pathol.* **164**, 1425 (2004).
18. GeneSeeker (www.geneseeker.org) was used to prioritize genes for biological candidacy by integrating information from diverse online databases (including Entrez Gene, Online Mendelian Inheritance in Man, PubMed, and Mouse Genome Informatics).
19. S. G. Rane *et al.*, *Nat. Genet.* **22**, 44 (1999).
20. R. V. Mettus, S. G. Rane, *Oncogene* **22**, 8413 (2003).
21. M. Maria *et al.*, *Diabetologia* **47**, 686 (2004).
22. J. Krishnamurthy *et al.*, *Nature* **443**, 453 (2006).
23. M. Mantani *et al.*, *Mol. Cell. Endocrinol.* **229**, 175 (2005).
24. M. Blanchette *et al.*, *Genome Res.* **14**, 708 (2004).
25. F. Pettersson, O. Jonsson, L. R. Cardon, *Bioinformatics* **20**, 3241 (2004).
26. S. Myers, L. Bottolo, C. Freeman, G. McVean, P. Donnelly, *Science* **310**, 321 (2005).
27. The International HapMap Consortium, *Nature* **437**, 1299 (2005).

28. We are grateful to all the study participants. We acknowledge the support of Diabetes UK, British Diabetic Association Research, the UK Medical Research Council, the Wellcome Trust, European Commission (EURODIA LSHG-CT-2004-512153), and Peninsula Medical School. Personal funding comes from the Wellcome Trust (E.Z., A.T.H., and L.R.C.); UK Medical Research Council (J.N.H.P.); Diabetes UK (R.M.F.); Throne-Holst Foundation (C.M.L.); Leverhulme Trust (A.P.M.); Research Councils UK (L.W.H.); and the Scottish Executive Generations Scotland Initiative (C.R.A.P., A.D.M.). M.N.W. is Vanderveil Foundation Research Fellow at the Peninsula Medical School. We are grateful to members of the DGI and FUSION teams for sharing data.

Membership of Wellcome Trust Case Control Consortium Management committee: Paul R. Burton,[†] David G. Clayton,[‡]

Jon R. Cardon,[3] Nick Craddock,[4] Panos Deloukas,[5] Audrey Duncanson,[6] Dominic P. Kwiatkowski,[7] Mark McCarthy,[8] Willem H. Ouwehand,[9,10] Nilesh Samani,[11] John A. Todd,[2] Peter Donnelly,[1]* Jeffrey C. Barrett,[1] Paul R. Burton, Dan Davison, Peter Donnelly, Doug Easton,[12] David Evans, Hin-Tak Leung,[2] Jonathan L. Marchini, Andrew P. Morris, Lon R. Cardon (Co-chair),[3] David G. Clayton (Co-chair)[5]

UK Blood Services and University of Cambridge controls: Antony P. Attwood,[5,8] James P. Boorman,[8,9] Barbara Cant,[8] Ursula Everson,[10] Judith M. Hussey,[10] Jennifer D. Jolley,[8] Alexandra S. Knight,[8] Kerstin Koch,[8] Elizabeth Meech,[10] Sarah Nutland,[2] Christopher V. Prowse,[10] Helen E. Stevens,[2] Niall C. Taylor,[8] Graham R. Walters,[8] Neil M. Walker,[2] Nicholas A. Watkins,[8,9] Thilo Winzer,[8] John A. Todd,[2] Willem H. Ouwehand[8,9]

1958 birth cohort controls: Richard W. Jones,[10] Wendy L. McArdle,[10] Susan M. Ring,[10] David P. Strachan,[10] Marcus Pembrey[10,11]

Bipolar disorder (Aberdeen): Gerome Breen,[11] David St. Clair, **(Birmingham)** [illegible] Catherine Jackson Whitehead, **(Cardiff)** Nigel Hayward, Claire K. Green, Dorothea Lindsay, Marian L. Hamshere, Peter A. Holmans, Ian R. Jones, George Kirov, Valentina Moskvina,[4] Ivan Nikolov, Michael C. O'Donovan, Michael J. Owen, Nick Craddock, **(London)** David A. Collier,[12] Amanda Elkin,[12] Anne Farmer,[13] Richard Williamson,[14] Peter McGuffin,[14] **(Newcastle)** Allan H. Young,[15] & Nicol Ferrier[15]

Coronary artery disease (Leeds): Stephen G. Ball,[16] Anthony J. Balmforth,[16] Jennifer H. Barrett,[16] D. Timothy Bishop,[16] Mark M. Iles,[16] Azhar Maqbool,[16] Nadira Yuldasheva,[16] Abetayo S. Hall[16] **(Leicester):** Peter S. Braund,[17] Paul R. Burton,[3] Richard J. Dixon,[17] Massimo Mangino,[18] Suzanne Stevens,[19] Martin D. Tobin, John R. Thompson, Nilesh J. Samani[18]

Crohn's disease (Cambridge): Francesca Bredin,[17] Mark Tremelling,[17] Miles Parkes,[17] **(Edinburgh):** Hazel Drummond,[20] Charles W. Lees,[21] Elaine R. Monmo,[21] Jack Satsangi[21] **(London):** Sheila A. Fisher,[22] Alastair Forbes,[23] Cathryn M. Lewis,[24] Clive M. Onnie,[25] Natalie J. Prescott,[24] Jeremy Sanderson,[25] Christopher G. Mathew[24] **(Newcastle):** Jamie Barbour,[26] M. Khalid Mohiuddin,[26] Catherine E. Todhunter,[26] John C. Mansfield,[27] **(Oxford):** Tariq Ahmad,[28] Fraser R. Cummings,[28] Derek P. Jewell,[1]

Hypertension (Aberdeen): John Webster,[1] **(Cambridge):** Morris J. Brown,[29] David G. Clayton,[5] **(Evry, France):** G. Mark Lathrop,[16] **(Glasgow):** John Connell,[17] Anna Dominiczak,[17] **(Leicester):** Nilesh J. Samani,[18] **(London):** Caroline A. Braga Marcano,[30] Beverley Burke,[30] Richard Dobson,[30] Johannie Gungadoo,[30] Kate L. Lee,[30] Patricia B. Munroe,[30] Stephen J. Newhouse,[30] Abiodun Onipinla,[30] Chris Wallace,[30] Mingzhan Xue,[30] Mark Caulfield,[30] **(Oxford):** Martin Farrall,[4]

Rheumatoid arthritis: Anne Barton,[20] The Biologics in RA Genetics and Genomics Study Syndicate (BRAGGS) Steering Committee,[a] Ian N. Bruce,[20] Hannah Donovan,[20] Steve Eyre,[20] Paul D. Gilbert,[20] Samantha L. Hider,[20] Anne M. Hinks,[1] Sally L. John,[20] Catherine Potter,[20] Alan J. Silman,[20] Deborah P. M. Symmons,[20] Wendy Thomson,[20] Jane Worthington[20]

Type 1 diabetes: David G. Clayton,[5] David B. Dunger,[2,31] Sarah Nutland,[2] Helen E. Stevens,[2] Neil M. Walker,[2] Barry Widmer,[2,31] John A. Todd[2]

Type 2 diabetes (Exeter): Timothy M. Frayling,[32,33] Rachel M. Freathy,[32,33] Hana Lango,[32,34] John R. B. Perry,[32,33] Beverley M. Shields,[33] Michael N. Weedon,[32,33] Andrew T. Hattersley,[32,33] **(London):** Graham A. Hitman,[35] **(Newcastle):** Mark Walker[36] **(Oxford):** Kate S. Elliott,[1,7] Christopher J. Groves,[7] Cecilia M. Lindgren, Nigel W. Rayner, Nicholas J. Timpson,[34] Eleftheria Zeggini,[1,7] Mark I. McCarthy[1,7]

Tuberculosis (Gambia): Melanie Newport,[37] Giorgio Sirugo,[37] **(Oxford):** Emily Lyons,[1] Fredrik Vannberg,[1] Adrian V. S. Hill[1]

Ankylosing spondylitis: Linda A. Bradbury,[38] Claire Farrar,[39] Jennifer J. Pointon,[39] Paul Wordsworth,[39] Matthew A. Brown[39,40]

Autoimmune thyroid disease: Jayne A. Franklyn,[38] Joanne M. Heward,[38] Matthew J. Simmonds,[38] Stephen C. L. Gough[38]

Breast cancer: Sheila Seal,[41] Breast Cancer Susceptibility Collaboration (UK),† Michael R. Stratton,[41,42] Nazneen Rahman[43]

Multiple sclerosis: Maria Ban,[44] An Goris,[45] Stephen J. Sawcer,[44] Alastair Compston[44]

Gambian controls (Gambia): David Conway,[37] Muminatou Jallow,[37] Melanie Newport,[37] Giorgio Sirugo,[37] **(Oxford):** Kirk A. Rockett, Dominic P. Kwiatkowski[7]

DNA, genotyping, data QC, and informatics (Wellcome Trust Sanger Institute, Hinxton): Suzannah J. Bumpstead,[5] Amy Chaney,[5] Kate Downes,[2,5] Mohammed J. R. Ghori,[5] Rhian Gwilliam,[5] Sarah E. Hunt,[5] Michael Inouye,[5] Andrew Keniry,[5] Emma King,[5] Ralph McGinnis,[5] Simon Potter,[5] Rathi Ravindrarajah,[5] Pamela Whittaker,[5] Claire Widden,[5] David Withers,[5] Panos Deloukas[5] **(Cambridge):** Hin-Tak Leung,[2] Sarah Nutland,[2] Helen E. Stevens,[2] Neil M. Walker,[2] John A. Todd[2]

Statistics (Cambridge): Doug Easton,[3,4] David G. Clayton,[5] **(Leicester):** Paul R. Burton,[1] Martin D. Tobin[1] **(Oxford):** Jeffrey C. Barrett,[1] David Evans,[2] Andrew P. Morris,[2] Lon R. Cardon[1] **(Oxford):** Niall J. Cardin,[11] Dan Davison,[12] Teresa Ferreira,[11] Joanne Pereira-Gale,[13] Ingileif B. Hallgrimsdottir,[11] Bryan N. Howie,[11] Jonathan L. Marchini,[11] Chris C. A. Spencer,[11] Zhan Su,[11] Yik Ying Teo,[2,11] Damjan Vukcevic,[11] Peter Donnelly

Principal investigators: David Bentley,[5] Matthew A. Brown,[40,49] Lon R. Cardon,[3] Mark Caulfield,[30] David G. Clayton,[5] Alastair Compston,[44] Nick Craddock,[27] Panos Deloukas,[5] Peter Donnelly,[11] Martin Farrall,[28] Stephen C. L. Gough,[38] Alistair S. Hall,[26] Andrew T. Hattersley,[32,33] Adrian V. S. Hill,[1] Dominic P. Kwiatkowski,[7,5] Christopher G. Mathew,[24] Mark I. McCarthy,[8,7] Willem H. Ouwehand,[8,9] Miles Parkes,[17] Marcus Pembrey,[10,50] Nazneen Rahman,[43] Nilesh J. Samani,[18] Michael R. Stratton,[41,42] John A. Todd,[2] John Worthington[20]

[1]Genetic Epidemiology Group, Department of Health Sciences, University of Leicester Adrian Building, University Road, Leicester, LE1 7RH, UK. [2]Juvenile Diabetes Research Foundation/Wellcome Trust Diabetes and Inflammation Laboratory, Department of Medical Genetics, Cambridge Institute for Medical Research, University of Cambridge, Wellcome Trust/MRC Building, Addenbooke's Hospital, Cambridge, CB2 0XY, UK. [3]Wellcome Trust Centre for Human Genetics, University of Oxford, Roosevelt Drive, Oxford OX3 7BN, UK. [4]Department of Psychological Medicine, University of Wales College of Medicine, Heath Park, Cardiff CF14 4XN, UK. [5]Wellcome Trust Sanger Institute, Wellcome Trust Genome Campus, Hinxton, Cambridge CB10 1SA, UK. [6]Wellcome Trust Centre for Human Genetics, Roosevelt Drive, Oxford OX3 7BN, UK. [7]Department of Medical Genetics, University of Cambridge, Cambridge Institute for Medical Research, Wellcome Trust/MRC Building, Addenbooke's Hospital, Hills Road, Cambridge CB2 0XY, UK. [8]National Health Service Blood and Transplant, Cambridge Centre, Long Road, Cambridge CB2 0PT, UK. [9]University of Cambridge, Department of Haematology, Long Road, Cambridge CB2 0PT, UK. [10]National Health Service Blood and Transplant, Oxford Centre, Oxford OX3 9BQ, UK. [11]Department of Cardiovascular Sciences, University of Leicester and Glenfield Hospital, Leicester, LE3 9QP, UK. [12]Department of Public Health and Primary Care, University of Oxford, Oxford OX3 7LF, UK. [13]Wellcome Trust Clinical Research Facility, Western General Hospital, Edinburgh EH4 2XU, UK. [14]Department of Psychiatry, University of Edinburgh, Royal Edinburgh Hospital, Morningside Park, Edinburgh EH10 5HF, UK. [15]Department of Medicine, University of Alberta, 562 Heritage Medical Research Centre, Edmonton, Alberta T6G 2S2, Canada. [16]Leeds Institute of Molecular Medicine, Wellcome Trust Brenner Building, St. James's University Hospital, Leeds LS9 7TF, UK. [17]Inflammatory Bowel Disease Research Group, Addenbrooke's Hospital, University of Cambridge, Cambridge CB2 2QQ, UK. [18]Department of Cardiovascular Sciences, University of Leicester, Glenfield Hospital, Leicester, LE3 9QP, UK. [19]Department of Medical Genetics, University of Cambridge, Cambridge Institute for Medical Research, Wellcome Trust/MRC Building, Addenbooke's Hospital, Hills Road, Cambridge CB2 0XY, UK. [20]Arthritis Research Campaign Epidemiology Research Unit, Manchester Musculoskeletal Research Institute, University of Manchester, Stopford Building, Oxford Road, Manchester M13 9PT, UK. [21]Department of Gastroenterology and Gastrointestinal Surgery, University of Edinburgh, Western General Hospital, Edinburgh EH4 2XU, UK. [22]Department of Medical & Molecular Genetics, King's College London School of Medicine, 8th Floor Guy's Tower, Guy's Hospital, London SE1 9RT, UK. [23]Institute for Digestive Diseases, University College London Hospitals Trust, London NW1 2BU, UK. [24]Department of Gastroenterology, Guy's and St Thomas' National Health Service Foundation Trust, London SE1 7EH, UK. [25]Department of Gastroenterology and Hepatology, University of Newcastle upon Tyne, Tyne Royal Victoria Infirmary, Newcastle upon Tyne NE1 4LP, UK. [26]Gastroenterology Unit, Aberdeen Royal Infirmary, University of Oxford, Oxford OX3 9DU, UK. [27]Medicine and Therapeutics, Aberdeen Royal Infirmary, Foresterhill, Aberdeen, Grampian AB25 2ZB, UK. [28]Clinical Pharmacology Unit and the Diabetes and Inflammation Laboratory, University of Cambridge, Addenbrooke's Hospital, Hills Road, Cambridge, CB2 0QQ, UK. [29]Centre National de Genotypage, 2 Rue Gaston Cremieux, Evry, Paris 91057, France. [30]British Heart Foundation Glasgow Cardiovascular Research Centre, University of Glasgow, 126 University Place, Glasgow G12 8LX, UK. [31]Novartis Pharmaceuticals and Barts and The London Genome Centre, William Harvey Research Institute, Barts and The London Queen Mary School of Medicine, Charterhouse Square, London EC1M 6BQ, UK. [32]Cardiovascular Medicine, University of Oxford, Wellcome Trust Centre for Human Genetics, Roosevelt Drive, Oxford OX3 7BN, UK. [33]Arthritis Research Campaign Epidemiology Research Unit, University of Manchester, Stopford Building, Oxford Road, Manchester, M13 9PT, UK. [34]Department of Paediatrics, University of Cambridge, Addenbrooke's Hospital, Cambridge CB2 2QQ, UK. [35]Institute of Cancer Research, Institute of Biomedical and Clinical Science, Peninsula Medical School, Barrack Road, Exeter EX2 5DW, UK. [36]Centre for Diabetes and Metabolic Medicine, Barts and The London Royal London Hospital, Whitechapel, London E1 1BB, UK. [37]Diabetes Research Group, School of Clinical Medical Sciences, Newcastle University, Framlington Place, Newcastle upon Tyne NE2 4HH, UK. [38]Medical Research Council Laboratories, Fajara, The Gambia. [39]Diamantina Institute for Cancer, Immunology and Metabolic Medicine, Princess Alexandra Hospital, University of Queensland, Woolloongabba, Queensland 4102, Australia. [40]Botnar Research Centre, Nuffield Orthopaedic Centre, Oxford OX3 7LD, UK. [41]Department of Medicine, Division of Medical Sciences, Institute of Biomedical Research, University of Birmingham, Edgbaston, Birmingham B15 2TT, UK. [42]Section of Cancer Genetics, Institute of Cancer Research, Sutton, Surrey SM2 5NG, UK. [43]Cancer Genetics Group, The Institute of Cancer Research, 15 Cotswold Road, Sutton, Surrey SM2 5NG, UK. [44]Department of Clinical Neurosciences, University of Cambridge, Addenbrooke's Hospital, Hills Road, Cambridge CB2 2QQ, UK.

*Members of the Biologics in RA Genetics and Genomics Study Syndicate (BRAGGS) Steering Committee are listed after the WTCCC list.

†Members of the Breast Cancer Susceptibility Collaboration (UK) are listed after the BRAGGS list.

‡Present address: Illumina Cambridge, Chesterford Research Park, Little Chesterford, Near Saffron Walden, Essex, CB10 1XL, UK.

Biologics in RA Genetics and Genomics Study Syndicate (BRAGGS) Steering Committee Anne Barton,[1] John D Isaacs,[2] Ann W Morgan,[3] Gerry O. Wilson[4]

[1]arc Epidemiology Unit, University of Manchester, Oxford Road, Manchester, M13 9PT, UK. [2]Department of Rheumatology, University of Newcastle-upon-Tyne, Framlington Place, Newcastle-Upon-Tyne NE2 4HH, UK. [3]Leeds Institute of Molecular Medicine, Section of Academic Unit of Musculoskeletal Disease Wellcome Trust Brenner Building, St. James's University Hospital, Beckett Street, Leeds LS9 7TF, UK. [4]Genomic Medicine, The University of Sheffield, Western Bank, Sheffield, S10 2TN, UK.

Breast Cancer Susceptibility Collaboration (UK) A. Ardern-Jones,[1] J. Berg,[2] A. Brady,[1] N. Bradshaw,[4] C. Brewer,[3]

G. Brice,[5] B. Bullman,[1] J. Campbell,[6] B. Castle,[7] R. Calmarty,[8] C. Chapman,[10] C. Chu,[11] N. Coates,[12] T. Cole,[10] R. Davidson,[4] A. Donaldson,[13] H. Dorkins,[1] F. Douglas,[2] D. Eccles,[6] R. Edes,[2] F. Elmslie,[6] D. G. Evans,[7] S. Gair,[4] S. Goodwin,[5] D. Gosden,[2] J. Gray,[14] L. Greenhalgh,[15] H. Gregory,[13] S. V. Hodgson,[9] T. Homfray,[6] R. S. Houlston,[2] L. Izatt,[16] L. Jackson,[1] L. Jeffries,[14] V. Johnson-Ratley,[12] F. Kavalier,[16] C. Kirk,[17] F. Lalloo,[7] C. Langman,[18] L. Locke,[4] M. Longmuir,[6] J. Mackay,[19] A. Magee,[13] S. Mansour,[6] Z. Miedzybrodzka,[20] J. Miller,[2] P. Morrison,[14] V. Murday,[4] J. Paterson,[21] G. Pichert,[16] M. Porteous,[8] N. Rahman,[5] M. Rogers,[15] S. Rowe,[22] S. Shanley,[1] A. Saggar,[5] G. Scott,[2] L. Side,[23] L. Snadden,[4] M. Steel,[2] M. Thomas,[5] S. Thomas,

[1]Clinical Genetics Service, Royal Marsden Hospital, Downs Road, Sutton, Surrey, SM2 5PT, UK. [2]Department of Clinical Genetics, Ninewells Hospital, Dundee, DD1 9SY, UK. [3]Medical and Community Genetics, Kennedy-Galton Centre, Level 8V, Northwick Park and St. Mark's NHS Trust, Watford Rd, Harrow, HA1 3UJ, UK. [4]Institute of Medical Genetics, Yorkhill NHS Trust, Dalnair Street, Glasgow, G3 8SJ, UK. [5]Clinical Genetics Department, Royal Devon and Exeter Hospital (Heavitree), Gladstone Road, Exeter, EX1 2ED, UK. [6]Department of Clinical Genetics, St. George's Hospital Medical School, Jenner Wing, Cranmer Terrace, London, SW17 0RE, UK. [7]Department of Medical Genetics, St. Mary's Hospital, Hathersage Road, Manchester, M13 0JH, UK. [8]South East of Scotland Clinical Genetics Service, Western General Hospital, Crewe Road, Edinburgh, EH4 2XU, UK. [9]Department of Medical Genetics, the Princess Anne Hospital, Coxford Road, Southampton, SO16 5YA, UK. [10]Clinical Genetics Unit, Birmingham Women's Hospital, Metchley Park Road, Edgbaston, Birmingham, B15 2TG, UK. [12]Yorkshire Regional Genetic Service, Department of Clinical Genetics, Cancer Genetics Building, St. James University Hospital, Becket Street, Leeds, LS9 7TF, UK. [12]Department of Clinical Genetics, Leicester Royal Infirmary, Leicester, LE1 5WW, UK. [13]Department of Clinical Genetics, St Michael's Hospital, Southwell Street, Bristol, BS2 8EG, UK. [14]Institute of Human Genetics, International Centre for Life, Central Parkway, Newcastle upon Tyne, NE1 3BZ, UK. [15]Institute of Medical Genetics, University Hospital of Wales, Heath Park, Cardiff, CF14 4XW, UK. [16]Department of Clinical Genetics, Alder Hey Children's Hospital, Eaton Road, Liverpool, L12 2AP, UK. [17]Clinical Genetics Centre, Argyll House, Foresterhill, Aberdeen, AB25 2ZB, UK. [18]Clinical Genetics, 9th Floor New Guy's House, Guy's Hospital, St. Thomas Street, London, SE1 9RT, UK. [19]Clinical Genetics Service, Belfast City Hospital Trust, Belvoir Park Hospital, Lisburn Road, Belfast, BT9 7AB, UK. [20]Clinical and Medical Genetics Unit, Institute of Child Health, 30 Guildford Street, London, WC1N 1EH, UK. [21]Department of Clinical Genetics, Addenbrooke's NHS Trust, Box 134, Hills Road, Cambridge, CB2 2QQ, UK. [22]Department of Clinical Genetics, Mostyn Lodge, Countess of Chester Hospital, Liverpool Road, Chester, CH2 1UL, UK. [23]Department of Clinical Genetics, Churchill Hospital, Old Road, Headington, Oxford, OX3 7LJ, UK.

Supporting Online Material

www.sciencemag.org/cgi/content/full/1142364/DC1
Materials and Methods
Figs. S1 to S8
Tables S1 to S10
References

9 March 2007; accepted 20 April 2007
Published online 26 April 2007
10.1126/science.1142364
Include this information when citing this paper.

A Genome-Wide Association Study of Type 2 Diabetes in Finns Detects Multiple Susceptibility Variants

Laura J. Scott,[1] Karen L. Mohlke,[2] Lori L. Bonnycastle,[3] Cristen J. Willer,[1] Yun Li,[1] William L. Duren,[1] Michael R. Erdos,[3] Heather M. Stringham,[1] Peter S. Chines,[3] Anne U. Jackson,[1] Ludmila Prokunina-Olsson,[3] Chia-Jen Ding,[3] Amy J. Swift,[3] Narisu Narisu,[3] Tianle Hu,[1] Randall Pruim,[4] Rui Xiao,[1] Xiao-Yi Li,[1] Karen N. Conneely,[1] Nancy L. Riebow,[3] Andrew G. Sprau,[3] Maurine Tong,[3] Peggy P. White,[3] Kurt N. Hetrick,[5] Michael W. Barnhart,[5] Craig W. Bark,[5] Janet L. Goldstein,[5] Lee Watkins,[5] Fang Xiang,[5] Jouko Saramies,[6] Thomas A. Buchanan,[7] Richard M. Watanabe,[8,9] Timo T. Valle,[10] Leena Kinnunen,[10,11] Gonçalo R. Abecasis,[1] Elizabeth W. Pugh,[5] Kimberly F. Doheny,[5] Richard N. Bergman,[7] Jaakko Tuomilehto,[10,11,12] Francis S. Collins,[3]* Michael Boehnke[2]*

Identifying the genetic variants that increase the risk of type 2 diabetes (T2D) in humans has been a formidable challenge. Adopting a genome-wide association strategy, we genotyped 1161 Finnish T2D cases and 1174 Finnish normal glucose tolerant (NGT) controls with >315 000 single-nucleotide polymorphisms (SNPs) and imputed genotypes for an additional >2 million autosomal SNPs. We carried out association analysis with these SNPs to identify genetic variants that predispose to T2D, compared our T2D association results with the results of two similar studies, and genotyped 80 SNPs in an additional 1215 Finnish T2D cases and 1258 Finnish NGT controls. We identify T2D-associated variants in an intergenic region of chromosome 11p12 contribute to the identification of T2D-associated variants near the genes *IGF2BP2* and *CDKAL1* and the region of *CDKN2A* and *CDKN2B*, and confirm that variants near *TCF7L2*, *SLC30A8*, *HHEX*, *FTO*, *PPARG*, and *KCNJ11* are associated with T2D risk. This brings the number of T2D loci now confidently identified to at least 10.

Type 2 diabetes (T2D) is a disease characterized by insulin resistance and impaired pancreatic beta-cell function that affects 170 million people worldwide (*1*). With first-degree relatives having 3.6 times as much risk as compared to individuals in the general middle-aged population (*2*), hereditary factors, together with lifestyle and behavioral factors, play an important role in determining T2D risk (*3*). To date, intense efforts to identify genetic risk factors in T2D have met with only limited success. This study, reports from our collaborators (*4*–*6*), and the recently published work of Sladek *et al.* (*7*) describe results of genome-wide association (GWA) studies that further define the genetic architecture of T2D and identify biological pathways involved in T2D pathogenesis.

We genotyped 1161 Finnish T2D cases and 1174 Finnish NGT controls on 317 503 SNPs on the Illumina HumanHap300 BeadChip in stage 1 of a two-stage GWA study of T2D (*8*). These samples are from the Finland–United States Investigation of Non–Insulin-Dependent Diabetes Mellitus Genetics (FUSION) (*9*, *10*) and Finnish 2002 (*11*) studies (tables S1 and S2A). Among the 317 503 GWA SNPs, 315 635 had >10 copies of the less common allele (minor allele frequency (MAF) > 0.002) and passed quality-control criteria (*8*). We tested these 315 635 SNPs for association with T2D using a model that is additive on the log-odds scale (Table 1 and tables S3 and S4) (*8*). We observed a modest excess (4 observed versus 3.1 expected, $P = 0.07$) of SNPs with P values $< 10^{-4}$ (fig. S1). These results argue against the existence of multiple common SNPs with a large impact on T2D disease risk but are consistent with the presence of multiple common SNPs that each confer modest risk. The results also suggest that the matching of cases and controls by birth province, sex, and age (*8*) has been successful; in support of this conclusion, the genomic control (*12*) correction value is 1.026.

Analyses of our Illumina HumanHap300 data allowed us to query much of the known SNP variation in the genome. To increase this proportion, we developed an imputation method (*8*) that uses genotype data and linkage disequilibrium (LD) information from the HapMap Centre d'Etude du Polymorphisme Humain (Utah residents with ancestry from northern and

[3]Department of Biostatistics and Center for Statistical Genetics, University of Michigan, Ann Arbor, MI 48109, USA. [2]Department of Genetics, University of North Carolina, Chapel Hill, NC 27599, USA. [3]Genome Technology Branch, National Human Genome Research Institute, Bethesda, MD 20892, USA. [4]Department of Mathematics and Statistics, Calvin College, Grand Rapids, MI 49546, USA. [5]Center for Inherited Disease Research (CIDR), Institute of Genetic Medicine, Johns Hopkins School of Medicine, Baltimore, MD 21224, USA. [6]Savitaipale Health Center, 54800 Savitaipale, Finland. [7]Division of Endocrinology, Keck School of Medicine, University of Southern California, Los Angeles, CA 90033, USA. [8]Department of Preventive Medicine, Keck School of Medicine, University of Southern California, Los Angeles, CA 90089, USA. [9]Department of Physiology and Biophysics, Keck School of Medicine, University of Southern California, Los Angeles, CA 90033, USA. [10]Diabetes Unit, Department of Epidemiology and Health Promotion, National Public Health Institute, 00300 Helsinki, Finland. [11]Department of Public Health, University of Helsinki, 00014 Helsinki, Finland. [12]South Ostrobothnia Central Hospital, 60220 Seinäjoki, Finland.

*To whom correspondence should be addressed. E-mail: boehnke@umich.edu (M.B.); francisc@mail.nih.gov (F.S.C.)

Table 1. Confirmed T2D susceptibility loci based on all available data from the FUSION, DGI, and WTCCC/UKT2D samples.

FUSION	Chr	Position (bp)	Genes	Risk allele / nonrisk allele	Stage 1 + 2 control risk allele freq.	FUSION stage 1 OR (95% CI)	FUSION stage 1 P	FUSION stage 2 OR (95% CI)	FUSION stage 2 P	FUSION stage 1 + 2 OR (95% CI)	FUSION stage 1 + 2 P	DGI All Data OR (95% CI)	DGI All Data P	WTCCC/UKT2D All Data OR (95% CI)	WTCCC/UKT2D All Data P	FUSION-DGI-WTCCC/UKT2D All Data OR (95% CI)	FUSION-DGI-WTCCC/UKT2D All Data P	Total sample size for 80% power**
New T2D Loci																		
rs4402960	3	186,994,389	*IGF2BP2*	T/G	0.30	1.13 (1.13–1.45)	1.2×10^{-5}	1.08 (0.96–1.22)	0.22	1.18 (1.08–1.28)	2.1×10^{-4}	1.17 (1.11–1.23)	1.7×10^{-8}	1.11 (1.05–1.16)	1.6×10^{-4}	1.14 (1.11–1.18)	8.9×10^{-16}	~4300
rs7754840[†]	6	20,769,229	*CDKAL1*	C/G	0.36	1.16 (1.02–1.30)	0.021	1.08 (0.96–1.22)	0.20	1.12 (1.03–1.22)	0.0095	1.08 (1.03–1.14)	2.4×10^{-3}	1.16 (1.10–1.22)	1.3×10^{-8}	1.12 (1.08–1.16)	4.1×10^{-11}	5300
rs10811661	9	22,124,094	*CDKN2A/B*	T/C	0.85	1.17 (0.98–1.39)	0.082	1.22 (1.04–1.44)	0.015	1.20 (1.07–1.36)	0.0022	1.20 (1.12–1.28)	5.4×10^{-8}	1.19 (1.11–1.28)	4.9×10^{-7}	1.20 (1.14–1.25)	7.8×10^{-14}	~3900
rs9300039[‡]	11	41,871,942		C/A	0.89	1.52 (1.24–1.87)	6.0×10^{-5}	1.45 (1.19–1.77)	2.7×10^{-4}	1.48 (1.26–1.71)	5.7×10^{-8}	1.14[¶] (0.95–1.42)	0.12	1.13[#] (0.99–1.29)	0.068	1.25 (1.15–1.37)	4.3×10^{-7}	~3400
rs8050136	16	52,373,776	*FTO*	A/C	0.38	1.03 (0.92–1.16)	0.58	1.28 (1.05–1.33)	0.0063	1.11 (1.02–1.20)	0.016	1.03[¶] (0.91–1.17)	0.25	1.23 (1.18–1.32)	7.3×10^{-14}	1.17 (1.12–1.22)	1.3×10^{-12}	~2700
Previously published T2D association																		
rs1801282	3	12,368,125	*PPARG*	C/G	0.82	1.30 (1.11–1.53)	0.0011	1.08 (0.93–1.26)	0.33	1.20 (1.07–1.33)	0.0014	1.09 (1.01–1.16)	0.019	1.23[#] (1.09–1.41)	0.0013	1.14 (1.08–1.20)	1.7×10^{-6}	~6400
rs13266634	8	118,253,964	*SLC30A8*	C/T	0.61	1.22 (1.08–1.38)	0.0010	1.14 (1.02–1.28)	0.026	1.18 (1.09–1.29)	7.0×10^{-5}	1.07 (1.0–1.16)	0.047	1.12 (1.05–1.18)	7.0×10^{-4}	1.12 (1.07–1.16)	5.3×10^{-8}	~5100
rs1111875[†]	10	94,452,862	*HHEX*	C/T	0.52	1.13 (1.01–1.27)	0.039	1.06 (0.94–1.19)	0.34	1.10 (1.01–1.19)	0.026	1.14 (1.06–1.22)	1.7×10^{-4}	1.13 (1.07–1.19)	4.6×10^{-6}	1.13 (1.09–1.17)	5.7×10^{-10}	~4200
rs7903146[§]	10	114,748,339	*TCF7L2*	T/C	0.18	1.39 (1.20–1.61)	1.2×10^{-5}	1.30 (1.12–1.50)	3.9×10^{-4}	1.34 (1.21–1.49)	1.9×10^{-8}	1.38 (1.31–1.46)	2.9×10^{-20}	1.37[#] (1.25–1.49)	6.7×10^{-13}	1.37 (1.31–1.43)	1.0×10^{-48}	1000
rs5219[‖]	11	17,366,148	*KCNJ11*	T/C	0.46	1.20 (1.07–1.36)	0.0022	1.04 (0.92–1.16)	0.55	1.11 (1.02–1.21)	0.013	1.15 (1.09–1.21)	1.0×10^{-7}	1.15[#] (1.05–1.25)	0.0013	1.14 (1.10–1.19)	6.7×10^{-13}	3700
Total sample size						2,335		2,473		4,808		13,781		13,965		32,544		
Number of cases/controls						1,161/1,174		1,215/1,258		2,376/2,432		6,529/7,252		5,681/8,284		14,586/17,968		

*rs10946398 WTCCC/UKT2D (r^2 = 1). †Multimarker tag for rs9300039 DGI and rs1514823 WTCCC/UKT2D (r^2 = 0.965). ‡rs5015480 WTCCC GWA only (r^2 = 1). §rs7901695 WTCCC/UKT2D (r^2 = 0.849). ‖rs5215 WTCCC/UKT2D (r^2 = 0.995). ¶DGI GWA samples. #WTCCC GWA samples. **Approximate total sample size for 80% power to detect T2D SNP association at significance level 0.05 is based on the FUSION control risk allele frequency and the risk ratio calculated from FUSION-DGI-WTCCC/UKT2D all-data analyses, assuming 0.10 T2D prevalence. The sample sizes vary slightly from those of (#) because study-specific allele frequencies were used in the calculations.

western European (CEU) samples to predict genotypes of autosomal SNPs not genotyped in our subjects. A total of 2.09 million HapMap CEU SNPs (*14*) had imputed MAF >1% in FUSION and passed our imputation quality-control criteria. In the HapMap CEU sample, imputed SNPs passing these criteria increased coverage of SNPs with MAF >1% from 71.9 to 89.1% at an r^2 threshold of 0.8.

To increase the statistical power to detect T2D predisposing variants, we compared our stage 1 results to GWA results from the Diabetes Genetics Initiative (DGI) and the Wellcome Trust Case Control Consortium (WTCCC). We selected 82 SNPs for FUSION stage 2 follow-up genotyping based on evidence from: (i) FUSION-genotyped and FUSION-imputed SNPs; (ii) a combined analysis of GWA results from FUSION, DGI, and WTCCC; and (iii) previous T2D association results. For (i) and (ii), we used a prioritization algorithm that advantaged SNPs based on genome annotation (*8*) (table S7) and gave preference to genotyped SNPs over nearby imputed SNPs. We successfully genotyped 80 of the 82 SNPs in our stage 2 sample of 1215 Finnish T2D cases and 1258 Finnish NGT controls (*8*) (table S2B) and carried out joint analysis of the combined FUSION stage 1 + 2 sample (table S5). DGI (*4*) and United Kingdom T2D Genetics Consortium (UKT2D) (*5*) investigators also followed up DGI and WTCCC GWAs by genotyping replication samples.

We confirmed well-established T2D associations with *TCF7L2*, *PPARG*, and *KCNJ11* (Table 1) (*15*–*18*). SNPs in *TCF7L2* reached genome-wide significance in the FUSION stage 1 + 2 sample [odds ratio (OR) = 1.34, $P = 1.3 \times 10^{-8}$] and in the FUSION-DGI-WTCCC-UKT2D "all-data" (i.e., all GWA and follow-up samples) meta-analysis (OR = 1.37, $P = 1.0 \times 10^{-46}$) (Table 1 and table S5). *PPARG* Pro^{12}→Ala^{12} (rs1801282) and *KCNJ11* Glu^{23}→Lys^{23} (rs5219) were not genotyped in the FUSION GWA, but nearby SNPs showed some evidence for T2D association, as did the imputed genotypes for the coding variants. All-data meta-analysis resulted in genome-wide significant T2D association with *KCNJ11* Glu^{23}→Lys^{23} (OR = 1.14, $P = 6.7 \times 10^{-11}$) and strong evidence for *PPARG* Pro^{12}→Ala^{12} (OR = 1.14, $P = 1.7 \times 10^{-6}$). The *PPARG* and *KCNJ11* results emphasize the value of combining data across studies and suggest that other T2D-associated loci remain to be found.

The combined samples from the three studies provide evidence for seven additional T2D loci. For the first three of these loci, we had strong evidence in the FUSION stage 1 GWA data and, for the latter four, our FUSION stage 1 evidence was more modest.

A cluster of variants in the *IGF2BP2* (insulin-like growth factor 2 mRNA binding protein 2) region was associated with T2D in our stage 1 sample (e.g., rs1470579 with OR = 1.27, $P = 1.6 \times 10^{-4}$) (Fig. 1A). The all-data meta-analysis for rs4402960 resulted in genome-wide significance (OR = 1.14, $P = 8.9 \times 10^{-10}$). Including the rs4402960 genotype as a covariate essentially eliminates evidence for T2D association for other variants in the cluster (Fig. 1A), which is consistent with all SNPs representing the same T2D-predisposing variant(s). IGF2BP2 is a paralog of IGF2BP1, which binds to the 5′ untranslated region of the insulin-like growth factor 2 (*IGF2*) mRNA and represses [illegible] translation (*19*). IGF2BP2 is a member of a small family of polypeptide growth factors involved in the development, growth, and stimulation of

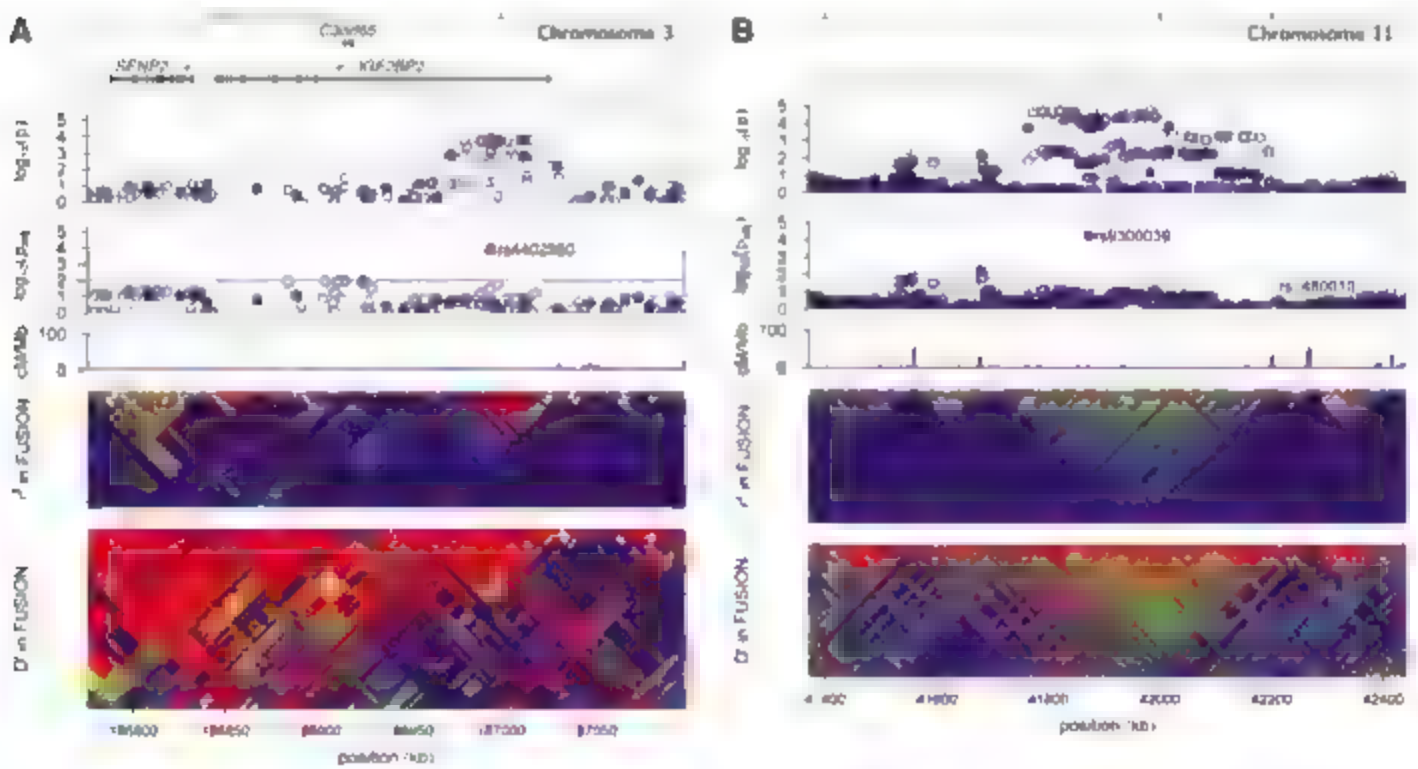

Fig. 1. Plots of T2D association and LD in FUSION stage 1 samples for regions surrounding *IGF2BP2* (**A**) and rs9300039 (**B**). (A) and (B) each contain six panels. The top panels display RefSeq genes; there are none in the rs9300039 region. The second panels (i.e., directly below the top panels) show the T2D association $-\log_{10} P$ values in FUSION stage 1 samples for SNPs genotyped in the GWA panel (closed blue circles) or imputed (open blue circles). The third panels show T2D association $-\log_{10} P$ values for each SNP in a logistic regression model correcting for the reference SNP (indicated by the red circle for rs4402960 in (A) and for rs9300039 in (B)). SNP rs7480010, reported by Sladek *et al.* (*7*), is also labeled in the rs9300039 plot (B) (green circle). A decrease in the $-\log_{10} P$ value from the second to the third panels indicates that the association signal of the tested SNPs can be explained, at least in part, by the reference SNP. In both regions, the reference SNP was chosen for convenience; the choice of another strongly associated SNP nearby would have resulted in a similar picture. The fourth panels show recombination rate in centimorgans per megabase for the HapMap CEU sample (*14*). The fifth and sixth panels show LD r^2 and D' based on FUSION stage 1–genotyped and FUSION stage 1–imputed data.

insulin action. The most strongly associated *IGF2BP2* SNPs are located in a 90-kb region within intron 2 (Fig. 1A); diabetes-predisposing variants may therefore affect regulation of *IGF2BP2* expression.

SNP rs13266634, a nonsynonymous $Arg^{325} \rightarrow Trp^{325}$ variant in the pancreatic beta-cell specific zinc transporter *SLC30A8* (*20*), showed (through our annotation-based algorithm) evidence for T2D association in stage 1 (Table 1 and fig. S2). Modest evidence in stage 2 resulted in stronger evidence in our stage 1 + 2 sample (OR = 1.18, $P = 7.0 \times 10^{-4}$) (Table 1 and table S5). Subsequent DGI and UKT2D genotyping results in strong evidence in the combined samples (OR = 1.12, $P = 5.3 \times 10^{-8}$). Sladek *et al.* (*7*) recently reported independent T2D association evidence with the same allele in two French samples ($P = 1.8 \times 10^{-5}$ and $P = 5.0 \times 10^{-7}$). SLC30A8 transports zinc from the cytoplasm into insulin secretory vesicles (*20*, *21*), where insulin is stored as a hexamer bound with two Zn^{2+} ions before secretion (*22*). Variation in *SLC30A8* may affect zinc accumulation in insulin granules, affecting insulin stability, storage, or secretion. In high-glucose conditions, overexpression of *SLC30A8* in insulinoma (INS-1E) cells enhanced glucose-induced insulin secretion (*21*).

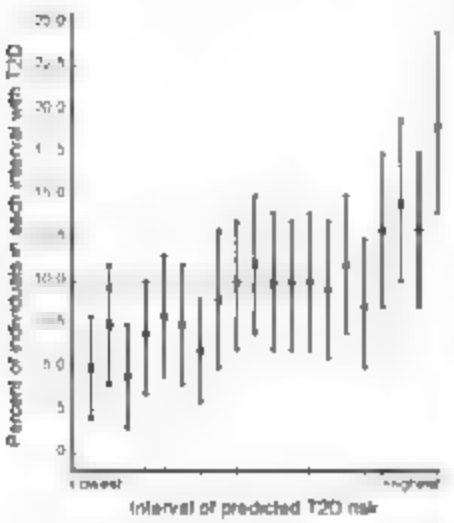

Fig. 2. Prediction of T2D risk in the FUSION sample with the use of 10 T2D susceptibility variants. T2D cases and NGT controls with complete genotype data were included in the analysis. To obtain a sample with a T2D prevalence of ~10%, we included nine copies of each of 2176 NGT controls and one copy of each of 2102 T2D cases. The predicted risk for each individual was estimated from a logistic regression model containing the 10 risk variants listed in Table 1. The proportion of T2D cases is shown for 20 equal intervals of predicted T2D risk. We constructed 95% confidence intervals (CIs) for the proportion of T2D cases in each interval using the original sample of 2102 cases and 2176 controls. The constructed sample T2D prevalence (0.096) is shown as a horizontal line. The proportion of T2D cases increases from ~5% in the lowest to 20% in the highest predicted risk categories.

SNP rs9300039 in an intergenic region on chromosome 11 showed evidence for T2D association in stage 1 (Table 1 and Fig. 1B); genotyping our stage 2 sample resulted in near genome-wide significance in our stage 1 + 2 sample (OR = 1.48, $P = 5.7 \times 10^{-8}$) (Table 1 and tables S3 and S5). In the WTCCC and DGI scans, the nearby SNP rs514823 ($r^2 = 0.97$ with rs9300039) provided weak evidence for T2D association with the appropriate allele; combining results across all three studies gave OR = 1.25 and $P = 4.3 \times 10^{-7}$. Fifty-six imputed SNPs and two more genotyped SNPs spanning 219 kb are in LD with rs9300039 and show substantial evidence for T2D association ($P < 10^{-4}$) in our stage 1 sample (table S4 and Fig. 1B). Including the genotype for rs9300039 as a covariate essentially eliminates evidence for T2D association with the remaining SNPs (Fig. 1B). This region includes three sets of spliced Expressed Sequence Tags but no annotated genes. The identification of a T2D-associated variant >1 Mb from the nearest annotated gene highlights the value of a genome-wide approach. Sladek *et al.* (*7*) reported strongly associated SNPs in two nearby regions on chromosome 11. SNP rs7480010 near hypothetical gene *LOC387761* is 131 kb centromeric to rs9300039. LD between rs9300039 and rs7480010 is essentially zero ($r^2 = 0.00063$ and $D' = 0.036$), and rs7480010 showed little evidence for association in our stage 1 + 2 sample (OR = 1.03, $P = 0.54$). Sladek *et al.* (*7*) also reported T2D association with three intronic variants of *EXT2* located ~2.4 Mb centromeric of rs9300039; we found no evidence for association with *EXT2* SNPs.

SNP rs4712523, located within intron 5 of *CDKAL1*, showed modest evidence for T2D association in our FUSION stage 1 sample which strengthened slightly in our combined stage 1 + 2 sample (OR = 1.12, $P = 0.0073$) (table S5). Nearby SNPs in strong LD with rs4712523 including rs7754840 showed modest evidence for T2D association in the DGI scan and considerably stronger evidence in the WTCCC scan. Including strong DGI and UKT2D replication data resulted in genome-wide significance (OR = 1.12, $P = 4.1 \times 10^{-11}$ for rs7754840) in the all-data meta-analysis (Table 1). CDKAL1 [cyclin-dependent kinase 5 (CDK5) regulatory subunit associated protein 1 like 1] shares protein domain similarity with CDK5 regulatory subunit associated protein 1 (CDK5RAP1), which specifically inhibits activation of CDK5 by CDK5 regulatory subunit 1 (CDK5R1) (*23*). Using quantitative reverse transcription polymerase chain reaction analysis of a panel of RNA samples from human tissues and cells, we detected the highest expression of *CDKAL1* in skeletal muscle and brain cells, as well as in 293T and Hepg2 cells (fig. S3A). The associated SNPs within intron 5, or SNPs in LD with them, may regulate expression of CDKAL1 and so affect the expression of CDK5. CDK5 and CDK5R1 activity is influenced by glucose and may influence beta-cell processes (*24*, *25*); overactivity of CDK5 in the pancreas may lead to beta-cell degeneration, especially under glucotoxic conditions (*26*).

SNP rs10811661 near cyclin-dependent kinase inhibitors *CDKN2A* and *CDKN2B* showed modest evidence for T2D association in our stage 1 + 2 sample (OR = 1.20, $P = 0.0022$) (Table 1 and table S5) and showed genome-wide significance in the all-data meta-analysis (OR = 1.20, $P = 7.8 \times 10^{-15}$). SNP rs10811661 is located upstream of *CDKN2A* and *CDKN2B*, may have a long-range effect on one of these genes, or may influence a gene not yet annotated. CDKN2A and CDKN2B inhibit the activity of CDK4 and CDK6. In mice, Cdk4 activity has been shown to influence beta-cell proliferation and mass, with loss of *Cdk4* leading to diabetes (*27*, *28*). We find *CDKN2A* to be expressed at high levels in islets, adipocytes, brain, and pancreas and at even higher levels in 293T, HeLa, and Hepg2 cells (fig. S3B). *CDKN2B* is expressed in islets and adipocytes and, to a lesser degree, in small intestine, colon, 293T, and Hepg2 cells (fig. S3C). *CDKN2A* and *CDKN2B* are also tumor suppressor genes and may play a role in aging (*29*).

SNPs rs1111875 and rs7923837 showed modest evidence of T2D association in the FUSION and DGI scans, much stronger evidence in the WTCCC scan, and genome-wide significant evidence (OR = 1.13, $P = 5.7 \times 10^{-10}$ for rs1111875) in the all-data meta-analysis. These SNPs are in LD ($r^2 = 0.70$) in a region that includes *HHEX* (hematopoietically expressed homeobox), which is critical for development of the ventral pancreas (*30*), the insulin-degrading enzyme gene *IDE*, and the kinesin-interacting factor 11 gene *KIF11*. Sladek *et al.* (*7*) recently reported independent genome-wide significant evidence for T2D association with these SNPs.

The WTCCC UKT2D groups identified evidence for T2D and body mass index (BMI) associations with a set of SNPs including rs8050136 in the *FTO* region, the T2D association appears to be mediated through a primary effect on adiposity (*5*, *6*, *31*). We observed modest evidence for association with T2D in the combined FUSION stage 1 + 2 sample (OR = 1.11, $P = 0.016$) (Table 1 and table S5).

T2D can be a component of a larger syndrome of metabolic abnormalities, and we were interested to assess the effects of T2D-related traits on our association results. We repeated our T2D association analysis for the 10 SNPs in Table 1 with one of several variables included as an additional covariate. Adjustment for BMI strengthened T2D association with *TCF7L2* and *SLC30A8*, weakened association with rs9300039 and *FTO*, and had little effect on the other loci. The effect of waist circumference was similar to that of BMI, blood pressure variables had essentially no effect.

We previously carried out T2D linkage analysis in the families of many of our stage 1 cases (*10*). None of the 10 loci in Table 1 had large T2D logarithm of the odds (LOD) scores, although those for *FTO* and *TCF7L2* were 0.63 and 0.60 and so were nominally significant. LOD scores for six of the 10 loci were greater than 0.2, as compared to 2.2 that would be expected for random genome locations. Thus, suggests enrichment for T2D-associated loci in regions with modest evidence of T2D linkage ($P = 0.01$) but that the power of the linkage approach was insufficient to distinguish these signals from background noise.

The ability to construct a list of ten robust and replicated T2D-associated loci (Table 1) represents a landmark in efforts to identify genetic variants that predispose to complex human diseases, although the specific predisposing variants and even the relevant genes remain to be defined. We examined the combined risk of T2D based on these 10 loci in our stage 1 + 2 sample by constructing a logistic regression model and predicting T2D risk for each person (*9*). We found a fourfold variation in T2D risk from the lowest to highest predicted risk groups, which is of potential interest for a personalized preventive-medicine program (Fig. 2). However these predictions from our data may be biased as compared to predictions based on the general population, likely owing to the overestimation of ORs due to the "winner's curse," enrichment for familial T2D cases, and exclusion of individuals with impaired glucose tolerance or impaired fasting glucose.

Thirty years ago, James V. Neel labeled T2D as "the geneticist's nightmare" (*42*), predicting that the discovery of genetic factors in T2D would be thoroughly challenging. Until recently, his prediction has proven true. Although large samples and collaboration among three groups were required, we can confidently state that new diabetes risk factors have been identified. Each gene discovery points to a pathway that contributes to pathogenesis, and all of these proteins and their relevant pathways represent potential drug targets for the prevention or treatment of diabetes. Based on the number of other interesting results observed in these studies, it is likely that there are additional T2D-predisposing loci to be found. Even though much remains to be done, we are at last awakening from Jim Neel's nightmare.

References and Notes

1. S. Wild, G. Roglic, A. Green, R. Sicree, H. King, *Diabetes Care* **27**, 1047 (2004).
2. S. S. Rich, *Diabetes* **39**, 1315 (1990).
3. J. Kaprio *et al.*, *Diabetologia* **35**, 1060 (1992).
4. Diabetes Genetics Initiative, *Science* **316**, 1331 (2007); published online 26 April 2007 (10.1126/science.1142358).
5. E. Zeggini *et al.*, *Science* **316**, 1336 (2007); published online 26 April 2007 (10.1126/science.1142364).
6. The Wellcome Trust Case Control Consortium, *Nature* in press.
7. R. Sladek *et al.*, *Nature* **445**, 881 (2007).
8. Materials and methods are available as supporting material on *Science* Online.
9. T. Valle *et al.*, *Diabetes Care* **21**, 949 (1998).
10. K. Silander *et al.*, *Diabetes* **53**, 821 (2004).
11. L. Saarinio *et al.*, *Diabetes Vasc. Dis. Res.* **2**, 67 (2005).
12. B. Devlin, K. Roeder, *Biometrics* **55**, 997 (1999).
13. Y. Li, P. Scheet, J. Ding, G. R. Abecasis, submitted for publication; manuscript available from G.R.A. (e-mail: goncalo@umich.edu).
14. International HapMap Consortium, *Nature* **437**, 1299 (2005).
15. S. F. Grant *et al.*, *Nat. Genet.* **38**, 320 (2006).
16. S. S. Deeb *et al.*, *Nat. Genet.* **20**, 284 (1998).
17. D. Altshuler *et al.*, *Nat. Genet.* **26**, 76 (2000).
18. A. L. Gloyn *et al.*, *Diabetes* **52**, 568 (2003).
19. J. Nielsen *et al.*, *Mol. Cell. Biol.* **19**, 1262 (1999).
20. F. Chiaromi, S. Devergnas, A. Favier, M. Seve, *Diabetes* **53**, 2930 (2004).
21. F. Chiasson *et al.*, *J. Cell Sci.* **119**, 4199 (2006).
22. M. F. Dunn, *Biometals* **18**, 295 (2005).
23. Y. P. Ching, A. S. Pang, W. H. Lee, R. Z. Qi, J. H. Wang, *J. Biol. Chem.* **277**, 15237 (2002).
24. M. Ubeda, D. M. Kemp, J. F. Habener, *Endocrinology* **145**, 3023 (2004).
25. F. Y. Wei *et al.*, *Nat. Med.* **11**, 1104 (2005).
26. M. Ubeda, J. M. Rukstalis, J. F. Habener, *J. Biol. Chem.* **281**, 28858 (2006).
27. S. G. Bone *et al.*, *Nat. Genet.* **22**, 64 (1999).
28. T. Tsuchiya *et al.*, *Mol. Cell. Biol.* **19**, 7011 (1999).
29. W. Y. Kim, N. E. Sharpless, *Cell* **127**, 265 (2006).
30. R. Bort, J. P. Martinez-Barbera, R. S. Beddington, K. S. Zaret, *Development* **131**, 797 (2004).
31. T. M. Frayling *et al.*, *Science* **316**, 889 (2007); published online 12 April 2007 (10.1126/science.1141634).
32. J. V. Neel, in *The Genetics of Diabetes Mellitus*, W. Creutzfeldt, J. Kobberling, J. V. Neel, Eds. (Springer-Verlag, Berlin, 1976), pp. 1–11.

33. We thank the Finnish citizens who generously participated in this study; our colleagues from the DGI, WTCCC, and UKT2D for sharing prepublication data from their studies; S. Erdos of FUSION and E. Krasnik, J. Gearhart, J. Bowen, M. Zeka, E. Ongaco, A. Robinson, R. King, M. Craig, and E. Hsu of CIDR for expert technical work; and D. Leja of NHGRI for expert assistance with a figure. Support for this research was provided by NIH grants DK062370 (M.B.), DK072193 (K.L.M.), HL084729 (G.R.A.), HG007651 (G.R.A.), and U54 DA021519 (National Human Genome Research Institute intramural project number 1 Z01 HG000024 (F.S.C.); a postdoctoral fellowship award from the American Diabetes Association (C.J.W.); a Wellcome-Gen Fellowship (L.P.C.); and a Calvin Research Fellowship (R.P.). Genome-wide genotyping was performed by the Johns Hopkins University Genetic Resources Core Facility (GRCF) SNP Center at CIDR with support from CIDR NIH (contract N01-HG-65403) and the GRCF SNP Center.

Supporting Online Material

www.sciencemag.org/cgi/content/full/1142382/DC1
Author Contributions
Materials and Methods
Figs. S1 to S3
Tables S1 to S7
References

17 March 2007; accepted 20 April 2007
Published online 26 April 2007
10.1126/science.1142382
Include this information when citing this paper.

Complex I Binding by a Virally Encoded RNA Regulates Mitochondria-Induced Cell Death

Matthew B. Reeves,[1]* Andrew A. Davies,[1] Brian P. McSharry,[2] Gavin W. Wilkinson,[2] John H. Sinclair[1]†

Human cytomegalovirus infection perturbs multiple cellular processes that could promote the release of proapoptotic stimuli. Consequently, it encodes mechanisms to prevent cell death during infection. Using rotenone, a potent inhibitor of the mitochondrial enzyme complex I (reduced nicotinamide adenine dinucleotide: ubiquinone oxidoreductase), we found that human cytomegalovirus infection protected cells from rotenone-induced apoptosis, a protection mediated by a 2.7-kilobase virally encoded RNA (β2.7). During infection, β2.7 RNA interacted with complex I and prevented the relocalization of the essential subunit genes associated with retinoid/interferon-induced mortality–19 in response to apoptotic stimuli. This interaction, which is important for stabilizing the mitochondrial membrane potential, resulted in continued adenosine triphosphate production, which is critical for the successful completion of the virus' life cycle. Complex I targeting by a viral RNA represents a refined strategy to modulate the metabolic viability of the infected host cell.

During primary infection or reactivation of human cytomegalovirus (HCMV), especially in the immunocompromised, the virus is able to replicate in a number of cell types, often resulting in life-threatening disease (*1*). HCMV exhibits a relatively protracted life cycle (upwards of 5 days) and at early times of infection (12 to 24 hours) encodes a highly abundant 2.7-kb RNA transcript (β2.7), accounting for >20% of total viral gene transcription (*2, 3*) of unknown function. The RNA may be associated with mitochondria (*4*), and no protein product of this RNA has ever been detected in infected cells (*3*), suggesting that it functions as a noncoding RNA (*5*).

We investigated the possibility that β2.7 could function as a noncoding RNA. A

[1]Department of Medicine, University of Cambridge, Addenbrooke's Hospital, Hills Road, Cambridge, CB2 2QQ, UK. [2]Section for Infection and Immunity, College of Medicine, University of Wales, Heath Park, Cardiff, CF14 4XX, UK.

*Present address: Novartis Institutes for Biomedical Research, 500 Technology Square, Cambridge, MA 02139, USA.
†To whom correspondence should be addressed. E-mail: js@mole.bio.cam.ac.uk

Northwestern screen of a human cDNA library with a β2.7 probe identified potential cellular interaction partners for the β2.7 RNA molecule. One of these proteins was a subunit of the mitochondrial enzyme complex I (reduced nicotinamide adenine dinucleotide ubiquinone oxido-reductase). Defective complex I activity has been implicated in numerous mitochondrial and genetic diseases, including Leigh's syndrome, Leber's hereditary optic neuropathy, and mitochondrial encephalopathy (*16*); and inhibition of complex I activity by reactive O or N species or by the direct binding of environmental toxins ultimately results in apoptosis (*17*).

We first tested whether HCMV infection (multiplicity of infection (MOI) = 5) and, specifically, β2.7 expression prevented cell death in neuronal U373 cells subjected to mitochondrial stress by treatment with rotenone, a highly effective complex I inhibitor (*9*, *10*). As expected, the addition of rotenone promoted substantial cell death in U373 cells (70% in Fig. 1). We then compared the effect of preinfection of cells with the Toledo strain of HCMV and a recombinant Toledo virus, in which the β2.7 gene had been deleted (Δβ2.7Tol) (*5*). Toledo-infected U373 cultures showed profoundly ($P < 0.001$) reduced levels of apoptosis (3%), in contrast to Δβ2.7Tol-infected cells (70% in Fig. 1A). Furthermore, the protective effect of β2.7 could be restored with a revertant virus (Fig. 1A) and by transfection of a β2.7 expression vector into U373 cells (Fig. 1B). Thus, HCMV-mediated protection of cells from rotenone-induced apoptosis correlated with expression of the viral β2.7 gene. Although the consensus is that the β2.7 transcript does not encode a protein product (*5*), we also analyzed a clinical isolate of HCMV (HCMV-3157), which would produce a heavily truncated nonsense protein if β2.7 were translated (*5*). HCMV 3157 was as efficient as Toledo at protecting cells from rotenone-induced death (fig. S1A). The protective effect of β2.7 was observed only in Toledo-infected cells (fig. S1B), whereas Δβ2.7Tol-infected cells routinely stained for both viral gene expression and terminal deoxynucleotidyl transferase mediated deoxyuridine triphosphate nick end labeling (TUNEL) (fig. S1B). The proportion of immediate-early (IE) positivity in the Δβ2.7Tol cells undergoing apoptosis was around 70% (fig. S1C). Given that only 45% of the whole population was infected, this finding implied that viral infection, in the absence of β2.7, actually rendered cells more sensitive to rotenone-induced apoptosis.

One role of the HCMV β2.7 transcript may be to mediate protection of the cell from apoptotic pathways activated by metabolic stress of complex I. Genes associated with retinoid interferon induced mortality (GRIM) 19 is a subunit of complex I that is essential for its assembly and function (*11*). HCMV infection up-regulates steady-state mRNA levels of some subunits of mitochondrial complexes I to V (*12*), but virus infection has no impact on GRIM-19 protein expression, up to 120 hours post infection (hpi) in U373 cells (fig. S2, A and B). We did, however, detect changes in GRIM-19 localization in response to rotenone and virus infection in U373 cells. GRIM-19 expression appeared to be diffuse throughout the cytoplasm of the cell (Fig. 2A), and it became relocalized into discrete perinuclear clumps after the addition of rotenone to uninfected U373 cells. However, preinfection with Toledo prevented this relocalization (Fig. 2A). GRIM-19 is known to localize to the nucleus under certain conditions (*13*), and it also interacts with the signal transducer and activator of transcription (STAT) 3 protein to prevent the nuclear import of STAT3 in a perinuclear location (*14*). Although the GRIM-19 in Toledo-infected U373 remained predominantly cytoplasmic within the cell, it did exhibit a more punctate pattern within the cytoplasm (Fig. 2A), perhaps suggesting more association with mitochondria. However, HCMV itself has profound effects on mitochondrial shape and localization after infection (*15*), and this may also partially account for the difference in GRIM-19 staining. In contrast, in Δβ2.7Tol-infected cells, the rotenone-induced perinuclear relocalization of the GRIM-19 protein was still observed (Fig. 2A), identical to that observed with uninfected cells treated with rotenone (data not shown in Fig. 2A). Thus, rotenone-induced mitochondrial stress promotes the relocalization of GRIM-19 within the cell, which can be abrogated by expression of the HCMV β2.7 transcript.

We next tested whether this effect on GRIM-19 relocalization was due to a physical interaction between the GRIM-19 protein and β2.7 RNA during infection. β2.7 RNA was specifically immunoprecipitated from infected cells with an antibody to GRIM-19 (Fig. 2B). We also observed an interaction with native complex I, which is found only on the inner mitochondrial membrane, suggesting that the interaction between β2.7 RNA and GRIM-19 targets complex I in mitochondria. No immunoprecipitation of a similarly abundant viral RNA (UL32 in Fig. 2, B and C) with GRIM-19, complex I, or complex V (Fig. 2C) was observed. As expected, analyses using the Δβ2.7Tol virus showed no β2.7-specific polymerase chain reaction (PCR) band (Fig. 2D).

In a reciprocal analysis, we captured β2.7 RNA with the use of biotin-labeled oligonucleotide probes (Fig. 2E). Immunoprecipitations (IPs) of the β2.7-captured complexes did contain GRIM-19 (Fig. 2F). Thus, β2.7 RNA specifically interacts with GRIM-19, but with few other proteins in vivo.

The observed physical interaction with GRIM-19 and complex I was investigated further. Active complex I supports the formation of an electrochemical gradient ($\Delta\Psi_M$) across the inner mitochondrial membrane, which is imperative for the efficient production of adenosine triphosphate (ATP) (*16*). Expression of β2.7 RNA during infection or transfection protected $\Delta\Psi_M$ stability from rotenone (fig. S3, A and B), suggesting that the β2.7 RNA interaction with complex I could affect mitochondrial energy production under oxidative stress after infection. Previous data have shown

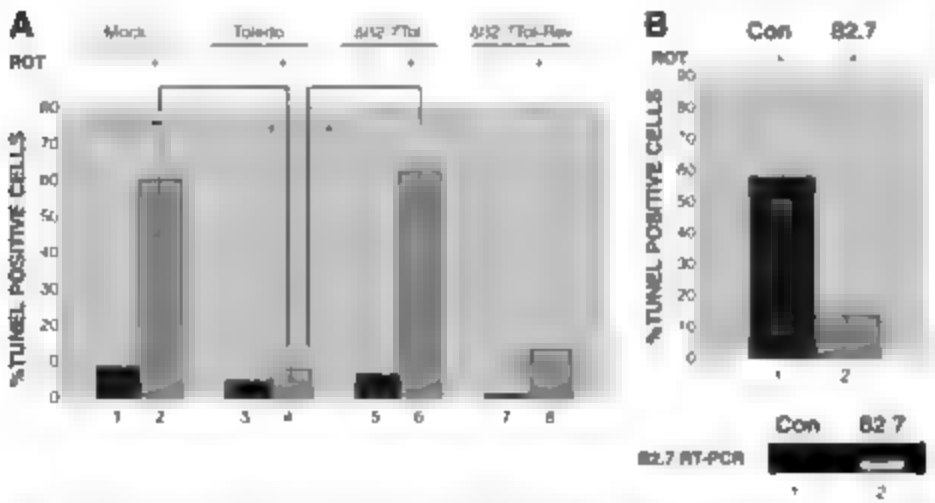

Fig. 1. HCMV protects cells from rotenone-induced apoptosis. (**A**) Percentage of TUNEL-positive cells in mock (1 and 2), Toledo- (3 and 4), Δβ2.7Tol- (5 and 6), and Δβ2.7Tol-Revertant (Δβ2.7Tol-Rev)–infected (7 and 8) U373 cells incubated with acetone (1, 3, 5, and 7) or rotenone (ROT) (2, 4, 6, and 8). $n = 3$ independent experiments. Asterisks denote $P < 0.01$ with Student's *t* test. Error bars indicate 1 SEM. (**B**) Percentage of TUNEL-positive pREP10- (Con) (1) and pREP10-β2.7–transfected (2) cells incubated with rotenone, from three independent analyses. Reverse transcription (RT)–PCR for β2.7 expression in pREP10- (lane 1) and pREP10-β2.7–transfected (lane 2) cells is shown.

that, unlike in herpes simplex virus (17), ATP levels in HCMV-infected cells are maintained at 24 hpi (19), a requirement probably attributable to HCMVs' comparatively protracted growth phase (19). We therefore analyzed the role of β2.7 in ATP production.

Rotenone substantially reduced ATP production in U373 cells (75% reduction, I and J in Fig. 3A). However, in Toledo-infected cells, only a 1.2-fold reduction was observed (84 to 67% in Fig. 3A), suggesting that HCMV protected ATP production in infected cells. In Δβ2.7Tol-infected cells, rotenone treatment resulted in a 2.5-fold depletion of intracellular ATP (77 to 33% in Fig. 3A). At 6 hpi, before β2.7 RNA expression, no protection from rotenone-induced ATP depletion occurred (fig. S4). Using a second strain of HCMV AD169 that encodes two copies of the β2.7 gene, we eliminated the possibility that green fluorescent protein (GFP) expression from the β2.7 gene locus would have a phenotypic effect because a recombinant AD169 virus still expressing GFP and one functional copy of the β2.7 gene maintained ATP levels (Fig. 3A). Thus, the β2.7 transcript is important for maintaining ATP production.

We hypothesized that the impact of β2.7 expression on ATP production may be more profound at later times of infection. Analysis in the absence of rotenone showed that ATP levels in Δβ2.7Tol dropped significantly ($P < 0.01$) at 5 days post infection (dpi), in direct contrast with Toledo-infected cells. Confirmation that the difference was not an artifact of GFP production was performed with the AD169-GFP infected cells, in which the levels of ATP were comparable to those of the parent virus AD169 (Fig. 3B).

Deletion of the viral β2.7 gene from HCMV has no significant effects on growth kinetics in fibroblasts (5) (Fig. 4A). At first, this appears to be contradictory; however, fibroblasts are particularly resistant to the induction of apoptosis by rotenone and oxidative stress (20), as compared with neuronal cells (21). However, a Δβ2.7Tol growth defect was observed when compared with the Toledo virus (Fig. 4B), which was more profound in the presence of rotenone (Fig. 4B), as is entirely consistent with the β2.7 transcript supporting virus production at times of metabolic stress. Tissue culture was performed in glucose-enriched media, and fibroblasts, particularly in times of diminished ATP production from the electron transport

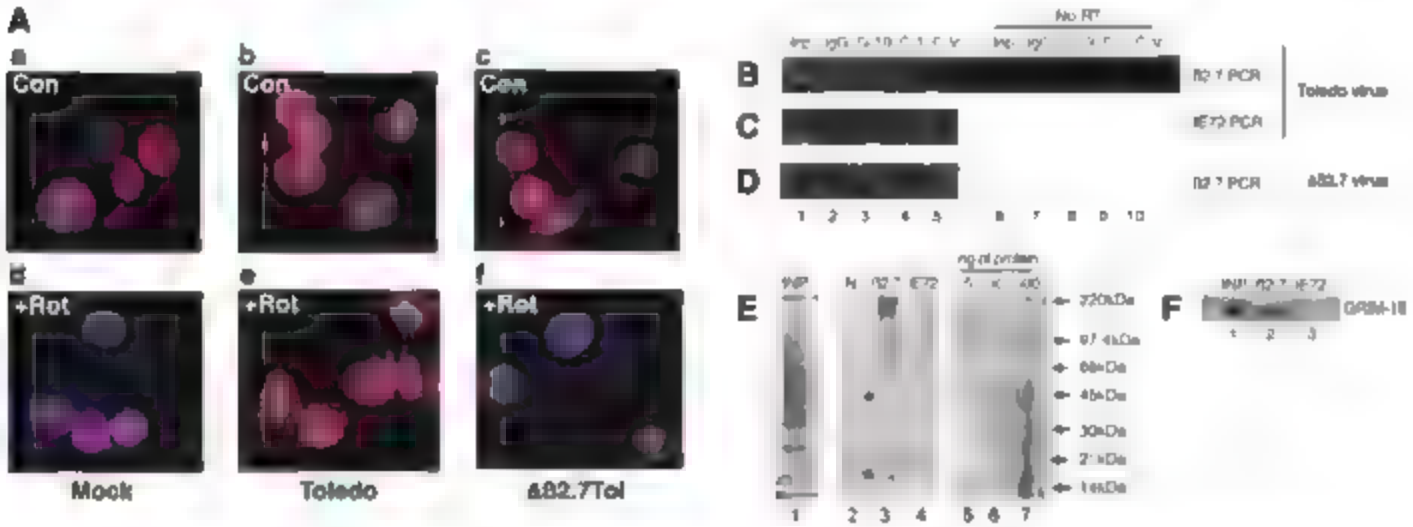

Fig. 2. HCMV interacts with and prevents the rotenone-induced relocalization of GRIM-19 in virally infected cells. (**A**) GRIM-19 localization (red) in mock- (a and d), Toledo- (b and e), and Δβ2.7Tol-infected (c and f) U373 cells incubated with solvent control (Con) (a, c, and e) or rotenone (b, d, and f) 24 hpi. (**B** to **D**) Immunoprecipitation of control immunoglobulin G (lane 2), GRIM-19 (G-19) (lane 3), native complex I (C-I) (lane 4), and native complex V (C-V) (lane 5) from Toledo- (B and C) or Δβ2.7Tol-infected (D) cells, and RT-PCR for β2.7 [(B) and (D), lanes 1 to 5], IE72 (C), or a β2.7 PCR with no prior RT [(B), lanes 6 to 10]. Inputs are shown in lane 1. (**E**) IPs on Toledo-infected cells with anti-sense oligonucleotides to β2.7 (lane 3) or IE72 (lane 4) or with no oligonucleotide (N) (lane 2). Silver stain of 1% input (INP) (lane 1), the immunoprecipitated proteins (lanes 2 to 4), and known protein loading controls (5 to 500 ng, lanes 5 to 7) is shown. (**F**) GRIM-19 expression in 10% input (lane 1) and the β2.7 (lane 2) and IE72 (lane 3) RNA-IP samples.

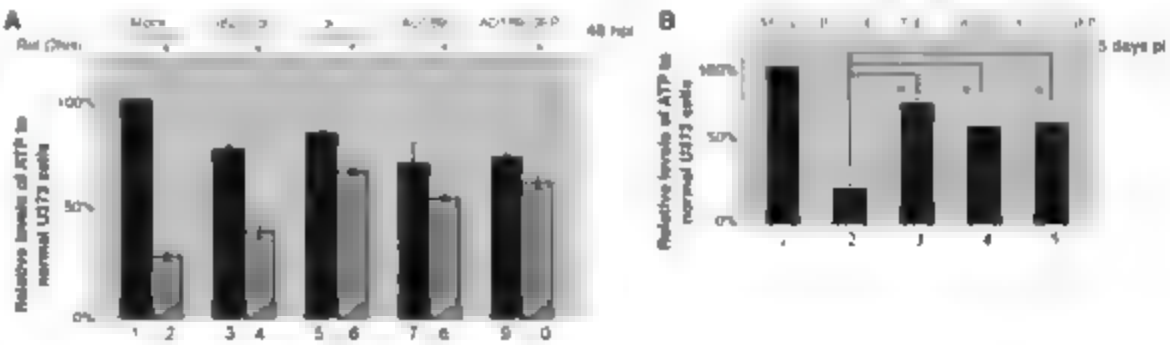

Fig. 3. β2.7 expression maintains ATP production in infected cells. (**A**) Percentage of ATP content of mock- (1 and 2), Δβ2.7Tol- (3 and 4), Toledo- (Tol) (5 and 6), AD169- and AD169-GFP–infected cells with (2, 4, 6, 8, and 10) or without (1, 3, 5, 7, and 9) rotenone for 2 hours was determined at 48 hpi, as compared to mock (1). (**B**) Percentage of ATP in mock- (1), Δβ2.7Tol- (2), Toledo- (3), AD169- (4), or AD169-GFP–infected cells (5) 5 dpi. $n = 3$ independent experiments. Asterisks denote $P < 0.01$ with Student's t test. Error bars indicate 1 SEM.

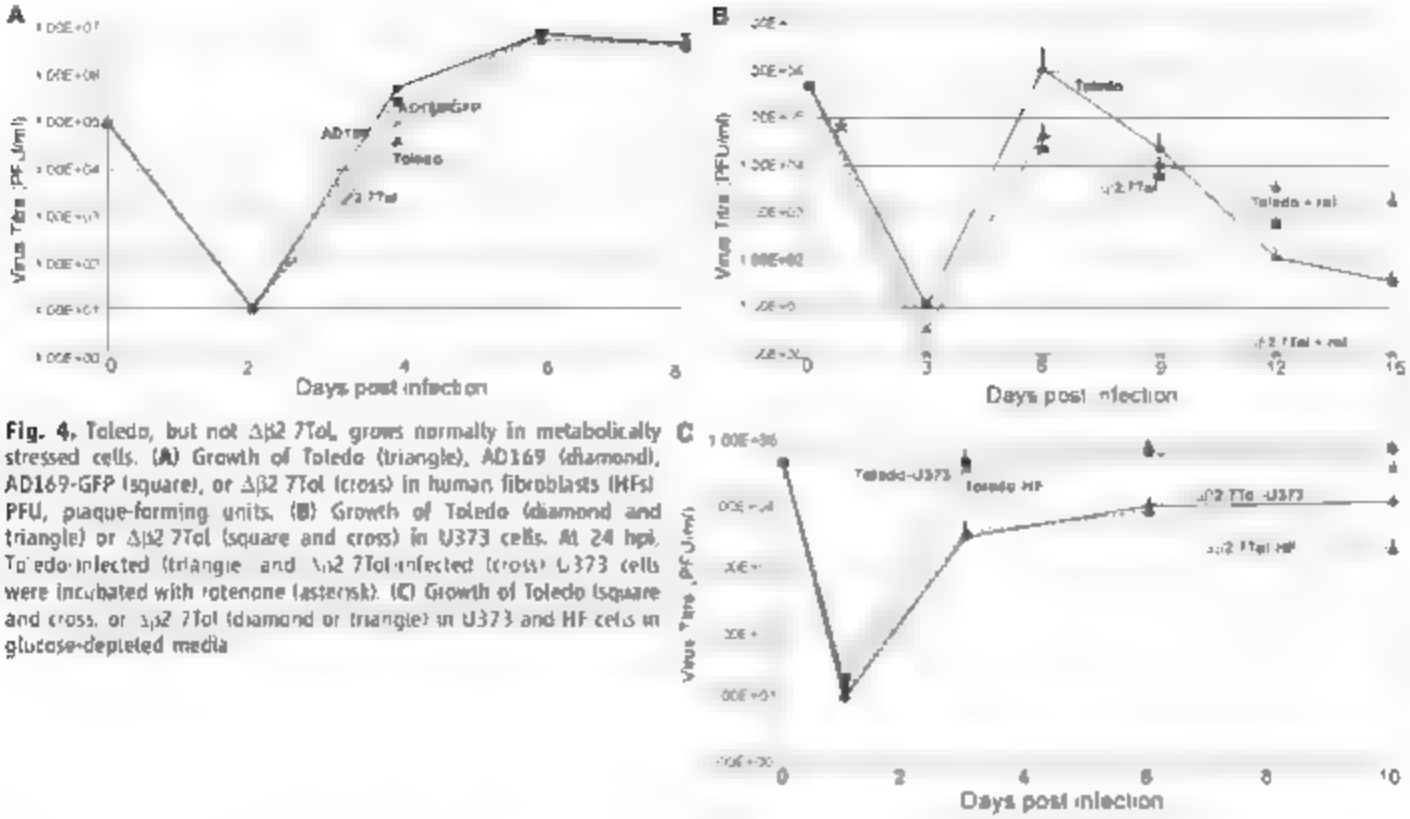

Fig. 4. Toledo, but not Δβ2.7Tol, grows normally in metabolically stressed cells. (**A**) Growth of Toledo (triangle), AD169 (diamond), AD169-GFP (square), or Δβ2.7Tol (cross) in human fibroblasts (HFs). PFU, plaque-forming units. (**B**) Growth of Toledo (diamond and triangle) or Δβ2.7Tol (square and cross) in U373 cells. At 24 hpi, Toledo-infected (triangle and Δβ2.7Tol-infected (cross) U373 cells were incubated with rotenone (asterisk). (**C**) Growth of Toledo (square and cross, or Δβ2.7Tol (diamond or triangle) in U373 and HF cells in glucose-depleted media.

chain (ETC), use this additional glucose to generate ATP via alternate pathways (22). We observed that glucose-depleted media impaired the growth of the Δβ2.7Tol virus in U373 and fibroblast cells, as compared with Toledo (Fig. 4C). This finding correlated with a drop in ATP production in Δβ2.7Tol-infected fibroblasts (fig. S5A) and the relocalization of GRIM-19 in Δβ2.7Tol-infected, but not Toledo-infected, cells (fig. S5B). Because cells in vivo are not exposed to such artificially high levels of glucose and are more reliant on the ETC for ATP production, the effects of β2.7 expression in vivo on metabolism are probably more overt than they are during tissue culture.

Metabolic dysfunction, the breakdown of mitochondrial integrity, and the release of pro-apoptotic stimuli are hallmarks of mitochondria-induced apoptosis (23). HCMV targets complex I for degradation promoting apoptosis (24), presumably by promoting the formation of reactive oxidative species. Because of the pivotal nature of mitochondria in cell death, it is not surprising that HCMV targets mitochondria function and makes a concerted effort to subvert the apoptotic response including UL36 (caspase inhibitor), UL37x1 (a B cell lymphoma 2 homolog with profound anti-apoptotic activity) (25, 26), and UL38, which protects infected cells from endoplasmic reticulum stress (27). UL37x1 is also known to promote mitochondrial membrane stability (26) and is predominantly active at late times of infection (~48 hpi) (28). In contrast, the β2.7 gene RNA is expressed much earlier during infection (~8 hpi); consequently, it is likely that HCMV has evolved multiple functions in order to hijack the mitochondria in the cell to enable continued energy production, as well as protection from cell death.

An intriguing aspect of this study is that an RNA molecule is used directly to exert these effects. Although at first appearing unusual, this may represent a highly refined viral strategy. First, because of the sheer numbers of mitochondria within the cell, the expression of a highly abundant RNA allows the virus to saturate these organelles effectively. Second, by dispensing of the need to translate the super-abundant β2.7 RNA, the virus can achieve this effect more quickly throughout the course of infection.

References and Notes

1. J. G. Stevens, M. Barr, M. R. Wills, *J. Infect.* **44**, 73 (2002).
2. D. H. Spector, *Intervirology* **39**, 361 (1996).
3. P. J. Greenaway, G. W. Wilkinson, *Virus Res.* **7**, 17 (1987).
4. J. M. Goaw, R. F. Greaves, *J. Virol.* **76**, 4441 (2002).
5. R. P. McSharry, P. Tamarac, M. L. Neale, G. W. Wilkinson, *J. Gen. Virol.* **84**, 2511 (2003).
6. G. K. Simon, D. R. Johns, *Annu. Rev. Med.* **50**, 111 (1999).
7. D. R. Green, G. Kroemer, *Science* **305**, 626 (2004).
8. M. Li *et al.*, *J. Biol. Chem.* **278**, 8516 (2003).
9. Materials and methods are available as supporting material on *Science* Online.
10. T. F. Singer, *Methods Enzymol.* **55**, 454 (1979).
11. G. Huang *et al.*, *Mol. Cell. Biol.* **24**, 8447 (2004).
12. L. Hertel, E. S. Mocarski, *J. Virol.* **78**, 11988 (2004).
13. J. E. Angell, D. J. Lindner, P. S. Shapiro, E. R. Hofmann, O. V. Kalvakolanu, *J. Biol. Chem.* **275**, 33416 (2000).
14. C. Lafer *et al.*, *EMBO J.* **22**, 1325 (2003).
15. A. L. McCormick, V. L. Smith, D. Chow, E. S. Mocarski, *J. Virol.* **77**, 631 (2003).
16. D. D. Newmeyer, S. Ferguson-Miller, *Cell* **112**, 481 (2003).
17. T. Murata *et al.*, *J. Gen. Virol.* **81**, 401 (2000).
18. W. E. Crowe, L. M. Maglova, P. Ponka, J. M. Russell, *Am. J. Physiol. Cell Physiol.* **287**, C1023 (2004).
19. K. M. Fish, C. Soderberg-Naucler, L. K. Mills, S. Stenglein, J. A. Nelson, *J. Virol.* **72**, 5661 (1998).
20. C. P. Baines *et al.*, *Nature* **434**, 658 (2005).
21. J. Li *et al.*, *J. Neurochem.* **92**, 482 (2005).
22. B. V. Chernyak, O. Y. Pletjushkina, D. S. Izyumov, K. G. Lyamzaev, A. V. Avetisyan, *Biochemistry (Moscow)* **70**, 240 (2005).
23. A. Eckert *et al.*, *Biochem. Pharmacol.* **66**, 1627 (2003).
24. J. S. Ladha, M. K. Tripathy, D. Mitra, *Cell Death Differ.* **12**, 1417 (2005).
25. A. Skaletskaya *et al.*, *Proc. Natl. Acad. Sci. U.S.A.* **98**, 7829 (2001).
26. V. S. Goldmacher *et al.*, *Proc. Natl. Acad. Sci. U.S.A.* **96**, 12536 (1999).
27. S. Terhune *et al.*, *J. Virol.* **81**, 3109 (2007).
28. M. Reboredo, R. F. Greaves, G. Hahn, *J. Gen. Virol.* **85**, 3555 (2004).

29. The authors thank L. Teague for excellent technical assistance and S. Brown for assistance with some of the preliminary studies. This study was funded by the Wellcome Trust.

Supporting Online Material

www.sciencemag.org/cgi/content/full/316/5829/1345/DC1

Figs. S1 to S5
References

26 March 2007; accepted 23 April 2007
10.1126/science.1142984

Regulation of CD8⁺ T Cell Development by Thymus-Specific Proteasomes

Shigeo Murata,[1,2]* Katsuhiro Sasaki,[1] Toshihiko Kishimoto,[3,4] Shun-ichiro Niwa,[5] Hidemi Hayashi,[3,5] Yousuke Takahama,[6] Keiji Tanaka[1]

Proteasomes are responsible for generating peptides presented by the class I major histocompatibility complex (MHC) molecules of the immune system. Here, we report the identification of a previously unrecognized catalytic subunit called β5t. β5t is expressed exclusively in cortical thymic epithelial cells, which are responsible for the positive selection of developing thymocytes. Although the chymotrypsin-like activity of proteasomes is considered to be important for the production of peptides with high affinities for MHC class I clefts, incorporation of β5t into proteasomes in place of β5 or β5i selectively reduces this activity. We also found that β5t-deficient mice displayed defective development of CD8⁺ T cells in the thymus. Our results suggest a key role for β5t in generating the MHC class I–restricted CD8⁺ T cell repertoire during thymic selection.

Proteasomes are multicatalytic proteinase complexes that are responsible for regulated proteolysis in eukaryotic cells and essential for the generation of antigenic peptides presented by major histocompatibility complex (MHC) class I molecules of the immune system in jawed vertebrates (*1*). Proteolysis is conducted by 20S proteasomes, which are large complexes composed of 28 subunits arranged as a cylinder in four heteroheptameric rings: α_{1-7}, β_{1-7}, β_{1-7}, and α_{1-7}. Among these, the three subunits called β1, β2, and β5 perform the catalytic function. In vertebrates, three additional β1i, β2i, and β5i subunits are induced by interferon (IFN)-γ and are preferentially incorporated into proteasomes. These immunoproteasomes produce antigenic peptides more efficiently than do constitutive proteasomes, and they play an important role in the elimination of virus-infected and tumor cells by CD8⁺ T cells (*2*).

During a search for proteasome-related genes in a genome database (www.ensembl.org), we found a previously unrecognized gene product with high homology to β subunits of 20S proteasomes. The gene encoding it is located adjacent to the gene for β5, and the gene product is encoded by a single exon in both human and mouse genomes (fig. S1A). Orthologous genes are found specifically in vertebrates, implying that this gene emerged synchronously with genes involved in adaptive immunity, evolutionarily as did the immunoproteasomes (*2*). The expression of this gene was biased toward the thymus in an expressed sequence tag database (UniGene Mm.42809). Multiple sequence alignments showed that its putative active-site threonine residue was preceded by a propeptide that ends with a glycine residue, a hallmark of active β subunits (fig. S1B). The dendrogram and homologies among catalytic β subunits indicated its close relation with β5 and β5i (Fig. 1A and fig. S1C), and we therefore named this gene *β5t*, as a thymus-specific β5 family member. Northern blot analysis confirmed the exclusive transcription of β5t in the thymus (fig. S1D). Immunoblot analysis of various mouse organs, with the use of an antibody specific to β5t (anti-β5t), further confirmed that the expression was thymus-specific (Fig. 1B). In comparison, β5t was predominantly expressed in a broad range of immune tissues (including the thymus and spleen) and to a lesser extent in lung and liver), and it further differed from the wide distribution of β5 (Fig. 1B).

We next examined how β5t is incorporated into proteasomes. Thymic extracts were immunoprecipitated with an antibody to the 20S proteasome (anti-20S), (cross-specific for all 20S proteasomes) and with anti-β5t. These antibodies coimmunoprecipitated 20S proteasomes and β5t, respectively (fig. S2A). Quantitative immunoblotting of α5, an invariable subunit of 20S proteasomes, revealed that ~20% of the 20S proteasomes in the thymus contain β5t (fig. S2B), β5 and β5i were barely detected in the β5t-containing proteasomes, indicating that β5t was incorporated into 20S proteasomes in place of β5 or β5i (Fig. 1C). Moreover, the IFN-γ inducible subunits β1i and β2i were preferentially incorporated into the β5t-containing proteasomes, in

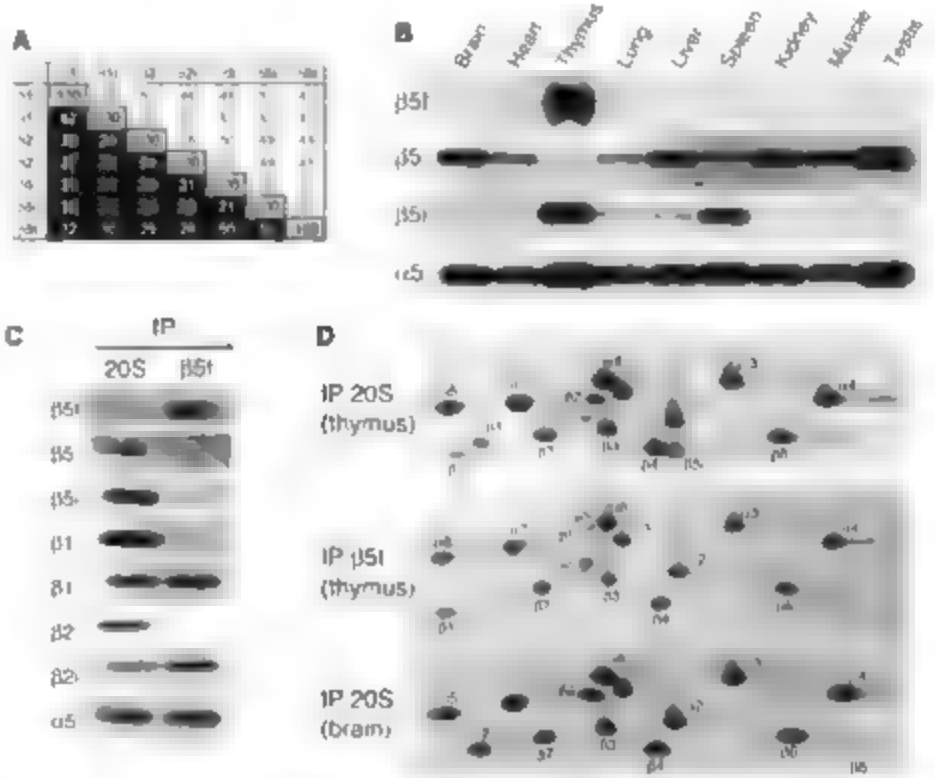

Fig. 1. β5t is a catalytic proteasome subunit in the thymus. (**A**) Percentages of amino acid sequence identities (boxed in black) and similarities (white box) among primary structures of mouse catalytic subunits obtained with the BLAST2 program (*28*). (**B**) Immunoblot analysis of various tissues of 3-week-old mice with the indicated antibodies. (**C**) Extracts of mouse thymus were immunoprecipitated with anti-20S or anti-β5t, followed by immunoblotting with the indicated antibodies. IP, immunoprecipitation. (**D**) 2D-PAGE analysis of samples in (C) with Coomassie staining. 20S proteasomes of brain extracts represent constitutive proteasomes. All spots were identified by tandem mass spectrometry. One of the β5t spots (represented by arrows) overlaps with that of α6.

[1]Laboratory of Frontier Science, Core Technology and Research Center, Tokyo Metropolitan Institute of Medical Science, Bunkyo-ku, Tokyo 113-8613, Japan. [2]Precursory Research for Embryonic Science and Technology, Japan Science and Technology Agency, Kawaguchi, Saitama 332-0012, Japan. [3]Proteome Analysis Center, Faculty of Science, Toho University, Funabashi, Chiba 274-8510, Japan. [4]Department of Biomolecular Science, Faculty of Science, Toho University, Funabashi, Chiba 274-8510, Japan. [5]Link Genomics, Chuo-ku, Tokyo 103-0024, Japan. [6]Division of Experimental Immunology, Institute for Genome Research, Graduate School of Medical Science, University of Tokushima, Tokushima 770-8503, Japan.

*To whom correspondence should be addressed. E-mail: smurata@rinshoken.or.jp

place of constitutive subunits β1 and β2 (Fig. 1C). The above findings were further confirmed by analysis of the precipitated products by two-dimensional polyacrylamide gel electrophoresis (2D-PAGE) (Fig. 1D). Spots for [illegible] and β5 were separately detected in the β5t-containing proteasomes, whereas spots for β5t emerged together with those for β1 and β2 (Fig. 1D, middle). We therefore propose to call this distinct subtype of proteasomes "thymoproteasomes."

Proteasomes are responsible for the production of MHC class I binding peptides and the sole enzymes that determine the C terminus of the peptides (*7*, *8*). Previous crystal structural studies of MHC class I complexes have revealed that the hydrophobic C-terminal anchor residues of the peptides are essential for high-affinity peptide binding into the clefts of MHC class I complexes (*9*). Some types of MHC molecules prefer basic C termini (*1*). The 20S proteasomes have at least three types of peptidase activities (chymotrypsin-like, trypsin-like, and caspase-like activities), which cleave peptide bonds after hydrophobic, basic, and acidic amino acids, respectively (*10*). The specificity is determined by the nature of the amino acids that compose the so-called S1 pocket (*11*, *12*). For the production of high-affinity MHC class I ligands, the chymotrypsin-like activity carried by β5 and β5t, whose S1 pockets are composed mostly of hydrophobic amino acids, is important (*13*). A comparison of the S1 pockets of the three β5 families revealed that the pocket of β5t is mainly composed of hydrophilic residues, in marked contrast to those of β5 and β5t (Fig. 2A), suggesting that thymoproteasomes have weaker chymotrypsin-like activity. To test this idea, we analyzed the peptidase activities of β5t-overexpressing cells, where ~90% of β5 was replaced by β5t (Fig. 2, B and C). We observed that the precursor forms of β5t were processed into mature forms after incorporation into 20S and 26S proteasomes (Fig. 2B, bottom left). In β5t-expressing cells, the chymotrypsin-like activity was exclusively reduced by 60 to 70%, without affecting the other two activities in both 20S and 26S fractions (Fig. 2B). Kinetic analysis of the chymotrypsin-like activity revealed that β5t reduced both the maximum velocity and the Michaelis constant values for the activity (Fig. 2D), which is opposite to the effect that β5 has on these quantities (*14*). However, these cells still possessed normal protein-degrading activity, as assessed by the

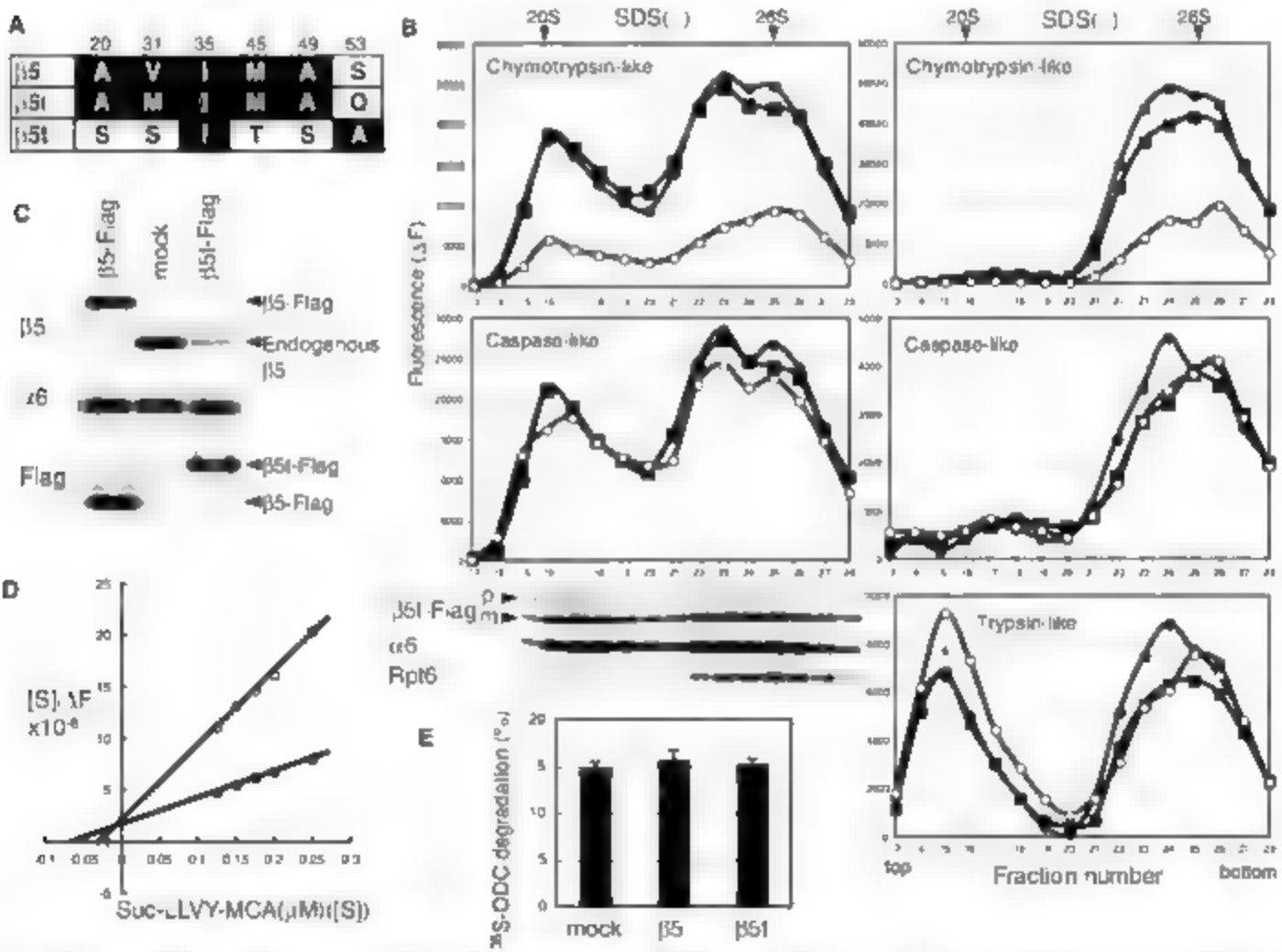

Fig. 2. β5t selectively reduces the chymotrypsin-like activity of proteasomes. (**A**) Alignment of amino acid residues organizing the S1 pockets of β5 families. The hydrophobic and hydrophilic amino acid residues are boxed in black and white, respectively. The numbers represent the position from the active-site threonine. (**B**) Peptidase activities of human embryonic kidney–293 T cells expressing human β5t-Flag (open circles), β5-Flag (black squares), or mock cells (black circles) in the presence (left) and absence (right) of 0.025% SDS. Arrowheads indicate the peak locations of 20S proteasomes and 26S proteasomes, proven by immunoblot analysis of each fraction (bottom left). p, precursor; m, mature; asterisk, nonproteasomal activity. (**C**) Fraction numbers 25 in (B) were immunoblotted for β5, α6, and Flag. (**D**) Hanes-Woolf plots for chymotrypsin-like activity of 26S proteasomes (pools of fraction numbers 24 to 26) from mock cells (black circles) and β5t cells (open circles). Suc-LLVY-MCA, succinyl-Leu-Leu-Val-Tyr-4-methylcoumaryl-7-amide; [S], substrate concentration. (**E**) Cell extracts from (B) were assayed for adenosine triphosphate–dependent protein degradation activity using ^{35}S-labeled ODC. Mean ± SD; $n = 3$ experiments.

degradation of ornithine decarboxylase (ODC) (Fig. 2E) (15).

The thymus is responsible for generating a T cell repertoire that specifically recognizes self-peptide MHC (self-pMHC) complexes and tolerates self-antigens. Thymic stromal cells represent a heterogeneous mixture of cell types and provide a proper microenvironment for developing thymocytes (16, 17). To identify a cell type that expresses β5t, we ran immunostaining sections of mouse thymus for β5t and markers for thymic stromal cells (Fig. 3, A and B). β5t was exclusively expressed in the thymic cortex, which is quite similar to the expression of Ly51, a marker for cortical thymic epithelial cells (cTECs). The distribution of β5t was distinct from that of cells that bind to *Ulex europaeus* agglutinin I (UEA-I), a marker for medullary TECs (mTECs), CD11c, a marker for dendritic cells, and MTS 5, a marker for fibroblasts (Fig. 3A) (16, 18). A magnified image of the cortex revealed that the reticular staining pattern of β5t is nearly identical to that of Ly51, indicating that β5t is exclusively expressed in cTECs (Fig. 3B).

To confirm this conclusion, different cell populations of the thymus were isolated. Immunoblot analysis demonstrated that β5t is specifically expressed in Ly51-positive cells and is not detected in any other stromal cells or in CD45$^+$ cells that are mostly composed of thymocytes (Fig. 3C). A comparison of Ly51-positive cells with mouse embryonic fibroblasts that were treated with or without IFN-γ [in which almost all the proteasomes are immuno- and constitutive proteasomes, respectively (19)] revealed that the majority of proteasomes in cTECs were thymoproteasomes containing β5t, together with β1i and β2i. Also, the expression levels of β5 and β5i were markedly down-regulated in cTECs (Fig. 3D).

To clarify the physiological role of β5t, we generated β5t-deficient mice. The β5t-coding sequence was substituted for cDNA encoding the protein Venus to identify β5t-expressing cells (Fig. 4A). The loss of β5t proteins in the β5t$^{-/-}$ thymus and the expression of Venus in the β5t$^{+/-}$ and β5t$^{-/-}$ thymuses were confirmed by immunoblotting (Fig. 4B). An inspection of β5t$^{+/-}$ and β5t$^{-/-}$ mice with fluorescence demonstrated that the expression of Venus (i.e., β5t) was limited to the cortex of the thymus with a reticular pattern similar to that of cTECs (Fig. S1, A to C). Cortical and medullary architectures as well as the size of the thymuses in β5t$^{-/-}$ mice were indistinguishable from those of β5t$^{+/+}$ mice (Fig. S1, B and C). When thymic stromal cells from β5t$^{-/-}$ mice were analyzed by flow cytometry, all Venus-expressing cells were MHC class II I-A^b positive (Fig. 4C). Furthermore, we examined the relationship between Venus and Ly51 expression in the I-A^b positive population (Fig. 4D). We identified three distinct populations. Among them, the Venus$^+$Ly51$^+$ population was the largest, constituting 50% of I-A^b positive cells. There was a smaller population of Venus$^+$Ly51$^-$ that constituted 11% of I-A^b positive cells. These results demonstrate that all β5t-expressing cells are I-A^{b+}Ly51$^+$ cTECs and that this population makes up ~80% of cTECs.

It has been suggested that cTECs are mainly responsible for positive selection by presenting ligands on MHC molecules to CD4$^+$CD8$^+$ double-positive (DP) thymocytes (17, 18). We therefore examined how β5t is involved in the function of cTECs. Flow cytometry analysis of thymocytes revealed that β5t deficiency was associated with a markedly low percentage of CD8$^+$ single-positive (SP) thymocytes but not with the percentage of CD4$^+$ SP thymocytes (Fig. 4E). A small proportion (8.7%) of wild-type (WT) CD8$^+$ SP thymocytes expressed high levels of T cell receptor β (TCRβ), resembling positively selected cells (Fig. 4F, left) (20). In contrast, a much smaller proportion (~0.2%) of CD8$^+$ SP thymocytes expressed high levels of TCRβ in β5t$^{-/-}$ mice (Fig. 4F, right), suggesting that many of the CD8$^+$ SP thymocytes of β5t$^{-/-}$ mice were immature thymocytes that are transitory intermediates between double-negative (DN) and DP thymocytes (21). Consequently, the ratio of CD4$^+$ SP cells to CD8$^+$ SP cells in β5t$^{-/-}$ mice was markedly higher than that in WT mice (Fig. 4G). The ratio was also significantly elevated in β5t$^{+/-}$ mice, although the difference was much smaller (Fig. 4G). Total numbers of DN, DP, and CD4$^+$ SP thymocytes in β5t$^{-/-}$ mice were nearly identical to those of β5t$^{+/+}$ and WT mice. However, a significantly low total number of CD8$^+$ SP thymocytes was observed in β5t$^{-/-}$ mice (Fig. 4H). Selective reduction of CD8$^+$ SP T cells was also observed in TCRβ$^+$ splenocytes of β5t$^{-/-}$ mice

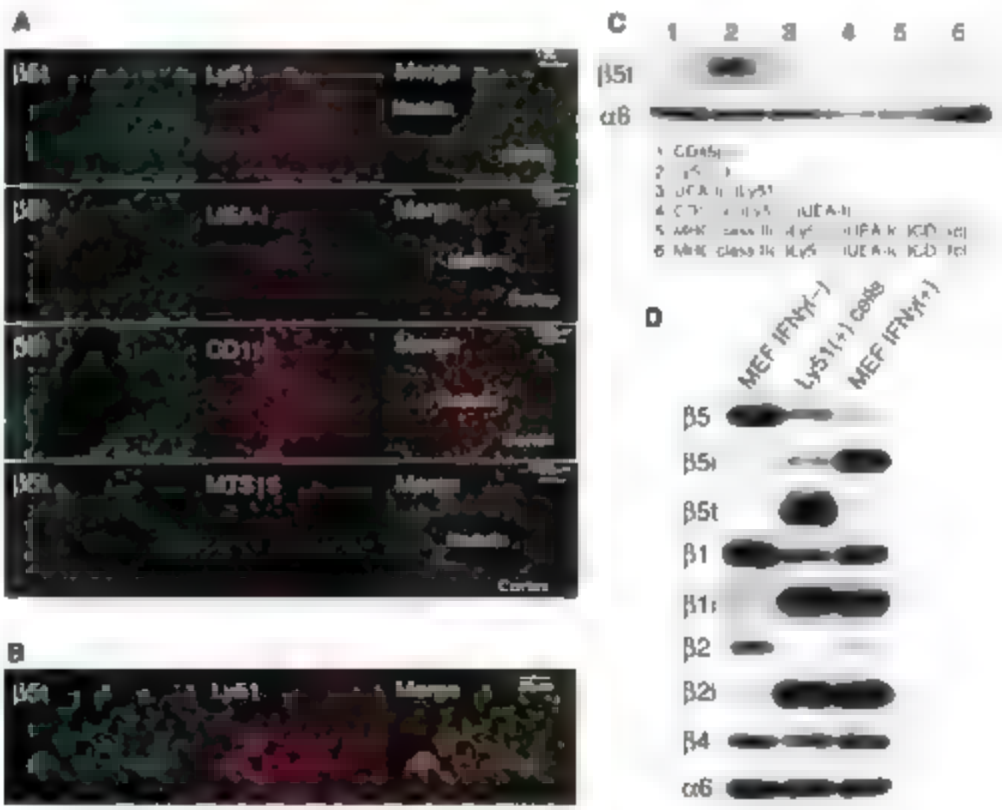

Fig. 3. β5t is specifically expressed in cTECs. (**A** and **B**) Cryosections of mouse thymus were immunostained for β5t, together with Ly51, UEA-I, CD11c, or MTS15. (**C**) Various populations of cells from the thymus were immunoblotted for β5t and α6 (a loading control for proteasomes). (**D**) Contents of thymoproteasomes in Ly51-positive cells were analyzed by immunoblotting. MEF, murine embryonic fibroblast.

(Fig. 4, I and J). These results demonstrate that β5t is required for the development of CD8$^+$ T cells in the thymus and suggest the possibility that β5t deficiency is associated with defective positive selection of CD8$^+$ T cells.

During positive selection, DP cells that interact with self-pMHC complexes expressed on cTECs with sufficiently low affinity or avidity are rescued from intrathymic death and induced to differentiate into CD4 or CD8 SP thymocytes. The recognition of MHC class I molecules results in commitment to the CD8 lineage (*22*, *26*). In contrast, DP cells that interact with high affinity or avidity with self-pMHC complexes are eliminated by the induction of apoptosis (*22*, *24*). To date, however, information about whether and how cTECs can offer specialized signals that are suitable for positive selection has been elusive. The present work demonstrates that β5t, which is specifically expressed in cTECs, plays a pivotal role in the development of CD8$^+$ T cells. What, then, is the mechanism for CD8$^+$ T cell development regulated by β5t? The thymic architecture was apparently normal in β5t$^{-/-}$ mice (fig. S3, B and C), suggesting that β5t is not essential for the differentiation and proliferation of cTECs. Normal development of CD4 SP thymocytes observed in β5t$^{-/-}$ mice supports this argument. Surface expression levels of MHC class I on β5t$^{-/-}$ cTECs were also comparable to those of β5t$^{+/+}$ cTECs (fig. S4). It is assumed that other β5 family members (e.g., β5 and β5 subunits) are incorporated in place of β5t in cTECs

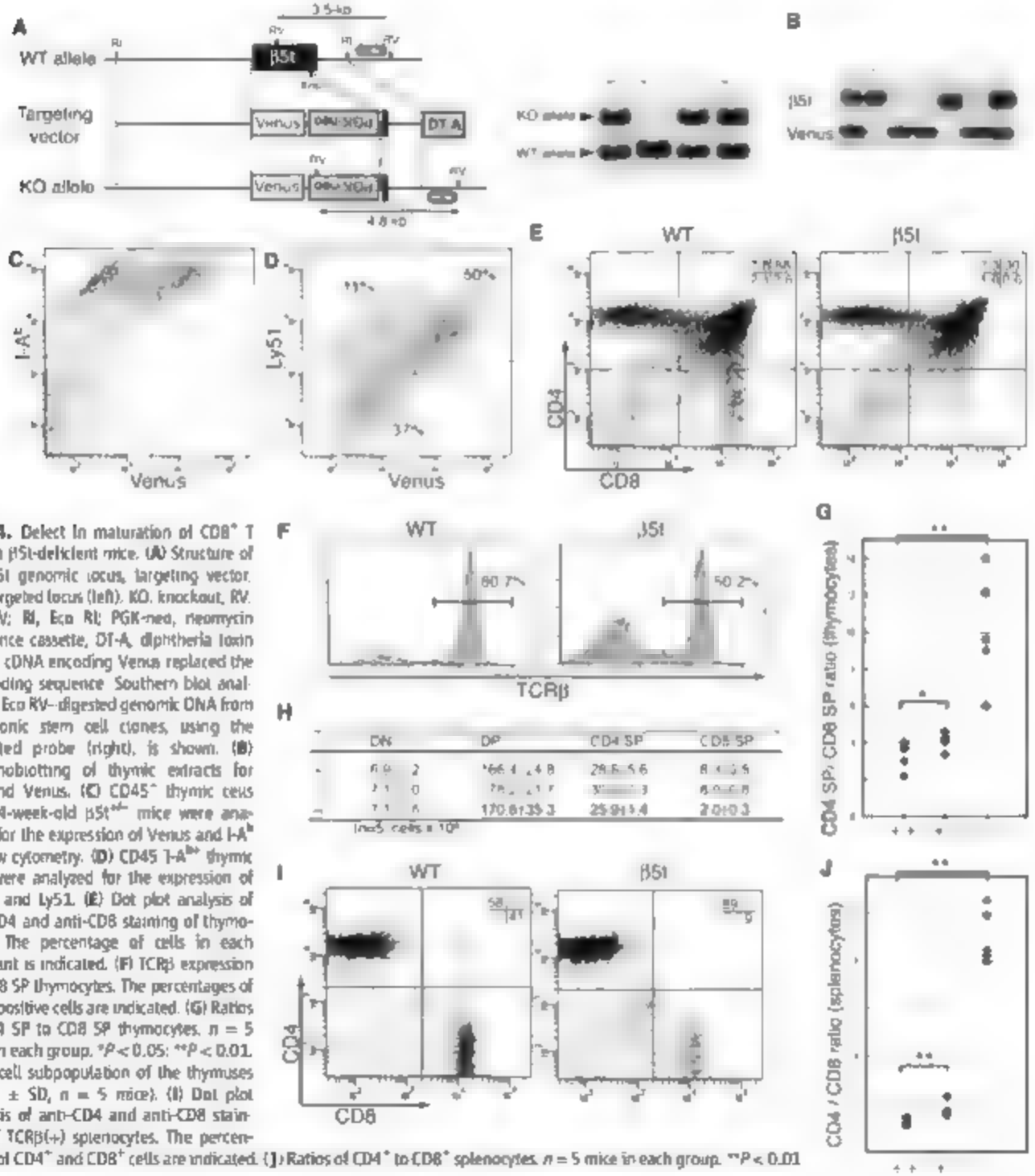

Fig. 4. Defect in maturation of CD8$^+$ T cells in β5t-deficient mice. (**A**) Structure of the β5t genomic locus, targeting vector, and targeted locus (left). KO, knockout; RV, Eco RV; RI, Eco RI; PGK-neo, neomycin resistance cassette; DT-A, diphtheria toxin A. The cDNA encoding Venus replaced the β5t coding sequence. Southern blot analysis of Eco RV–digested genomic DNA from embryonic stem cell clones, using the indicated probe (right), is shown. (**B**) Immunoblotting of thymic extracts for β5t and Venus. (**C**) CD45$^+$ thymic cells from 4-week-old β5t^{Ven} mice were analyzed for the expression of Venus and I-A^b by flow cytometry. (**D**) CD45 I-A^{bh} thymic cells were analyzed for the expression of Venus and Ly51. (**E**) Dot plot analysis of anti-CD4 and anti-CD8 staining of thymocytes. The percentage of cells in each quadrant is indicated. (**F**) TCRβ expression on CD8 SP thymocytes. The percentages of TCRβ-positive cells are indicated. (**G**) Ratios of CD4 SP to CD8 SP thymocytes. $n = 5$ mice in each group. $^*P < 0.05$; $^{**}P < 0.01$. (**H**) T cell subpopulation of the thymuses (mean ± SD, $n = 5$ mice). (**I**) Dot plot analysis of anti-CD4 and anti-CD8 staining of TCRβ(+) splenocytes. The percentages of CD4$^+$ and CD8$^+$ cells are indicated. (**J**) Ratios of CD4$^+$ to CD8$^+$ splenocytes. $n = 5$ mice in each group. $^{**}P < 0.01$

RNAi:
MICRORNA PACKS A WALLOP

MicroRNAs play a hitherto unsuspected, integral role in regulating gene expression. But their short length, sequence similarities, multiplicity of mRNA targets, and unpredictable pairing to those targets make studying them tricky. The good news: Methods for analyzing more familiar RNA species have been adapted for investigation of these extraordinary molecules and improved technologies are constantly becoming available. **By Bruce Goldman**

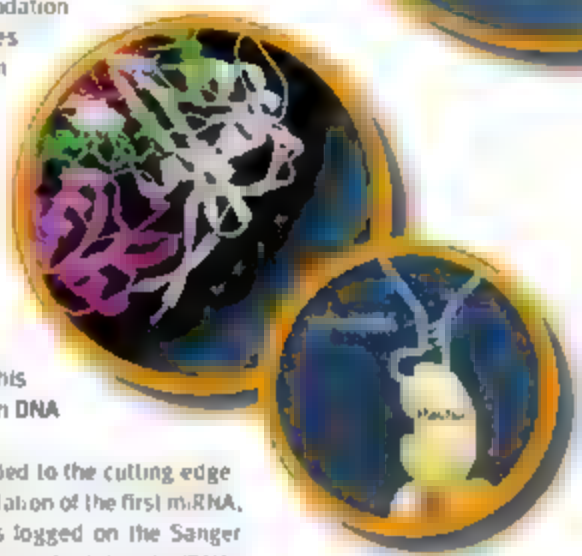

Wait! Stop. Don't toss out that small-RNA fraction just yet. It took researchers a while to break that habit. Tiny pieces of RNA were long thought to be mere degradation fragments of more important longer molecules. But it's now obvious that the famous formulation enshrined as the Central Dogma of Molecular Biology "DNA makes RNA makes proteins" is only partly true. Small noncoding RNAs called microRNAs (miRNAs), typically about 21 or 22 nucleotides in length, exert a powerful posttranscriptional regulatory influence. By binding to untranslated regions of messenger RNAs (mRNAs), miRNAs stall ribosomal output of the proteins encoded by the target mRNA, fine-tuning translation and on occasion, marking the target mRNA for degradation. Gregory Hannon at **Cold Spring Harbor Laboratory** and his colleagues recently reported findings implicating miRNA in **DNA** methylation, too.

From being regarded as an oddity, miRNA has proceeded to the cutting edge of biomedical research. After a sluggish start following isolation of the first miRNA, from *C. elegans* in 1993, the number of human miRNAs logged on the Sanger Institute's miRBase Sequences Database (a central repository of validated miRNAs in the public domain) has exploded in the past few years, and has now reached almost 500.

"Smart scientists that we are, we managed to miss this entire class of incredibly important regulatory molecules until the 21st century," says Eric Lader, associate director of research and development at **Qiagen**, a Germany-based supplier of nucleic acid sample preparation materials and polymerase chain reaction (PCR) kits.

But researchers are making up for lost time. While only four papers on miRNA were published as recently as 2001, last year the number exceeded 600. "The likely impact of miRNAs in mammalian biology is enormous," says Carl Novina, of the **Dana-Farber Cancer Institute**. "They play roles in differentiation and development, chromosomal segregation and division, cell type–specific functioning, metabolism, and apoptosis." Alterations of miRNA expression, Novina continues, have been correlated with numerous cancers and, at least in mice, with diabetes, sparking the investigation of miRNA as a potential diagnostic and therapeutic tool.

One reason for the field's accelerating advance: The tools were already mostly in place. "Over the last 20 years, an extraordinarily large number of really smart molecular biologists worked out every technique you could ever desire to study small RNAs while somehow scrupulously avoiding discovering too much about them, so that people of my generation would have something to do," marvels Philip Zamore, professor of biomedical sciences and biochemistry at the **University of Massachusetts School of Medicine** in Worcester.

> "We managed to miss this entire class of incredibly important regulatory molecules until the 21st century."

Cell Signaling 2 — June 22
Microarray Technologies — August 24
Genomics 2 — October 19

Inclusion of companies in this article does not indicate endorsement by either AAAS or Science, nor is it meant to imply that their products or services are superior to those of other companies.

IMAGES COURTESY OF KATHARINE SUTCLIFF/SCIENCE

Those tools did require some modification. Early RNA methodologies weren't optimized for ultrashort species such as miRNA, which got tossed out with the buffer solution. Nowadays, companies selling sample-preparation tools, such as Qiagen and **Ambion** (acquired last year by **Applied Biosystems**), offer kits adapted for isolating small RNAs.

Once you've found a given miRNA, figuring out which mRNAs it targets is nontrivial, at least in animals, as only six or seven of the 21 or 22 nucleotides in an miRNA sequence (the seed region) bind to their mRNA targets in a strict antisense fashion. This "fuzzy pairing," with the seed sequence dictating much, but not all, of binding strength, makes it hard to predict mRNA targets computationally—all the more so with the recent discovery that miRNA transcripts get "edited": Enzymatic nucleotide substitutions differentiate them from their DNA sense-strand progenitors.

Finding New miRNAs

The sequencing of the human genome and partial elucidation of miRNAs' structural features made it possible to do computational searches for nucleotide stretches that could fold into characteristic hairpin structures and are conserved across species lines. Unfortunately, the vast majority of computational hits were false positives.

Rosetta Genomics, an Israeli company that presciently began life with an miRNA focus in 2000, created a sophisticated algorithm that located some 11 million hairpin structures, eliminated most of them (those that are thermodynamically unstable, structurally suspect, or located on protein-coding sequences or in repetitive elements), and then filed patents on thousands of candidate miRNAs. Ronit Aharonov, executive vice president for intellectual property and computational biology, says Rosetta has internally validated many miRNAs not yet listed on the Sanger database. In a highly cited 2005 article, Rosetta Genomics scientists claimed that a significant number of these novel miRNAs are conserved among primates but not other mammals, and may therefore have played a major evolutionary role in the higher complexity of primates, including humans.

Massively parallel oligonucleotide sequencing now appears to be outstripping computational approaches for discovering novel miRNAs and is even unveiling entirely new realms of small RNAs. In the past year alone, groups led by David Bartel of **Whitehead Institute at MIT** and by Hannon at Cold Spring Harbor have used this methodology to discover two small RNA classes, each consisting of tens of thousands of members, whose defining features differ considerably from those of miRNA and from one another's.

454 Life Sciences, previously a Curagen subsidiary, was selling its sequencing instrument along with reagents via a marketing agreement with **Roche Diagnostics**, who has now purchased the company outright. Each sequencing run yields between 200,000 and 400,000 readouts of 100 to 250 nucleotides. A newer machine by **Solexa** (now owned by **Illumina**) can deliver up to 20 million short readouts of about 27 nucleotides. Although Solexa's device may truncate slightly longer small-RNA sequences—some species run 30 bases—Hannon, who has used both companies' instruments, says it usually provides enough information to identify a novel miRNA.

While the huge number of sequence readouts per run makes the per sequence cost ultracheap, a single run is still quite expensive. "You don't need a computer to figure out 99.9 percent of all the miRNAs in a human being," comments Zamore. "You just need a big budget."

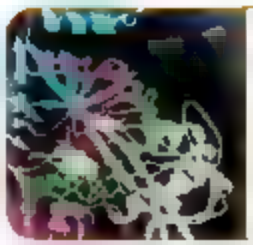

You don't need a computer to figure out 99.9 percent of all the miRNAs in a human being. You just need a big budget."

There is a feeling among those in the field that miRNA discovery, per se, is hitting the point of vanishing returns. "The numbers of new miRNAs we're detecting are diminishing," confirms Novina.

What's Different?

Meanwhile, expression profiling of miRNA molecules, once they're found, is a growth area. Microarray techniques for profiling RNA expression, which were quite advanced by the time the study of miRNA began, merely had to be adapted for use with smaller species. Planar arrays are ideal for comparing small numbers of samples for patterns of over- or underexpression of large numbers of miRNAs.

Ambion was one of the first companies to focus on the miRNA tools market. This company and its diagnostics-and-services spinoff, **Asuragen**, have licensed Rosetta Genomics' candidate miRNAs for their microarrays, which feature capture probes representing 13,349 sequences: several hundred of them from the public domain but the vast majority from Rosetta. Scott Hunicke Smith, vice president and general manager of Asuragen's service group, says, "You can update a database every month. But you can't update content on an array cost-effectively every month. We think most of the near-term future releases of the Sanger database will probably already be represented by these sequences." Based on its own preliminary initial validation studies (looking for expression in a small number of normal human tissues), Asuragen has already identified three to five times the number of miRNAs that show up in the Sanger database. Hunicke Smith thinks this multiple could go to as high as 10 when more tissues are examined.

Invitrogen is another big player in the miRNA-microarray space. Invitrogen's microarray methodology makes it easy to detect differences in miRNA expression between two samples—for example tumor versus normal tissue—whose respective miRNA fractions fluoresce simultaneously at different frequencies, thus allowing comparison of samples processed under identical conditions. Invitrogen sells the microarray itself, the labeling kit, and a real-time PCR kit for validating array data, says Invitrogen's research and development lead, Christopher Adams. In May 2006, Invitrogen launched a kit for specifically amplifying small RNAs. "A lot of people in the stem cell field don't have a lot of cellular material available—in some cases as few as 100 cells," Adams notes. "Evaluating miRNA expression in those circumstances can be a real challenge." The ultimate goal, he says, is to profile a single cell without any amplification or other manipulation.

For some academic laboratories, an alternative to buying arrays is to buy the probes and have them spotted onto arrays at their institutions' own facilities. One leading probe supplier is **Exiqon**, a Danish company that manufactures "locked nucleic acids" (LNAs). Unlike RNA, whose ribose backbone is quite flexible, continued >

Exiqon's synthetic oligonucleotide is chemically constrained, locking the probe's bases into a hybridization-friendly conformation. Whereas miRNAs' short size makes optimizing probe-melting temperatures tricky, individual LNAs' compositions can be modulated to give them very similar melting temperatures.

When a researcher doesn't need to look at the entire universe of known miRNAs, but rather wants to select a set of them for, say, exploring a diagnostic application, **Luminex** offers a new bead-based technology that can multiplex up to a thousand samples—less costly per run than microarrays—testing each against probes representing 320 miRNAs from the Sanger database. "The number of miRNAs that will turn out to be relevant for a particular condition may be 20, or 10, or five," says Keld Sorensen, director of research and development. "We expect scientists profiling miRNA for a particular medical condition to want to run large numbers of samples. If you have a thousand samples, you're going to want a multiplex system."

Unlike sequencing methodologies, hybridization techniques such as Luminex's confront the dual challenge posed by miRNAs' short sequences and the fact that they often cluster in families whose members may differ by as little as a single nucleotide. That doesn't leave much room for discrimination. To tell them apart, Luminex turned to Exiqon's capture probes, Sorensen says.

Time and Place

An miRNA's role in development practically guarantees that it will often exhibit transient or highly tissue-specific expression. Chemistries that increase the stringency of binding, as LNAs do, enhance in situ analysis, performed to locate cells or tissues where a particular miRNA is being expressed at a particular time in the developmental cycle.

If locating miRNAs is getting easier, finding out what they do there is still difficult. Attempts to learn about miRNA function usually boil down to painstaking, labor-intensive experimentation, says Bartel of Whitehead Institute. "You can use antisense reagents that will inhibit the miRNA," he says. "But because each miRNA has hundreds of targets, you'll still be at a bit of a loss as to what's the real mechanism for any effect you see." Also, while miRNA function can be transiently knocked down with standard or modified antisense or RNAi approaches, cell division dilutes such agents. Furthermore, different cell types vary in their susceptibility to transfection with these substances. "There's no good, universal, or conventional way of transfecting multiple, different cell lines," says Robert Setterquist, senior manager of research and development at Ambion. "Each of them has to be optimized. And once you get that worked out, you still may not be able to get good miRNA inhibition."

How Do miRNAs Work?

As the number of relevant miRNAs in humans approaches saturation, and as ever more of them are subjected to expression profiling and characterization within particular tissues or during various developmental stages and disease states, attention is turning to the thorny matter of target identification.

Typical computational approaches grossly overpredict the number of targets, as a random search of seven-nucleotide sequences will yield more than 500 hits, says Deepak Srivastava, director of the **Gladstone Institute of Cardiovascular Disease** in San Francisco. Srivastava hopes to soon make public a more sophisticated computational algorithm. "Only around 20 or so miRNA targets have been validated at the level of protein regulation. Virtually all of them have something in common. The target site in the mRNA is located in a stretch of RNA that is physically accessible to the miRNA." Srivastava's algorithm, in addition to searching the genome for spots amenable to binding to miRNA seed regions, also screens out DNA stretches whose transcripts would be likely to form secondary RNA structures rendering them inaccessible to a corresponding miRNA. Srivastava says this appears to significantly increase specificity, although perhaps at the expense of sensitivity.

Says Bartel, "Learning the biological function of particular miRNA-target interactions is certainly possible. But it's a lot of work. I don't see any way around it."

Complicating things, there can be several miRNA-binding sites on a single mRNA transcript. In a study published in early 2007, Bartel's group picked a target mRNA with not one but seven predicted binding sites for miRNA, all of which sat on a section of the molecule whose deletion, via a translocation in the corresponding gene, was known to be associated with oncogenesis in humans. To see if the loss of translational regulation by miRNA was indeed responsible, Bartel and his colleagues created point mutations in each of the mRNA's seven miRNA-target sites—and observed the same tumor phenotype. "You get the same results as if you had that translocation," he says. "That tells us that at least part of what's going on in those human tumors is the loss of suppression of that gene."

Bartel, who has long been out in front of the pack, says he's accustomed to inventing his own techniques, but "companies are making it a lot easier for people who haven't been working on miRNAs for the last six years."

A strong motive in any business, naturally, is to make money. But there are other incentives in play, not least intellectual ones. "When you find out some miRNA is 100-fold downregulated in an early cancer cell," says Lader of Qiagen, "and you know one miRNA could affect the expression of 100 genes, the allure of figuring out what's going on is powerful."

Bruce Goldman, a freelance science writer, lives in San Francisco.

Featured Participants

454 Life Sciences
www.454.com

Ambion
www.ambion.com

Applied Biosystems
www.appliedbiosystems.com

Asuragen
www.asuragen.com

Cold Spring Harbor Laboratory
www.cshl.edu

Dana-Farber Cancer Institute
www.dfci.harvard.edu

Exiqon
www.exiqon.com

Gladstone Institute of Cardiovascular Disease

University of California, San Francisco
www.ucsf.edu

Illumina
www.illumina.com

Invitrogen
www.invitrogen.com

Luminex
www.luminexcorp.com

MIT/Whitehead Institute
www.wi.mit.edu

Qiagen
www.qiagen.com

Roche
www.roche.com

Rosetta Genomics
www.rosettagenomics.com

Solexa
Solexa.com

University of Massachusetts, Worcester
www.umassmed.edu

Tissue Homogenizer

The benchtop Prece lys 24 is dedicated to the gr nding, lysis, and homogen zation of biologica samples It can handle difficult samples such as microorganisms and bacteria spores, ha d tissues such as teeth and bone, kidney, muscle, and hair, soi samples, plants, and more It can load up to 24 tubes simultaneously Protocols are flexible and easy to set Buffer and samples are added n 2 ml tubes prefilled with specific beads, either glass, ceramic, or meta The single-use tubes prevent cross contamination The high speed and spec fic motion guarantee homogeneous and eff cient grind ng for rep oducible, high-qua ity resu ts.

Bertin Technologies

For nformation +331 39 30 61 69

www.bert n.fr

Multi-blocking Oligonucleotides

The Multi-Blocking Morpholino oligonucleotides inhibit the activity of a targeted miRNA by blocking several steps of its maturation. The oligonucleotides inhibit that activity by sterically interfering with: Drosha cleavage of pri-messenger RNA, Dicer cleavage of pre-miRNA, loading of miRNA onto the RNA induced silenc ng complex (R SC), and recognition of miRNA targets by the miRNA strand on RISC. The strategy is to synthesize a 31-base Morpholino oligonucleotide that is complementary to the miRNA and extends one base over the flanking sequence past the Drosha cleavage site, with the balance of the bases extending into and complementary to the loop sequence. Because the loop contains many unpaired bases, the Multi-blocking Morpholino has many single-stranded bases available for nucleate pairing and strand invasion. The duplex portion of the miRNA sequence is not perfectly paired, favoring invasion of the miRNA sequence by the Multi-blocking Morpholino.

Gene Tools

For nformation 541 929 7840

www.gene too s com

miRNA Expression Analysis

A complete suite of reagents, instruments, and protocols is dedicated to the investigation of miRNAs by quantitative reverse transcription-polymerase chain reaction (qRT-PCR). The mirVana miRNA Isolation Kit, TaqMan miRNA RT Kit, TaqMan miRNA assays, and 7900HT Fast Real-Time PCR System provide a reliable and ready-to-use approach for quantitation of miRNA expression levels from a variety of sample types. The products offer a lower barrier to getting started and reduced technical variability n experiments backed by solid technical support.

A bion, an Applied B systems Business

For nformation 512-651-0200

www.ambion com catalog/workflows. miRNA

Small Interfering RNA

FlexiTube siRNA (small interfering-RNA) enhances the flexibility of Qiagen's range of RNA nterference (RNAi) solutions by providing a cost-effective option for analysis of small numbers of human or mouse genes. FlexiTube siRNAs are provided in economical 1-nmol amounts. They are designed using neural network technology based on a large set of data from siRNA exper ments. The siRNA design is then checked for homology to all other sequences of the genome using an up-to-date, nonredundant sequence database and a proprietary homology analysis tool. Design features include 3' untranslated region/seed region analysis, single nucleotide polymorphism avoidance, and interferon motif avoidance

Q agen

For nformation 800-426-8157

www.qiagen com, siRNA

Linker Oligonucleotides for miRNA Cloning

Three different adenylated linker oligonucleotides are available for miRNA library construction without the use of ATP. Linker-1 contains a Ban-1 restriction site. Linker-2 contains Ava and Sty-I restriction sites. Linker-3 contains EcoR I and Msp-I restriction sites. All three linkers are modified to prevent self ligation and can improve the cloning efficiency of miRNAs that have a 5 phosphate and react unfavorably when attaching linkers using RNA ligase in the presence of ATP. Traditionally, RNA ligase makes use of ATP to adenylate the 5'-end of a single-stranded nucleic acid sequence. The activated adenylated o igomer is then ligated to the 3'-OH of a second single-stranded sequence. n the absence of ATP, these adenylated oligonucleotides containing a pyrophosphate linkage are substrates for T4 RNA ligase.

ng ated DNA Technolo gies DT

For nformation 800-328 2661

www.idtdna.com

Eukaryotic mRNA

The capping of in vitro transcribed RNA improves the stability and in vivo translation efficiency of transfected messenger RNA (mRNA) in most eukaryotic cells. Capped mRNA is also more efficiently translated in some in vitro translation system. The ScriptCap m7G Capping System builds the Cap 0 structure found on the 5'-end of most eukaryotic mRNA molecules. Based on the trifunctional vaccinia virus capping enzyme, this system includes all of the components necessary to convert RNA containing a 5'-triphosphate to Cap 0 RNA.

Epi centre B otechnologies

For nformation 800-284-8474

www.epibio com, scriptcapvce asp

Internet Access to RNA

An array of RNA samples available through an e-commerce site include those from common cancers such as breast and colon cancer. The company plans to add thousands of RNA samples from a wide range of diseases. Each sample of total RNA is from an individual donor and supplied n 5-mg aliquots. Each sample includes clinica data and pathology report details so the clinical context of the RNA can be understood. Each sample has been quality-assured through the use of the Ag lent Bioanalyzer and confirmed to have an RNA integrity number of at least 6. This ensures that the materials are suitable for all forms of gene expression analysis, from Northern blots to Affymetrix chips.

A le and

For nformation 313 263-0960

solutions.asle rand.com

POSITIONS OPEN

STAFF ASSOCIATE

The candidate will be expected to lead and conduct standard molecular and genetic analysis experiments designed to resolve the molecular bases of the response to hypoxia in the context of the role of early growth response-1 in both in vitro (cell culture) and in vivo (animal) studies. The candidate will address the question of the role of egr-1 in the biological response to hypoxia at the transcript, protein, and activity level of a variety of candidate genes. To accomplish these goals, the candidate will be required to design and carry out these studies with the following expertise essential as follows: Duties will involve cell culture (both passaged commercially available cell lines and primary isolates from animal tissues), molecular and cellular biology assays (it is required that the successful candidate be fully proficient in RNA/DNA manipulation, subcloning, PCR, electrophoresis, and molecular cloning). Affymetrix gene chip expression arrays, and biochemical assays (Western blotting, protein expression, and analysis of signal transduction pathways). The applicant must be able to remove primary endothelial and inflammatory cells, such as monocytes and T and B lymphocytes, from mouse tissues and peripheral blood. Thus, additional duties will include the maintenance of the colonies of animals necessary for these studies. This includes animal handling (complex breeding, genotyping, including preparation of genomic DNA, [illegible] digestions, Southern blotting, and PCR). Additionally, he/she will perform other related duties necessary to the functioning of the laboratory, research project, or work unit as assigned. It is expected that the successful candidate will be able to perform each of the above duties independently and report findings to the principal investigator on a daily basis.

The candidate must have a doctoral degree and at least five years of experience in research, including experience in each of these areas:

[illegible] Inquiries to: **Karen Evans, Divisional Administrator, Division of Surgical Sciences, Department of Surgery** [illegible] **kme1@columbia.edu.**

[illegible] an Internship, Lien Equal Opportunity Employer.

RESEARCH ASSOCIATE (POSTDOCTORAL) POSITIONS

Fluorescence Spectroscopy and Plasmonics

Two Research Associate positions are available in metal-enhanced fluorescence sensing.

Qualifications: A Ph.D. in physical chemistry, fluorescence spectroscopy, or related discipline is required. Qualifications in biochemistry and/or cell biology are also desirable. Expertise in fluorescence based sensing and cellular spectroscopy measurements will be given preference. The ideal candidate will have significant experience in fluorescence spectroscopy, fluorescence sensing, and biochemistry. Working knowledge of micro fluorescence microscopy, data collection, time domain calculations, and/or fabrication of noble metal nanostructures is also desirable.

Salary: Commensurate with experience.

Applications: Please send a letter of application indicating position #3001-S, your 3001-93 [illegible] interest, and [illegible] three individuals to the following: **Dr. Chris D. Geddes, Professor, Director, The Institute of Fluorescence, Medical Biotechnology Center, University of Maryland Biotechnology Institute, 725 West Lombard Street, Baltimore, MD 21201. E-mail: geddes@umbi.umd.edu.**

Closing date: Until a suitable candidate is selected.

RESEARCH PROFESSOR, Institute for Shock Physics, Washington State University. The Institute for Shock Physics invites applications from outstanding experimental physicists with ten to 15 years of post Ph.D. experience in shock wave research. U.S. citizenship is required. This position is available immediately. Applicants should view the position at website http://www.shock.wsu.edu/opportunities for the application procedures. *Equal Employment Opportunity/Affirmative Action.* 4/24

POSITIONS OPEN

USDA ARS Agricultural Research Service
www.ars.usda.gov

RESEARCH PLANT PATHOLOGIST
GS-0434-11/12
$52,912 to $82,446 Per Annum

The USDA Agricultural Research Service, Sugarbeet and Potato Research Unit at Fargo, North Dakota, is seeking a permanent, full-time, Research Plant Pathologist to conduct research to alleviate disease losses and enhance efficiency of sugarbeet production. The mission of the Sugarbeet and Potato Research Unit is to improve the quality and profitability of sugarbeet and potato production through fundamental research on germplasm development, crop protection and postharvest physiology. Research results will identify biochemical mechanisms underlying pathogenicity and/or virulence possessed by sugarbeet fungal and viral pathogens; provide detection strategies for important sugarbeet pathogens at the species and strain levels; and identify genes and their markers and biocontrol agents that condition natural resistance in sugarbeet to pathogens of importance to sugar production. A comprehensive benefits package includes paid sick leave and annual leave, life and health insurance, a savings and investment plan (401K type), and a federal retirement plan. For more information on the research program and/or position, contact **Jamie Wadzinik** at **telephone: 701 239-1203.** Complete information and application procedures may be obtained at **website: http://www.afm.ars.usda.gov/divisions/hrd/index.html.** To have a printed copy of the vacancy announcement mailed to you, call **telephone: 701 239-1203** or **e-mail: wadzinkj@fargo.ars.usda.gov.** Mail applications to: **USDA-Agricultural Research Service, Human Resources Division, Attn: Kelli A. Martin, 5601 Sunnyside Avenue, Stop 5106, Beltsville, MD 20705-5106, fax: 301 504-1535; e-mail sdrecruit@ars.usda.gov.** Applications must be marked **ARS-NPW-0212** and be postmarked by **July 13, 2007.** *U.S. citizenship is required. USDA/ARS is an Equal Opportunity Employer and Provider.*

CHIEF of RESEARCH SERVICE

The Minneapolis VA Medical Center invites applicants for the position of Associate Chief of Staff (ACOS) for Research. This person will be responsible for the oversight of all research conducted at the Medical Center including departmental management, program oversight and coordination, compliance, strategic planning, and academic affiliations for research. Candidates must hold an M.D. or Ph.D. degree and be eligible for appointment at the University of Minnesota Medical School at the **ASSOCIATE PROFESSOR** or **PROFESSOR** level. Experience within the VA system is highly desirable. Applicants should have a record of distinguished accomplishments in academic research and substantial experience in administration. The successful candidate will be expected to maintain an active research program and to facilitate growth of new and existing research programs at the VA including collaborative research with the University. Successful experience in mentorship is essential. The successful candidate must demonstrate an ability to balance all elements of the VA's mission and to work collaboratively across all departments at the VA and with appropriate departments at the University of Minnesota. Interested candidates should submit a letter of interest and curriculum vitae to:

Jan Ochsendorf
Minneapolis VA Medical Center HRMS (05)
1 Veterans Drive
Minneapolis, MN 55417

Or at fax: 612-725-2287. Telephone: 612-725-2060.

NIDDK Tenure-Track Position in Endocrinology and Metabolism and Human Obesity
National Institute of Diabetes and Digestive and Kidney Diseases

We seek an outstanding scientist to direct a vigorous, innovative research program in the Clinical Endocrine Section of the Clinical Endocrinology Branch to advance knowledge in the area of obesity and weight regulation with particular emphasis on the neuroendocrine aspects of weight regulation and the role of sleep in obesity. Applicants must be highly motivated and have a demonstrated track record through publications that address significant contributions to the field of endocrinology and metabolism. The successful candidate is expected to develop an independent, world-class research program complementary to current investigations within the Branch. The position comes with generous start up funds and on-going support.

The Clinical Endocrinology Branch, NIDDK is located on the main NIH campus in Bethesda, Maryland, a suburb of Washington DC. The Branch represents interests similar in range to those of an academic department. There are strong interactions among the independent research groups, and the position offers unparalleled opportunities for interdisciplinary collaboration within NIDDK and throughout NIH. Applicants should submit a curriculum vitae, bibliography, copies of three major publications, a summary of research accomplishments, a brief statement of future research goals, and arrange for three letters of reference to be sent to:

Dr. James Bulow, Chair, Search Committee, c/o Glynnis Vance, NIDDK, 9000 Rockville Pike, Building 10-CRC Room 5-2551, National Institutes of Health, Bethesda, MD 20892

Application Deadline: **June 30, 2007**

NIDDK Tenure-Track Position in Human Energy Metabolism
National Institute of Diabetes and Digestive and Kidney Diseases

We seek an outstanding scientist to direct a vigorous, innovative research program in human energy metabolism and serve as Director of the newly established Metabolic Core Laboratory (MCL) in Clinical Endocrinology Branch, NIDDK. The MCL performs a number of analyses including exercise testing, physical activity monitoring, body composition measurement, and 24-hour energy expenditure analyses in health and disease. Applicants must be highly motivated and have a demonstrated track record through publications that address significant contributions in the areas of energy expenditure and physical activity as it relates to metabolism and weight regulation. The successful candidate is expected to develop an independent, world-class research program complementary to current investigations within the Branch and to successfully oversee the functioning of the MCL. The position comes with generous start up funds and on-going support.

The Clinical Endocrinology Branch, NIDDK is located on the main NIH campus in Bethesda, Maryland, a suburb of Washington DC. The Branch represents interests similar in range to those of an academic department. There are strong interactions among the independent research groups, and the position offers unparalleled opportunities for interdisciplinary collaboration within NIDDK and throughout NIH. Applicants should submit a curriculum vitae, bibliography, copies of three major publications, a summary of research accomplishments, a brief statement of future research goals, and arrange for three letters of reference to be sent to:

Dr. James Bulow, Chair, Search Committee, c/o Glynnis Vance, NIDDK, 9000 Rockville Pike, Building 10-CRC/Room 5-2551, National Institutes of Health, Bethesda, MD 20892

Application Deadline: **June 30, 2007**

WWW.NIH.GOV

NIDDK Tenure-Track Position in Clinical Research in Diabetes and Kidney Disease
National Institute of Diabetes and Digestive and Kidney Diseases

We seek an outstanding scientist to direct a vigorous, innovative clinical research program in the epidemiology, physiology, and treatment of type 2 diabetes, diabetic nephropathy, and related disorders. Applicants must be highly motivated and have a demonstrated track record through publications that address significant issues of causation, prevention, and treatment of these conditions. Applicants must also be licensed to practice medicine in one of the United States and have substantial experience in community relations, recruitment, and clinical research among U.S. minority groups. The successful candidate is expected to develop an independent, world-class research program complementary to current investigations within the Phoenix Epidemiology and Clinical Research Branch (PECRB). The position comes with generous start up funds and on-going support.

The PECRB, NIDDK, is located in Phoenix, Arizona. The Branch represents interests similar in range to those of an academic department. There are strong interactions among the independent research groups, and the position offers unparalleled opportunities for interdisciplinary collaboration within NIDDK and throughout NIH. Applicants should submit a curriculum vitae, bibliography, copies of three major publications, a summary of research accomplishments, a brief statement of future research goals, and arrange for three letters of reference to be sent to:

Dr. James Balow, Chair, Search Committee, c/o Glynnis Vance, NIDDK, 9000 Rockville Pike, Bldg. 10-CRC /Rm. 5-2551, National Institutes of Health, Bethesda, MD 20892

Application Deadline: **June 30, 2007**

NIDDK POSTDOCTORAL FELLOWSHIPS IN MOLECULAR AND CELL BIOLOGY
National Institute of Diabetes and Digestive and Kidney Diseases (NIDDK)

We are seeking outstanding postdoctoral candidates holding a PhD, an MD or an MD-PhD with a background in molecular and cell biology and genetics interested in the following research topics:

A) IDENTIFICATION OF NOVEL REGULATORS OF MESENCHYMAL STEM CELL SPECIFICATION

The laboratory studies the transcriptional regulation of adipogenesis and is currently interested in the characterization of novel molecules that can influence adipocyte cell lineage specification. If you would like to apply for a postdoctoral position in this laboratory, please send your curriculum vitae with a cover letter to Dr. Christa Buecker (buecherc@mail.nih.gov). To learn more about our research, please visit our lab website at **http://intramural.niddk.nih.gov/research/faculty.asp?People_ID=1702**

B) SKELETAL MUSCLE STEM CELL REGULATION

Our laboratory studies the role of TGF-beta family members in skeletal muscle development and metabolism. A postdoctoral position is available to study the regulation of adult skeletal muscle stem cell quiescence and activation. Please send your curriculum vitae with a cover letter to Dr. Alexandra McPherron (mcpherra@niddk.nih.gov). To learn more about our research, please visit our lab website at **http://intramural.niddk.nih.gov/research/faculty.asp?People_ID=1701**

C) BIOLOGY OF SPHINGOLIPID SIGNALING

The laboratory studies the signaling functions of sphingolipids, a diverse group of cellular lipids, with focus on their roles in immunity and inflammation. If you would like to apply for a postdoctoral position in this laboratory, please send your curriculum vitae with a cover letter to Dr. Richard Proia (proia@nih.gov). To learn more about our research, please visit our lab website at **http://intramural.niddk.nih.gov/research/faculty.asp?People_ID=1533**

Applications will be reviewed upon receipt. The selected candidates will be contacted for an interview within a month from the application.

NIDDK

Tenure-Track Positions
Liver Diseases Branch

New Research Initiative – Fatty Liver Disease & Obesity - Tenure Track Position

The Liver Diseases Branch of the National Institute of Diabetes and Digestive and Kidney Diseases (NIDDK), National Institutes of Health (NIH) invites applications for one tenure track position from scientists interested in basic and/or clinical research involving non-alcoholic fatty liver disease and metabolic syndrome. Specific areas of research interest include pathogenesis and mechanisms of metabolic derangement in non-alcoholic fatty liver disease and its pathophysiological link to insulin resistance and obesity. Priority will be given to applicants at the Assistant Professor level in traditional universities or those finishing their post-doctoral fellowship positions.

New Research Initiative – Liver Stem Cells - Tenure Track Position

The Liver Diseases Branch of the National Institute of Diabetes and Digestive and Kidney Diseases (NIDDK), National Institutes of Health (NIH) invites applications for one tenure track position from scientists interested in basic and/or clinical research involving mammalian adult stem cells. Specific areas of research interest include functional differentiation and mechanisms of development of adult tissue-derived stem cells, especially those of the liver, and potential clinical application of stem cell therapy in liver diseases. Priority will be given to applicants at the Assistant Professor level in traditional universities or those finishing their post-doctoral fellowship positions.

The applicant must have a proven record of accomplishments and will be expected to propose and pursue an independent research program in one of these fields. The position offers unparalleled opportunities for interdisciplinary collaboration within NIDDK and throughout NIH. The Liver Diseases Branch at NIDDK is located on the main intramural campus of the NIH in Bethesda, Maryland, a suburb of Washington, D.C. Interested applicants should send a Curriculum Vitae and list of publications, copies of three major publications, a summary of research accomplishments, a plan for future research, and three letters of recommendation to **Ms. Michelle Brown, Search Committee, Liver Diseases Branch, NIDDK, Building 10-9B16, NIH, Bethesda, MD, 20892-1800**. Application deadline: **September 15, 2007**.

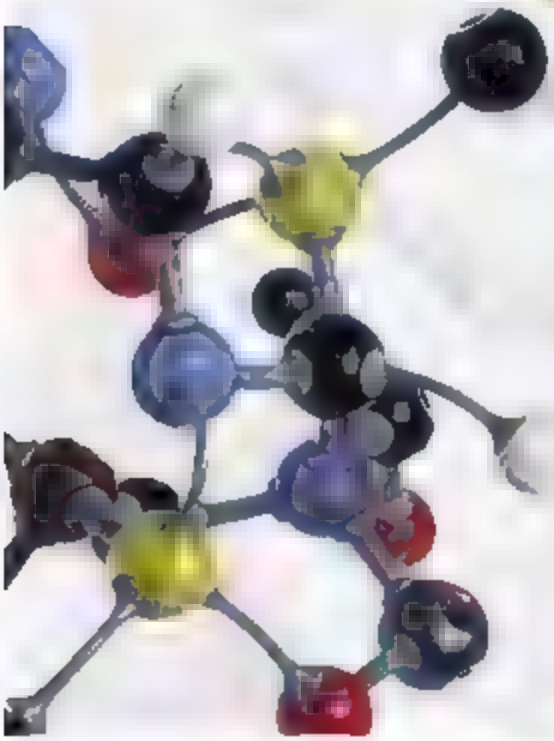

Postdoctoral Research Training at NIH

Launch a career to improve human health

Work in one of 1250 of the most innovative and well-equipped biomedical research laboratories in the world

Explore new options in interdisciplinary and bench-to-bedside research

Develop the professional skills essential for success

Earn an excellent stipend and benefits

Click on www.training.nih.gov

Office of Intramural Training and Education

Founding President

King Abdullah University of Science and Technology

KAUST

"The creation of KAUST with its high aspirations, bold design, and remarkable resources is an event of singular significance, not only for the Kingdom of Saudi Arabia, but for the region and the world."

The University

The King Abdullah University of Science and Technology (KAUST) is [illegible] a new age of scientific achievement [illegible] the region, and beyond. As an independent, graduate-level research university, KAUST [illegible] to open in 2009.

The Research

KAUST will focus on research that applies science and technology [illegible] development. Rather than organizing around academic disciplines, KAUST will focus on cross-disciplinary, problem-oriented research [illegible]

- [illegible]
- Materials Science and Engineering
- Biosciences and Engineering
- Applied Mathematics and Computational Science

[illegible] **Global Research Partnership** [illegible] Collaborative Research Centers, KAUST Investigators, and KAUST Research Fellows around the world.

The Students

KAUST [illegible] talent of all nationalities and religious faiths. The initial class of 250–150 KAUST graduate students will begin classes in 2009. At [illegible] KAUST will [illegible] PhD programs.

Two programs will be offered:

- **The KAUST Discovery Scholarship** is a pre-[illegible] that will support undergraduate students at [illegible] before entering KAUST as master's degree candidates.
- **The King Abdullah Scholars**, with four-year [illegible] developed along the lines of the Fulbright, Rhodes, and [illegible] support outstanding students at leading [illegible]

Qualifications

A distinguished international academic and private-sector search [illegible] KAUST Founding President. The search is open to academic and non-academic candidates of significant [illegible]

- [illegible]
- [illegible]
- [illegible]
- [illegible]
- [illegible]
- Experience in fostering collaborations with academia, industry [illegible]
- Entrepreneurial instincts, organizational skills
- [illegible] significance of KAUST
- [illegible] to inspire the [illegible] internal constituencies and external [illegible]

Contact Information

Korn/Ferry International, which is assisting the KAUST Presidential Search Committee, invites confidential inquiries, applications, and nominations.* All communications will be held in absolute confidence. [illegible] information, including email address. The position is available January 2008 or as soon thereafter as possible.

Korn/Ferry International
KAUSTpresident@kornferry.com

[illegible]
Washington, DC 802-765-4543

Edward Hardwick
[illegible]
Dubai, UAE 971-42-04-55-738

*KAUST does not discriminate on the basis of gender, nationality, or religious belief.

KENT STATE UNIVERSITY

Faculty Positions in Liquid Crystals and Biological Materials

Liquid Crystal Institute, Chemical Physics Interdisciplinary Program, and Department of Biological Sciences

In a major joint venture the Liquid Crystal Institute/Chemical Physics Interdisciplinary Program and the Department of Biological Sciences at Kent State University are recruiting two new full-time faculty members to work in the interdisciplinary field of experimental soft matter biomaterials, biological physics, and molecular biology.

The positions are funded by the State of Ohio and Kent State University, one with appointment in the Liquid Crystal Institute/Chemical Physics Interdisciplinary Program and one in the Department of Biological Sciences, beginning January 2008.

The positions offer remarkable opportunities for work in the area of liquid crystals, biopolymers, soft and complex systems. The Liquid Crystal Institute is a leader in basic and applied liquid crystal science, with a broad range of research activities, exemplary facilities, and a vibrant scientific atmosphere. The Department of Biological Sciences houses extensive core genomic, proteomic, microscopy and imaging facilities, and supports a dynamic cross-disciplinary research culture. Further information is available on the websites **http://www.lci.kent.edu** and **http://www.kent.edu/biology**.

For the Liquid Crystal Institute position, we seek an experimental scientist focused on the physical properties of soft matter and biomaterials. Responsibilities include conducting a vigorous program of innovative and funded research, supervising graduate students, and teaching doctoral and masters level classes. Qualifications: PhD in Physics, Chemical Physics, Biophysics, Materials Science, or related field. Applicants must also have an established record of high quality scholarly research and ability to secure extramural funding.

For the Biology position, we seek a molecular biologist focused on cross-disciplinary interactions between biological systems and liquid crystal and other biomaterials. The successful candidate will have an integrated approach to studies at the cellular and molecular level, and interest in applying advanced biomolecular and materials science concepts to biology and/or medicine. **Qualifications:** PhD in Biology, biochemistry, or related field and postdoctoral experience. Applicants must have an established record of high quality scholarly research and will be expected to seek and secure extramural funding. Current extramural funding is required for applications for senior ranks.

Review of applications will begin **August 15, 2007** and continue until the positions are filled. To apply, please submit a letter of application, C.V. and contact information for three references to: **Prof. Jonathan V. Selinger, Ohio Eminent Scholar in Soft Matter Theory, Liquid Crystal Institute, Kent State University, Kent OH 44242-0001. Tel: 330-672-2654, fax: 330-672-2796. E-mail: search2007@lci.kent.edu**

Kent State University is an Affirmative Action Equal Opportunity Employer and encourages applications from candidates who would enhance the diversity of the University's faculty.

Founding Director and Ontario Research Chairs

Biorefining Research Initiative (BRI)

Lakehead University is seeking outstanding scholars to fill two positions in fields relevant to biorefining processes that transform low-value biomass feedstocks into multiple higher-value products. Candidates with experience developing university-industry partnerships will be highly valued.

Founding Director & Senior Ontario Research Chair

(one position)

Prospective candidates must be senior scholars with an international reputation for leadership and research excellence, a PhD in related discipline(s), and a demonstrated track record of attracting external funding. The incumbent will be responsible for the overall leadership and success of establishing a new Biorefining Research Initiative (BRI) which will eventually become a research institute pending Senate and Board approval. BRI is expected to become a world-class centre of excellence dedicated to developing transformative technologies and products from biomass. The Founding Director will also be responsible for developing interdisciplinary research programs and mentoring junior scientists and highly qualified personnel. Lakehead University is committed to providing the resources required for BRI's success, including space and the recruitment of faculty and technical staff as well as provision of administrative assistance. The successful candidate will be appointed at the full-professor level with tenure and with no teaching responsibilities.

Ontario Research Chair in Biorefining Technologies

(one position)

Prospective candidates are expected to have a PhD in a related discipline(s), be scholars who have achieved or have the potential to achieve international recognition in their field, and have a demonstrated track record of attracting external funding. The successful candidate will be given a tenure-track or tenured appointment at the associate or full-professor level depending on credentials and experience and will have minimal teaching responsibilities.

The BRI has been made possible through a grant awarded by the Ontario Ministry of Research and Innovation which will be endowed in perpetuity by Lakehead University. The successful candidates will be provided with competitive salaries and substantial start-up funding.

Lakehead University is a comprehensive university of 7,700 students, 2,250 faculty and staff, and an active and growing research environment with its main campus in Thunder Bay and a branch campus in Orillia. We have nine faculties including a Faculty of Medicine. Lakehead University was designated "Canada's Research University of the Year" in the undergraduate category for research intensity and growth in 2006. Additional information about Lakehead University can be found on our website at **www.lakeheadu.ca**

lakeheadu.ca | thunderbay.ca | orillia.ca

Applicants should submit a covering letter, curriculum vitae, brief five-year research plan (candidates for Founding Director position should also provide a vision statement for the BRI), samples of research, and names of three references to:
Dr. Rui Wang, Vice-President Research, Lakehead University
955 Oliver Road, Thunder Bay, Ontario, Canada P7B 5E1
fax: (807) 346-7748 e-mail: rui.wang@lakeheadu.ca

Review of applications will begin on September 15, 2007.

We are committed to employment equity and welcome diversity in the workplace and encourage applications from all qualified candidates including women, aboriginal persons, persons with disabilities and members of visible minorities. In accordance with the Ontario Human Rights Code, preference will be given to Canadian citizens or permanent residents. We thank all applicants for their interest; however, only those selected for an interview will be contacted. Personal information contained in applications will be used for employment purposes only. Lakehead University is committed to accessible employment practices. Please advise us if you require accommodation during the recruitment process. Lakehead University is committed to employment practices that respect the dignity of persons with disabilities. Please advise us if you require accommodation during the recruitment process. Lakehead University is committed to employment practices that respect the dignity of persons with disabilities.

Lakehead UNIVERSITY

Universität Karlsruhe (TH)
Forschungsuniversität · gegründet 1825

KIT

The Universitaet Karlsruhe (TH) and the Forschungszentrum Karlsruhe are joining forces to form the Karlsruhe Institute of Technology (KIT) and are planning to integrate their research activities both structurally and strategically. Within the framework of this award-winning concept for the future, funded by the German Excellence Initiative, we seek applications for the position of

Professor (W3) for Theoretical Quantum Optics

at the Department of Physics. This position includes resources equivalent to an endowed chair.

We are looking for an expert in the area of theoretical quantum optics with links to condensed-matter theory. The research of the applicant should focus on (i) the realization of quantum-optics concepts in solid-state or hybrid systems, (ii) many-particle effects in ultra-cold gases or (iii) quantum-information processing and quantum simulation.

The position offers excellent opportunities for collaboration within the Department of Physics and with other departments of the university, with the Research Center Karlsruhe (FZK) in the framework of KIT, within the 'DFG-Center for Functional Nanostructures (CFN)' and the 'Karlsruhe School of Optics and Photonics (KSOP)'.

Teaching duties include participation in the education of physics students as well as of students majoring in other natural sciences or engineering.

The University of Karlsruhe aims to increase the number of female professors and especially welcomes applications from women. Handicapped persons with equal qualifications will be preferred.

In the case of a first appointment to a professorship the contract will not be tenured initially. Exceptions from this rule are possible.

Applications with the usual credentials, copies of the five most important publications and a statement about past and planned research and teaching activities should be sent before **June 23, 2007** to the **Dean, Department of Physics, Universitaet Karlsruhe (TH), D-76128 Karlsruhe, Germany.**

NAVAL RESEARCH LABORATORY
Superintendent, Space Science Division

NRL • Naval Research Laboratory • www.nrl.navy.mil
4555 Overlook Ave SW, Washington DC 20375

Senior Executive Service Career Opportunity
ES-1301/1310/1330: $111,676 to 168,000 per annum*
***Rate limited to that rate for Level II of the Executive Schedule (5 U.S.C. 5304 (g) (2))**

Become a member of an elite research and development community involved in basic and applied scientific research and advanced technological development for tomorrow's Navy and for the Nation.

- Manages, directs, and administers a recognized scientific work force conducting a broad spectrum research program in astrophysics, solar-terrestrial physics, upper middle atmospheric science, and astronomy.
- Executive direction and technical leadership in the development of policies and objectives necessary in conducting a program of research, development, and evaluation leading to the creation, adoption and application of improved and new concepts, principles, methods, sensors, and techniques applicable to understanding and observing the space environment.
- Principal consultant to the Navy, other agencies and nations on the science and developing applications for the R&D programs under his/her cognizance.
- Applicants should be recognized as national/international authorities and should have planned and executed difficult programs of national significance or specialized programs that show outstanding attainment in their field of research.
- Optional Application for Federal Employment (OF-612), Application for Federal Employment (SF-171), or resume along with technical qualifications and executive Core Qualifications (ECQs) **must be received by 30 June 2007**. In order to receive full consideration, all technical qualifications and ECQ's must be discussed in detail.
- Apply to: **Naval Research Laboratory, Announcement #NE7-XXXX-80-KS4-0001-SES, 4555 Overlook Avenue SW, Washington, DC 20375-5320**. Faxed or emailed applications will not be accepted. To view full vacancy announcement and or to apply online visit **https://hrol.nrl.navy.mil/jobs/index.htm**
- For further information contact **Kathy Weaver**, Human Resources Office, NRL at **Kathy.weaver@nrl.navy.mil** or **(202) 404-8305**.

NRL is an Equal Opportunity Employer

New Scientists, Senior scientists and Department Research Director positions offered at Novo Nordisk China R&D center

Zhongguancun Life Science Park, Beijing, China

Novo Nordisk is a Danish healthcare company and a world leader in diabetes care. Novo Nordisk China R&D (NNCD) is an early stage part of Novo Nordisk's growing international R&D organization. Building on its extensive expertise in protein expression and purification, NNCD actively identify and validate novel drug targets in the areas of cancer immunology and inflammatory diseases.

NNCD has three departments: Molecular Biology, Protein Chemistry and Cell Biology. We are now announcing new scientist positions in these departments and we are seeking for highly motivated scientists who plan to advance their career in China. The new scientists will take part in the following responsibilities: 1) Expression, purification and analysis of therapeutic proteins like e.g. mAbs produced and optimized at laboratory to pilot scale; 2) Novel drug target identification and evaluation of opportunities in immunotherapy of cancer and inflammation.

The successful candidates must have the following qualifications: 1) Ph.D in immunology combined with one of the following core technologies: cell biology, biochemistry, molecular biology or protein chemistry; 2) >2 years (Post Doc.) hands-on experience and a good scientific track record within immunology, inflammation and/or cancer research; 3) preferentially industry and/or international experience; 4) independent innovator and at the same time a strong team-player, enjoy problem solving and love the challenge of achieving ambitious goals; 5) excellent communication skills in English which is the official company language. In addition, the candidates for Research Director of Protein Chemistry must have excellent track record in protein chemistry, and industrial & management experience.

Title and compensation will be dependent on the individual candidate's qualifications. For detailed information regarding individual positions, please check the website **www.ebiotrade.com/jobf**, or send an inquiry via e-mail to **nnsf@novonordisk.com**.

Associate Director, Scientific Affairs
Montreal Neurological Institute and Hospital
McGill University

The Montreal Neurological Institute and Hospital will hire an Associate Director for Scientific Affairs to implement the scientific mission of the Institute and Hospital under the guidance of the Director. This person will be responsible for the success of the scholarly mission of the Institute, which has both basic research and clinical components, and engages about 75 faculty and 400 staff members. He or she will play a central role in the recruitment of new faculty, organizing the Institute's internal grant review program, preparing scientific reports, planning scientific retreats, and organizing large institutional grant applications. He or she will also serve as the liaison with McGill University and the McGill University Hospital Centre for academic and research issues. Strong interpersonal skills and expertise in writing are essential talents for this position. Applicants with MD or PhD degrees and experience in university or industry-based research organizations, or in foundations that fund medical research will be of particular interest. Applications should be sent by email to **scientific-affairs.mnhi@mcgill.ca** or by mail to:

Dr. David Colman
Director, Montreal Neurological Institute
3801 University Street, Room 776
Montreal, Quebec, H3A 2B4
www.mni.mcgill.ca

Deadline for receipt of applications is July 15, 2007. All qualified candidates are encouraged to apply; however Canadians and permanent residents of Canada will be given priority. McGill University is committed to Equity in Employment.

DEPUTY DIRECTOR

National Institute of Diabetes and Digestive and Kidney Diseases
Department of Health and Human Services
National Institutes of Health

THE POSITION: The National Institute of Diabetes and Digestive and Kidney Diseases (NIDDK) is seeking exceptional candidates for the position of **Deputy Director** of the Institute. The incumbent serves as an active partner with the NIDDK Director in the leadership of a $1.8 billion national organization that conducts and supports biomedical and behavioral research. The NIDDK supports and conducts research to understand, treat and prevent a wide array of the most common and severe diseases affecting the nation's health and disseminates research findings and health information to health care professionals, patients and the public through various health promotion and education programs. http://www2.niddk.nih.gov has positions offers a unique and exciting opportunity for an experienced leader dedicated to sharing responsibility, providing strong and visionary leadership to an organization dedicated to uncovering new knowledge and technologies with wide public benefit. The NIDDK seeks candidates who have a commitment to science, excellence, a high energy, enthusiasm and innovative thinking necessary to help lead major strategic planning initiatives and their subsequent careful implementation. The Deputy will be expected to represent the Institute and the Director and the Institute before Members of Congress and their staffs, high-level Government officials, leaders of national voluntary and professional health organizations and leaders in business, science and academia.

QUALIFICATIONS REQUIRED: Applicants must possess an M.D., Ph.D., or equivalent degree as well as senior level research experience or knowledge of research programs in one or more of the following disease areas: diabetes, endocrinology and metabolic diseases, digestive diseases and nutrition, and kidney, urologic and hematologic diseases. Candidates should be nationally recognized and respected within their professions as distinguished individuals of outstanding competence. Applicants should also demonstrate the ability to: think strategically; work collaboratively and use a consultative approach to policy setting and decision making.

SALARY/BENEFITS: Salary is commensurate with experience and a full package of Civil Service benefits is available, including retirement, health and life insurance, long term care insurance, leave and savings plan (401K equivalent). This position is subject to a background investigation.

HOW TO APPLY: A C.V., curriculum vitae, bibliographies and three letters of recommendation must be received by **July 2, 2007**. Application packages should be sent to the **National Institutes of Health (NIH), National Institute of Diabetes & Digestive & Kidney Diseases (NIDDK), 31 Center Drive, MSC 2560, Building 31, Room 9A-16, Bethesda, Maryland 20892**. For more information, please call (301) 594-7777. All information provided by candidates will remain confidential and will not be released outside the NIDDK search process without a signed release from candidates.

DHHS and NIH are Equal Opportunity Employers

THE OHIO STATE UNIVERSITY

Faculty Position
Small Animal Imaging

The Department of Surgery of The Ohio State University Medical Center seeks a motivated individual for a tenure track faculty member at the levels of Assistant or Associate Professor to develop a research program in small animal imaging in the context of the Division of Cardiothoracic Surgery and the Davis Heart and Lung Research Institute. The successful candidate is a PhD and or MD with a record of active extramural research funding and publications in cardiovascular biology. This position holds a co-appointment in the Department of Biomedical Engineering.

Candidates should send a curriculum vitae and a statement of current research funding activities to the Chair of the Search Committee:

Professor Chandan K. Sen
Vice Chairman of Research
Department of Surgery
chandan.sen@osumc.edu
Ph 614-247-7786
Fax 614-247-7818

The Ohio State University is an Equal Opportunity/Affirmative Action Employer. Women, minorities, veterans and individuals with disabilities are encouraged to apply.

Department of Health and Human Services
National Institutes of Health
National Heart, Lung and Blood Institute

Medical Officer (Deputy Director), AD-602-0/0, Division of Lung Diseases

The National Heart, Lung and Blood Institute (NHLBI) at the National Institutes of Health (NIH) seeks a dynamic physician-scientist to provide strategic leadership and advice to the Division Director, Branch Chiefs, and other Division staff in programmatic and administrative aspects of the Division of Lung Diseases (DLD). DLD operations and overall direction of its extramural and international research programs. DLD supports research on the causes, prevention and treatment of lung diseases and sleep disorders. Research is funded through investigator-initiated and institute-initiated grant and contract programs in disease areas including asthma, chronic obstructive pulmonary disease, cystic fibrosis, cell biology and sleep. Critical care and acute lung injury, developmental biology and perinatal pulmonary diseases, immunology and tissue, lung cell and vascular biology, and pulmonary complications of AIDS and tuberculosis. The Deputy will have a major role in shaping the national programs in pulmonary research and in maintaining and developing interactions with professional, voluntary and patient organizations. The Deputy will work with Division staff to implement the latest research developments in the extramural scientific community as well as identifying research gaps and needs, obtaining advice from experts in the field, and implementing programs to address new opportunities. Research supported by the DLD encompasses a broad spectrum of science ranging from stem cell biology to medical management of lung diseases as well as supporting training and development, dissemination of research results, and public education for these areas of research. The Division has a major responsibility for research in all the major and rare pulmonary diseases with the exception of lung cancer and certain infectious diseases. The DLD has three Branches: Airway Biology and Disease Branch, Lung Biology and Disease Branch, and the National Center on Sleep Disorders Research. The incumbent of this position will be appointed indefinitely into the excepted service under title 42 at a salary commensurate with his/her qualifications.

Selective Factors: Applicants must possess an M.D. degree as well as senior level research experience, evidence of leadership and ability to interact successfully with a broad range of individuals. The successful candidate will be a respected accomplished scientist who matures integrity and outstanding communication skills with the ability to view leadership as service. Applicant may be subject to a background investigation.

Benefits: Excellent health, life investment and personal leave benefits. In addition, a recruitment bonus may also be considered. **Position requirements** and detailed application procedures are provided in the vacancy announcement. Please apply online by accessing **www.usajobs.opm.gov** and refer to **NHLBI-07-186565**. You may also submit a resume, c.v., bibliography or other format to: **Mechelle Young, Human Resources Specialist, 2115 East Jefferson Street, Room 1E 133, Rockville, MD 20852**. All applications must be postmarked by the closing date **07-18-07**. For additional information, contact Mechelle Young at (301) 443-3358.

DHHS and NIH are Equal Opportunity Employers

GRANTS

Funding for Antimalarial Drug Discovery Research in Sub-Saharan Africa

- Funding of up to 1 million Euros over three years is available for research in Africa
- The aim is to build long-term sustainable institutional capacity in the field of antimalarial drug discovery

Funding is supported by the EU FP6 financed AntiMal project in collaboration with MIM/TDR

Full details are available at
http://www.antimal.eu



GRANTS

DISTINGUISHED PROFESSOR POSITIONS IN CELL AND MOLECULAR BIOLOGY

The Department of Molecular Biosciences at the University of Kansas on the beautiful Lawrence campus seeks outstanding applicants for two endowed distinguished professorships. The **Irving Johnson Distinguished Professor of Molecular Biology** is a tenured appointment at the rank of distinguished professor. The successful candidate will be a molecular biologist who has a well-established, internationally recognized program of research. We also invite applicants for a **Distinguished Professor of Cell and Molecular Biology**. We seek outstanding applicants who conduct basic research on genes and proteins that control fundamental processes in living cells.

Applicants for either position must have a Ph.D. (or equivalent) and sufficient post-doctoral experience to qualify for a tenured distinguished professorship at the University of Kansas. For additional guidelines & information on required qualifications for an appointment as a Distinguished Professor, please refer to:
https://www.provost.ku.edu/policy/faculty/dp_guidelines.shtml

Successful candidates will be expected to have and maintain an active research program and contribute to the teaching mission of the department.

For full position descriptions refer to **www.molecularbiosciences.ku.edu**. Applicants should submit a cover letter describing their qualifications and interest in the position, future research plans, teaching philosophy and experience, curriculum vitae, and the names and contact information of at least five references in a single PDF file to **molbiosearch@ku.edu** or by mail to **Linda Wiley, Administrative Associate, Molecular Biology Search, Department of Molecular Biosciences, University of Kansas, 1200 Sunnyside Ave., Room 2034, Lawrence, KS 66045-7534**. Initial review of applications will begin **September 7, 2007** and will continue until the positions are filled.

EOE

GRADUATE PROGRAM

BIOZENTRUM
Universität Basel

UNI BASEL

OPPORTUNITIES FOR EXCELLENCE

International PhD program at the BIOZENTRUM of the University of Basel, Switzerland

The **Biozentrum** together with the **Werner Siemens-Foundation (WSF), Zug (Switzerland)** launches the **International PhD program in Molecular Life Sciences** and encourages excellent students to apply for one of the prestigious WSF fellowships.

The Biozentrum provides an internationally renowned research environment centered around three focal areas (Infection Biology, Growth and Development, Neurobiology) and two core programs (Structural Biology & Biophysics and Genome Scale Biology & Bioinformatics) and is dedicated to basic molecular and biomedical research (http://www.biozentrum.unibas.ch/). We offer advanced, interdisciplinary training in the field of modern biology, a lively and interactive educational atmosphere, and competitive salaries with respect to European standards. University graduates admitted to the Program receive theoretical and practical training, and conduct a three-year research project under the supervision of a Biozentrum faculty member, monitored by a Thesis Advisory Committee.

Applications to the program have to be submitted online. Application forms, requirements, and additional information can be found under: http://www.biozentrum.unibas.ch/phd/
Application deadline: July 1st, 2007

MEETINGS

RNAiEurope.com SELECT

POSITIONS OPEN

Department of Health and Human Services
National Institutes of Health
National Heart, Lung and Blood Institute

MEDICAL OFFICER OR HEALTH SCIENTIST ADMINISTRATOR
Pulmonary and Sleep Disorders Medicine, Vascular and Developmental Lung Biology, Immunobiology

The Department of Health and Human Services and the National Institutes of Health (NIH) are seeking to hire a person with scientific knowledge and research expertise in neonatal, pediatric, vascular, or sleep disorders medicine, developmental or stem cell biology, with emphasis on understanding function and application to human lung development; vascular or respiratory biology; circadian molecular biology; immunobiology or molecular genetics in the context of normal lung function and adult or pediatric lung disease. This position represents an excellent career opportunity to work in a visible, high priority program area that has the potential to alter in a substantive way the direction of pulmonary medicine at the national level.

U.S. citizenship is required and the applicant may be subject to a background investigation. For the **basic qualification requirements**, refer to dir. NI. s guidance for Health Scientist Administrators **http://www.nhlbi.nih.gov/about/jobs/hsguide.htm** and Medical Officers **www.opm.gov/qualifications/SUBCHAPTER/GS0600/0602.HTM**

Benefits: Appointment will be made at the GS-13/14/15 grade level depending on qualifications. A Physician Comparability Allowance may be paid up to $30,000 per year. In addition, a recruitment bonus may also be considered. Excellent health, life, investment, and personal leave benefits.

Position requirements and detailed application procedures are provided in three separate vacancy announcements. Please apply online by accessing **www.usajobs.opm.gov** and refer to **NHLBI-07-186569-MP** for Health Scientist Administrator (merit promotion), **NHLBI-07-186567-DE** for Health Scientist Administrator candidates without government status and **NHLBI-07-186570-DH** for Medical Officer. You may also submit a resume, c.v./bibliography or other format to: Meschelle Young, Human Resources Specialist, 2115 East Jefferson Street, Room 1M-102, Bethesda, MD 20892-8502. All applications must be postmarked by the closing date **07-18-07**. For additional information, contact Meschelle Young at (301) 443-3358.

DHHS and NIH are Equal Opportunity Employers

POSITIONS OPEN

Argonne NATIONAL LABORATORY

The X-ray Science Division at Argonne National Laboratory invites applications for staff positions within X-ray Operations and Research. We are seeking candidates in all experimental x-ray areas with particular emphasis on inelastic x-ray scattering, magnetism, small-angle x-ray scattering, surface scattering, and x-ray imaging. Positions are entry level to senior appointments.

Candidates should have a strong background in synchrotron radiation research; considerable skill in developing instrumentation (such as x-ray optics and detectors) and in state-of-the-art techniques; considerable skill in designing and implementing x-ray optics; considerable skill in understanding abstract concepts; experience in hardware and software for computer control/data collection systems and high heat load x-ray optics is beneficial.

The Advanced Photon Source at Argonne provides a stimulating intellectual environment, and offers the successful candidates many opportunities to interact with world-class facilities and researchers.

Successful candidates will have a Ph.D., postdoctoral experience and a demonstrated ability to conduct high quality independent research in the field.

Argonne is a U.S. Department of Energy laboratory managed by UChicago Argonne, LLC. Argonne's site is approximately 25 miles southwest of Chicago on a beautiful 1500-acre campus-like environment. Interested candidates should send a detailed CV by August 24, 2007, along with a list of publications, and the names and addresses of three references through the Argonne website at **http://www.anl.gov/jobs** job search for the following requisitions:

XSD 311367 (Assistant Physicist)
XSD 311262 (Physicist)
XSD 311364 (Physicist)

For additional technical information, please contact Dr. George Srajer at **XSDpositions@aps.anl.gov**

Argonne is an equal opportunity employer, and we value diversity in our workforce.

FACULTY POSITION in REPRODUCTIVE/PERINATAL ENDOCRINOLOGY ASSISTANT or ASSOCIATE PROFESSOR University of Maryland School of Medicine

The Department of Obstetrics/Gynecology and Reproductive Sciences and the Center for Studies in Reproduction at the University of Maryland School of Medicine are seeking an established investigator to fill a Tenure Track Faculty Position in the area of reproductive and/or perinatal endocrinology. Candidates should have the Ph.D. and/or M.D., post-doctoral training in reproductive endocrinology/physiology, a strong background in molecular biology, *U.S. citizenship*, a sound record of scholarly activity, and active NIH R01-type research grant funding. Opportunities exist for collaboration with existing faculty in several areas of reproductive biology/medicine, on a NICHD U54 Cooperative Centers Program in Reproductive Sciences, and on translational research in the area of maternal fetal medicine. Active areas of research in the Center include endometrial and placental angiogenesis, fetal-placental development and cardiovascular function, ovarian follicular development, steroid hormone action, neuroendocrine regulation of behavior and gonadotropin secretion, et cetera. The University of Maryland at Baltimore has recently undergone aggressive growth in its new research and clinical facilities and $380 million in research grant funding. Submit letter of interest, abbreviated NIH biosketch, and full curriculum vitae to **Eugene D. Albrecht, Ph.D., Director, Center for Studies in Reproduction, Department of Obstetrics/Gynecology and Reproductive Sciences, Bressler Research Laboratories Room 11-019, 655 West Baltimore Street, Baltimore, MD 21201. E-mail: ealbrecht@umaryland.edu.**

ASSISTANT PROFESSOR of CHEMISTRY Department of Chemistry Bethune-Cookman University

The Department of Chemistry is accepting applications for a full-time, nine-month tenure track position. The successful candidate will be expected to teach general chemistry and biochemistry among other courses which coincide with training. Additional responsibilities include student advisement and service on departmental and institutional committees. Development of an active, externally funded research project, which provides opportunities for undergraduate participation, is expected. Salary is competitive and based on qualifications. A Ph.D. in biochemistry is required. Preference will be given to applicants with experience in biochemistry. Applicants should submit a letter of application including a statement of research interest, curriculum vitae, graduate and undergraduate transcripts, and three letters of reference to:

Thomas O. Richardson, Ph.D.
Head, Chemistry Department
Bethune-Cookman University
640 Mary McLeod Bethune Boulevard
Daytona Beach, FL 32114
Telephone: 386 481 2692
Fax: 386 481 2662
E-mail: richardt@cookman.edu

Tampa, Florida-based orthopedic device manufacturer seeking an experienced **BIOMEDICAL ENGINEER.** R&D and manufacturing businesses devices for orthopedic surgery. Experience with collagen preferred. M.S. in biomedical engineering and/or biomechanics required. Experience with orthopedic musculoskeletal tissues preferred. Three to five years of experience in biomedical manufacturing preferred. Qualified candidates please submit resume and salary requirements to e-mail: rollins@trimedx.com.

Colorado State University

Microbiology, Immunology and Pathology
Post-Doctoral Position (Mtb)
Dobos-Elder Lab

Qualified applicants will work on NIH funded tuberculosis grants and contracts to coordinate day-to-day research activities. Studies on these projects range from generating recombinant and native products derived from *Mycobacterium tuberculosis*, generation of new reagents for the detection of Mtb and tissues infected with Mtb, and coordination of research efforts with our collaborators studying various aspects of Mtb physiology and the immune response to Mtb. Qualified applicants must possess a broad range of experience in biochemistry, tissue culture based assays, animal studies, quantitative and qualitative analyses, and BSL-3 experience. Qualified applicants must also possess strong written and verbal communication skills. PhD or equivalent required.

Applications received by **June 8, 2007** given full consideration. Applications accepted until position filled. Electronic submission (preferred) to include letter stating research interests, curriculum vitae and names and email addresses of three references to:

Karen.Dobos-Elder@ColoState.EDU

CSU is an EEO/AA Employer

Colorado State University

Microbiology, Immunology and Pathology
Post-Doctoral Position (TB)
Dobos-Elder Lab

Qualified applicants will work on an NIH funded tuberculosis contract generating recombinant antigens and use these highly purified reagents to study the delayed-type hypersensitivity response in a guinea pig model of tuberculosis. In addition candidates will study protein-protein interactions and the relationship of these interactions in the host immune response to tuberculosis. Qualified applicants must possess experience in protein biochemistry and in tissue culture based assays and have strong written and verbal communication skills. Experience in mass spectrometry, animal studies, and BSL-3 experience preferred. PhD or equivalent required.

Applications received by **June 8, 2007** given full consideration. Applications accepted until position filled. Electronic submission (preferred) to include letter of intent stating research interests, curriculum vitae and names and email addresses of three references to:

Karen.Dobos-Elder@ColoState.EDU

CSU is an EEO/AA Employer

USDA Agricultural Research Service
www.ars.usda.gov

Research Entomologist/ Research Chemist
GS-12/13/14
$63,417.00-$115,848.00 per annum

The U.S. Department of Agriculture, Agricultural Research Service, San Joaquin Valley Agricultural Sciences Center, Parlier, California, invites applications for a Research Entomologist/Research Chemist position (GS-12/13/14 @$63,417.00-$115,848.00 per annum). Position is responsible for planning and leading fumigation research on fresh or dried fruit, nuts and durable commodities such as grains, beans and spices, as well as conducting research on fumigation programs for commodity processing facilities. The ideal candidate has experience in urban entomology and/or pest control and is familiar with commodity marketing. For information call **Denise Chambers at 559-596-2940.**

For a copy of the full agency announcement, application procedures and qualifications for the position go to www.usajobs.com (Announcement Number **ARS-NCW-0233**). Closing date for applications is **July 31, 2007.** Applications must be received by the closing date of the announcement. This is a competitive, permanent appointment and U.S. citizenship is required.

The USDA is an Equal Opportunity Provider and Employer

MBL Biological Laboratory in Woods Hole

Chief Academic & Scientific Officer

The Marine Biological Laboratory in Woods Hole, MA, is seeking candidates for the position of Chief Academic and Scientific Officer (CASO). Established in 1888, the MBL serves as an international resource to biological education, the world's best and brightest in the areas of basic biology, biomedicine, and environmental sciences as well as providing a stimulating and productive research base for scientists from across the globe.

The MBL is searching for a senior level person, equivalent to a Dean, in an academic setting, to be responsible for leadership, planning and oversight of all academic programs, to develop and oversee policies relating to scientific research, to cooperate/interact/collaborate with part-time scientists. The position will advise and work closely with the Director/CEO of the MBL and participate in the development of strategic direction of the laboratory.

The successful candidate should have an outstanding record in scientific research and education, have strong leadership and administrative skills, possess superior interpersonal and communication skills, understand the realities of small marine institutions, have experience with science education at all levels, and have experience with funding projects, developing and administering budgets, and the scientific grants process.

Further information about the MBL is available at www.mbl.edu. Review of applications will begin **July 1, 2007.**

Letters and applications to: Chair, CASO Search Committee, c/o Susan Leon, Marine Biological Laboratory, MBL Street, Woods Hole, MA 02543.

An Equal Opportunity, Affirmative Action Employer
and welcomes candidates

RUSH UNIVERSITY MEDICAL CENTER

CHAIR
Department of Behavioral Sciences

Rush Medical College of Rush University Medical Center is seeking a new Chair of the Department of Behavioral Sciences (Psychology). The Department currently includes twenty three salaried faculty, eighteen full time and five part time and fifty six affiliated faculty. This multi faceted department maintains a strong research and clinical presence within the University.

The Department houses two laboratories with extensive histories of NIH funding: Sleep and Sleep Disorders and Biological Rhythms. Clinically, the current strengths include Sleep and Sleep Disorders, Neuropsychology, Psychosocial Oncology, Outpatient Psychotherapy, Pediatric Psychology and Geropsychology and Rehabilitation. The Department is deeply involved in basic medical education and has one of the most popular elective clerkships within the Medical College. In addition, the Department has a highly competitive, APA-approved internship with eight positions per year.

The preferred candidate will have a Ph.D. in Psychology with an internationally recognized scientific and clinical reputation and a proven NIH track record of funding. Candidates must possess a commitment to innovation in the field and the leadership skills necessary to oversee the growth and development of a multi-disciplinary translational research program. The successful candidate is expected to provide visionary and entrepreneurial leadership and development of junior faculty in their clinical, research, and academic missions of Rush University.

Rush Medical College is the oldest medical college in Chicago, established in 1837, and is part of Rush University Medical Center, one of the largest private academic medical centers in Illinois. Rush is a thriving center for basic and clinical research with more than 1,600 active investigations. The University is located in the Illinois Medical District that includes the John H. Stroger Hospital of Cook County, University of Illinois at Chicago, and the Westside Veterans Administration Hospital.

Letters of interest that include a curriculum vitae will be accepted through **October 1, 2007** and should be sent to:

Rick Sumner, Ph.D.
Chair, Search Committee for Chair of Behavioral Science
Rush University Medical Center
600 South Paulina, Rm 507
Chicago, Illinois 60612

Or preferably electronically to:
Julie_Karstrand@rush.edu

Rush is an Equal Opportunity Employer

Chinese Academy of Sciences

Max-Planck-Gesellschaft

The Chinese Academy of Sciences (CAS) and the Max-Planck-Gesellschaft (MPG)

are searching for up to two **department directors** for the

CAS – MPG PARTNER INSTITUTE FOR COMPUTATIONAL BIOLOGY (PICB) in Shanghai

Legally and administratively the Partner Institute is an institute of the CAS, located on the CAS Campus of the Shanghai Institutes for Biological Sciences (SIBS).

The aim of this interdisciplinary and theoretically oriented institute is to account for the increasing involvement of mathematical, computer science and engineering methods in modern biology and to allow for novel approaches of research at the interfaces between disciplines (e.g. bioinformatics, computational biology, systems biology, computational biophysics, theoretical neurobiology or evolutionary biology).

The proximity to experimentally oriented, internationally competitive research institutes on the SIBS campus guarantees close scientific cooperation and interaction between theoretical and experimental research. Strong collaboration with one or more Max Planck Institutes in Germany is expected from the directors and will be expressively documented and fostered by appointing them as External Scientific Members of MPG.

To aid the final definition of promising research areas and the identification of suitable candidates, the Chinese Academy of Sciences and the Max Planck Gesellschaft will jointly organize a

Symposium on Perspectives in Computational and Theoretical Biology

to be held in Shanghai on 24 – 25 Oct, 2007.

We invite applications from scientists with an outstanding international research record who are willing to take full advantage of the unique challenge of leading this area of this interdisciplinary and theoretical/computational institute by cooperating with the experimental institutes on the SIBS campus and in association with a Max Planck Institute in Germany.

The recruitment and appointment procedure for the director positions will be carried out jointly by CAS and MPG. The positions will offer full scientific and economic independence comparable to that of a director/head of department at a Max Planck Institute.

The initial appointment will be for five years and can be extended after review by the institute's internationally composed Scientific Advisory Board.

Qualified candidates should submit a curriculum vitae, a short statement of research interests and scientific goals, reprints of key publications and the topic (or abstract) of the intended presentation at the symposium.

To ensure full consideration, please submit a hard copy of your application before **July 31, 2007** to

CHEN Zhu (Vice President of CAS)
Chinese Academy of Sciences
52 Sanlihe Road
Beijing 100864
P.R. China

and PDF files of your application to the contact persons in Munich and Shanghai.

Barbara **SPIELMANN**
E-mail: spielmann@gv.mpg.de

Max Planck-Gesellschaft zur Förderung der Wissenschaften
Hofgartenstrasse 8

D – 80539 München, Germany

Tel. +49-89-2108 - 365
Fax +49-89-2108 - 041

CHEN Yi
E-mail: ychen@sibs.ac.cn

CAS/MPG Partner Institute for Computational Biology
Shanghai Institutes for Biological Sciences
Chinese Academy of Sciences
319 Yue Yang Road
Shanghai 200031, P.R. China

Tel. +86-21-5492-0456
Fax +86-21-5492-0451

HUMAN FRONTIER SCIENCE PROGRAM

12 Quai Saint-Jean 67080 Strasbourg Cedex FRANCE
Phone +33 (0)3 88 21 51 27/34 Fax +33 (0)3 88 32 88 97
E-mail **fellow@hfsp.org** Web site **http://www.hfsp.org**

2008 POSTDOCTORAL FELLOWSHIPS IN THE LIFE SCIENCES

The Human Frontier Science Program (HFSP) supports basic research in the life sciences with emphasis on novel, innovative, and interdisciplinary approaches that involve scientific exchange across national boundaries. The dynamic fields at the interface of biological and physical sciences open up new approaches to understand the mechanisms of living organisms. This indicates a clear need for participation of scientists from outside the life sciences to reveal the structures and networks that characterize the living state. Therefore the HFSP supports postdoctoral investigators who explore new areas within the life sciences or who, in the cross-disciplinary program, use their expertise in chemistry, physics, mathematics, engineering or computer science to bear on a biological question. Two types of fellowships are available:

Long-Term Fellowships

For applicants with a PhD degree in the life sciences who are expected to **broaden their horizon and to move into a new research area** that is **different from their doctoral studies or previous postdoctoral training**. Applicants that propose a significant departure from their previous research are viewed favorably.

Cross-Disciplinary Fellowships

For applicants with a PhD degree in physics, chemistry, mathematics, engineering or computer sciences who wish to **gain research experience in the life sciences by proposing a significant change in discipline**. While previous expertise should be reflected in the project, applicants are expected to be exposed to new techniques and literature.

Important deadlines:

Compulsory pre-registration for password: **16 August 2007**

Submission of applications: **30 August 2007**

The online submission system will become available in summer 2007 on the HFSP web site.

Nationals from one of the HFSPO supporting countries can apply to work in any country, while other nationals can apply for training only in a supporting country. Current supporting members are: *Australia, Canada, the European Union, France, Germany, India, Italy, Japan, the Republic of Korea, New Zealand, Switzerland, the United Kingdom, and the United States of America.*

Applicants must be within 3 years after receiving their doctoral degree. The program provides initial support for postdoctoral training in another country by means of an individual stipend (~150K USD over 3 years) that is composed of a living allowance and funds for research and travel. Fellows can apply for 3 months paid parental leave and receive a contribution towards the cost of child care. As a rule, fellows who choose to return to their home country can defer their final year for up to two years and are invited to apply for a **Career Development Award** (currently 300K USD over 3 years) to establish themselves as independent young investigators. HFSP requires the maintenance of stipends for research scholars and has the policy that its fellowship stipend cannot be subject to mandatory deductions for social security contributions. Applications from female PhD recipients are encouraged.

Short-Term Fellowships

Short-Term Fellowships are intended for researchers early in their careers who already hold a PhD and provide up to 3 months of support to **learn techniques in a new area of research or establish new collaborations in another country.** Applications are accepted throughout the year.

Europe's most important interdisciplinary forum

Learn about new trends and directions in research, business, science policy and funding
Network with the leaders of the world science community
Communicate your leading research and ideas to an international audience
Participate in the debate, the discussion and the excitement of European science and technology
Meet and **talk** to scientific journalists from Europe and around the world
Develop your career, your future projects, your horizons and your contacts

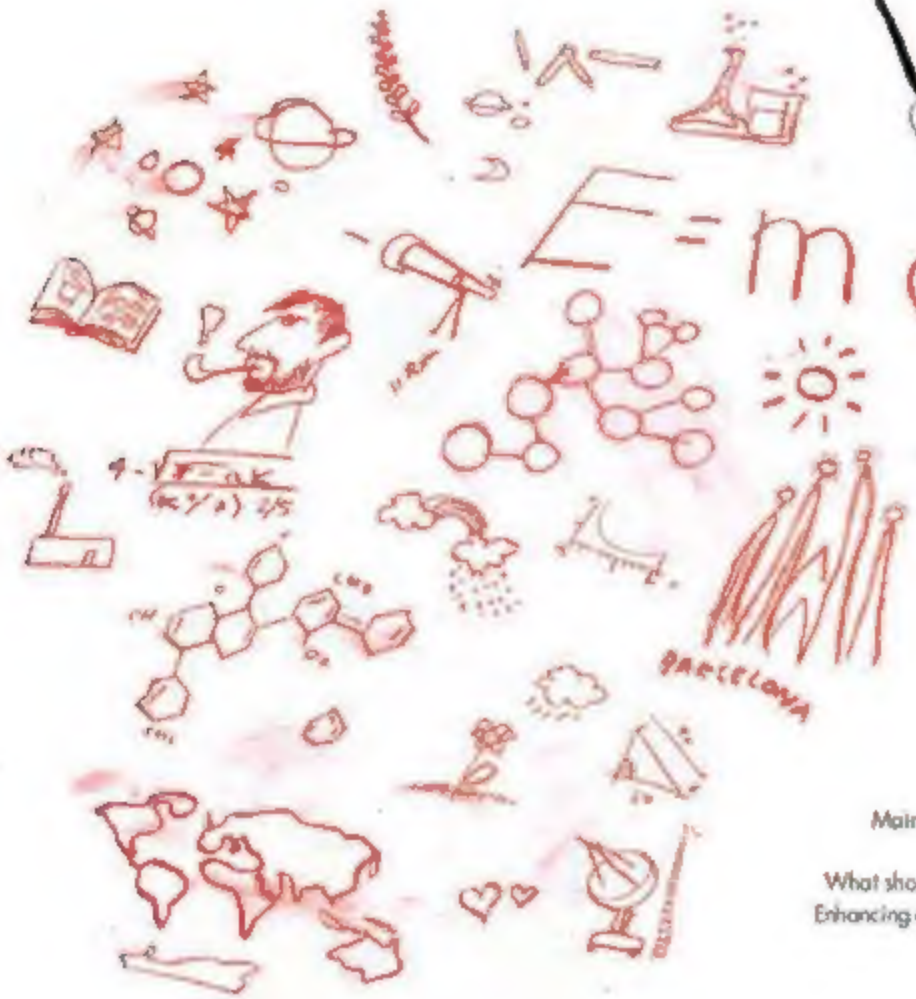

ANSWER THE CALL!
www.esof2008.org
SUBMIT A PROPOSAL

ESOF2008

Scientific themes

The human mind and behaviour
The very big and the very small
Maintaining an open society through science
Engineering the body
What should we eat and how should we look like?
Enhancing energy security, fighting global warming
Science policy
Science and art
Demography in an ageing Europe
Screening: burdens and benefits

A FORUM FOR LEADING SCIENTISTS, YOUNG RESEARCHERS, POLICY MAKERS, BUSINESS PEOPLE AND JOURNALISTS

EUROSCIENCE OPEN FORUM
ESOF 2008
SCIENCE FOR A BETTER LIFE
BARCELONA, JULY 18-22

POSITIONS OPEN

USDA ARS Agricultural Research Service
www.ars.usda.gov

The Soybean Genomics and Improvement Laboratory, Beltsville, Maryland, is seeking a permanent full-time **RESEARCH GENETICIST** (Plants), to conduct research aimed at the development and application of molecular genetic markers in soybean. The selectee will be expected to use new DNA sequence analysis tools combined with in silico approaches for single nucleotide polymorphism (SNP) discovery coupled high throughput SNP detection technologies to undertake whole genome analyses of plant germplasm. Salary range: $66,767 to $103,220 per annum, plus benefits. *Candidates must be U.S. citizens.* For details and application directions for announcement number ARS-X7E-0187, see **website: http://www.afm.ars.usda.gov/divisions/hrd/index.html,** or call **telephone: 301-504-1482.** Applications must be postmarked by June 15, 2007. *USDA/ARS is an Equal Opportunity Provider and Employer.*

The Children's Nutrition Research Center of the Baylor College of Medicine announces the availability of **TENURE-TRACK POSITIONS** in nutrition at the molecular, cellular, and whole organism levels, including translational human nutrition research. Although positions are not limited to these areas, specific interests are fetal, neonatal, and early childhood nutrition (including fundamental mechanisms for the developmental origins of adult health and disease) and obesity (including fundamental adipose tissue biology, regulation of appetite and satiety, development of eating and physical activity behaviors, and prevention/intervention studies).

The level of appointment will be consistent with the candidate's qualifications. Candidates should have a record of achievement through publications in peer-review journals and successful competition for extramural funding. In addition to a strong independent research program, the successful candidate will be expected to have significant potential for research collaboration with existing research programs within the Children's Nutrition Research Center.

Interested candidates should submit their curriculum vitae, a statement of research interests, and three letters of recommendation sent by regular mail to: **Dennis M. Bier, M.D., Director, Children's Nutrition Research Center, Baylor College of Medicine, 1100 Bates, Houston, TX 77030-2600.**

Baylor College of Medicine is an Equal Access/Equal Opportunity/Affirmative Action Employer.

POSTDOCTORAL RESEARCH POSITIONS
Diabetes, Oxidative Stress, Vascular Biology

New positions are available in the Laboratory of Cellular and Molecular Cerebral Ischemia to investigate translational-based medicine that focuses upon novel mechanisms of cell plasticity, degeneration, and immune function (*Journal of the American Medical Association* **293**:90, 2005; *Cell Signal* **19**:1150, 2007). Expertise in molecular biology with cell culture and animal models is required. Please forward curriculum vitae to: **Kenneth Maiese, M.D., Wayne State University, Detroit, MI. E-mail: kmaiese@med.wayne.edu.** *Wayne State University is an Equal Opportunity/Affirmative Action Employer.*

POSTDOCTORAL FELLOW

Position available to study the cellular and molecular mechanisms underlying neurodegeneration (**website: http://www.utdallas.edu/biology/faculty/research/dimello.html**). Applicants must have a Ph.D. degree with strong background and research experience in signal transduction mechanisms and/or rodent neurodegeneration models. Please send curriculum vitae to: **Santosh R. D'Mello, Department of Molecular and Cell Biology, University of Texas at Dallas, Richardson, TX 75083-0688.** *University of Texas, Dallas, is an Affirmative Action/Equal Opportunity Employer.*

ASSOCIATE or FULL PROFESSOR
Inhalation Toxicology and Cardiology/ Tenure Track
Comparative Biomedical Sciences

Biomedical Department with a well-equipped inhalation research facility seeks a faculty person in inhalation toxicology and cardiology. Required qualifications: Ph.D. or equivalent degree in biological/biomedical sciences or related field; postdoctoral experience; research background in inhalation toxicology and cardiology; significant extramural funding; ability to teach in professional and graduate programs. Responsibilities: maintains an extramurally funded research program, contributes to the graduate and professional program, expands collaborative usage of inhalation research facility. Salary and rank will be commensurate with qualifications. An offer of employment is contingent on a satisfactory pre-employment background check. Application deadline is July 6, 2007, or until candidate is selected. Submit letter of application and resume (including e-mail address) to:

Dr. Arthur Penn
Department of Comparative Biomedical Sciences
School of Veterinary Medicine
Louisiana State University
Reference: #027599
Baton Rouge, LA 70803
Telephone: 225-578-9889
E-mail: apenn@vetmed.lsu.edu

Louisiana State University is an Equal Opportunity/Equal Access Employer.

NATIONAL SCIENCE FOUNDATION
Integrative Organismal Systems

The National Science Foundation's Division of Integrative Organismal Systems (IOS) is seeking qualified candidates for a permanent position of **PROGRAM DIRECTOR** in the areas of Developmental Systems. Program Directors are responsible for program planning and administration, and for furthering the goals of the NSF and IOS. More information about IOS can be found on the **website: http://www.nsf.gov/div/index.jsp?div=IOS**. Applicants must possess a Ph.D. or equivalent experience in biology or a related area. In addition you must have six or more years of successful research, research administration, or managerial experience in developmental biology beyond the Ph.D. Familiarity with NSF policies and practices, administrative experience, and recognized stature among peers are desirable. Annual salary range is $93,822 to $146,213 depending on qualification and experience. Applicants should submit a resume to: **National Science Foundation, Attn: Myra Loyd, Division of Human Resource Management, 4201 Wilson Boulevard, Arlington, VA 22230.** For details regarding terms of employment, contact: **Myra Loyd, telephone: 703-292-4363.** For scientific or programmatic information, contact: **Dr. Bill Zamer, Acting Deputy Division Director, telephone: 703-292-8420; e-mail: wzamer@nsf.gov.**

NSF is an Equal Opportunity Employer.

POSTDOCTORAL POSITIONS

Postdoctoral positions funded by the National Institutes of Health are available, to study the roles of insulin, nitric oxide and protein tyrosine phosphatases in regulation of vascular smooth muscle cell signaling and neointima formation in vascular injury. Our projects address important basic science questions and also have relevance to clinical problems. Experience in molecular biology and/or rat and mouse surgery is essential. Competitive salary is offered. Please send curriculum vitae and the names of three references to: **Dr. Aviv Hassid, Department of Physiology, University of Tennessee, 894 Union Avenue, Memphis TN 38163. E-mail: ahassid@tennessee.edu, fax: 901-448-7126.** *The University of Tennessee is an Equal Employment Opportunity/Affirmative Action Title VI/Title IX/Section 504/ADA/ADEA Institution in the provision of its education and employment programs and services.*

GILEAD

SENIOR RESEARCH SCIENTIST I
Requisition Number: BF 7-386
Foster City, California

Gilead Sciences is a biopharmaceutical company that discovers, develops, and commercializes innovative therapeutics in areas of unmet medical need. Our mission is to advance the care of patients suffering from life-threatening diseases worldwide. Headquartered in Foster City, California, Gilead has operations in the United States, Europe, and Australia. We currently have a great opportunity in Foster City for an experienced, well-organized professional to join our Biology Department.

Responsibilities: The successful candidate will join multidisciplinary research teams focused on the discovery of new therapeutics for hepatitis C virus (HCV) and human immunodeficiency virus (HIV). He/she will be responsible for biological characterizations of drug candidates by developing state-of-the-art cell-based assays, and will plan and direct in vivo pharmacology studies. Additional responsibilities include management of associate and Ph.D. level scientists, providing project updates to internal research committees, and participating in business development opportunities. Publication and presentation of company research are expected.

Position requires: This position requires a Ph.D. in biomedical sciences with a minimum of six years of relevant postdoctoral experience. Extensive knowledge and hands-on research expertise in immunology and familiarity with in vitro and in vivo models are required. Experience in the host response to pathogens, innate immunology, and/or tumor immunology strongly preferred. Excellent track record and strong interpersonal and oral/written communication skills are essential.

Reference requisition number BF 7-386 and apply online today at **website: http://www.gilead.com/wt/sec/careers.**

We are an Equal Opportunity Employer.

CONFERENCE

The THIRD INTERNATIONAL CONFERENCE on B CELLS and AUTOIMMUNITY: FOCUS on INFECTION

Copacabana, Rio de Janeiro, Brazil
18 to 20 August 2007

Website: http://www.histo.ufrj.br/LIB/satellite

MARKETPLACE

Believe it!

DNA Sequencing for $2.50 per reaction.

- Read length up to 900 bases.
- High quality electropherograms.
- Fast turnaround.
- Plasmid and PCR purification available.

$2.50 per reaction!

POLYMORPHIC
Polymorphic DNA Technologies, Inc.™

www.polymorphicdna.com
info@polymorphicdna.com

1125 Atlantic Ave., Ste. 102
Alameda, CA 94501

Polymorphic exclusively uses ABI 3730XL sequencers.
Data delivered via secure FTP, email or CD.
No charge for standard sequencing primers.
384 sample minimum order.
96 well plates only—no tubes.

888.362.0888

For more information please visit
www.polymorphicdna.com

More siMPLE, stress-free, successful RNAi experiments.

Make your RNAi research as simple and successful as possible with expert help selecting the right tools.

With Invitrogen on your side, you can count on guidance throughout your entire RNAi experiment, from selecting between synthetic RNAi and vector-based RNAi to finding the right transfection and qRT-PCR reagents—you'll always have the right products and guaranteed results. Start to simplify your RNAi research now using our new RNAi Sourcebook. It's available, along with the answer to this Sudoku puzzle, at **www.invitrogen.com/siMPLE**.

invitrogen™